

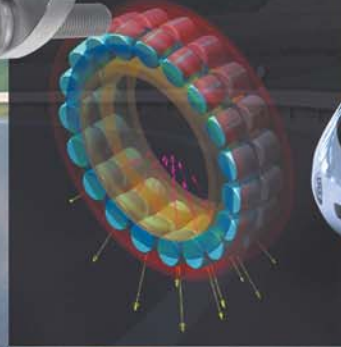
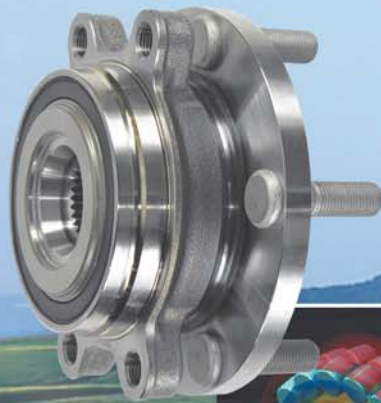
For New Technology Network

**NTN**®

# TECHNICAL REVIEW

No.  
**79**

**Special Issue;**  
**Automotive Technologies**  
November 2011





# TECHNICAL REVIEW

**No.79**

**Special Issue:**  
**Automotive Technologies**

# NTN TECHNICAL REVIEW No.79

## CONTENTS

<b>Preface</b>	Yoshikazu FUKUMURA	1
<b>Contribution</b>	<b>Prospects for Environmental and Energy-related Vehicle Technologies</b> Yasuhiro DAISHO Professor, Waseda University Graduate School of Environment and Energy Engineering	2
<b>Perspective</b>	<b>Market and Technology Trends in the Automotive Industry</b> Makoto OKASAKA	12
<b>Special Issue for Electric Vehicle ● Earth-friendly NTN - Pioneering Technologies for Tomorrow</b>		
	<b>In-Wheel Motor System</b> Yuichi ITOH, Kayo SAKAI and Yusuke MAKINO	22
	<b>Development of In-Wheel Motor System for Electric Commuters</b> Tetsuya YAMAMOTO, Aiko ISHIKAWA and Wataru YAMADA	29
	<b>One Motor Type Electric Vehicle Drive System</b> Fumihiko ISOBE, Yoshinori ITAKURA, Yusuke OOSUMI and Guodong LI	33
	<b>Development of a New Steer-by-wire System</b> Katsutoshi MOGI, Tomohiro SUGAI, Ryo SAKURAI and Nobuyuki SUZUKI	42
	<b>Development of Two-seat Electric Vehicles with In-Wheel Motors</b> Akira YAMAGATA, Aiko ISHIKAWA, Chinami ITOU, Tomomi GOTOU, Kayo SAKAI, Yukiko TAKEKAWA, Kaori TOMODA and Daisuke MATSUOKA	51
<b>● Automotive Products and Engineering</b>		
	<b>Hub Bearing with Integrated Multi-axis Load Sensor</b> Kentaro NISHIKAWA	58
	<b>Hub Bearing for Severe Environments</b> Yasushi SHIBATA	64
	<b>Lightweight and High-efficiency Drive Shafts for Rear-wheel-drive Cars</b> Tatsuro SUGIYAMA and Yuichi ASANO	69
	<b>Ball Screw Unit for Automotive Electro-actuation</b> Koji TATEISHI	73
	<b>Low-torque Deep-groove Ball Bearings for Transmissions</b> Katsuaki SASAKI	78
	<b>Technology Trends in Auto Tensioners</b> Seiji SATO	83
	<b>NTN-SNR Low-torque Strut Bearing for Severe Environments</b> Gérald MIRABEL and Susumu YAMAJI	90
	<b>NTN-SNR Low-torque High-capacity Pulley Bearing Unit for Water Pumps</b> Sebastien BRISSON	94
	<b>Development of a System for Rolling Bearing Design Optimization</b> Daisuke IMADA, Tsuyoshi NIWA, Takashi UENO and Tomohisa UOZUMI	98
<b>● Technical Papers Technical Articles New Products</b>		
	<b>Rapid Evaluation of Shear Fatigue Properties of Rolling Bearing Steels for Lifespans Up to the Gigacycle Range</b> Noriaki SAKANAKA, Yukio MATSUBARA, Yoshinobu SHIMAMURA and Hitoshi ISHII	104
	<b>Two-Dimensional Dynamic Analysis of Cage Stress for Needle Roller Bearings that Support Connecting Rods in Reciprocating Engines</b> Tomoya SAKAGUCHI	111
	<b>Integrated Bearing Dynamic Analysis System (IBDAS)</b> Mariko SEKIYA	119
	<b>Hybrid PEEK Sliding Bearing</b> Takuya ISHII and Ken YASUDA	125
	<b>Air Spindle for Ultra High-precision Machine Tools</b> Teruyoshi HORIUCHI and Kazuyuki AONO	130
<b>● Our Line of Award Winning Products</b>		
	<b>"2010 'CHO' MONODZUKURI Innovative Components Awards" Automotive Component Award</b> <b>Torque Diode for Seat Lifter</b> Masahiro KAWAI	136
	<b>The First Approval of Tribology Inheritance</b> <b>Journal Rolling Bearing for the 0 "Zero" Series Shinkansen Trains</b> Kouya OHIRA and Masanori UENO	137
<b>Our Line of New Products</b>		138

*Introduction to this special issue  
on automotive technologies*



**Yoshikazu FUKUMURA**  
Managing Director

As measures to reduce greenhouse gases and balance power supplies and demands in the energy field, the utilization of renewable energy sources, including the generation of power with wind and solar, has been accelerating. In the automotive field, the development of next-generation automobiles, including hybrid cars and electric vehicles, has been advancing.

In this changing environment, we are further improving the technologies that we have cultivated thus far at NTN, and we are developing green products based on the themes of reducing their torque, increasing their life spans, and making them more compact and lightweight in order to increase the conservation of resources and energy. Furthermore, we established our EV System Division in April 2011 to accelerate the development and commercialization of drive systems, steering systems, and control systems for electric cars, one type of the next generation of vehicles.

We have worked to publish this issue of our Technical Review, which features technologies and products for cutting-edge automobiles, in time for the 42nd Tokyo Motor Show that will be held over 10 days, December 2–11, with the theme “Mobility can change the world.” This issue starts with “Prospects for Environmental and Energy-related Vehicle Technologies,” a contribution by Professor Yasuhiro Daisho who is an authority in the automobile environment and energy field at the Waseda University Graduate School of Environment and Energy Engineering. Following this, in our Special Feature on Electric Vehicle Technologies, we introduce our in-wheel motor system, one-motor-type drive system, and steer-by-wire system for electric vehicles. We have been conducting research and development for these systems from standpoints that are completely different from the past.

At NTN, we will celebrate our 100th anniversary in fiscal 2017. Following our theme, “For New Technology Network: We shall contribute to international society through creating new technologies and developing new products,” we are striving to expand our business in the three years from fiscal 2011. To do this, we are implementing our Global Advance 2013 medium-term management plan, in which we stand on a foundation that puts “technology first” and we seek to realize a strong corporate composition that does not rely on scale. With this plan, we are also promoting the development of products that are better for the environment and contribute to the sustainable advancement of society.

**For New Technology Network**

# Prospects for Environmental and Energy-related Vehicle Technologies

## Improving Conventional Technologies and Electrifying Vehicles



**Yasuhiro DAISHO**

**Professor, Faculty of Science and Engineering, Waseda University**

To comply with increasingly stringent emission regulations, automakers are being forced to develop ultra-low-emission engine systems by optimizing combinations of technologies related to combustion, exhaust after-treatment and fuels. These vehicles are expected to retain their importance with state-of-the-art technologies for two decades to come. More emphasis will be placed on improving fuel economy and promoting the popularity of hybrid and electric vehicles, decreasing vehicle weights, and utilizing renewable energy and fuels to reduce oil dependency in the transportation sector, thereby mitigating global warming. High-performance and cost-effective components are essential for these electrified vehicles. While keeping an eye on these trends in the global market, we should develop a comprehensive technology strategy.

### 1. Introduction

In the industrialized nations, not only are entire-car manufacturers continuing to develop and commercialize novel technologies but the various automotive material and component manufactures have formed a big industrial field for commercializing these technologies. The common use of automobiles, as a means of mobility and transportation, has brought convenience and abundance to our lifestyles. On the other hand, automobiles consume a large amount of petroleum, and are a main source of emissions that cause urban air pollution and CO<sub>2</sub>, which are typically considered greenhouse gas. We can expect, however, that by the middle of this decade, vehicles ranging from passenger cars to heavy trucks will become compliant with strengthening restrictions on exhaust emissions, and the problem of air pollution will have been largely overcome in the industrialized nations.<sup>1)</sup>

To address global warming, Japan, in fiscal 2008 began a five-year effort with the goal of reducing greenhouse gases by 6% when compared to fiscal 1990 levels to meet the mandate of the Kyoto Protocol. In 2013, each country must set forth new target values for reducing greenhouse gases by 2020.

Currently, 17% of the total CO<sub>2</sub> emissions in Japan are from automobiles, and measures to reduce them are becoming an even more serious concern.

According to the World Energy Outlook 2010, which is a report by the International Energy Agency, the primary energy demand of the entire planet is

expected to increase 40% by 2030 if current measures are left unchanged. Above all, 60% of petroleum use will be in the transportation field, primarily caused by the remarkable increase in demand for petroleum in emerging nations, in particular, China, India and countries in South East Asia, where motorization is progressing considerably.<sup>2)</sup>

Under these circumstances, the development of technologies that improve fuel efficiency even more and the diversification of energy sources have become indispensable. Automobile manufacturers, betting on their own survival in the international market, are working on the development of technologies related to these things. In this paper, I will examine the prospects for automotive technological problems related to the environment and energy and their solutions from a medium and long-term perspective, while offering my own opinions.

### 2. Improvement in Conventional Vehicles

#### 2.1 Fuel economy improvements for gasoline-powered automobiles

For gasoline-powered automobiles, emission controls against the three pollutants—NO<sub>x</sub>, hydrocarbons (HC) and CO—are advancing greatly through the combination of more accurate electronically-controlled fuel injection systems and three-way catalytic converter systems. In Japan, reduced taxes on green cars and purchase subsidy

programs are succeeding, so most gasoline automobiles are now super-low emission models that emit one quarter of the regulated upper limits of NO<sub>x</sub> and HC, and impacts on the atmosphere have been greatly curtailed. While it can be said that this is a trend shared by other industrialized nations, the situation is serious in emerging nations, which have air pollution caused by traffic congestion and the resulting automobile emissions in large cities. Stronger regulations to improve fuel characteristics including reductions in sulfur content as well as the incorporation of sophisticated emissions control technologies are now thought to be necessary.

From now on, in addition to maintaining low exhaust emissions, improving fuel economy is becoming an even more critical issue for gasoline-powered cars. In Japan, the fiscal 2010 fuel economy standard<sup>3)</sup> was achieved ahead of schedule, and a standard for fiscal 2015 has been proposed that seeks fuel economy increases that are 23.5% better than that of fiscal 2004.<sup>4)</sup> Furthermore, Corporate Average Fuel Efficiency (CAFE) standards are being applied toward strengthening the fiscal 2020 standards for passenger cars, and considering the popularization of hybrid cars, a proposal has been made to seek an average of 20.3 km/L, which is a 24.1% improvement from the composition of vehicles in fiscal 2009. The plan to increase fuel economy numbers for hybrid vehicles will be determined next year.<sup>5)</sup> Specifically, after determining fuel economy target values for each vehicle weight class, what is sought for each company is that the weighted harmonic mean value from the actual fuel economy values for the number of vehicles of each class shipped does not go below the weighted harmonic mean value for the number of vehicles shipped according to the fuel economy target values set for each class.

In the EU, corporate average fuel efficiency standards based on CO<sub>2</sub> emission amounts have been set, and from the 130 g/km target value for 2012 to 2015, 95 g/km has been proposed for 2020. Even in the USA, as though chasing after Japan and Europe, stronger standards for 2017 to 2025 have been proposed.

Specific examples of technologies to achieve these targets, including fuel economy improvement measures that were considered during investigations of the above fiscal 2020 fuel economy standards, and their improvement ratios are shown in **Table 1**.<sup>5)</sup> They include the use of a variety of advanced engine variable geometries, direct injection and other fuel supply system control refinements, CVT, DCT and other more efficient transmission systems, engine size reduction through the use of supercharging systems,

**Table 1** Fuel economy improvement measures and their ratios for the proposed 2020 Japanese passenger car fuel economy standards

Fuel economy improvement measure		Fuel economy improvement ratio
Engine improvements	Friction reduction	1%
	4 valve	1%
	2 valve + 2-point ignition	2%
	Variable valve actuation	1~6%
	Electromagnetic valve actuation	10%
	Direct injection engine	2~10%
	Variable cylinders	7%
	Miller cycle	6%
	High-volume exhaust gas recirculation (EGR)	2%
	Heat management (cooling loss reduction, heat recapture, etc.)	2%
	Switching to variable compression	10%
	Supercharging size reduction	8%
Auxiliary equipment loss reduction	Electric power steering	2%
	Electrification (electric-powered wipers etc.)	1%
	Recharging control	0.5%
Improvements related to drive	Idling neutral control	1%
	Increasing automatic transmission (AT) stages	2%
	Expanding AT lockup range	2%
	Continuously variable transmission (CVT)	7%
	Semi automatic transmission (AMT), Dual clutch transmission (DCT)	9%
	Manual transmission (MT)	9%
Running resistance reduction	Rolling resistance reduction	1%
	Aerodynamic improvements	1%
Others	No idling (other than hybrid automobiles)	7%
	Diesel vehicles	20%
	No idling + energy recovery (other than hybrid automobiles)	10%

and the reduction of mechanical friction in every part as well as the reduction of parasitic losses from auxiliary systems. Furthermore, as I will discuss later, hybridization and vehicle weight reduction are also effective, and these must be integrated into seeking large overall fuel economy improvements. Until now, fuel economy improvements of 10 to 20% or so have been achieved. For engine technologies themselves, we can predict that, having meeting the strengthened standards of fiscal 2020, we will enter a period of decreasing returns as we approach an improvement of about 20%.

## 2.2 Countermeasures for exhaust gas and new combustion methods for diesel vehicles<sup>6)</sup>

Diesel engines have good fuel economy, and are a type of motor that will continue to be popular in the future for trucks and buses, which require high output and durability. On the other hand, NO<sub>x</sub>, black smoke and particulate matter (PM) are emitted at the same time due to combustion of non-uniform fuel spray, so emissions that are as clean as those from gasoline

vehicles are sought in Japan, America and Europe. Last year, in accordance with the world harmonized test cycle (WHTC), regulated values for emission gas testing methods for NOx and PM to be implemented in 2016 were proposed at 0.40 and 0.01 g/kWh, respectively, in Japan.<sup>1)</sup>

As shown in Fig. 1, NOx countermeasures include exhaust gas recirculation (EGR) and injection timing control. Measures to improve fuel economy and PM include the utilization of variable compression mechanisms and multistage turbocharging systems, as well as common rail systems capable of high-pressure, and flexible multistage fuel injection thanks to electronic control. We predict that supercharging will improve emissions even more, allowing engine size to be reduced further. Departing from the present fuel injection pressure of around 200 MPa, it is possible that there will be demand for pressure of nearly 300 MPa, and it will also be necessary to address demands for greater rigidity, reliability and durability in related parts.

Furthermore, as emission after-treatment technologies, in addition to diesel particulate filters, it is necessary to combine urea-based selective catalytic reduction (SCR) and NOx storage catalytic reduction. It is also necessary to ensure reliability and durability as well as the clear-cut division of roles with combustion technologies. Issues related to managing the costs of the overall system must also be overcome. We can predict that eventually these types of technologies will converge into optimal systems that are common to any manufacturer.

Moreover, although diesel passenger cars, which have achieved high performance, comprise about 50% of all passenger cars in the EU, due to smoke and noise issues, they have been held back in Japan, and they had disappeared from the market with the increasing costs of exhaust emissions control. Recently, however, Nissan Motors and Mitsubishi

Motors have introduced clean diesel passenger cars that conform to the Post New Long Term Regulations.<sup>1)</sup> For Japan, from the perspective of product balances in petroleum refining and CO<sub>2</sub> reduction, there are expectations for the revival of diesel cars, but the keys to their popularization on a broad basis are the development of NOx catalytic reduction with high purification capability and the cost reduction for the overall exhaust system.<sup>7)</sup>

### 3. Electrification of Automobiles<sup>8)</sup>

#### 3.1 History and background of electrification

After the oil shock that broke out in 1973, there was interest in electric vehicles (EV), but development did not advance, in part because of the eventual decline in the price of crude oil. Then, in the 1990s, the US state of California enacted a low-pollution vehicle program. As one part of this, it was proposed that one in every ten passenger cars sold in the state would be required to be a zero emission vehicle (ZEV).<sup>9)</sup> EVs are really the only kind of ZEVs, so a development boom occurred, but they were not well-received by consumers, and the program was revised to allow gasoline vehicles with low-polluting exhaust emissions. As a result, EVs did not achieve mainstream popularity. In every case, the batteries, which are the key components, were heavy and bulky, required a long time to recharge and only allowed short travel distances, not to mention being expensive. These drawbacks prevented their popularization.

Then, starting in the 1990s in the United States, the Partnership for a New Generation of Vehicles (PNGV) was started as a national project to triple mileage<sup>10)</sup> The big three American automakers worked on hybridization as the main technology, but they did not achieve the goal on a commercially acceptable level.

Prompted by this, however, Japanese auto manufacturers created hybrid cars that were ready for consumer use by the late 1990s. Furthermore, EVs that carry higher performance batteries, as well as fuel-cell vehicles (FCV) that use hydrogen as fuel have also appeared recently. Through this process, as shown in Fig. 2, research and development advanced greatly in areas ranging from batteries and motors to inverters, DC-DC converters and other electronic devices, as well as in power electronics, including power-energy management, vehicle weight reduction, high-efficiency engines for hybrids and fuel cell systems. Japan currently has a great lead in these technological fields. I will discuss it later, but as an example, in Fig. 3, I provide an overview of the electric system of the Mitsubishi Motors i-MiEV, which is the first EV in the world to be a truly mass-produced.

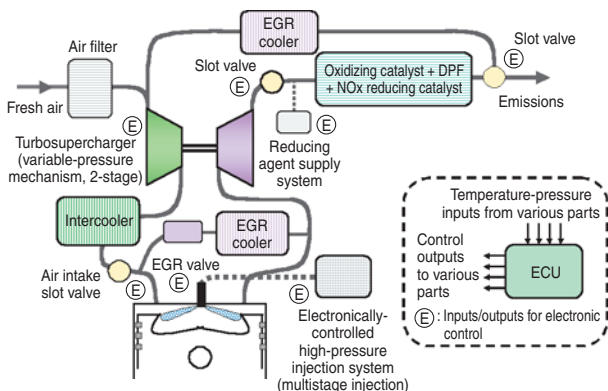


Fig.1 Typical example of measures to meet future diesel emission regulations

I expect that the determining factors for more common use of electric vehicles will depend on performance of lithium-ion (Li-ion) batteries in terms of both energy density and power density: more common use of Li-ion batteries will be promoted by further improvement in efficiency and lower cost. Furthermore, the most common electric motors used in vehicles are high output variants of highly efficient water-cooled permanent magnet AC synchronized type motors using neodymium and dysprosium. Long-term availability of raw materials of these rare earths will pose another challenge.

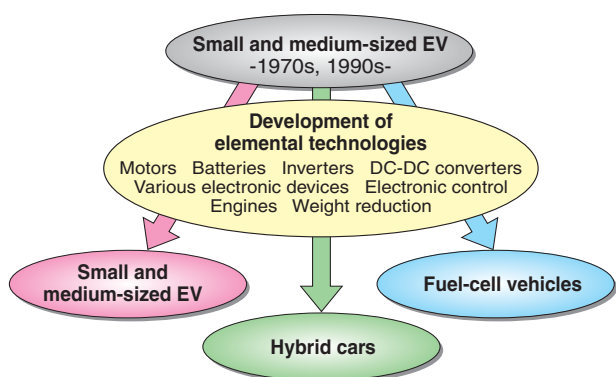


Fig. 2 Future trends in the electrification of vehicles

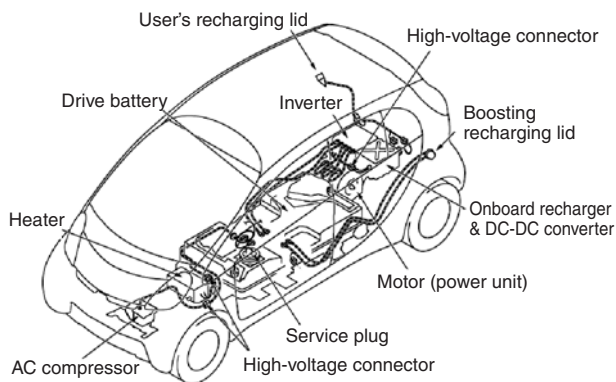


Fig. 3 Electric drive system of i-MiEV (Source: Mitsubishi Motors Corporation)

### 3.2 Hybrid vehicles<sup>8, 11)</sup>

Currently, as indicated in the background above, hybrid technologies that combine engines, motors, generators and batteries are the most promising of technologies that greatly improves fuel economy compared to conventional engine-powered cars. Types of hybrid systems can be classified as shown below, and the structures of types [2] and [3] are illustrated in Fig. 4. Toyota and Honda are already mass-producing such vehicles and cost reductions are in progress. At this time, their popularization is ahead of EVs, which still have high costs.

[1] Micro hybrids: The engine is started and stopped by a motor (stop idling) and regenerative braking occurs during deceleration to recharge. With these functions, fuel economy is increased by about 5–15%. The motor may be incorporated into the transmission system and used as a starter-alternator, leading to size reduction of the vehicle.

[2] Mild hybrids: In addition to the functions of micro type hybrids, these have systems to provide power assistance (parallel type). Fuel economy improvement is about 20–50%. Examples include Honda Motor Company's Insight, Fit and CR-Z, which all use Ni-H batteries, and Nissan Motor Company's FUGA hybrid, which uses lithium batteries.

[3] Full hybrids: This type of hybrid includes a motor and power generator. There are series types whose engines are used only to generate electric power, and dual types, which have both series and parallel functions. Fuel economy improvement ranges from about 50 to 100%. Examples of dual type hybrids are Toyota Motor Corporation's Prius and SAI, which are series/parallel types that use Ni-H batteries.

★Micro hybrids have stop idling and regeneration functions but do not have power assistance functions.

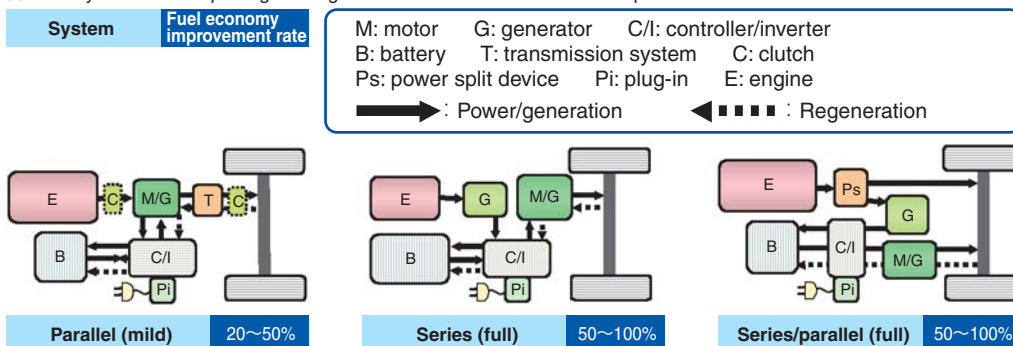


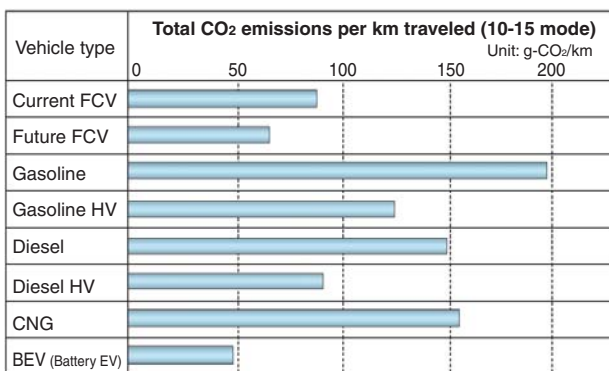
Fig. 4 Various hybrid systems

Gasoline hybrid vehicles almost double fuel economy at best, exceeding the fuel economy of diesel cars. For still better fuel economy, diesel hybrid cars must be developed. However, due to increased costs for diesel passenger cars, that include exhaust emissions controls, we can predict that achieving commercialization will not be easy. At the same time, in response to future strict CO<sub>2</sub> restrictions in the EU, as described above, the trend to apply parallel hybrid systems particularly with high-class gasoline cars and diesel cars, has increased in the last 2 or 3 years.

Moreover, various companies have been releasing diesel trucks for regional transportation and highway buses that are parallel hybrid vehicles in Japan. These achieve fuel economy improvements of 20 to 30%, but because of the large size of the vehicles, further improvements, including size reduction of hybrid system and batteries, are necessary.

**3.3 Electric vehicles<sup>8)</sup>**

As discussed above, since exhaust cleaning technologies for conventional vehicles have greatly advanced, for example, the necessity of the zero emission feature of EVs has declined, and interest has been focused on their CO<sub>2</sub> emission reduction and energy conservation features. Considering the current power source composition, Well-To-Wheel (overall performance from the production of fuel from primary resources and energy to transportation, storage and vehicle operation) energy efficiency and CO<sub>2</sub> emissions are both far superior to other types of vehicles. This is demonstrated clearly in results of comparative evaluations of the current Well-to-Wheel efficiency and CO<sub>2</sub> emissions of various types of automobiles provided by the Japan Hydrogen & Fuel Cell Demonstration Project, as shown in Fig. 5.<sup>12)</sup>



Current FCV: Calculated using top values from JHFC empirical results for hydrogen station and FCV data and top values from literature for other data

Future FCV: Calculated using a Future FC system efficiency of 60% for FCV and top values from literature

Power source composition: Average power supply composition for Japan

**Fig. 5** Comparison of CO<sub>2</sub> emissions in various vehicles (Source: JHFC, March 2006)

Features of these overall systems include the merits that the motors have high-efficiency in a wide operation range and that the battery loss during recharging and discharging is low. In addition, EVs and hybrid vehicles use their motors as generators to generate electricity while braking and store it in their batteries, allowing them to recover part of their operation energy during deceleration. By doing this, a significant energy conservation effect is achieved. This type of braking is called “regenerative braking” and is a method that is applied in conjunction with mechanical brakes.

Following the beginning of sales of Mitsubishi Motor Company’s i-MiEV cars, which carry Li-ion batteries, in 2009, Nissan Motor Company’s Leaf appeared in the market as a mass-produced EV at the end of 2010. Electric power has the great merit of being significantly less expensive than gasoline, considering the practice of discounted electric power rates at night, for example. On the other hand, since the batteries are expensive, they are still fairly expensive vehicles at present. However, Toyota and Honda will also enter the EV market in 2012 with models based on the iQ, RAV4 and Fit.

Furthermore, compared to conventional engine vehicles, the number of parts in EVs is 20 to 30% less, and a manufacturing approach with a so-called horizontal specialization of work is possible by combining major types of parts in modules. In fact, venture businesses in the United States have started manufacture and sales using this type of approach. In addition, while on a small-scale, sales of simple compact cars for short distance travel with limited speed and modification kits for gasoline cars have begun. Assuring safety for these vehicles, however, seems to be a challenge. Existing automobile manufacturers can be said to have advantages when they decide to mass-produce vehicles, which allows costs to be reduced, and in establishing networks that include sales, repair and maintenance. Anyway we look at it, however, we can see that a diverse variety of EV types will appear that respond to the different needs of a wide range of regions and income levels in the future.

**3.4 Plug-in hybrid vehicles**

Recently, a type of automobile called a “plug-in hybrid vehicle (PHEV)” has begun to enter the mainstream both in Japan and abroad. These vehicles feature the combination of both a charge depleting (CD) mode of travel that uses electric power charged from an external source and a charge sustaining (CS) hybrid travel mode. With this combination, these vehicles benefit from both the low CO<sub>2</sub> emission advantage of the power source

itself and the low cost of recharging, as well as the ability to travel long distances in CS mode. This can be said to offer the benefit of eliminating driver concern about running out of battery energy. In 2009, the Ministry of Land, Infrastructure and Transport presented a method to measure exhaust emissions and fuel economy for this type of vehicle.<sup>13)</sup>

Toyota Motor Corporation began limited sales of 600 Prius Plug-ins, its first PHEV, in 2010 and is conducting demonstration tests. Using a Li-ion battery, this model is capable of traveling 23.4 km as an EV. General sales are scheduled to begin in 2012. Another example is the mass-market sale of the Chevy Volt begun by GM at the end of 2010. In addition, Honda and Suzuki also plan to start sales of PHEVs. Honda plans to release a model based on the Inspire in 2012 and Suzuki plans to release a model based on the Swift in 2013.

Obviously, if the size of the battery in a PHEV is increased, the travel distance in CD mode can be extended, but this invites increased costs and greater energy consumption due to the increased weight. Further improving the performance of the batteries and reducing costs are challenges, but compared to EV, they already have both cost and convenience on their side when it comes to potential popularization. In any case, it is necessary to estimate the average daily travel distance of ordinary drivers and determine the optimal amount of batteries to be included onboard.

### 3.5 Measures to support EV and PHEV popularization

The Ministry of Economy, Trade and Industry has set target values for improving the performance of batteries for EVs and PHEVs and lowering their costs, as shown in **Table 2**.<sup>14)</sup> In particular, improving energy density, which leads to weight reduction, is the most important issue. Research and development support is also being provided through NEDO and other organizations.

**Table 2** Targets for developing Li-ion batteries for electric vehicles (Source: NEDO and METI, 2006)

Phase	Present	Improvement 2010	Advancement 2015	2020?	Innovation 2030
Application	Compact EVs for electric power companies	EVs and HVs for limited commuting	EVs, FCVs and plug-in HVs for commuting	High-performance plug-in HVs	Widespread adoption of EVs
Performance	1	1	1.5	3	7
EV	Energy density 100Wh/kg Output density 400W/kg	100 1,000	150 1,200	— —	700 1,000
HV	Energy density 70Wh/kg Output density 1,900W/kg	70 2,000	100 2,000	200 2,500	— —
Cost (¥10,000/kWh)	1 (20)	1/2 (10)	1/7 (3)	1/10 (2)	1/40 (0.5)
Development structure	Led by private sector	Led by private sector	Cooperation among industry, government and academia		Universities Research organizations

Furthermore, in order to realize their widespread adoption, along with manufacturer efforts to reduce costs, programs that respond to their current high costs, including reduced national taxes and purchase subsidies to cover the differences in prices over ordinary vehicles, the establishment of recharging stations and greater common awareness about their use, which is limited to short and medium distances, are necessary. Overseas, plans are being made to popularize these vehicles with levels of one million vehicles by 2015 in the United States and two million and one million vehicles by 2020 in France and Germany, respectively. In all these countries, we can predict that these five and ten year points will be critical to achieving widespread adoption.

In the United States in particular, since the change to the Obama administration, as part of an energy policy to reduce dependence on petroleum, plans are being implemented to construct a smart grid that will use IT to network conventional electric power sources with renewable energy sources, and policies are being advanced to support the popularization of EVs and PHEVs that will utilize this grid.

As a support policy for these types of vehicles in Japan, the Ministry of Economy, Trade and Industry designated 11 cities as “EV & pHV Towns” in fiscal 2009 with the goal of achieving a total of 3,200 vehicles and installing 10,000 boosting and regular recharging equipment units. These designations were made in order to take the lead in EV and PHEV (also abbreviated PHV) adoption and work on how they are used and resolve related problems. Since then, additional designations have continued to be made.<sup>15)</sup>

Furthermore, through support from the Agency for Natural Resources and Energy, the Committee for Next Generation Energy and Social Systems was started in 2010 with the purpose of investigating the potential for the effective use of smart grids, including the recharging of vehicles. Yokohama, Nagoya, Kyoto Keihanna Science City and Kita Kyushu City have been designated for their investigations, and empirical testing has begun in these four regions.<sup>16)</sup> As an example, let me introduce a smart house proposal that Toyota is working on. As shown in **Fig. 6**, it includes installation of a home energy management system (HEMS) that can manage energy use by PHEVs and EVs as well as within the residence. This system enables the comprehensive management and regulation of overall supply and demand, including electricity from power companies and energy generated by the household from solar and other sources. In addition, this system provides information to residents and vehicle users and allows them external control.

The sudden occurrence of the Great East Japan Earthquake this past March 11, however, reduced the ratio of nuclear power generation, which has been a major source of power for EVs and PHEVs, and caused an increase in the ratio of thermal power generation. For this reason, although the trend is an increase in the basic unit of CO<sub>2</sub> emissions, the potential exists for greater use of power generated from renewable energy sources, including solar, wind, geothermal and biomass. In this respect, we can expect that this will lead to eventual reduction in CO<sub>2</sub> emissions. In addition, many ideas have been proposed for using the batteries of these vehicles to store electricity generated by residential solar power and as emergency power sources.

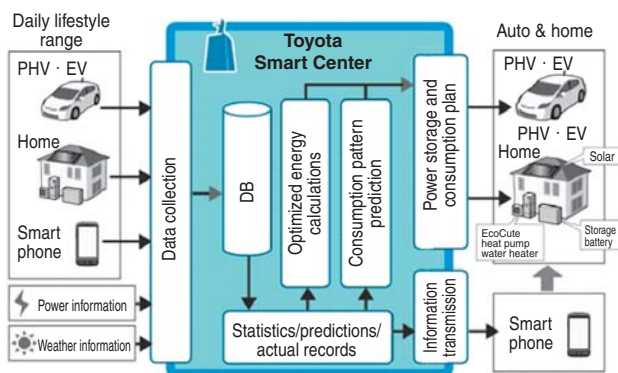


**Fig. 6** Toyota Smart Center energy management system—service will start in 2012 (Source: Toyota Motor Corporation, October 2010)

#### 4. Use of New Fuels and Energy Sources

The promotion of the use of new fuels and energy sources to supplement the amount of gasoline and diesel used is an important task in consideration of such issues as reducing fuel consumption, diversifying energy sources and taking measures against global warming. As shown in Fig. 7, diverse options can be suggested to supplement fossil fuels. Electricity for electric vehicles and hydrogen for fuel cells, as discussed above, are also included in these.

As for renewable fuels, we have bioethanol and biodiesel, which use biomass for their raw materials.<sup>17, 18)</sup> These fuels can be utilized with minimal change to the fuel infrastructure and to the vehicles themselves. Moreover, since they are liquids, they are similar to and more compatible with conventional fuels. Bioethanol is produced through the fermentation of sugarcane, corn and other sugars and starches, as well as cellulose-based raw materials using a variety of processes. Biodiesel is produced from vegetable

oil, including used oil, and other oils that have been converted to methyl ester. In Japan their use in already existing vehicles is permitted by the Act on the Quality Control of Gasoline and Other Fuels if mixed in concentrations of 3% (volume) in gasoline and 5% (mass) in diesel.

Moreover, in order to prevent the competition with food supplies that has occurred recently, as well as related to Post Kyoto Protocol efforts, an international movement is occurring that seeks an appropriate evaluation of CO<sub>2</sub> reduction effects, including all aspects of the process from the use of land to manufacturing and transportation.<sup>19)</sup> In any event, biomass resources are not very abundant in Japan, so their use must be limited. On the other hand, through the development of new fuel production methods, there are expectations that we can contribute to its use abroad.

If I am to make a few remarks on fuel-cell vehicles that use hydrogen as fuel, the fact is that their CO<sub>2</sub> reduction effect will not be great as long as the manufacture of hydrogen depends on petroleum, natural gas, coal and other fossil fuels. Eventually, systems for manufacturing and supplying hydrogen that eliminate dependence on fossil fuels and achieve great reductions in CO<sub>2</sub> emissions must be realized. If these conditions can be met, hydrogen could become popular, but many other obstacles must also be overcome, such as the storage and supply of hydrogen, how it is carried in vehicles and its user-friendliness. Other obstacles are issues related to the fuel cell stacks themselves, including their performance, reliability and durability and cost reduction. At present, long-term research and development must be continued with the support of the national government. Specifically, 30 companies have made a joint declaration targeting 2015 as the starting point for the real expansion of this technology.<sup>20)</sup>

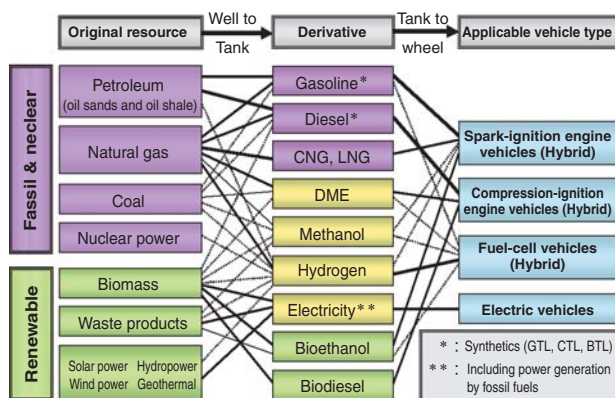


**Fig. 7** Future paths of fuel and energy generation for vehicles

### 5. Techniques to Reduce Vehicle Weight

I want to emphasize that techniques that reduce vehicle weight are also extremely important for fuel economy improvements. Fig. 8 shows a comparison of the energy consumption caused by vehicle weight, rolling resistance and air drag while driving based on a light vehicle traveling city streets. Fig. 9 is an example of a quantitative estimation that I prepared through the nondimensionalization of this data. It shows the impacts that reducing these effects could have on energy consumption when driving. These figures make clear that, among these three factors, the effect of weight reduction on improving fuel economy could be very large. It goes without saying that this is an important technique for both hybrid vehicles and electric vehicles. As shown in Fig. 10, weight reduction not only improves the operation performance of vehicles, but also enables the downsizing of power systems and the reduction of emissions purification loads, creating a virtuous circle.

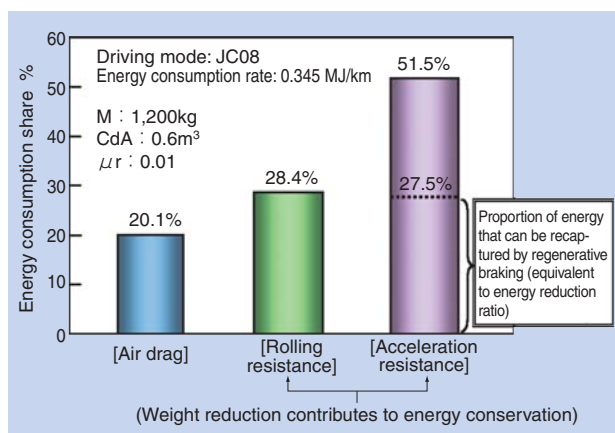


Fig. 8 Energy consumption when driving a vehicle

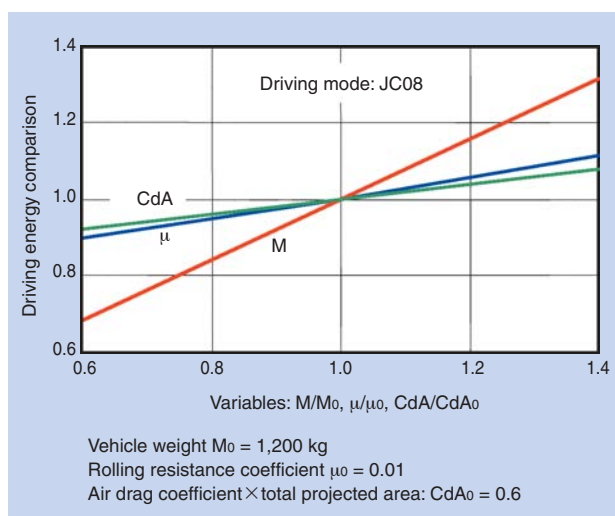


Fig. 9 Resistance factors and required energy for driving a vehicle

In order to achieve weight reduction of vehicles in their entirety, efforts must be made in a wide range from structural parts to the component level, including making items more compact. Of course, these types of weight reductions have the benefit of improving fuel economy not only for passenger cars but also for commercial vehicles.

As a specific example, I will introduce the World Auto Steel project that has been undertaken since 2008 by 16 major international steel manufacturers. In this project for electric vehicles and hybrid vehicles, they are seeking to reduce vehicle weights by about 30% to improve fuel economy by 20% while assuring safety by using high tension and super high tension steels that are 2 to 4 times as strong as previous materials.<sup>21)</sup> These types of vehicles tend to become heavy compared to gasoline vehicles, so reducing their weight can be said to be necessary. Japanese steelmakers have a lead in this field, and the application of their results is steadily beginning to expand.

In addition, the use of aluminum and other lightweight metals, as well as plastics, including CFRP, is also being advanced. Hopes are high for the advancement of the popularization of technologies that use these materials as the benefits of each type of material are utilized and the obstacles, which include difficulties related to molding, finishing and joining with different types of parts, increased costs and the globalization of production, are overcome.

With these materials, another important issue will be assuring control of vehicle vibrations and noise as well as collision compatibility between vehicles. Structural optimizations that minimize harm to people and the damage caused by heavier vehicles to lighter vehicles during collisions are needed. I want to point out that these types of vehicle weight reductions also motivate research and development for cutting-edge technologies that seek to increase comfort, provide collision safety and prevent accidents.

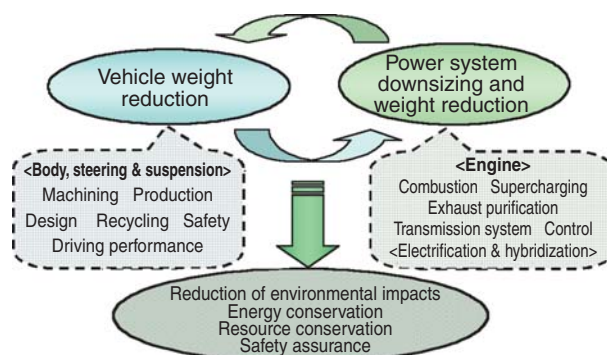


Fig. 10 Synergy between power system downsizing and vehicle weight reduction

## 6. Future Prospects and Conclusion

After conforming to the planned final emissions regulations in Japan, America and Europe by the middle of the second decade of the 21st century, developments and advancements will continue for gasoline and diesel vehicles with an emphasis on fuel economy improvement technologies. I expect that they will continue to have an important role for at least the next 20 years. In their advancement, assuming that fuel characteristics improve, the combination and optimization of elemental technologies related to combustion technologies and exhaust after-treatment technologies will be indispensable.

In addition to these conventional technologies, the reduction of vehicle weights and the use of hybrid and electric vehicles as well as biofuels, for example, are necessary. Fig. 11 shows the results of predictions about future CO<sub>2</sub> reductions resulting from these technologies. In this chart, a ■ indicates a current technology, a ● indicates a reduction resulting from the power system, and a ☆ indicates a reduction from another technology. The horizontal bars indicate the range of the effect depending on differences in the technology. This chart also shows us that the CO<sub>2</sub> reduction potential of EVs is very high. At the Next Generation Vehicle Strategic Research Meeting sponsored by the Ministry of Economy, Trade and Industry, international standardization, establishing recharging infrastructure and securing resources were suggested as important strategies related to EVs and batteries.<sup>22)</sup> The same research meeting provided a forecast of comparative sales shares of next-generation vehicles in 2020 and 2030, as shown in Table 3. We can expect that it would be possible for adoption to occur even more quickly with proactive government support compared to if only businesses make efforts.

Moreover, assuming the wider adoption of Intelligent Transport Systems (ITS) that utilize telecommunication technologies, which are expected to advance even more in the future, reviewing the use of all types of vehicles and advancing performance increases are necessary. These include traffic flow smoothing and controlling suitable traffic volumes, increasing the efficiency of freight traffic, promoting the use of public transportation, shifting to rail transportation, and reevaluating commercial habits and lifestyle patterns that depend on automobiles (such as the promotion of green driving).

If we can advance these measures comprehensively, the potential CO<sub>2</sub> reduction is predicted to possibly be about 50% by 2030 and 80% by 2050, as shown in Fig. 12. To achieve these

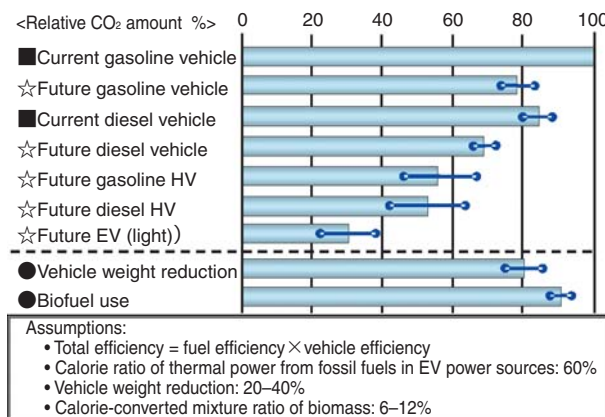


Fig. 11 Comparison of vehicle CO<sub>2</sub> emissions in the 2020s (Baseline: current gasoline vehicle)

Table 3 Projected sales shares of next generation vehicles in 2020 and 2030  
 (Source: Next Generation Vehicle Strategic Research Meeting, METI, March 2010)

<Private sector effort model>		
	2020	2030
Conventional vehicles	80% or more	60~70%
Next-generation vehicles	20% or less	30~40%
Hybrid vehicles	10~15%	20~30%
EVs & plug-in hybrid vehicles	5~10%	10~20%
Fuel cell vehicles	Minimal	1%
Clean diesel vehicles	Minimal	~5%

<Government targets>		
	2020	2030
Conventional vehicles	50~80%	30~50%
Next-generation vehicles	20~50%	50~70%
Hybrid vehicles	20~30%	30~40%
EVs & plug-in hybrid vehicles	15~20%	20~30%
Fuel cell vehicles	~1%	~3%
Clean diesel vehicles	~5%	5~10%

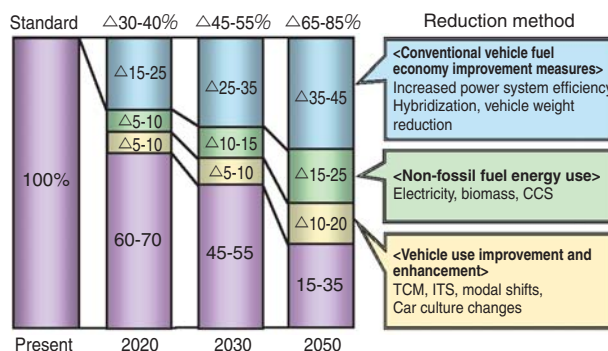


Fig. 12 Projected medium and long-term reductions in vehicle CO<sub>2</sub> emissions

predictions, medium and long-term outlooks for securing resources, conserving energy, and reducing CO<sub>2</sub> are necessary along with the execution of national support measures to realize them. While keeping an eye on the international marketplace, including emerging nations, and energy policies, the industry should also devise and execute technological strategies accordingly.

NTN has been conducting the development and manufacture of power transmission systems, related bearings and similar parts for automobiles. Recently, however, the company has also been advancing the development of technologies related to the trend toward vehicle electrification. These are indispensable technologies for the next generation of vehicles, and I have great expectations for your future advancements with them.

## Reference

- 1) Forms of vehicle exhaust gas reduction measures in the future, reports 2–10 of the Central Environmental Council, 1997–2010.
- 2) World Energy Outlook 2010, IEA (<http://www.iea.org/weo/2010.asp>), 2010.
- 3) Fiscal 2010 fuel economy standards for passenger cars and other vehicles, Ministry of Economy, Trade and Industry, and Ministry of Land, Infrastructure and Transport (<http://www.meti.go.jp/feedback/data/iscar00j.html>), 2010.
- 4) Final arrangement of fiscal 2015 fuel economy standards for cars and other vehicles, Ministry of Economy, Trade and Industry, and Ministry of Land, Infrastructure and Transport ([http://www.mlit.go.jp/kisha/kisha07/09/090202\\_2\\_.html](http://www.mlit.go.jp/kisha/kisha07/09/090202_2_.html)).
- 5) Fiscal 2010 fuel economy standards for passenger cars and other vehicles, Ministry of Economy, Trade and Industry, and Ministry of Land, Infrastructure and Transport (<http://www.meti.go.jp/feedback/data/iscar00j.html>), 2010.
- 6) Daisho, Y., Environmental and regulatory trends related to automobiles—the past ten years, Journal of the Society of Automotive Engineers of Japan, Jan. 2010.
- 7) Report of an investigative commission related to the popularization of and future prospects for clean diesel passenger cars, Ministry of Economy, Trade and Industry (<http://www.meti.go.jp/report/downloadfiles/g50418b01j.pdf>), April 2005.
- 8) Osaka, T., Daisho, Y., et al., Electric Automobile Handbook, Maruzen, 2001.
- 9) State of California (USA) website (<http://www.arb.ca.gov/msprog/levprog/levprog.htm>).
- 10) US PNGV program (<http://www.fueleconomy.gov/feg/pngv.shtml>).
- 11) Kihara, R., Daisho, Y., Research on High-performance Hybrid Vehicles, Sankaido, 2005.
- 12) Japan Hydrogen & Fuel Cell Demonstration Project (<http://www.jhfc.jp/j/index.html>), 2002–present.
- 13) Measurement methods for the exhaust gas and fuel economy of plug-in hybrids, Ministry of Land, Infrastructure, Transport and Tourism ([www.mlit.go.jp/common/000046352.pdf](http://www.mlit.go.jp/common/000046352.pdf)), 2009.
- 14) Roadmap for Technological Development of Storage Batteries for Next-generation Automotive Electric Power Systems, NEDO (<https://app3.infoc.nedo.go.jp/informations/koubo/other/FANedooothernews.2009-05-29.2374124845/>), 2009.
- 15) EV & pHV Towns Concept, Ministry of Economy, Trade and Industry (<http://www.meti.go.jp/policy/automobile/evphv/index.html>) 2009.
- 16) Ministry of Economy, Trade and Industry, Next-generation Energy and Social Systems Demonstration Areas ([http://www.meti.go.jp/policy/energy\\_environment/smart\\_community/community.html](http://www.meti.go.jp/policy/energy_environment/smart_community/community.html)), April 2010.
- 17) Increasing the utilization of green transportation fuels, Green Fuel Use Promotion Committee, Ministry of the Environment ([http://www.env.go.jp/earth/ondanka/conf\\_ecofuel/](http://www.env.go.jp/earth/ondanka/conf_ecofuel/)), 2006.
- 18) Daisho, et al., The Frontline of Biodiesel (Revised Edition), Kogyo Chosakai Publishing Co., Ltd., June 2008.
- 19) Report on the “Investigative committee on sustainability standards and other matters concerning the adoption of biofuel use,” Ministry of Economy, Trade and Industry (<http://www.meti.go.jp/press/20100305002/20100305002.html>), March 2010.
- 20) Toyota Motor Corporation ([http://www2.toyota.co.jp/jp/news/11/01/nt11\\_0106.html](http://www2.toyota.co.jp/jp/news/11/01/nt11_0106.html)), Jan. 2011.
- 21) Efforts by WorldAutoSteel (<http://www.worldautosteel.org/About.aspx>).
- 22) Next-Generation Vehicle Plan 2010, Ministry of Economy, Trade and Industry (<http://www.meti.go.jp/press/20100412002/20100412002-3.pdf>), March 2011.

### <Author biography>

#### Yasuhiro Daisho

Professor, Faculty of Science and Engineering, Waseda University  
 Dean, Graduate School of Environment and Energy Engineering  
 Director, Environmental Research Institute  
 Professor, Department of Modern Mechanical Engineering, Graduate School of Creative Science and Engineering

- 1976 Received Ph.D. from Faculty of Science and Engineering, Waseda University Graduate School
- 1980 Became Assistant Professor of Department of Science and Engineering, Waseda University
- 1985 Became Professor of Department of Science and Engineering, Waseda University

### [Research fields]

- Engine combustion, exhaust purification, efficiency improvement and new fuel utilization technologies
- Manufacture, performance evaluation and other studies of electric, hybrid and fuel-cell vehicles

### [Academic society and committee affiliations]

- Vice President, International Federation of Automotive Engineering Societies (FISITA)
- Advisor, Ministry of the Environment Central Environment Council
- Member, Ministry of Land, Infrastructure and Transport Transportation Policy Council and Social Capital Policy Council
- Member, Advisory Committee on Energy and Natural Resources
- Director, Japan Automobile Research Institute
- Member or chairman, other committees related to vehicles and the environment and energy, etc.

# Market and Technology Trends in the Automotive Industry

Makoto OKASAKA\*



After the collapse of Lehman Brothers, the Ministry of Economy, Trade and Industry announced a new strategy to build long-term and short-term responses for the automotive industry and society as a whole in April 2010. The results of the Next-Generation Vehicle Strategy Research Association were published as the Next-Generation Vehicle Plan 2010. We have begun to see signs of revival even in the domestic auto industry, and discrepancies with this scenario have begun to arise in 2011.

In this report, we look at the present and future market and technology trends in the automotive industry as a developer of automotive bearing and related products.

## 1. Introduction

In April 2010, the Ministry of Economy, Trade and Industry (METI) officially published the Next Generation Auto Strategy 2010.<sup>1)</sup>

This strategy is the product from the Research Conference on Next Generation Auto Strategy were experts from METI and the Ministry of Land, Infrastructure and Transport (MLIT), automakers and automotive component manufactures in Japan took part, in order to develop a new strategy for medium and long term activities to be taken by the entire society in Japan including Japan's automakers and automotive component manufactures that were experiencing difficulties after the Lehman Brothers shock.

In the global automotive industry, a period of great success with six consecutive years of record-breaking car production numbers continued until the Lehman Brothers shock, and then, a rapid decline in demand followed, and both the US Big Three and the Japanese automakers fell into the red. Later, numerous aid measures and economic stimulus policies have started the recovery of demand, but it is still stagnant at a low level.

In contrast, the emerging markets, in particular, Brazil, Russia, India and China (the BRIC countries), experienced temporary stagnation, but their recoveries were remarkable. In addition, as a result of the changing conditions of the global economy with the acceptance of a high yen, the Japanese industry

has changed from the export of vehicles produced domestically to the production of both parts and vehicle bodies in the emerging markets themselves. With these changes, however, the automobile market is continuing to expand.

At the same time, out of concern for preventing global warming and other worldwide environmental problems, as well as in response to energy concerns due to the steep rise in crude oil prices, the development of electric vehicles (EV), hybrid vehicles (HEV) and fuel cell vehicles (FCV) has begun to flourish in many countries. On the other hand, in response to changes in the automotive market, development of technologies for conventional vehicles with gasoline and diesel engines that consume fossil fuels has also become vigorous. These include ways to increase fuel economy, reduce weight and purify exhaust gases, as well as to promote greater electrification and control-by-wire utilization.

## 2. Changes in Automotive Market

### [Bipolarization of the automobile market]

Within the global automobile market, the Chinese market has grown and surpassed the North American market, which includes Canada and the United States, exceeding 13,790,000 vehicles in 2009. Meanwhile, the Japanese domestic market was stuck at 8,000,000 vehicles.

In the Next Generation Auto Strategy 2010, trends

\* Automotive Business HQ. Automotive Engineering Dept.

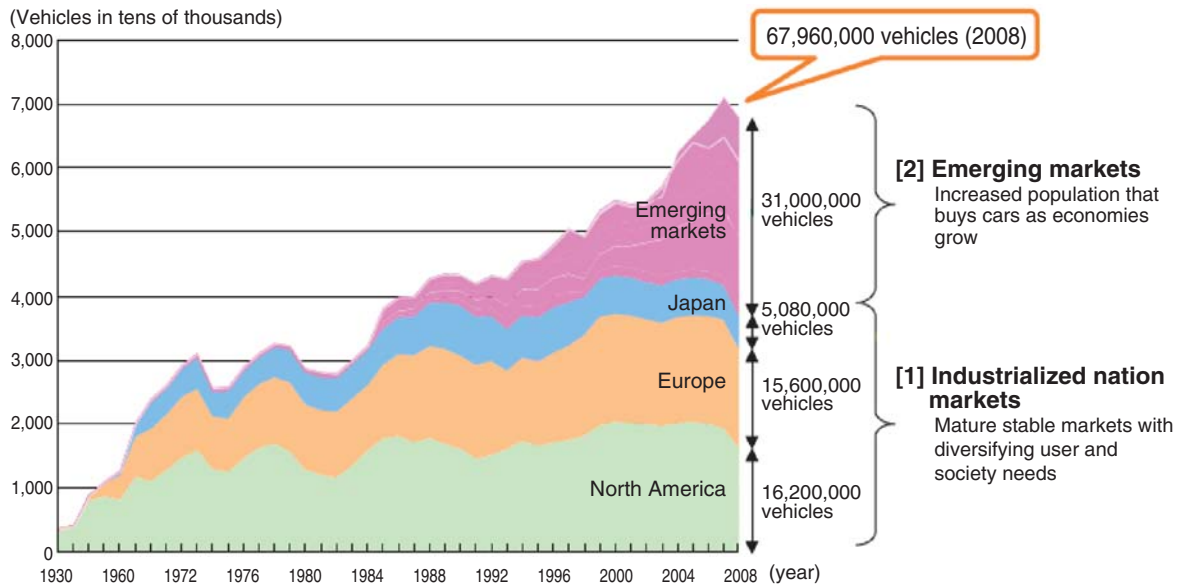


Fig. 1 Changes in the global auto market Reference: Next Generation Auto Strategy 2010<sup>1)</sup>

in the global automobile market are summarized as shown in Fig. 1. The growth of the markets in India, China and other emerging countries in recent years is particularly notable.

The rapid growth of the emerging markets, looked at in another way, suggests the beginning of a bipolarization of automobile markets into those of the industrialized countries and those of the emerging countries.

**[Responding to markets with difficult environmental conditions]**

In the markets of emerging nations where demand is increasing rapidly, in addition to responding to environments that range from extremely cold temperatures to very hot and humid conditions, measures that are sufficient to deal with mud are necessary because there are many regions that have insufficient road infrastructure.

As an example, Fig. 2 illustrates road conditions in a region with a difficult environment. The deep ruts and mud on the road surface create a difficult environment that is hard to imagine in an industrialized



Fig. 2 Poor road conditions in area with difficult environment

country market. Initially, carmakers did not foresee the severity of these conditions.

Furthermore, in addition to countermeasures against salt damage from snow-melting agents and muddy water, since the frequency of car-washing to clean off mud that adheres to vehicles is also great, consideration for high-pressure car-washing is also necessary.

**[Changes in power sources: breaking away from fossil fuels]**

Based on the Copenhagen Accord from the previous 15th Conference of the Parties (COP15) of the United Nations Framework Convention on Climate Change, Japan has proposed a target of reducing greenhouse gases by 25% from 1990 levels by 2020.

In addition, the price level of fossil fuels for vehicles has remained high with the increased cost of crude oil since the 2008 Lehman Shock, as well as because of the expansion of thermal power generation due to problems related to nuclear power generation in Japan.

As a result, development of alternatives, such as electric vehicles (EV), hybrid vehicles (HEV) and fuel-cell vehicles (FCV), has become active in various nations. At the same time, various carmakers have also begun developing various means of improving fuel efficiency for the internal combustion engines that will continue to use fossil fuels.

Both government and private parties are predicting the popularization of these types of next-generation vehicles. The Ministry of Economy, Trade and Industry's Conference on Next Generation Auto Strategy predicts that, with private efforts, the usage

ratios shown in **Table 1** will be achieved in 2020 and 2030 for these vehicle types.

In addition, the Conference on Next Generation Auto Strategy indicates that groupings can be made for these next-generation vehicles according to vehicle size and driving distance capability, as shown in **Fig. 3**.

In summary, they can be grouped into EVs as commuters for transporting small numbers of people over short distances within a community, HEVs for driving medium distances, and FCVs for traveling relatively long distances.

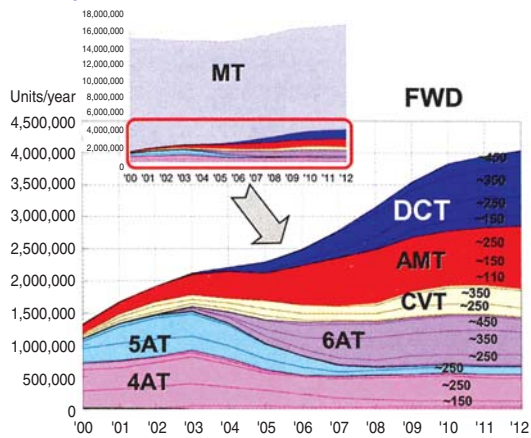
**[Changes in transmission types: reducers vs. transmissions more gear stages]**

If the power source is an EV motor with a wide torque band, as used in EVs and FCVs, a transmission is unnecessary and a reducer is utilized. For HEVs and conventional fossil-fuel automobiles that use internal combustion engines with narrow torque bands, however, multistage transmissions or continuously variable transmissions are necessary.

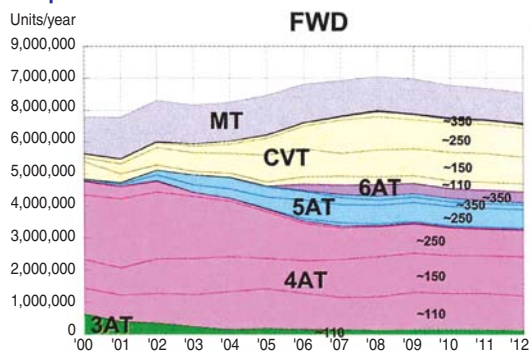
In addition to manual transmissions (MT), automatic transmissions (AT) and continuously variable transmissions (CVT), other transmission types include automated manual transmissions (AMT) and dual clutch transmissions (DCT).

As an example of the market trends for these types of transmissions, **Fig. 4** shows the changes in transmission type in front-engine, front-drive (FF)

<European market>



<Japanese market>



<North American market>

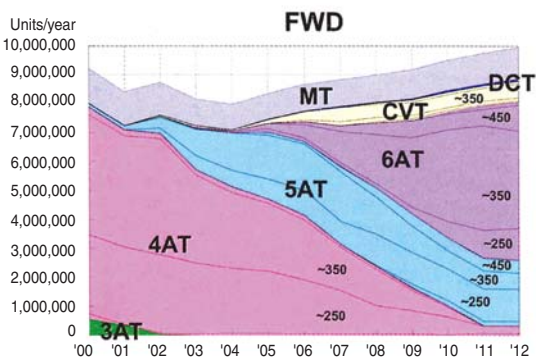


**Fig. 4** Changes in transmission type used in FF cars <sup>2)</sup>

**Table 1** 2020 & 2030 forecast for car types<sup>1)</sup>

	2020	2030
Conventional vehicles	80% or more	60~70%
Next-generation vehicle	20% or less	30~40%
Hybrid vehicles	10~15%	20~30%
Electric vehicles		
Plug-in hybrid vehicles	5~10%	10~20%
Fuel cell vehicles	Minimal	1%
Clean diesel vehicles	Minimal	~5%

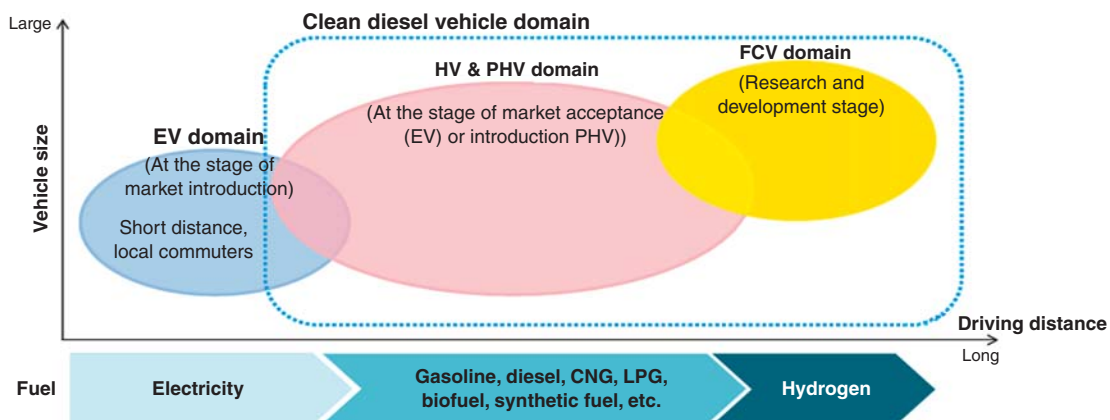


**Fig. 3** Future groupings by vehicle type <sup>1)</sup>

passenger cars in the markets of Europe, Japan and North America. Since lowering the engine speed should improve fuel economy, multistage transmissions with greater numbers of transmission gear stages have increased rapidly in recent years.

In the European market, MTs continue to be popular, but AMTs and DCTs, which make driving easier and have good acceleration and fuel economy characteristics, are rapidly increasing in popularity.

In the Japanese market, CVTs are steadily gaining popularity and ATs are shifting to 5- and 6-speed multistage versions.

On the other hand, in the North American market, ATs are as dominant as ever, but the common number of stages in them has increased from 3~5 speeds to 5~6 speeds.

**[Changes in growing passenger car markets]**

While the bipolarization of the markets of industrialized nations and emerging nations and the transition to EVs, HEVs, FCVs and other next-generation vehicles are occurring, the recovery of growth in the passenger car market, excluding trucks and buses, since the Lehman Shock has been fueled by India, China and other emerging markets.

According to the totals from the Japan Automobile Manufacturers Association (JAMA), in fiscal 2010, global production of automobiles, including trucks and buses, was 77,610,000 vehicles, of which 58,270,000 were passenger cars. Given the ever-increasing production of passenger cars in India, China and other countries, one private research institution has predicted that the number of passenger cars alone will exceed 72 million in 2020, as shown in Fig. 5.<sup>3)</sup>

In summary, the prediction is that the markets for passenger cars in Europe, Japan, North America and other industrialized nations will not grow any more

than they have. In contrast, the market for passenger cars is expected to continue growing globally, primarily in emerging markets, with the number of passenger cars alone exceeding 100 million by 2030.

**[Relative loss of interest in cars among young people]**

The ratio of licensed drivers among men and women between 18 and 24 years old has not changed much from 30 years ago in Japan. JAMA, however, has conducted a survey related to the "loss of interest in cars among youth."<sup>4)</sup>

The results of this survey, which ranked commodities according to the level of interest of college-aged respondents of that generation, showed that younger generations had decreasing interest in cars.

- College students 20 to 30 years ago (40~50 years old at present): 7th
- College students 10 to 20 years ago (30~40 years old at present): 10th
- Current college students (18~24 at present): 17th

Among the recent younger generation, which does not have much interest in cars and has low buying power, cars are merely one means of transportation, and they tend to prioritize economic issues (good fuel economy, low vehicle price and inexpensive maintenance). From the results of this survey, we can see that the trend will be for inexpensive compact cars to sell well.

**3. Recent Engineering Trends in Automotive Industry**

From these market trends, we can see that for the Japanese automotive industry to remain competitive and survive as a top global industry, developing the following technologies and advancing well-balanced production strategies in emerging markets are crucial.

- Development of EVs, HEVs, FCVs and other next-generation vehicles that combine energy conservation and environmental protection
- Development of fuel economy improvements and weight reduction for internal combustion engine vehicles to maintain competitiveness in this field

Table 2 shows engineering trends for improving electrical economy and fuel economy in the automotive industry.

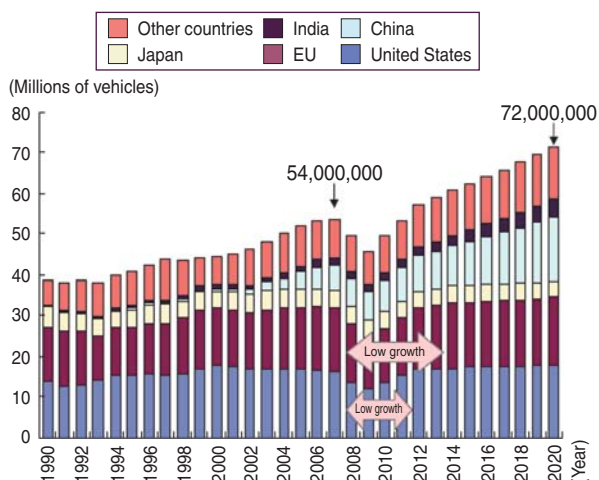


Fig. 5 World car sales forecast<sup>3)</sup>

**Table 2** Recent trends in the automotive industry

Area of application		Engineering trend		
EV motors		● Low friction motors	● High-RPM compact motors	● Motor bearing torque reduction
Engines	Fuel-related improvements	● High-pressure fuel injection	● Lean burn	
		● Miller cycle	● Hybrids	● Incorporation of rolling bearing in fuel pump
	Precision control	● Stop idling	● Cutting fuel supply during deceleration	
		● Fuel-air ratio control and ignition control		● Electric drive of auxiliary equipment
	Application of new mechanisms	● Downsizing by introduction of turbo superchargers		● Variable pressure mechanisms
		● Variable valve movement mechanisms (variable valve timing and variable lift)		
Friction reduction	● Low viscosity engine oil	● Dry sump lubrication	● Incorporation of rolling bearing onto crankshafts	
	● Oil pump size reduction		● Incorporation of rolling bearing onto camshafts	
	● Low-tension auxiliaries drive belt systems		● Incorporation of rolling bearing onto balancer shafts	
	● Reduced friction loss in valve powertrains		● Incorporation of rolling bearing onto chain levers	
Power trains	AT improvements	● CVTs with secondary transmission	● DCTs	● ATs with more stages
		● Ball-screw driven automatic transmissions (AMT)		● ATs with built-in EV motors
Chassis	Weight reduction	● Increased use of resins and high-tension steels		● Reduction in hub bearing weight
		● Low $\mu$ tires	● Zero lift bodies	● Reduction in hub bearing torque
Others		● Reduction of air drag coefficient	● Reduction of glass area	● Control-by-wire

## 4. NTN's Efforts for Next-Generation Vehicles

### [In-wheel motor drive systems]

Among electric vehicles (EV), which are next-generation vehicles, the type with the best performance is the EV with in-wheel motors that carry all of its drive parts inside its axle.

As shown in Fig. 6, in-wheel motors require coordinated control between the left and right wheels, but they also have the latent potential to create new automobile driving features because each wheel can be controlled separately. For this reason, NTN has been developing its propriety in-wheel motor drive systems that include controls using, for example, inverters.

### [One-motor-powered EV systems]

NTN is also developing one-motor-powered EV systems that can readily replace internal combustion engines because the structures of car bodies for this type of EV system are the simplest among electric vehicle forms. Fig. 7 shows an outline of this type.

This one-motor-powered EV system was developed through a combination of an automatic 2-stage reducer and constant velocity joint that fully reflects considerations related to an EV motors output characteristics. This system is capable of more common use as it can be used not only in front-wheel drive electric vehicles, but also for the rear wheels on electric four-wheel drive vehicles.

### [Low torque bearings for EV motors]

As for the bearings of next-generation vehicles using EV motors, including EVs, HEVs and FCVs, NTN has developed two types of low torque bearings.

#### <Grease-lubricated type>

Fig. 8 shows a grease-lubricated type of low-torque, sealed, deep-groove ball bearing for EV motors.

This bearing uses specially-designed cage pockets to scrape off excess grease and prevent the influx of excess grease onto the rolling contact surface, reducing stirring resistance. Furthermore, by using grease that has a base oil and thickener with low viscosity and excellent heat resistance properties, rotation torque is reduced 50% compared to previous products.

#### <Oil-lubricated type>

Fig. 9 shows NTN's oil-lubricated, high-speed low-torque deep-groove ball bearing for EV and HEV motors.

In the future, oil-cooling systems will be used to cool EV motors in order to make them more compact by enabling super-high-speed rotation.

As a result, motor shaft support bearings will be oil-lubricated, so we developed this bearing to meet this need.

Stirring resistance inside the bearing is reduced by optimizing the form of the cage and controlling the influx of oil into the bearing. Furthermore, cage deformation caused by centrifugal force during super-high-speed rotation can be inhibited by using a resin-

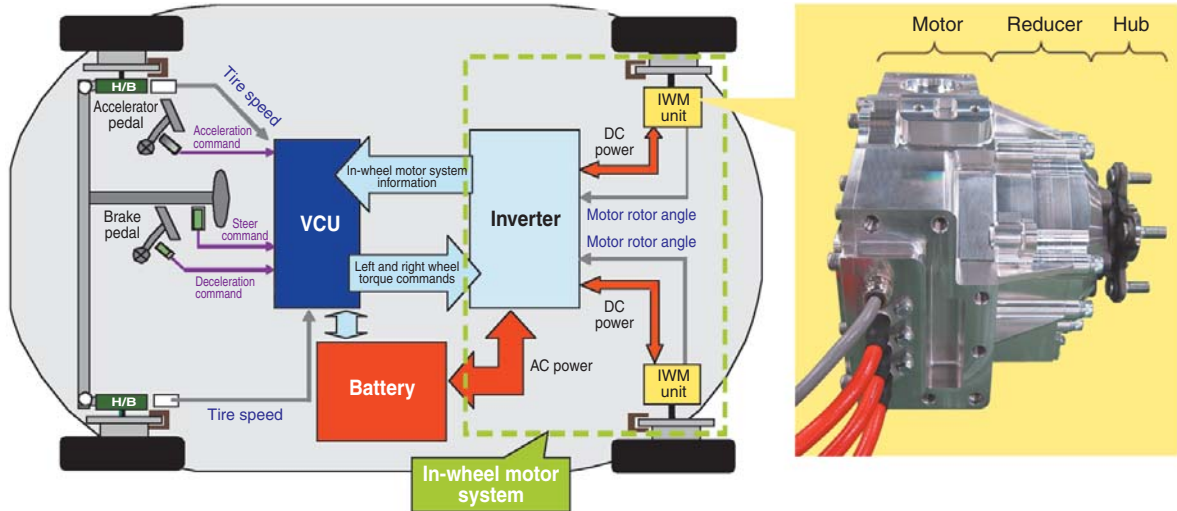


Fig. 6 In-wheel motor drive system

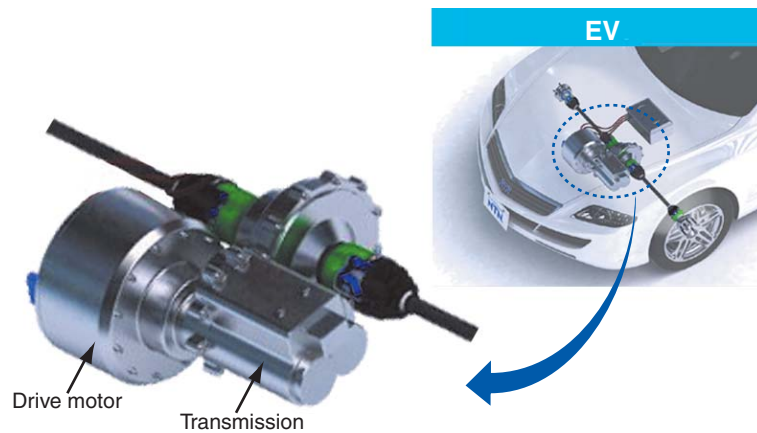


Fig. 7 One-motor-powered EV system

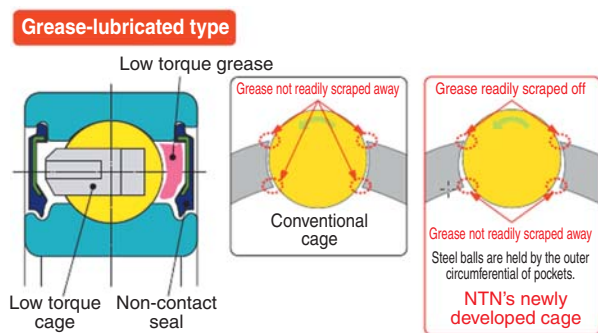


Fig. 8 Low-torque sealed deep-groove ball bearing for EV motors

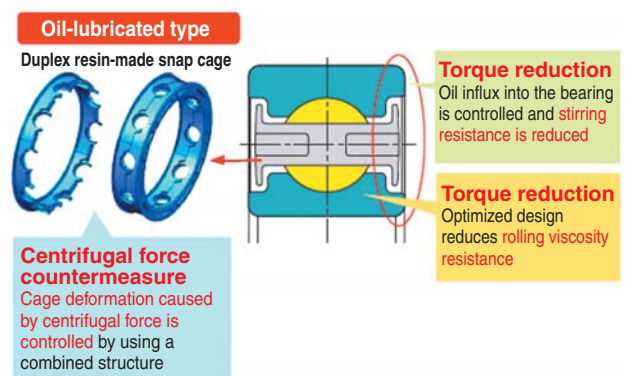


Fig. 9 High-speed low-torque deep-groove ball bearings

made duplex cage for higher bearing rigidity; thereby the bearing is capable of positively withstanding super-high-speed applications at 30,000 min<sup>-1</sup> and reduces rotary torque by more than 40% compared to conventional bearings.

## 5. NTN's Efforts for High Fuel Economy Vehicles

The main impediments to better fuel economy for vehicles, taking automatic transmission vehicles as an example, are shown in Fig. 10.

In order to increase fuel economy in hybrid vehicles and vehicles that use the fossil fuels of gasoline and diesel, NTN is developing optimized low-torque bearings for each place where they are used, as well as developing modular products for vehicle electrification.

### [Items that improve the fuel economy of fossil fuel engines]

Fig. 11 shows examples of items that NTN has developed for the purpose of improving the fuel economy of fossil fuel engines that use gasoline and diesel.

The rolling bearings introduced here are receiving

attention as items that improve fuel economy because, compared to sliding bearings, they have considerably lower torque at lower speed ranges. This reduces engine friction loss when a vehicle starts to move and when it accelerates, which are times when fuel consumption is high.

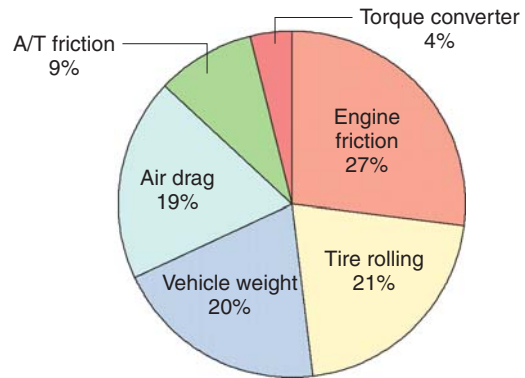


Fig. 10 Impediments to fuel efficiency (in HWY mode)<sup>5)</sup>

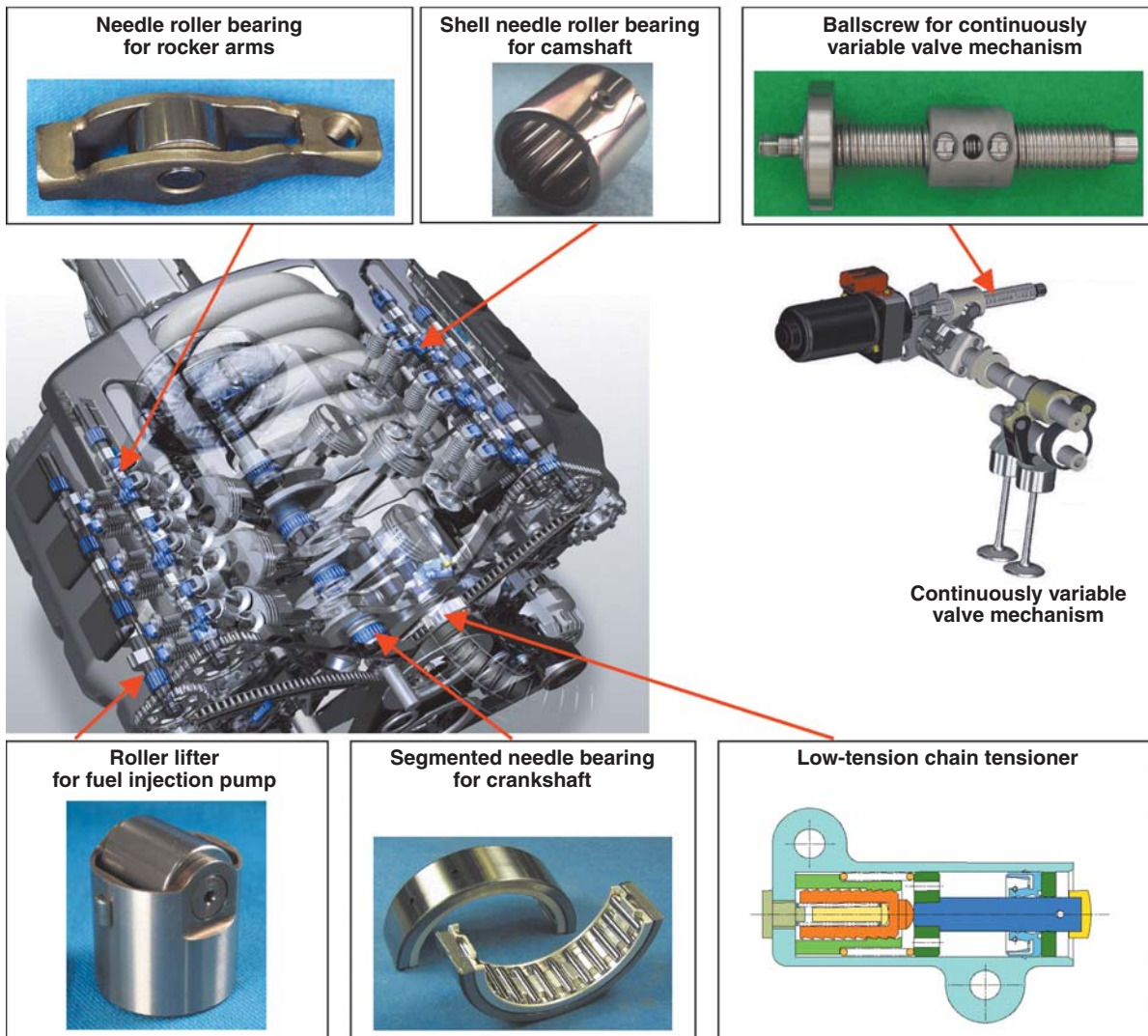


Fig. 11 NTN's products for improving the fuel economy of combustion engines<sup>6)</sup>

In addition, as a fuel economy improvement item for the engine valve system, a low-friction chain lever, as shown in Fig. 12 is adopted; where each raceway surface on the chain lever for applying tension to the timing chain as well as on the chain guide for guiding the timing guide is altered from the conventional sliding type to rolling type.

Previously, the chain lever and chain guide, which puts tensile load on the timing chain and guides it, has typically been made of cast iron. Recently, the use of lightweight alloys and polyamide resin materials has begun, but the drag torque acting on the chain is still great because the contact mode between the chain lever and chain guide with the chain is sliding contact.

NTN focused on this issue and has increased rotating contact with the chain and reduced friction torque by up to 18% at low speed ranges by placing a lot of thick-plate shell needle bearings in multiple locations on each of the chain levers and guides. As a result of this, a fuel economy improvement effect of a little less than 1% has been confirmed by measuring fuel economy in actual engines.



Fig. 12 Low-friction chain lever

[Items that improve the fuel economy of powertrains]

NTN has been at the vanguard in the development of low-torque tapered roller bearings for many years. However, even though further torque reduction had been thought to be difficult, we have beaten the competition in developing a low-torque deep-groove ball bearing as an item to reduce transmission friction loss further.

As an example of this, as shown in Fig. 13, we have developed a non-sealed low-torque deep-groove ball bearing. The insides of the cage pockets of deep-groove ball bearings are made concave, reducing the friction loss at the contact surface between the ball and the cage by 25%.

In addition to the application of this bearing in automotive transmissions, use of them in all the axial bearings for the cranks, cams and transmissions of

motorcycles, which frequently start travel and accelerate, fuel economy improvements of 1-3% have been achieved in actual motorcycles.

Moreover, the energy conservation effect of using several of these low-torque ball bearings in the EV motor and reducer on electric motor cycles has been confirmed to be a 35W electricity consumption reduction, which is equivalent to the amount used by the front light for illumination.

Furthermore, in place of the conventional tapered roller bearings for the differential side, we have a deep-groove ball bearing for high thrust loads. This is an altered form of a deep-groove ball bearing that has a thrust load capacity equivalent to that of low-gradient tapered roller bearing and reduces torque by 56% compared to tapered roller bearings, as shown in Fig. 14.

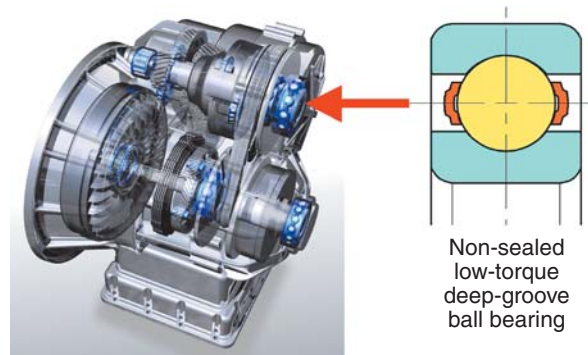


Fig. 13 NTN's bearing product for transmission for improved fuel-efficiency

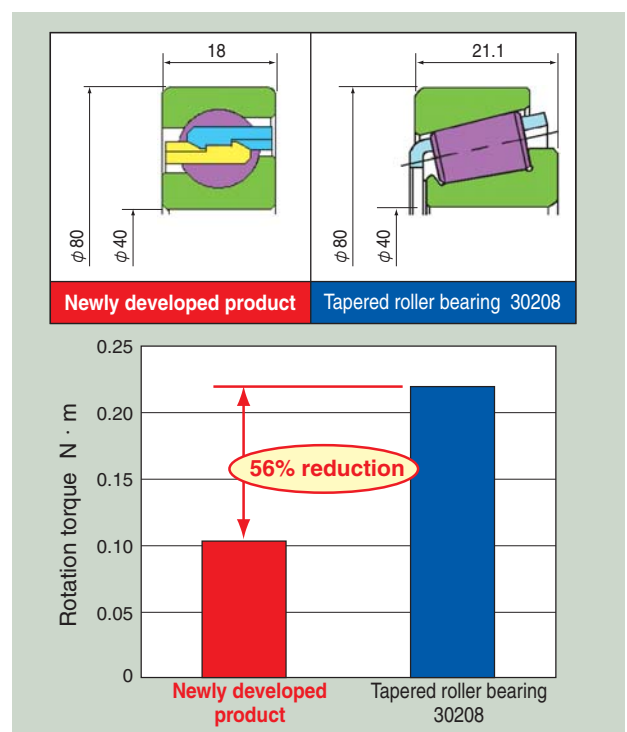


Fig. 14 NTN's deep-groove ball bearing for high thrust loads

This deep-groove ball bearing capable of high thrust loads, as a differential bearing with reduced torque, is expected to contribute to improving the fuel economy of vehicles.

**[Items that improve chassis and affect the fuel economy]**

Representative examples of items that improve the chassis for better fuel economy, which primarily reduce hub bearing friction and weight, are shown in Fig. 15.

Recently, hub bearings are beginning to be adopted even on vehicles in regions with poor driving conditions. Certain bearings that incorporate seals with a dual side lip structure have been used, to improve performance in severe mud-water conditions. By changing the seal to a rubber material and revising the form, however, not only is mud-water resistance improved, torque is also reduced, contributing to improved fuel economy for the vehicle.

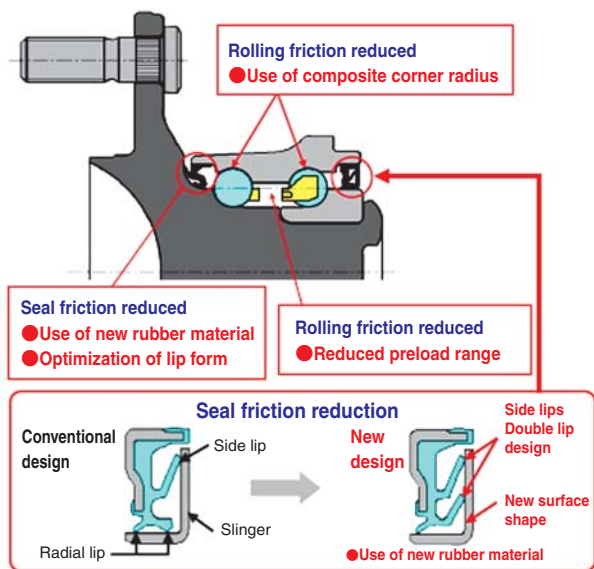


Fig. 15 NTN's low friction hub bearing

**6. Efforts in Response to Electrification**

In EVs, FCVs and other next-generation vehicles, internal combustion engines are no longer used as power sources for energizing the auxiliaries; consequently, the negative pressure from an engine when drawing in air can no longer be used.

Moreover, for engines with high fuel economy and HEVs that continue to use fossil fuels; auxiliary equipment, including hydraulically operated variable valve mechanisms and power steering, are superseded with electric mechanisms and the oil pumps that can inhibit fuel economy improvements are replaced with smaller capacity pumps whose capacity is just sufficient to lubricate the internal combustion engine.

Furthermore, hydraulic foot brakes and hand parking brakes that were boosted by engine negative pressure are also being replaced with electric mechanisms, and automatic transmissions that use electric shifting mechanisms have also been adopted by a number of vehicles.

We predict that the electrification of these types of auxiliary equipment and control systems will develop as they are and be transformed into control-by-wire equipment. Taking these conditions into account, NTN is anticipating the electrification and future control-by-wire transitions in next-generation vehicles and is developing a variety of modular products in response to electrification needs.

**7. Conclusion**

The vehicle market has overcome numerous trials in the past and will continue to grow even as the locations and forms of production change. The most important things in the automotive industry are being first to predict the latest market needs of each era and planning and developing novel new products.

Immediately, based on a new theme of improving electric economy and fuel economy, developments are advancing with efforts toward production in emerging markets and efforts toward electrification in the form of EVs and other next-generation vehicles, as well as efforts for technologies that improve the fuel economy of fossil fuel vehicles, which are the foundations for expansion of the automobile market.

After these have advanced, around the time when next-generation vehicles have become mainstream, I believe that the future development of vehicles will once again begin, focusing on their original purposes of reaching destinations quickly, safely, in comfort and at will. At NTN, we intend to continue developing new products for automobiles in the future.

## Reference

- 1) Ministry of Economy, Trade and Industry, Next Generation Auto Strategy 2010, April 12, 2010.
- 2) Sanei Shobo, Motor Fan illustrated, Vol. 21, June 15, 2008. (Data source: CSM Worldwide/Jatco CTI Symposium, June 12-14, 2007, Detroit, MI, USA.)
- 3) Kitagawa, F., The automotive industry after 2010–what we can see next, Nomura Research Institute, Ltd., Feb. 5, 2009; "Fuel economy strategies and newly developing country strategies: the Run-up to 2025" and "HIS Automotive's automobile market forecast," Automotive Technology, Nikkei Business Publications, Inc., July, 2011.
- 4) Japan Automobile Manufacturers Association, Inc., "Passenger car market trend investigation–attitudes toward cars of generations entering the car market," March 2009.
- 5) Industry and Science Systems Co., Ltd., Engine friction reduction technology text, Engine Friction Reduction Technology, Fujita, Y. (Nissan Motor Company, Powertrain Division Headquarters); Ryouno, Y., NTN Technical Review, Vol. 76, P. 80-87, 2008.

Photo of author

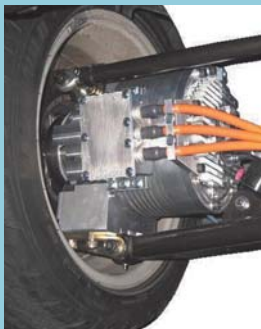
---



**Makoto OKASAKA**  
Automotive Business HQ  
Automotive Engineering Dept.

# In-Wheel Motor System

Yuichi ITOH\*  
 Kayo SAKAI\*  
 Yusuke MAKINO\*\*



With increasing global environmental concerns, much attention has been paid to electric vehicles for their high environmental performance. In-wheel motor drive systems for electric vehicles have the advantages of effectively maximizing interior space and providing vehicle driving performance due to the independent traction control ability of each wheel. NTN has developed an in-wheel motor system with a sensor-based control system for the dawning electric vehicle age. This paper describes evaluations of its decelerator and motor. In addition, it reports on results of vehicle tests with the developed system.

## 1. Introduction

Under the current circumstances in which more attention is being paid to environmental performance and problems concerning energy, the automobile industry, academic research institutes and a number of similar organizations are engaged in the technological development of electric vehicles (EV) as a next-generation automobile candidate.

Two different drive systems are available for EVs. The first is the one-motor system in which a motor is installed in the body and the power is transmitted to both the left and right wheels via a differential device and a drive shaft. The other is the in-wheel motor (IWM) system in which motors are installed in the wheels.

Since the motors and reducers are installed directly in the wheels, an IWM system does not need a differential, drive shaft or other parts<sup>1-8)</sup> when compared to a one-motor system. Free of the layout restrictions caused by these drive system components, the degree of freedom in vehicle design is increased greatly by an IWM system. In addition, with the removal of the differential and the drive shaft, energy loss is reduced and this allows for a reduction in electricity consumption required when running, thereby allowing the driving range per charge to be increased.

Furthermore, this system is capable of not only controlling the driving force of individual wheels

independently but also of directly transmitting the driving force to the tire without the intervention of a drive shaft. This makes it possible to achieve highly-responsive control of the driving force. Making the most of this drive characteristic allows the vehicle driving performance to be improved significantly.

Noting that IWM systems provide driving systems suitable for next-generation EVs in this way, we have developed the NTN-IWM System that incorporates an IWM, which is composed of a reducer and a motor, and a control system linked with sensor-based information.

This paper reports the results of evaluation tests of the IWM reducer and motor sections, and of a road evaluation test done on an IWM-equipped vehicle.

## 2. Specifications and structure of the developed product

### 2.1 Specifications

With a compact automobile with a displacement of 1500 cc in mind, we designed an IWM system assuming installation in the two rear wheels of such an automobile. We adopted a wheel size of 15 inches. The appearance and specifications of the IWM developed are shown in [Fig. 1](#) and [Table 1](#).

\*EV System Division Driveline System Engineering Dept.

\*\*EV System Division Control System Engineering Dept.



Fig. 1 Appearance of in-wheel motor

Table 1 Specifications of in-wheel motor

Maximum output	30 kW
Maximum torque	500 Nm
Maximum rotational speed	1350 min <sup>-1</sup> (equivalent to 150 km/h with a 0.6m tire diameter )
Reducer type	Cycloid reducer system
Reduction ratio	1/11
Motor type	Radial gap type permanent magnet synchronous motor
Cooling system	Air-cooled

## 2.2. Structure

Fig. 2 is a cross-section of the IWM system, which has a structure that aligns the hub, reducer section and the motor section in a series configuration. Compared with other driving systems, an IWM system equipped with the driving section in the wheels has larger unsprung mass, putting it at a disadvantage in terms of vehicle stability and riding comfort. For this reason, reduced physical size and weight is an important challenge in developing an IWM system.

In an IWM system, the motor section accounts for a significant portion of its weight, and since the physical size of the motor is usually dependent on the maximum torque it has to develop, reducing the required motor torque is effective in reducing the weight of the IWM system. During development reduction of the physical size and weight of the IWM system was achieved by adopting a reducer to reduce the torque required of the motor.

The lubrication system is based on an internal circulation scheme in which a built-in oil pump driven by the output shaft force-feeds the lubricating oil. The force-fed oil passes through an oil passage installed inside the motor housing and flows through an internal oil passage installed inside the rotor shaft and the reducer input shaft that rotates in conjunction with the rotor shaft and reaches the motor and interior of the reducer. This forced oil circulation not only lubricates the bearings and reducer but also cools the motor

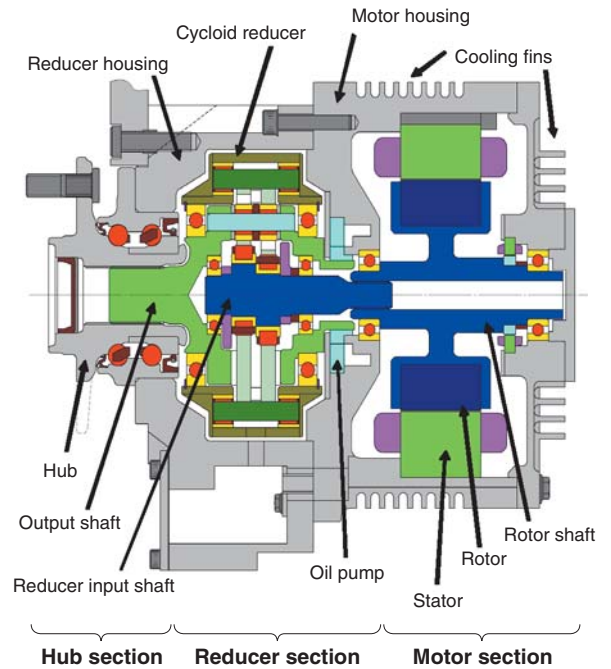


Fig. 2 Cross-section of IWM

stator (including the coil) and rotor. Furthermore, to help actively cool the stator and lubricating oil, the housing has cooling fins on its outer periphery and side faces so that the IWM is air-cooled.

Automatic transmission oil has been adopted as the lubricating oil to reduce the pipeline drag with the oil being pressure-fed by the built-in oil pump, and to reduce stirring loss due to rotating members in the rotor and reducer, as well as to ensure sufficient durability for the bearings and reducer.

In developing the IWM, we repeated a variety of durability tests such as water-submersion tests and vibration tests under severe conditions, which were identical to those under which NTN hub bearings are tested, to ensure sufficient reliability during actual running on roads.

### 2.2.1 Reducer section

A cycloid reducer equipped with a K-H-V-type planetary reducer mechanism<sup>9)</sup> has been adopted that not only requires less space but also provides a high reduction ratio. To reduce loss within the reducer, roller bearings have been adopted in the internal gear that contacts the oscillating-rotating external gear and the output shaft.<sup>7), 8)</sup>

### 2.2.2 Motor section

Table 2 shows the specifications of the motor. A concentrated winding system has been adopted to shorten the axial length. Using both magnetic field analysis and stress analysis, we derived the specifications for the shapes of the stator and rotor

cores and for the layout of permanent magnets in order to achieve a reduction in the power loss in the motor section to help realize an air cooled system as well as high speed rotary motion.

**Table 3** shows the specifications of the inverter. The inverter is provided with higher reliability through enhancements of a self-diagnostic function and circuit checking.

**Table 2** Motor specifications

Motor type	Radial gap type permanent magnet synchronous motor
Winding system	Concentrated winding
Maximum torque	45 Nm
Maximum output	30 kW
Maximum rotational speed	15,000 min <sup>-1</sup>

**Table 3** Inverter specifications

Drive power supply voltage	DC 400 V
Control power supply voltage	DC 12 V
Output	30 kW × 2
Carrier frequency	10 kW × 2
Drive system	Sinusoidal wave PWM
Cooling system	Water-cooled

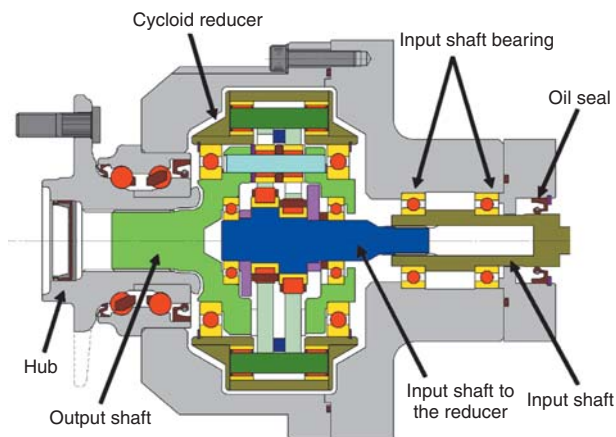


**Fig. 3** Cross-section of test reducer (including the hub)

**Table 4** Test conditions for reducer efficiency measurement

Maximum input shaft rotational speed	15,000 min <sup>-1</sup>
Maximum input shaft torque	45 Nm
Lubricant	Automatic transmission oil
Lubricant supply temperature	70 °C
Lubrication system	Forced oil supply from the outside

running of the IWM, was taken as the reverse input condition.

### 3. Bench Test (Efficiency Measurement)

#### 3.1 Reducer section

##### 3.1.1 Sample and test conditions

**Fig. 3** shows the structure of the sample used in measuring the efficiency of the reducer and **Table 4** shows the test conditions. The sample was composed of a reducer and a hub as principal components. The input shaft and the input shaft to the reducer were structured separately, with the power between them conveyed by means of a splined joint. Matching the developed IWM, the hub bearing was grease-lubricated and the reducer was oil-lubricated. The oil lubrication system in the reducer section was configured so that a lubrication unit, which was installed externally, circulated the lubricant to supply it to the different parts of the reducer. The heater installed in the circulation path kept the temperature of the oil supplied at 70 °C.

The operating condition in which power was conveyed from the input shaft of the reducer to the output shaft, which simulates the power running of the IWM, was taken as the forward input condition. In contrast to this, the operating condition in which power was conveyed from the output shaft to the input shaft of the reducer, which simulates the regenerative

#### 3.1.2 Test results

**Figs. 4** and **5** show the results of the measurement of the reducer transmission efficiency under the forward and backward input conditions. These charts show the efficiency of the reducer alone, with the power loss from the hub, the bearing of the input shaft, and oil seal in contact with the input shaft excluded. The horizontal and vertical axes denote, respectively, the rotational speed and the torque of the input shaft. The sign of the input shaft torque is positive for the forward direction input condition and negative for the reverse input condition.

The maximum efficiency was 98% under the forward input condition and 97.5% under the reverse input condition. With no noticeable difference observed in the transmission efficiency between the forward direction and the reverse direction, about the same efficiency was obtained for both power running and regenerative running.

#### 3.2 Motor section

**Table 5** shows the test conditions for measuring the motor efficiency. To match the developed IWM, the motor section was configured so that a lubrication unit, which was installed externally, circulates the lubricant to supply it to the rotor and stator of the motor.

**Fig. 6** shows the results of the measurement of

motor efficiency. The horizontal axis shows the rotational speed and the vertical axis is the motor torque. The maximum efficiency of the motor section was 94.7%.

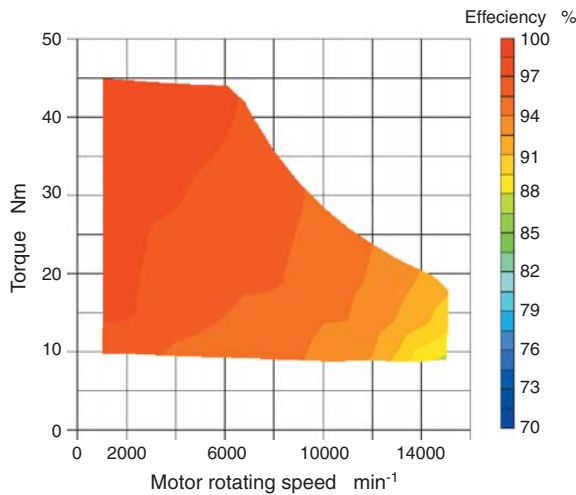


Fig. 4 Reducer transmission efficiency (for forward input)

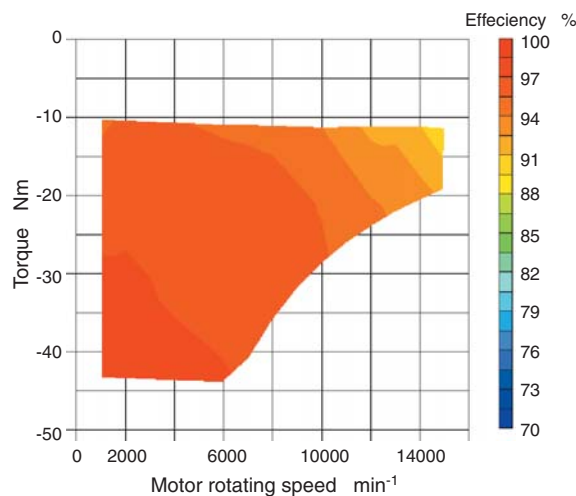


Fig. 5 Reducer transmission efficiency (for reverse input)

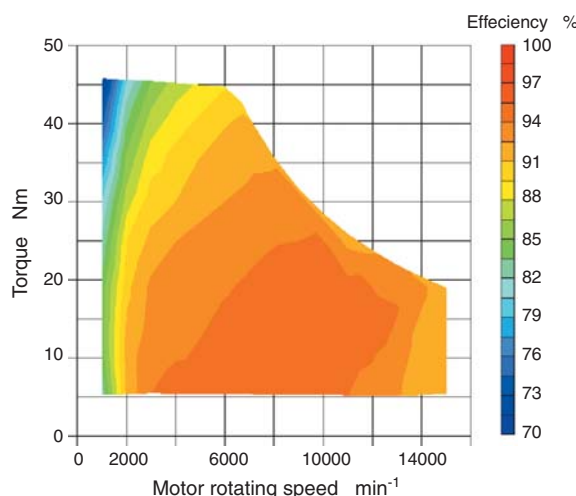


Fig. 6 Motor efficiency

Table 5 Test conditions for motor efficiency measurement

Maximum rotational speed	15,000 $\text{min}^{-1}$
Maximum torque	45 $\text{Nm}$
Lubricant	Automatic transmission oil
Lubrication system	Forced lubrication from the outside

### 3.3 IWM

#### 3.3.1 Test conditions

An efficiency measurement test was conducted in the power running mode on the IWM system shown in Fig. 2, which consists of a hub, a reducer and a motor.

In the power running mode, load was provided by making the built-in motor act as the power source and allowing an externally installed motor to absorb the power generated. To measure the output torque, a torque meter was placed between the IWM and the power-absorbing motor.

Table 6 shows the test conditions.

Table 6 Test conditions for IWM efficiency measurement

Maximum rotational speed	1365 $\text{min}^{-1}$
Maximum torque	500 $\text{Nm}$
Lubricant	Automatic transmission oil
Lubrication system	Built-in pump

#### 3.3.2 Test results

Fig. 7 shows the results of the measurement of the efficiency of the IWM under power running conditions. The horizontal axis shows the wheel rotational speed and the vertical axis shows the output torque. Table 7 shows the specifications of an EV comparable to a typical 1500cc-class compact automobile, and Fig. 8 shows the vehicle driving power calculated on the basis of these specifications.

As shown in Fig. 7, the maximum efficiency of the developed IWM was 90%, with a maximum power output of 30 kW and a maximum torque of 500  $\text{Nm}$  being achieved. In addition, a power output of 26 kW at a maximum rotational speed of 1365  $\text{min}^{-1}$ , which corresponds to a vehicle speed of 154  $\text{km/h}$ , was obtained. The results of calculations of driving power shown in Fig. 8 demonstrate that this is equivalent to the power performance necessary to achieve a running speed of 150  $\text{km/h}$  on a road with a zero-degree incline for a common 1500cc-class compact automobile propelled by two-wheel drive.

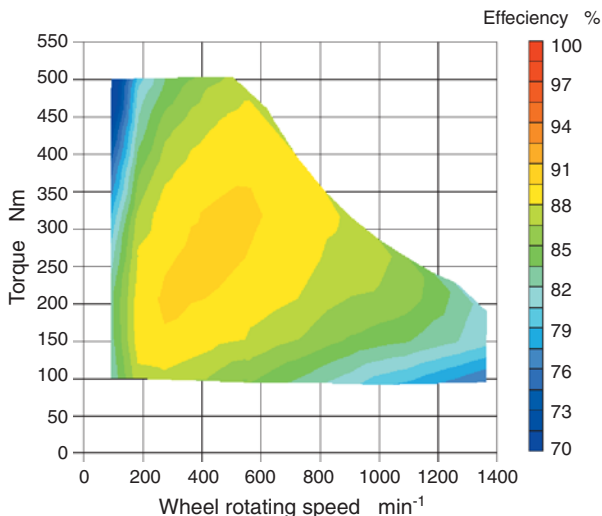


Fig. 7 IWM efficiency

Table 7 Specifications of a typical 1500cc compact vehicle class EV

Vehicle mass	1300 kg (including 110 kg for the weight of 2 passengers)
Frontal projected area	2.6m <sup>2</sup>
Coefficient of drag	0.32
Rolling resistance coefficient	0.015

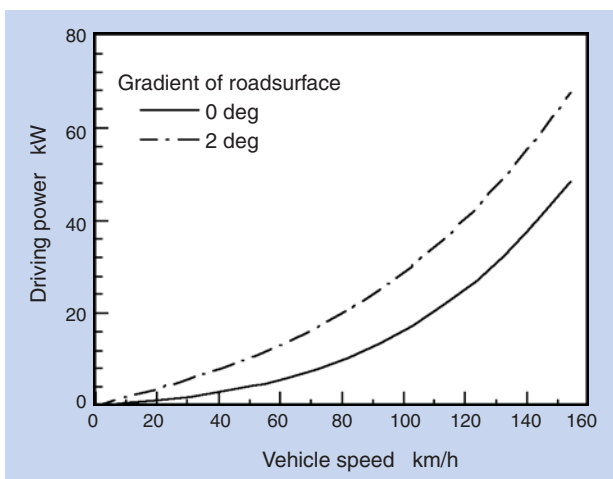


Fig. 8 Vehicle driving power of a 1500-cc compact class EV

## 4. Test in Actual Car

### 4.1 Test vehicle

Fig. 9 shows the appearance of the underbody of a vehicle equipped with the developed IWM. The vehicle is based on a commercially-available FF-vehicle, with the rear wheels equipped with the IWM. The suspension type is based on a double wishbone system, with the auxiliaries being motorized and installed in the engine compartment with a battery dedicated to powering them.

Fig. 10 shows the structure of the vehicle control system.

The main constituent elements of the test vehicle are the IWM system, a vehicle control unit (VCU) and a lithium-ion battery. The VCU gives the inverter torque commands for the motors so that suitable driving power is generated in the right and the left IWMs independently in accordance with the driving conditions on the basis of information from the driver, including acceleration, deceleration and cornering commands. Following a torque command, the inverter converts DC power from the battery into the AC power required to drive the motor installed in the IWM.



Fig. 9 IWM mounted in a vehicle (on the rear left wheel)

### 4.2 Temperature characteristics test

The temperature characteristics of an IWM while installed in a vehicle were assessed. The continuous rating characteristic, one of the important performance indexes of an IWM, is determined by the heat balance between the heating of the IWM itself and the external cooling action. In the assessment of the temperature characteristics of this IWM that is air-cooled, testing in an actual car is effective for reproducing the running wind. However, such a test poses difficulty in the securing of the battery capacity necessary for continuous running and stabilizing the running load. To solve this problem, we conducted tests using a chassis dynamometer on which a blast duct was installed as shown in Fig. 11. In accordance with the

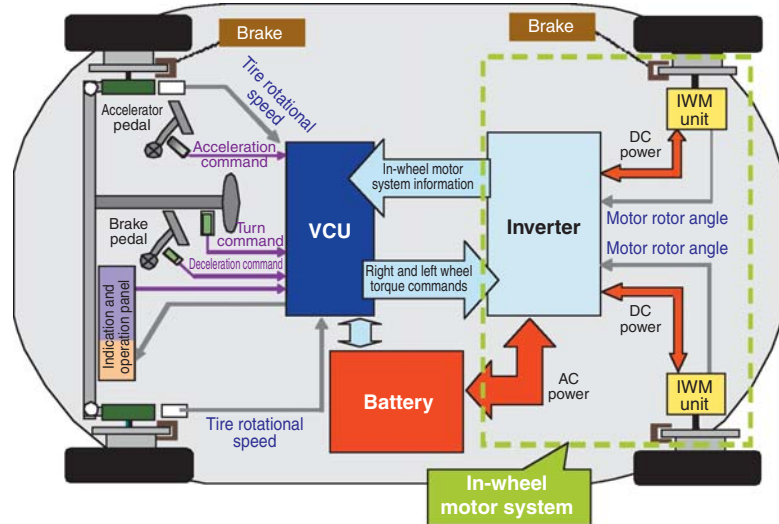


Fig. 10 Composition of vehicle control system

speed of the rotation of the drum of the dynamometer, which corresponds to the vehicle speed, air simulating running wind was blown from the blast duct around the IWM.

With the aim of supplying electricity in a stable manner, an external power supply was used as the drive power supply for the IWM instead of the onboard battery.

In the test, the temperature of the motor coil section and that of the internal lubricant were measured under running conditions, with the vehicle speed and hill-climbing conditions used as parameters.

In this test, the allowable upper limit of the coil temperature was set at 180°C from the viewpoint of the heat resistance of the coil insulation film. In addition, with the aim of preventing a reduction in the durability of the bearings and reducer parts used in the IWM, the allowable upper limit of the lubricant temperature was set at 120°C.

As shown in Table 8, the test was conducted under the conditions of running resistance and a running

wind speed that correspond to a case where the vehicle is running at a speed of 70 km/h on a slope with a gradient of 2 degrees. Fig. 12 shows the test results. Both the coil and the lubricant reached saturation temperatures that were below their allowable upper temperatures. The lubricant exhibited a smaller difference between the allowable upper limit temperature and the saturation temperature reached. Considering that this temperature difference is about 10°C, the assessment shows the possibility of continuous running under the load conditions shown in Table 8 if the outside air temperature is below 35°C or so.

Table 8 Conditions for the temperature characteristics test

Vehicle speed (Wheel rotational speed)	Equivalent to 70 km/h (655 min <sup>-1</sup> )
Wind speed	Equivalent to 70 km/h
Hill climbing resistance	Equivalent to an incline of 2 degrees
Running air temperature	25°C

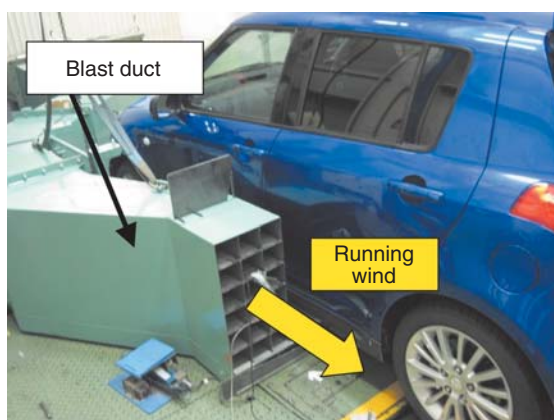


Fig. 11 Vehicle test with chassis dynamometer

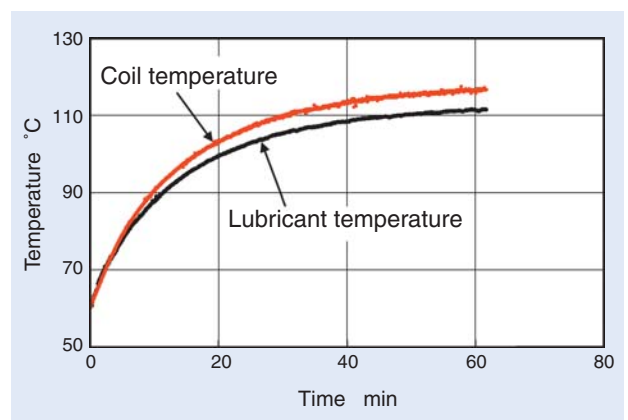


Fig. 12 Results of temperature characteristics test

As shown in Fig. 8, the drive power for a car running at a speed of 70 km/h on a slope with a 2-degree gradient is nearly equal to the driving power for a car running at a speed of 100 km/h on a level road surface. If, for simplification of assessment, variation in the efficiency of the IWM due to variation in operating conditions is ignored, we may conclude that NTN's newly-developed IWM system is capable of cruising at 100 km/h on a level road surface (zero degrees gradient) because increased car velocity results in a greater forced convection cooling effect.

## 5. Conclusion

Assuming installation in the two rear wheels of a 1500cc-displacement compact automobile, we developed the NTN-IWM System in which a control system driven by sensor-generated information is incorporated into each IWM, which consists of a cycloid reducer and a motor.

The efficiency of each element of the IWM system was assessed. The highest efficiencies achieved were 98% in the forward direction and 97.5% in the reverse direction for the reducer section, 94.7% for the motor section, and 90% for the IWM. In addition, we obtained power equivalent to that which allows a common 1500cc-class compact automobile with two-wheel drive to run at a speed of 150 km/h on a road with no incline.

Furthermore, we conducted a temperature characteristic test using a chassis dynamometer with the newly-developed IWM system onboard a vehicle, confirming that it is possible for the vehicle to run continuously at a speed of 100 km/h on a road with zero-degree incline in ambient air temperatures below 35°C.

We are continuing road tests using a test vehicle with the objective of further improving reliability and commercializing our IWM system as early as possible.

## Reference

- 1) Imayanagita, A. et al., "Development of In-wheel Motor System for Large-size Bus using 22.5-inch Wheel Mounted Motor," Toyo Denki Review, No. 113, pp. 9-14, 2006.
- 2) Tahara, Y. et al., Development of the In-Wheel Motor System, Transactions of the Society of Automotive Engineers of Japan, No. 131-06, 2006.
- 3) Okamoto, Y. et al., Development of High Efficiency In-wheel Motor System for using 20-inch Wheel Mounted Motor, Toyo Denki Review, No. 117, pp. 12-17, 2008.
- 4) Kaneko, Y. et al., Development of Compact and High Power In-Wheel-Motor unit, Transactions of the Society of Automotive Engineers of Japan, No. 7-09, 2009.
- 5) Murata, S., Development of In-Wheel Motor Drive Unit, Transactions of the Society of Automotive Engineers of Japan, No. 28-10, 2010.
- 6) Akaho, D., Development of Vehicle Dynamics Control System for In-Wheel-Motor Vehicle, Transactions of the Society of Automotive Engineers of Japan, No. 120-10, 2010.
- 7) Suzuki, M. et al., NTN Technical Review, No. 73, pp. 56-59, 2005.
- 8) Suzuki, M. et al., NTN Technical Review, No. 75, pp. 46-52, 2007.
- 9) Morozumi, M., Theory and Design Calculation Method of Planetary Gears and Differential Gears, Nikkan Kogyo Shimbun Ltd., pp. 1-6, 1989.

## Photo of authors



Yuich ITOH

EV System Division  
Driveline System  
Engineering Dept.



Kayo SAKAI

EV System Division  
Driveline System  
Engineering Dept.



Yusuke MAKINO

EV System Division  
Control System  
Engineering Dept.

## Development of In-Wheel Motor System for Electric Commuters

Tetsuya YAMAMOTO\*  
Aiko ISHIKAWA\*  
Wataru YAMADA\*\*



NTN has developed an In-wheel Motor System for commuter vehicles that could become a stepping stone that promotes the spread of electric vehicles (EV). The in-wheel motor unit that was developed can be installed in 14-inch wheels. In the test EV, it was shown that space in the car was able to be utilized effectively. This paper introduces the In-wheel Motor system that was developed and the test EV.

### 1. Introduction

In general, two problems exist in promoting the widespread use of electric vehicles (EVs). One is the reduced cruising range when compared to that of ordinary automobiles with internal combustion engines and the other is the higher initial costs of batteries. These two problems are expected to be solved in the future as technologies advance. For example, to solve the first problem of a reduced cruising range, what is important is not only technological progress for improved battery performance but also ubiquitous availability of battery-recharging infrastructure. For these problems, it is hoped that efforts are made by both the government and the private sector in order to realize the widespread use of EVs<sup>1)</sup>.

Against this backdrop, the Ministry of Economy, Trade and Industry planned the Next-Generation Vehicle Strategy 2010<sup>2)</sup> with the aim of spreading the use of next-generation vehicles. On the basis of the roadmap shown in the METI strategy, focused support for the development of infrastructure, such as the creation of "electric vehicle/plug-in hybrid vehicle (EV/PHV) towns," will be undertaken.

Vehicles that will be desired in such EV/PHV towns in the future are thought to be of the following types.

- 1) Fixed route buses that can be operated and recharged on schedules
- 2) Delivery vehicles that are used in limited areas and

- 3) Commuters intended for use in short-to-medium range distances from residences (daily travel of less than 40 km)

The services required of the commuter vehicle type in item 3 could be met to a certain extent by small-sized one-person commercial delivery vehicles if equipped with a large cargo compartment. To achieve the widespread use of EVs, however, creating a market intended for general users, not just commercial users, is essential. A fiscal 2009 survey, focusing on the uses of vehicles with small displacement engine, showed that about half of the users mainly used their vehicles for shopping and picking up family members. Needs for electric commuters are expected to be high in similar applications, as well.

Taking this into consideration, the electric commuter could be a vehicle that meets a wide variety of needs and fulfills the promise of extensive popularization if measures are taken to seat two or more passengers while maintaining the compact size of this type of vehicle.

Furthermore, designing a vehicle for use over short to medium distances makes it possible to reduce the weight load of the battery and thus the cost. A case of development of EVs for which costs were reduced from this point of view has been reported.<sup>4)</sup>

Securing space to accommodate luggage and similar cargo is also important for commuter vehicles.

\*EV System Division Driveline System Engineering Dept.

\*\*EV System Division Control System Engineering Dept.

To power EVs, motors replace the internal combustion engines of conventional automobiles. Compared to ordinary EVs, in which power is conveyed to the wheels via the drive train, in-wheel EVs with motors installed in their wheels will allow for increases in passenger and luggage space without enlarging the vehicle size.

For this reason, taking note of two-seater commuters for short-to-medium distance travel, NTN developed an in-wheel motor system for use in electric commuters. This system is composed of in-wheel motors that can be mounted in the wheels and an inverter for motor control, and was designed with the aim of increasing freedom in vehicle body design and usable cabin space. This paper reports on the concept behind this newly developed product, its characteristics, and a vehicle equipped with this system.

## 2. Specifications of this in-Wheel Motor System

Under current legal restrictions in Japan, the two-seater four-wheeled vehicle covered by this paper falls under the category of a small-displacement engine vehicle, assuming that the restrictions on its vehicle size and prime mover output are met. In Europe, a special standard applied to the two-seater commuter is already in effect.

Taking the current situation and trends of legal restrictions into account, the specifications for an in-wheel motor system were defined as shown in **Table 1**.

This in-wheel motor was designed so that it could be placed inside a 14-inch wheel. **Fig. 1** shows the appearance of the in-wheel motor that was developed. This in-wheel motor is composed of a motor section, a reducer section and a hub section. To reduce the size of the entire assembly, the mounting part to the suspension was incorporated into the housing.

Assuming that the commuter does not run on expressways but rather on urban streets in most cases, its highest speed was set at 60 km/h, the legal upper limit on ordinary roads. **Fig. 2** shows the results of measurement of the efficiency of the developed in-wheel motor. Based on the upper limit of 60 km/h for urban the target was to have the highest efficiency at the frequently used low-to-medium speed range (20-40km/h) and this was achieved per **Fig. 2**.

**Table 1** Target specifications of the in-wheel motor system

In-wheel motors	Maximum output	2kW
	Maximum torque	132Nm
	Suitable wheel size	14 inch
Cooling system	In-wheel motor	Air-cooled
	Inverter	Water-cooled
Battery voltage		96V
Maximum vehicle speed		60km/h

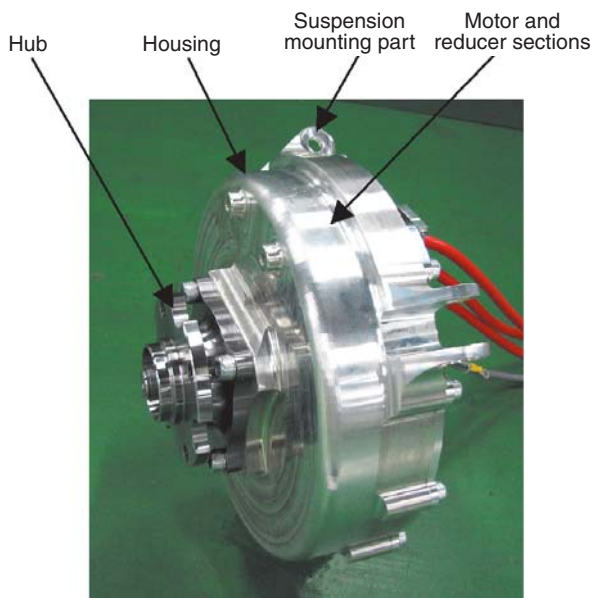


**Fig. 1** Exterior view of the in-wheel motor

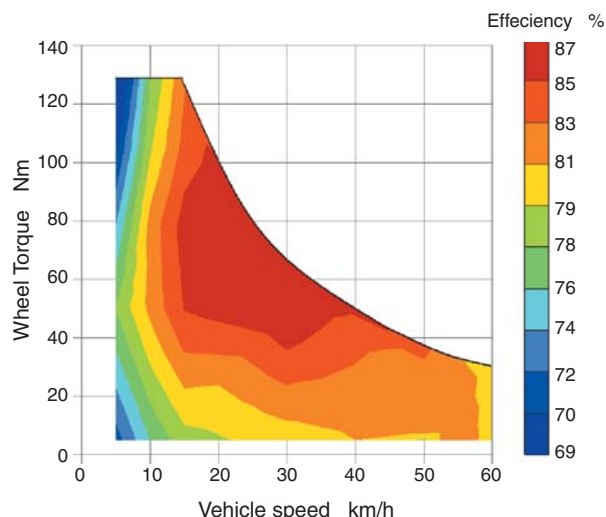


**Fig. 2** In-wheel motor efficiency

### 3. Test Vehicle

A test vehicle equipped with this in-wheel motor system was prototyped. **Table 2** shows the vehicle specifications.

**Fig. 3** shows a diagram of the configuration of the test vehicle and **Fig. 4** shows the appearance of the unit when installed on the vehicle.

The vehicle control unit (VCU) determines the torque required for the motor on the basis of stroke information from the accelerator operated by the driver and sends torque commands to the inverter. In turn, the inverter converts the DC power from the battery into the AC power necessary to drive the right and left motors, enabling them to generate suitable driving power according to the driving conditions.

A running test was conducted on this test vehicle in straight-ahead driving, cornering, and slalom conditions, and the achievement of smooth and powerful acceleration, which is characteristic of EVs, and of satisfactory stability drive control were confirmed.

**Fig. 5** shows a photograph of the space behind the seats of the test vehicle. A usable space with a volume of about 40 L was created between the right-hand and left-hand suspensions each supporting the

in-wheel motor. This space can be used as a luggage compartment when luggage-carrying capacity is considered important. In this vehicle, a Li-ion battery is installed below the seats in the center of the body. When emphasis is placed on the cruising range, the usable space described above can be used to carry additional batteries. Optimized vehicle frame and suspension system will help realize more efficient utilization of the space within the vehicle.



**Fig. 4** Test EV (above) and mounted in-wheel motor (below)

**Table 2** Specifications of the test EV

Vehicle weight	315 kg (not including the body cowl)	
Vehicle size (L×W×H)	2580mm×1390mm×1350mm	
Tire size	155/55R14	
Drive wheels	Two rear wheels	
Maximum output	2kW×2	
Maximum output torque	132Nm×2	
Battery	Type	Li-ion
	Capacity	3.1kWh

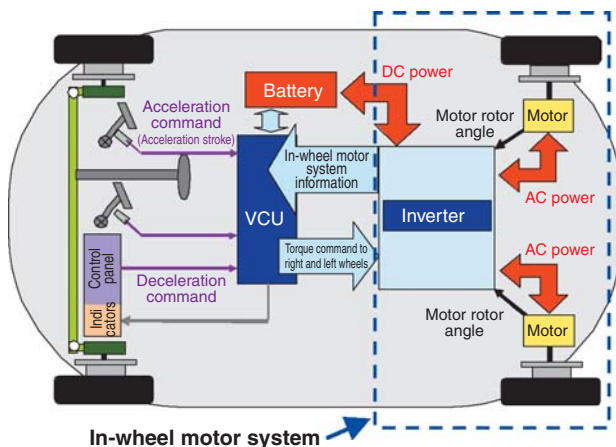


**Fig. 3** Schematic of EV with in-wheel motor system



**Fig. 5** Luggage space behind seats

## 4. Conclusion

Taking note of two-seater commuters that will provide a springboard for the popularization of EVs, NTN has developed an in-wheel motor system that has an advantage in creating cabin space. The running test on the test vehicle equipped with the NTN's newly developed in-wheel motor system has confirmed the smooth and powerful acceleration performance associated with EVs as well as satisfactory stability in drive control.

We will continue our development efforts toward the improvement of performance and reliability with the goal of contributing to the popularization of two-seater EV commuters.

## Reference

- 1) Ministry of Economy, Trade and Industry, Guidebook for Installing Charging Facilities for Electric Vehicles and Plug-In Hybrids, 2010.
- 2) Ministry of Economy, Trade and Industry, Next-Generation Vehicle Strategy 2010, 2010.
- 3) Japan Automobile Manufacturers Association, Report on Investigation of the State of Light Car Utilization, 2010.
- 4) Shimamura, K., Hirose, H., Development of Next Generation EV Concept "C•ta" (third report), Transactions of the Society of Automotive Engineers of Japan, No. 51-1020105142, 2010.
- 5) European Commission, 558340 DT Two- or Three-wheel vehicles and Quadricycles Impact Assessment, SEC (2010) 1152, 2010.

## Photo of authors

---



Tetsuya YAMAMOTO

EV System Division  
Driveline System  
Engineering Dept.



Aiko ISHIKAWA

EV System Division  
Driveline System  
Engineering Dept.



Wataru YAMADA

EV System Division  
Control System  
Engineering Dept.

# One Motor Type Electric Vehicle Drive System

Fumihiko ISOBE\*  
Yoshinori ITAKURA\*  
Yusuke OSUMI\*  
Guodong LI\*\*



In order to increase the cruising range per charge of one-motor type electric vehicles by improving power train efficiency, a one-motor type electric vehicle drive system that utilizes a 2-speed transmission has been successfully developed. To reduce the size and weight of the transmission while keeping high torque capability, a two-way roller clutch has been adopted as the shifting mechanism. This paper describes the composition of the developed system, the structure of the transmission, the principle of the gearshift, and the results of gearshift tests on a test bench and a test vehicle.

## 1. Introduction

In response to global warming and problems associated with energy, the development of hybrid and electric vehicles has been accelerating. In these circumstances, mass production of electric vehicles of the one-motor type, which are driven by power conveyed from a single onboard electric motor to the right and left wheels via a differential and a driveshaft, has already begun.

Many of the commercialized one-motor-type electric vehicles are equipped with reducers that lack speed-shifting functionality, and their maximum torque and maximum rotational speed are determined by a tradeoff between the acceleration performance and the maximum speed required with the reduction ratio of the reducer. Setting the reduction ratio to a lower value while increasing the maximum motor torque results in the size of the motor itself becoming larger. In contrast, setting the reduction ratio at a higher value while increasing the maximum rotational speed of the drive motor results in an increase in the power loss of the reducer, and hence in a reduction in efficiency.

In response to these problems, with the aim of improving the electricity consumption ratio of one-motor-type electric vehicles, for EV-use, NTN has developed a two-speed transmission and a drive module composed of a smaller, lighter drive motor and a differential, along with an NTN one-motor-EV drive system integrating a drive-motor inverter and a shift

controller for controlling the shifting action. This paper reports on the structure of the transmission, the principle of gear shifting, the results of shifting tests on a test bench and the results of shifting tests on an experimental vehicle.

## 2. Development Concept

### 2.1 Effectiveness of two-speed transmissions

As mentioned above, the performance required of a drive motor with a fixed reduction ratio is determined specifically by the reduction ratio, the output torque the vehicle requires and the vehicle speed. When a drive motor with a larger maximum torque is used with the reduction ratio set to a lower value this leads to an increase in the size and mass of the motor. For this reason, setting the reduction ratio at a higher value is effective for reducing motor weight.<sup>1)</sup> In this case, however, it is necessary to increase the maximum rotational speed of the drive motor. This results in greater power loss in the reducer, leading to decreased transmission efficiency.

Fig. 1 shows the concept behind the advantage of introducing a two-speed transmission system. Switching appropriately between the high reduction ratio gear and the low reduction ratio gear, for either low or high speeds respectively, allows the maximum torque of the drive motor to be set at a lower value than that of a fixed-reduction-ratio motor without increasing the maximum motor rotational speed. This

\*EV System Division Driveline System Engineering Dept.

\*\*EV System Division Control System Engineering Dept.

makes it possible to reduce the motor weight and increase the transmission efficiency at the same time.

The efficiency of the drive motor and that of the inverter vary depending on the rotational speed and torque, and the ranges of rotational speed and torque in which operation at higher efficiencies is allowed are limited. As shown in Fig. 1, adopting a two-speed transmission system enables the range in which operation at higher efficiencies is possible to be extended. It is possible, from this viewpoint also, to increase the system efficiency further and to reduce the electricity consumption necessary to drive a vehicle.

In the past, the effectiveness of the two-speed transmission scheme has been verified several times by means of simulation and other methods, and it has been reported that this scheme is capable of reducing the rate of electric power consumption by over 10% compared with a fixed reduction ratio scheme.<sup>1)-3)</sup>

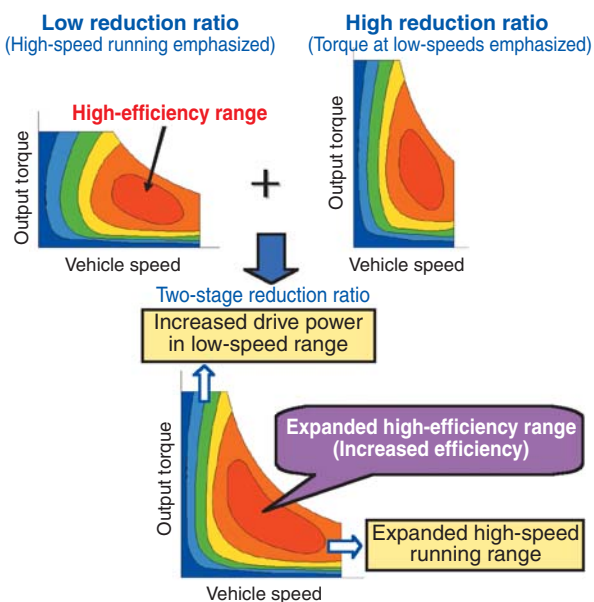


Fig. 1 Expansion of the high-efficiency range by employing a two-speed transmission scheme

## 2.2 Development specifications

A small-sized automobile with a 1000cc-class displacement was set as the target of development, and the specifications of the vehicle to be developed were defined as shown in Table 1.

The reduction ratios were defined using the following process. In the present development work, the major purpose was to reduce the power loss in the transmission associated with an increase in the rotational speed. For this reason, the second speed stage is selected when running at relatively low speed and load or running at high speed, while the first

speed stage is selected in the low-to-medium speed range when great driving power is needed. First, the reduction ratio of the second speed stage is selected temporarily, depending on the allowable maximum rotational speed of the motor selected and the planned maximum vehicle speed. On the basis of this temporarily-selected second speed stage reduction ratio, the first speed stage is selected temporarily so that adequate drive power in the low-to-medium speed range can be achieved while reducing the size of the drive motor and that smooth shifting between the first and the second speed stages is achieved.

Adjustments of the reduction ratios, temporarily selected as described above, were made to increase system efficiency on the basis of the efficiency characteristics of the inverter and the transmission section, with the reduction ratios being set as shown in Table 1.

Table 1 Development specifications

System		Maximum output		60 kW
		Maximum output torque		1000 Nm
		Maximum applicable vehicle speed		150km/h
Drive module	Motor	Type		IPM
	Transmission	Reduction ratio (including the final reduction ratio)	First speed	1/9.9
	Second speed		1/5.6	

## 3. Structure and Operating Principle of Transmission

### 3.1 Features of typical transmission mechanisms

Since the change from a fixed reduction ratio scheme to a two-speed shifting scheme leads to an increase in the transmission mass, it is important for the gear change mechanism to be lightweight and compact. This is to ensure that its weight does not offset the decrease in weight achieved by reducing the drive motor weight. In addition, it is also important for such a shifting mechanism to be a highly efficient transmission from the viewpoint of improving the rate of electricity consumption.

Typical automotive automatic transmissions include automatic transmissions (AT), continuously variable transmissions (CVT), dual clutch transmissions (DCT) and automated manual transmissions (AMT). The features of each of these transmissions are described below.

#### (1) AT

Recent progress in electronic hydraulic control has made it possible to change gears with little shock. However, the necessity of placing a torque converter

between the prime mover and the transmission is a disadvantage in terms of size and efficiency. The hydraulic pump and hydraulic circuit necessary to control the oil pressure are also factors that increase the size and cost.

**(2) CVT**

The most common type of automotive CVT is the metal-belt type. This CVT achieves smooth shifting without shock. However, the necessity for two pulleys, one each on the primary and the secondary sides, and the mainstay structure consisting of a torque converter as in an AT generally tend to make CVTs larger in size and mass and more expensive than other transmissions. In addition, the transmission of power by means of friction between the pulley and the metal belt requires large belt clamping force, and the generation of high oil pressure for this purpose increases power loss, which in turn lowers the transmission efficiency. An effective use of a CVT is to use it in combination with a prime mover that can operate in a wide range of gear change ratios, which is a notable CVT feature.

**(3) DCT**

Recently, DCTs have been adopted for use in internal combustion engine vehicles in an increasing number of cases. Although a DCT allows quick gear changes, it needs a dual clutch unit consisting of two wet multi-plate disk clutches or dry single-plate disk clutches and a clutch changeover actuator between the prime mover and the transmission. Moreover, the main body of the transmission requires two or more input shafts, which increases the part count.

**(4) AMT**

Based on a manual transmission (MT), an AMT has a basic structure consisting of a main clutch (usually a dry single-disk clutch) between the prime mover and the transmission and two or more actuators with which to perform shifting operations. An AMT allows an automatic transmission to be formed with a relatively simple structure, and it excels in terms of efficiency since it is based on an MT. However, the installation of a main clutch results in larger transmission dimensions, and the need to cut off power by means of the main clutch in order to change gears can result in a longer shift time when compared to other transmissions.

**3.2 Structure of the transmission to be developed**

In the present development work, the characteristics required of a two-speed transmission were set as follows.

- (1) Lightweight and compact
- (2) High transmission efficiency
- (3) Quick shifting
- (4) Non-use of oil pressure in shifting control

The conventional shifting mechanisms described in Section 3.1 were judged to not be capable of meeting all these requirements, so a scheme using a roller clutch in the shifting mechanism was devised.

Fig. 2 shows the structure of the newly developed drive module. The transmission consists of three shafts, namely, an input shaft that conveys power from the motor, a differential connected to the output shaft of the reducer (a constant velocity joint), and a countershaft that connects the input shaft and the differential. The first-speed and the second-speed gear trains are of the constant mesh type, and the torque output from the drive motor is transmitted to the countershaft via one of the two gear trains and from there to the differential and the constant velocity joint.

The countershaft is equipped with the first-speed and second-speed gears, each of which incorporates a roller clutch, and the roller clutch on/off control mechanism is placed between them. In this transmission, a separately-installed motorized speed-change actuator operates the roller clutch on/off control mechanism, thereby engaging and disengaging the two roller clutches to switch between the first and second speeds.

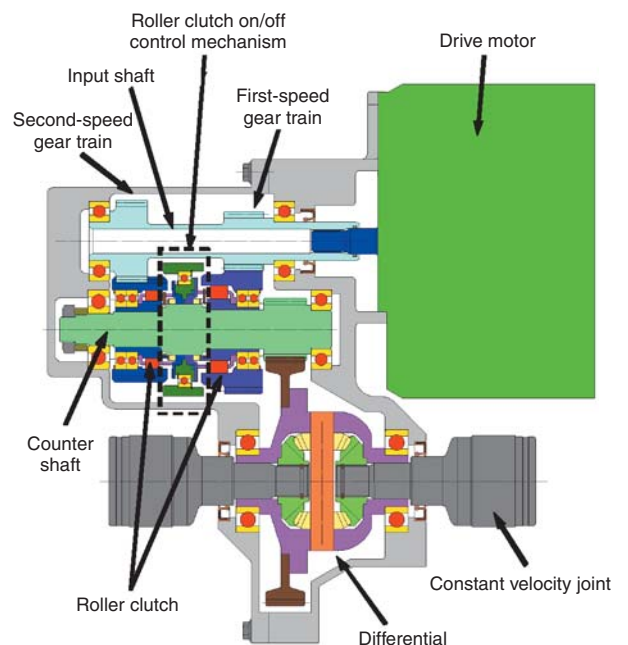


**Fig. 2** Basic structure of newly developed motor module

Some advantages of the roller clutch over other clutch mechanisms, such as wet multi-plate disk clutches, are: (1) the large torque transmission capacity allows for the size (outside diameter) to be reduced; (2) the structure is simple; and (3) the drag torque in the disengaged condition is small. The first and second advantages make it possible to place a clutch section that has sufficient load capacity within the bore of the gear to form a small, lightweight transmission. Since it is based on a parallel biaxial gear reduction scheme like that of an MT, this transmission has higher efficiency over a wide range of operating conditions. The third advantage described above allows for high efficiency to be achieved if it is used in a two-speed transmission.

The roller clutch can be engaged even if the outer ring and the inner ring of the clutch to be engaged are not perfectly synchronized with each other in terms of their respective rotational speeds. For this reason, the synchronous action of the drive motor alone can change speeds quickly and with less shock compared to the friction-based synchronizers used in DCTs and AMTs. Furthermore, the elimination of a synchronizer also eliminates the necessity of installing a main clutch to cut off power between the motor and the transmission, contributing to a reduction in the size and weight of the transmission.

Using a roller clutch in the shifting mechanism makes it possible to achieve all four of the necessary functions described above and realize a two-speed transmission suitable for electric vehicles.

A trial calculation carried out with the conditions that the maximum output, maximum output torque, maximum vehicle speed, and maximum motor rotational speed were equivalent shows that the mass of NTN's newly developed drive module combining the transmission drive motor is smaller by about 20% than

that of a drive module with a fixed reduction ratio.

### 3.3 Gear shifting principle

Fig. 3 shows the operating principle of the roller clutch. The torque transmitting section of a roller clutch consists of an inner ring with two or more cam faces on the outer circumference, an outer ring with a circular rolling face on the inner circumference, rollers installed between the inner ring cam face and the inner circumferential face of the outer ring, and the cage that holds the rollers at the same intervals in the circumferential direction. This design forms a wedge-shaped space between the inner ring cam face and the inner circumferential face of the outer ring. A return spring that is installed between the inner ring and the holder allows the energizing force, acting in the direction that negates the gripping of the roller in the wedge-shaped space, to act on the cage.

Fig. 4 shows in detail the structure around the countershaft. The roller clutch on/off control mechanism consists of two friction disks, one each for the first and second speeds, and a friction disk retainer. Each friction disk is fitted into the counterpart cage in such a manner so as not to allow relative rotation but to allow axial movement. The operation of the transmission actuator causes the shift fork to be driven axially, and the shift fork in turn causes the friction disk retainer and the friction disk to move axially. By moving the friction disk toward the roller clutch with which the friction disk is to be engaged and allowing the friction disk to come in contact with the outer ring, a frictional force that transmits the rotation of the outer ring to the friction disk is generated, and the rotation of the outer ring is transmitted to the cage via the friction disk. The transmission actuator is controlled so that frictional force sufficient to allow the outer ring to rotate together with the cage is produced.

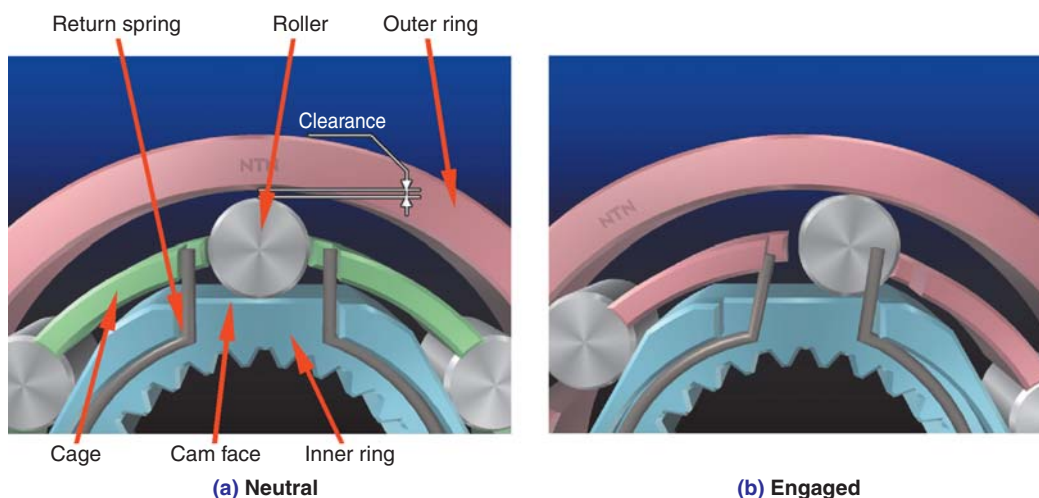


Fig. 3 Roller clutch operating principle

When frictional force does not act between the outer ring and the friction disk, the cage and the roller are held at the central position (the neutral position) of the cam face by the force of the return spring. In this condition, clearance occurs between the roller and the outer ring or inner ring, and the inner and the outer ring are put into a neutral state allowing relative rotation. On the other hand, when a frictional force larger than the force of the return spring acts on the outer ring and the friction disk, the relative rotation of the inner and the outer ring causes the cage, rotating together with the outer ring, to move the roller into the wedge-shaped space (the position of engagement) as shown in Fig. 3 (b), with the inner and the outer ring engaged with each other via the roller.

This roller clutch is a so-called two-way clutch that can transmit torque both clockwise and counterclockwise, so it is capable of transmitting torque not only in the power running mode but also in the regenerative mode.

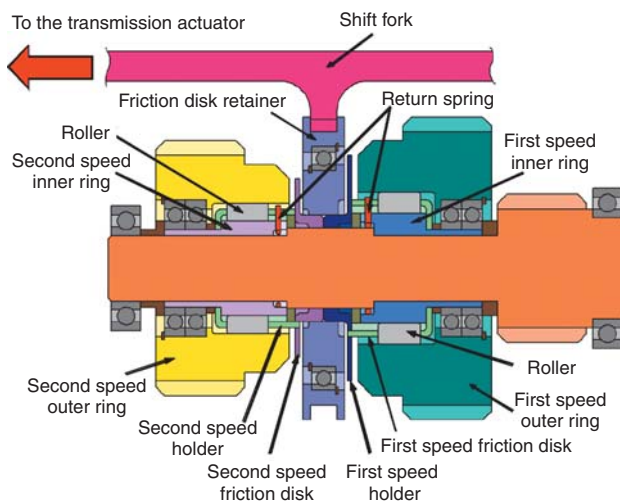


Fig. 4 Detail of countershaft section

## 4. Shifting Performance

### 4.1 Shifting control

In a roller clutch, the engagement of the roller is maintained as long as the transmission torque is above zero even if the holder does not push the roller into the wedge-shaped space. For this reason, the engagement of the roller clutch is maintained as long as torque transmission is continued, even after the contact of the outer ring with the friction disk by means of the action of the roller clutch on/off control mechanism is released. For this reason, shifting operations are performed in the following order:

- (1) First, the shift fork is moved from the current speed stage position to neutral to stop contact between the outer ring and the friction disk.
- (2) The motor torque is lowered to nearly zero to stop the engagement of the roller clutch.
- (3) The drive motor is accelerated or decelerated until the rotational speeds of the inner ring and the outer ring of the roller clutch of the next shifting stage match (synchronization).
- (4) Concurrently with the start of synchronization, the shift fork is made to start moving toward the next shifting stage. In this step, the speed of the synchronization is adjusted, so that the completion of the synchronization does not lag behind the completion of the movement of the shift fork, that is, the time of generation of the frictional force between the outer ring of the roller clutch of the next shifting stage and the frictional disk.
- (5) After completing synchronization, the movement of the shift fork to the next shifting stage is completed, with the outer ring of the roller clutch of the next stage allowed to come in contact with the friction disk.
- (6) Entering the drive motor, torque again causes the roller clutch of the next shifting stage to be engaged, with the torque transmission started and the shifting operation completed.

The information on the input/output rotational speed necessary for the control of shifting is obtained from a rotational angle detection sensor built into the drive motor on the input side and from the  $\text{min}^{-1}$  detection sensor installed in the differential section on the output side. Information about the position of the shift fork is detected by a position sensor attached to the shift fork.

### 4.2 Bench shifting test

#### 4.2.1 Testing equipment

To carry out the bench test, a dummy differential integrating the ring gear and the shaft (the output shaft), instead of the original differential, was

incorporated into the drive module specimen. Load was provided by making the motor, built into the drive module, act as the power source and allowing an externally installed motor to absorb the power generated. To measure the output torque, a torque meter was placed between the specimen and the power-absorbing motor.

**4.2.2 Test method**

To shift upward, the first speed stage is selected beforehand. To shift downward, the second speed stage is selected beforehand. The initial condition is defined as follows: the external motor for the power absorption purpose is operated at a fixed rotational speed through the rotational speed control and the drive motor produces constant positive torque. The positive torque in this case is that which accelerates the vehicle in the forward direction.

Beginning with this condition, the drive motor and the transmission actuator are controlled in the sequence described in Section 4.1 to change speeds.

**4.2.3 Results of the test**

**Figs. 5 and 6** show the results of upshifting and downshifting from an output rotational speed of 441 min<sup>-1</sup> (equivalent to a vehicle speed of about 50 km/h with a tire of 600mm diameter) at a drive motor torque of 60 Nm.

The shifting time is defined as the time required during which the output torque from the drive module is lowered to nearly zero for shifting and, after the completion of shifting, the drive module starts outputting torque again. Under the conditions of a drive motor torque of 60 Nm and an output rotational speed of 441 min<sup>-1</sup>, the time required for upshifting

was about 0.23 sec and for downshifting was about 0.27 sec.

The reason why downshifting takes more time is that the torque of the drive motor is lowered to zero to disengage the roller clutch and the standby time to maintain this condition is set. As described in Section 4.1, the roller clutch is not disengaged as long as the transmission torque does not become zero. For this reason, when the torque transmission direction immediately before shifting and the direction in which the drive motor torque is generated in the synchronization are the same as in the case of downshifting, it is necessary to lower the torque of the drive motor to zero once and to wait for the disengagement of the roller clutch.

In upshifting, on the other hand, the torque transmission direction immediately before shifting and the direction in which the drive motor torque is generated in the synchronization are opposite to each other even in the same accelerating condition, with the synchronization itself acting to end the engagement of the roller clutch. This eliminates the time waiting for disengagement. For this reason, downshifting takes 0.04 sec longer than upshifting does. Conversely, when the shifting occurs in a state in which the torque to decelerate the vehicle is output from the drive module as in the case when the regenerative brake is on downshifting takes a shorter time than upshifting does.

The shifting test was conducted on a bench up to a maximum vehicle speed of 80 km/h with a tire diameter of 600 mm and in a drive motor torque range of 20 Nm to 60 Nm and confirmed that smooth shifting is achieved without the occurrence of excessive torque.

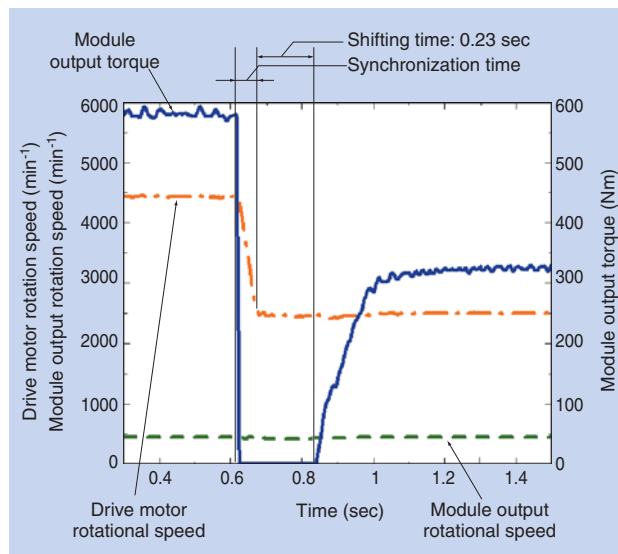


**Fig. 5** Results of upshifting test

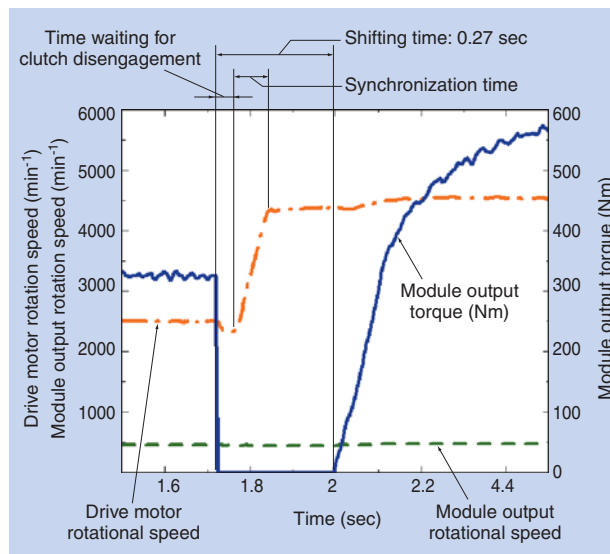


**Fig. 6** Result of downshifting test

The effect of the vehicle speed and the drive motor torque on the shifting time is shown in Figs. 7 and 8, with the former showing upshifting and the latter downshifting. In the vehicle speed range of 20 km/h to 80 km/h, upshifting took about 0.22 sec to 0.24 sec while downshifting took about 0.26 sec to 0.28 sec. This shows that the shifting time is nearly constant regardless of the vehicle speed. The shifting time is defined as the time required for the torque output from the drive module to become zero and to rise again. This time is determined by the time required for the roller clutch at the current shift stage to be disengaged, the time for the shift fork to move, and the time lag between the reentry of the drive motor torque and the engagement of the next shift stage roller clutch. With these times not dependent on the vehicle speed and output torque at the time of shifting, the shifting time is nearly constant. The time for the rotational speed synchronization depends on the vehicle speed. However, with the synchronization able to be completed within the shift fork moving time for the entire speed range, the time for the rotational speed synchronization does not affect the shifting

time. Under these circumstances, the moving time of the shift fork is the major factor for determining the shifting time, and improving the performance of the shift actuator responsible for the shift fork movement could bring about further reduction in the shifting time.

An irregularity of about 0.02 sec that is observed in the shifting time during upshifting or downshifting is due to the irregularity in the time lag from the reapplication of drive motor torque to the engagement of the next shift stage roller clutch. That is, due to the irregularity in the time required to move the shift fork to cause the roller clutch outer ring to contact the frictional disk and then, due to the torque input from the drive motor, for the roller of the roller clutch to move from the center position of the cam face (neutral position) to the wedge space (engaged position).

### 5. Onboard Test

The actual vehicle test drive was conducted with the aim of assessing the shifting performance under actual usage conditions that are difficult to reproduce in a bench test.

#### 5.1 Test vehicle configuration

Fig. 9 shows the drive module mounted on the vehicle and Fig. 10 the major system configuration for the test vehicle.

A commercially available FF vehicle was utilized for the test. The engine and transmission were removed, with the engine compartment modified so as to accommodate a drive module and its inverter.

The drive motor was water-cooled, with the cooling water being circulated between the radiator, inverter, and drive motor by a newly-installed electric pump.

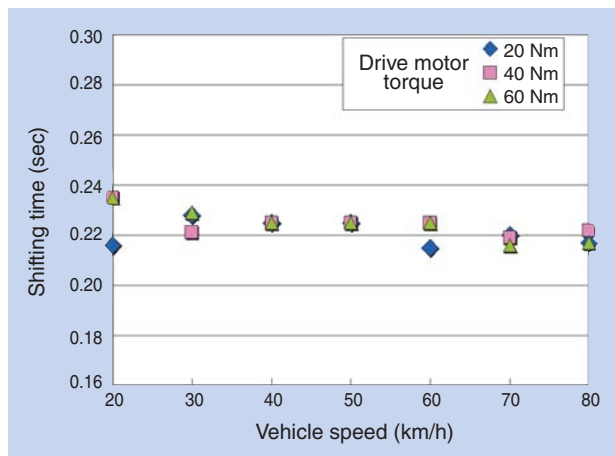


Fig. 7 Time needed for upshifting

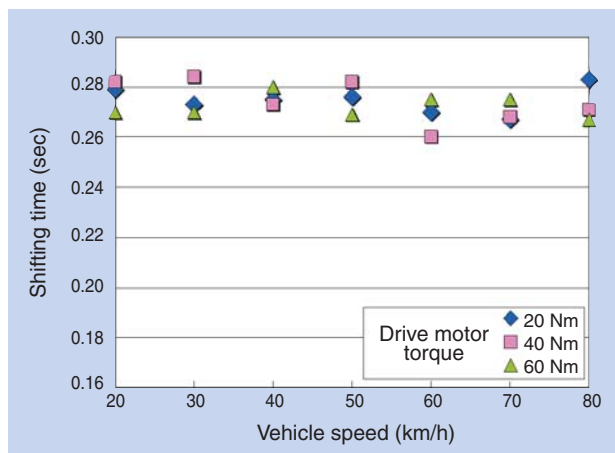


Fig. 8 Time needed for downshifting

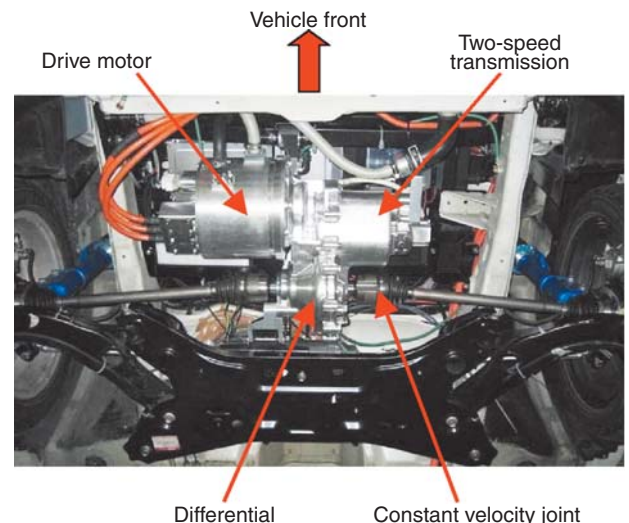


Fig. 9 Module mounted in the test vehicle

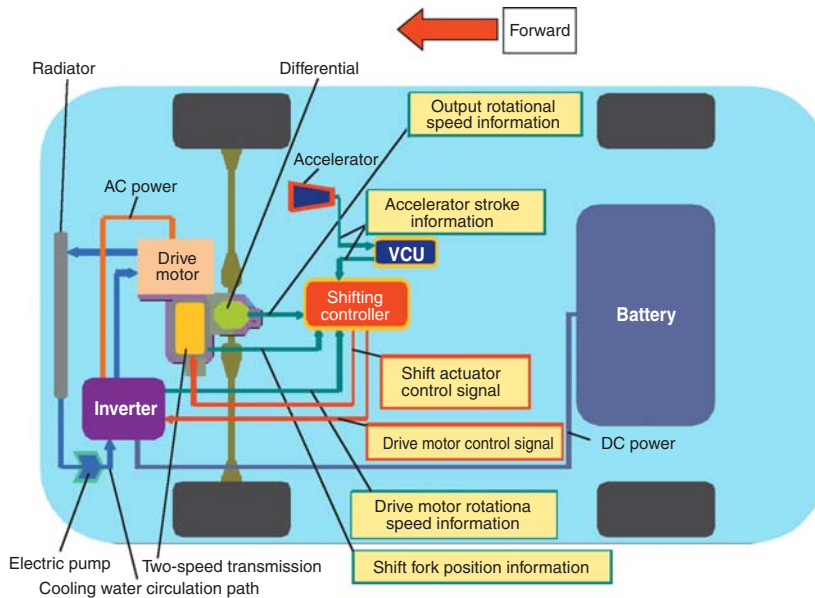


Fig. 10 Drive system for a one-motor-type electric vehicle

The drive battery was placed in the space that had been occupied by the gasoline tank.

A shifting controller was installed to control the shifting of the drive module, based on accelerator travel, drive motor rotational speed, output rotational speed, and shift fork position information.

## 5.2 Shifting tests

### 5.2.1 Test method

With the shift controller installed in the cabin, the tests were conducted by manipulating the controller manually so that speed could be changed at any time. The tests were conducted at vehicle speeds between 20 km/h and 60 km/h.

### 5.2.2 Results of the tests

Figs. 11 and 12 show the results of upshifting and downshifting at a vehicle speed of about 50 km/h.

In these tests, the output torque from the drive module was measured by a wheel torque meter mounted on the left wheel. The wheel output torque data shown in Figs. 11 and 12 are the measured values. Since they were measured on a single wheel only, they show about half of the actual torque output from the module.

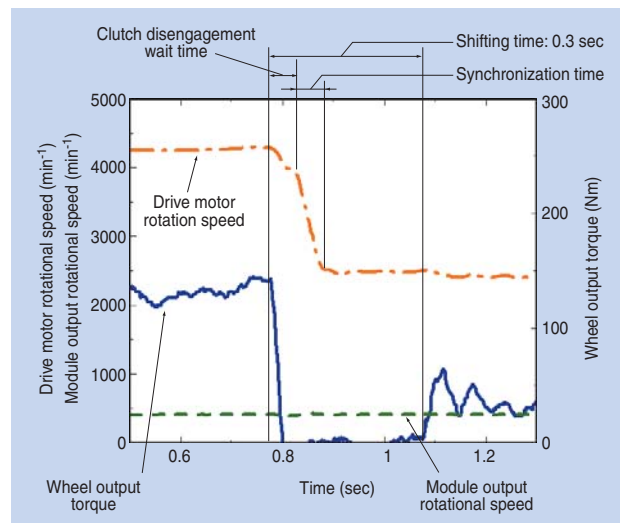


Fig. 11 Results of actual vehicle upshifting test

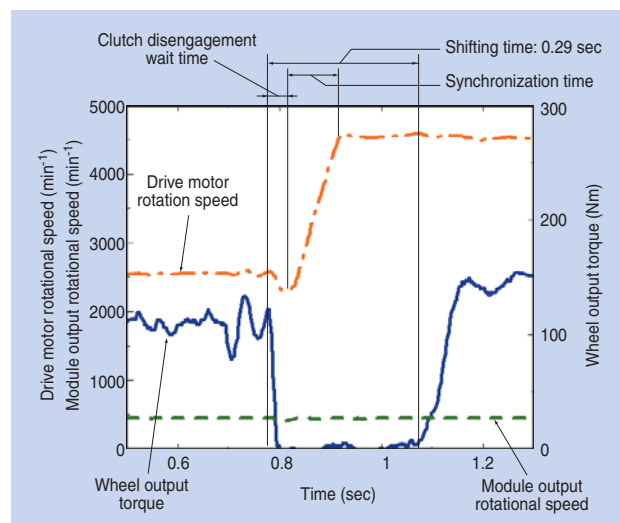


Fig. 12 Results of actual vehicle downshifting test

**Table 2** shows the shifting times required for upshifting and downshifting at 25 km/h, 50 km/h and 65 km/h.

**Table 2** Time needed for gear shifting in the test vehicle

Vehicle speed (km/h)		25	50	65
Shifting time (sec)	Upshifting	0.29	0.30	0.30
	Downshifting	0.29	0.29	0.30

Like the results of the bench tests, the tests on an actual vehicle showed that the effect of the vehicle speed on the shifting time is small. Unlike the bench test, however, the shifting times for upshifting and downshifting are about the same. This is due to the clutch disengagement waiting time, which was considered only for downshifting in the bench test, but was set also for upshifting in this test. This was done with the aim of assuring the engagement and disengagement of the clutch in actual vehicle running conditions in which vehicle speed and torque vary from time to time.

In addition, a comparison between **Figs. 6** and **12** reveal that, in spite of the same clutch disengagement waiting time and the same vehicle speed condition, the downshifting time on the test vehicle is longer by 0.02 sec than the result of the bench tests. The cause for this time difference is thought to be due to the fact that the variation in the vehicle speed, namely the output rotation speed, in actual vehicle running causes the synchronization time of the outer and the inner rings to increase. Furthermore, it can be supposed that a greater variation of the difference in the rotational speeds of the outer and the inner rings occurs until the roller clutch closes after the completion of synchronization compared to the bench test.

In the future, a reduction of the clutch disengagement waiting time in upshifting, set in the actual vehicle test, will be implemented by improving shift control through repeated in vehicle testing, until the shift time is shortened to that of the bench test.

## 6. Conclusion

With the aim of improving the rate of power consumption of one-motor-type electric vehicles, a one-motor EV drive system was developed that combines a reducer with a two-speed gear shifting mechanism and a drive motor.

Using a roller clutch in the shifting mechanism enabled the reducer size and weight to be decreased. At the same time, it was confirmed that shifting within the required time of 0.3 sec was possible at speeds of up to 80 km/h in a bench test and at speeds of up to 65 km/h in actual vehicles.

This potential for reducing the shifting time is great due to possible measures such as improvement of actuator performance and optimization of the control method. **NTN** will make efforts to further improve the shifting performance and will continue practical assessment tests on experimental vehicles.

## Reference

- 1) Eberleh, B. and Hartkopf, T., A high speed induction machine with two-speed transmission as a drive for electric vehicles, 2006 International Symposium on Power Electronics, Electrical Drives, Automation and Motion, pp. 249-254, 2006.
- 2) Sorniootti, A., Boscolo, M., Turner A. and Caballino, C., Optimisation of a 2-speed gearbox for an electric vehicle, AVEC 2010, pp. 755-760, 2010.
- 3) Meier, T., Rinderknecht, S. and Fietzek, R., Electric power train configurations with appropriate transmission systems, 2011 SAE World Congress, No. 2011-01-0942, 2011.

Photo of authors



Fumihiro ISOBE  
EV System Division  
Driveline System  
Engineering Dept.



Yoshinori ITAKUTRA  
EV System Division  
Driveline System  
Engineering



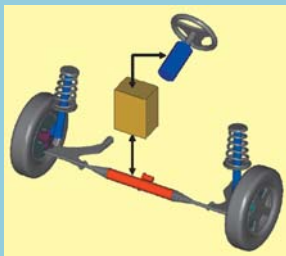
Yusuke OSUMI  
EV System Division  
Driveline System  
Engineering Dept.



Guodong LI  
EV System Division  
Control System  
Engineering Dept.

# Development of a New Steer-by-wire System

Katsutoshi MOGI\*  
 Tomohiro SUGAI\*  
 Ryo SAKURAI\*  
 Nobuyuki SUZUKI\*



NTN has been developing a new steer-by-wire system. In addition to steering functions, this steering system makes it possible to adjust the toe angle. The steering system that was developed has fail-safe functions that can respond to various failures in the system. We replaced the original steering system of an electric vehicle with the one developed and evaluated the adjustable toe angle mechanism and the fail-safe function when a motor for steering is out of order. An analysis of vehicle dynamics shows that the adjustable toe angle prevents wheels from slipping.

## 1. Introduction

Steer-by-wire (SBW) systems allow the amount of steering wheel operation to be transmitted in the form of electric signals to the vehicle wheels. These systems help improve control performance for vehicle safety while increasing vehicle design freedom. Thus, this type of system seems to have promise as a next-generation automotive steering system. SBW systems can be classified into the three types shown in Fig. 1.<sup>1)</sup> The features of each type can be summarized as follows.

### 1) Type I

A scheme in which the difference in the angle between the steering wheel and steered wheels can be controlled. This scheme is capable of controlling the steering angle independently of the steered wheel angle. However, since the steering reaction force is transmitted mechanically, this system cannot directly control the steering reaction force.

### 2) Type II

When the system is in a normal state, there is no mechanical link between the steering wheel and the steered wheels. Note, however, this system is provided with a backup feature that allows the steering wheel to be linked to the steered wheels by means of a clutch if the system fails. This system is also capable of controlling steering reaction force.

### 3) Type III

With this type, the system layout is the same as with the type II system, but the backup system is different.

For this backup system, rather than using a mechanical clutch plate, a system using electromechanical features is used. Type III boasts higher degrees of control and design, and can accommodate novel car steering systems that incorporate control means such as joysticks.

Aware of the greater freedom of Type III SBW steering systems, NTN has developed a unique SBW (hereafter referred to as the NTN-SBW) through improvements to increase functionality while assuring a high level of reliability. This paper reports on the

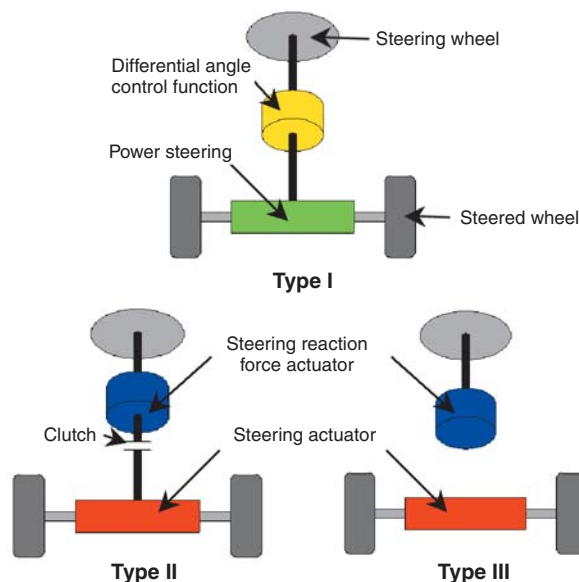


Fig. 1 Types of steer-by-wire systems

\*EV System Division Chassis System Engineering Dept

results of a function assessment test of the NTN-SBW and on theoretical consideration of the effectiveness of the toe angle adjustment function, which is a feature of the NTN-SBW.

## 2. NTN-SBW System

The NTN-SBW system consists of a steering actuator, a steering reaction force actuator and a controller.

The steering actuator drives a steering rod (a rack shaft) axially to steer the right and left wheels.

The steering reaction force actuator detects the steering wheel angle, and simultaneously transmits the state of the vehicle, which is conveyed from the tires, to the driver in the form of reaction force torque.

The controller is a unit that controls the steering actuator and the steering reaction force actuator in harmony with each other and judges whether or not the system is functioning normally to help the fail-safe mechanism operate.

### 2.1 Steering actuator

Fig. 2 shows the appearance of NTN's newly-developed steering actuator, Fig. 3 depicts its structure, and Table 1 summarizes its major specifications.

As shown in Fig. 3, the steering actuator includes two motors (main and sub), screws, a ball screw and a ball spline. The ball screw shaft and the ball spline shaft are arranged coaxially and coupled with each other by means of screws, forming a steering rod.

The rotation of the main motor is converted into linear motion via gearing by means of the ball screw. This mechanism allows the steering rod to move laterally, with the link mechanism consisting of a tie rod and a knuckle arm to steer the tires. The components shown in blue in Fig. 3 are those associated with steering.

The rotation of the sub motor causes the ball spline shaft to rotate via gearing, causing the coupling length of the screw to change. As the coupling length of the screw changes, so does the total length of the steering rod, allowing the toe angle of the tire to be adjusted. The components shown in red in Fig. 3 are associated with the toe angle adjustment. As shown in Fig. 4, the toe angle refers to the angle of each of the right-hand and left-hand tires relative to the vehicle traveling directly forward or backward as viewed from above.

As described later, should the main motor fail, the power transmission path is switched over to the sub motor, helping the vehicle maintain steering capability. In this way, when the main motor is operating

normally, the sub motor adjusts the toe angle of the steered wheel, and if the main motor fails, the sub motor functions as a backup motor for steering. The toe angle adjustment function can contribute to increasing the precision of vehicle control.<sup>2)</sup> For this reason, NTN's new steering actuator can be regarded as a mechanism that has achieved functional improvement while assuring reliability.

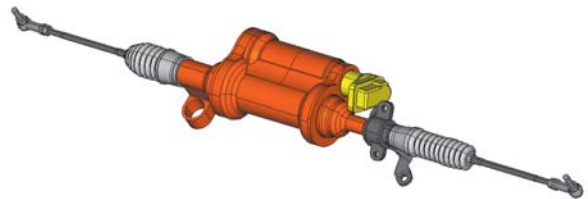


Fig. 2 Appearance of NTN's steering actuator

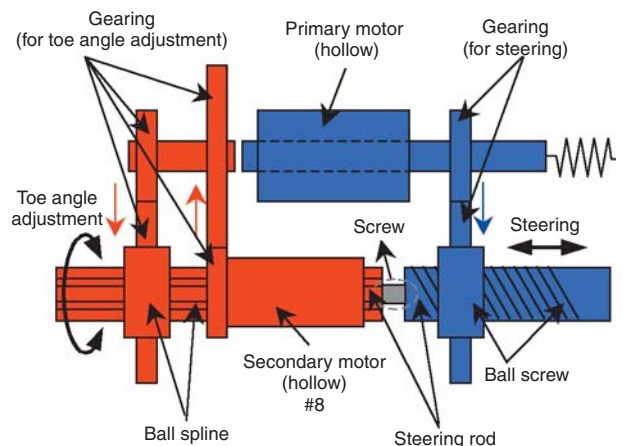


Fig. 3 Structure of steering actuator

Table 1 Specifications of steering actuator

Motor type	DC brushless
Steering system	Ball screw type
Power supply	48 V
Maximum thrust of steering rod	10 kN
Steering angle range when installed in vehicle	$\pm 31$ deg
Toe angle adjustment range when installed in vehicle	$\pm 2$ deg

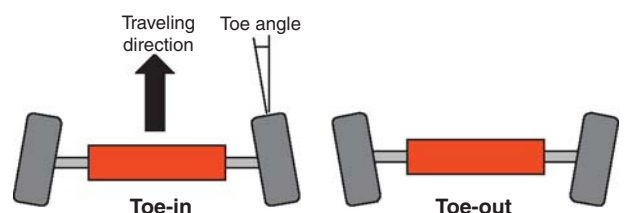


Fig. 4 Definition of toe angle

**2.2 Steering reaction force actuator**

Fig. 5 shows the appearance of NTN’s new steering reaction force actuator, Fig. 6 depicts its structure, and Table 2 summarizes its major specifications.

The torque damper, the steering angle limiting mechanism, the reducer, the motor and the angle sensor are installed on a common shaft to reduce the size and weight of the actuator.

In order to provide the driver with a comfortable feeling when steering, the damping effectiveness of the torque damper is increased by filling the space between the output shaft and housing with a high viscosity fluid.

**2.3 Controller**

Fig. 7 is a block diagram of the control system of NTN’s new SBW system. The electronic control unit (ECU) consists of the three ECUs—ECU-A, ECU-B and ECU-C—that control the actuator motors. The differential torque between the steering torque  $T_h$  of the driver and the steering reaction force torque causes the steering wheel to rotate, and the angle of the rotation is detected by the angle sensor. According to the steering wheel angle, ECU-A controls the position of the steering mechanism.

The external force acting on the steering mechanism is detected by a steering torque estimator. Then, a target reaction force torque is generated on the basis of the external force detected, and according to which the ECU-C controls the torque of the reaction force motor.

The vehicle control unit (VCU) that controls the motion of the entire vehicle sends toe angle command signals to ECU-B and ECU-A to control the main and sub motors of the steering actuator in coordination. This makes the center line of the steering column coincide with the lateral midpoint of the steering

actuator system to make adjustments to obtain a laterally-equal toe angle. It is possible to set up a steering angle on either side independently of the other to cope with the current traveling conditions of the vehicle.

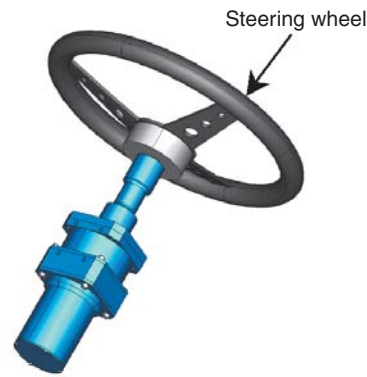


Fig. 5 Appearance of reaction force actuator

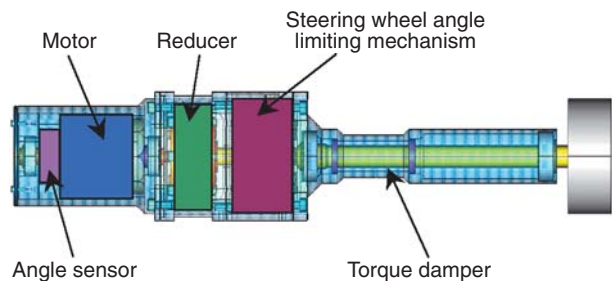


Fig. 6 Structure of reaction force actuator

Table 2 Specifications of reaction force actuator

Motor type	DC brushless
Power supply	48 V
Maximum reaction force torque	15.5 Nm
Steering wheel angle resolution	0.01 deg

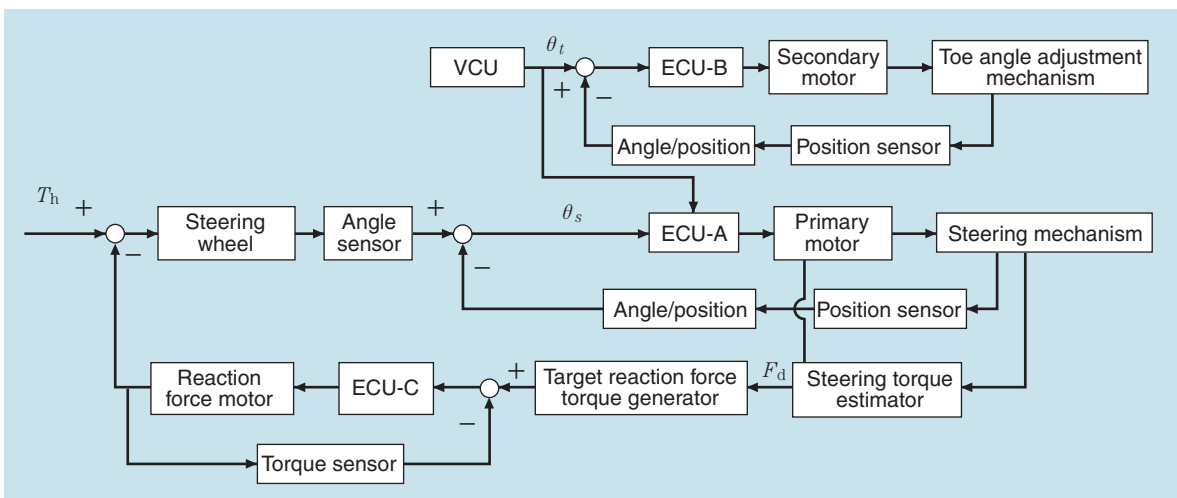


Fig. 7 Block diagram of control system

### 3. Fail-Safe Mechanism

The most critical challenge for an SBW system is to maintain its functionality even when there is a failure, in other words, to ensure its fault tolerance. This system was designed by taking into account the loss of power, disconnected wires, failed motors or sensors, malfunction and failure of the ECU, and failed mechanisms. This section describes the motor switching mechanism of the steering actuator that switches over to the sub motor to maintain steering capability even if the main motor has failed for any reason.

**Fig. 8** schematically illustrates the state of a steering actuator with a failed main motor. The schematic diagram of the steering actuator in **Fig. 3** shows the case when the main motor condition is normal.

At the end of the motor switching shaft that penetrates the main motor, a spring is provided to switch the power transmission mechanism. When the main motor operates normally, this spring is maintained in an energized state. Should the main motor fail, the spring is released, with the motor switching shaft moved to the left by the compressive force of the spring as shown in **Fig. 8**. Consequently, the clutch mechanism installed in the motor switching shaft trips to create a new power transmission path from the sub motor to the ball screw. At the same time, the power transmission from the sub motor to the ball spline is interrupted. Even if the rotor of the main motor seizes, the power is transmitted because the motor switching shaft penetrates the hollow rotor. In this way, the sub motor helps maintain the wheel steering function of the SBW even when the main motor has failed.

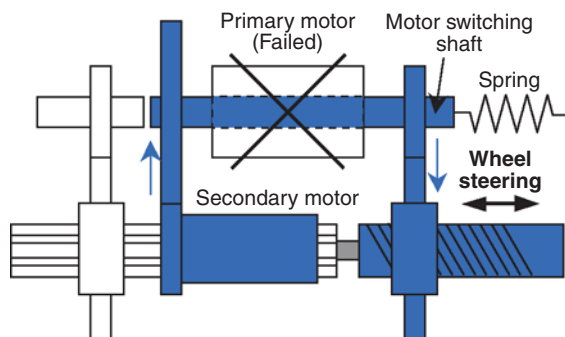


**Fig. 8** Schematic view of malfunctioning steering actuator

### 4. Verification of Motor Switching Mechanism

#### 4.1 Bench assessment test

To verify operation of the motor switching mechanism of the steering actuator, a bench test was conducted. **Fig. 9** illustrates the configuration of the test rig used for this bench test.

Assuming that the main motor failed while the vehicle was turning with the steering wheel maintained at a certain position, the steering rod of the steering actuator was given three levels of axial load—0 kN, 3 kN and 6 kN. The load was applied by an air cylinder. Because of the assumption that the steering wheel was kept at a particular angle, the axial position of the steering rod was kept controlled.

Under these conditions, the switching time and quality of the motor switching mechanism were assessed. The switching time was defined as the time span required, beginning with sending the command signal for releasing the spring and ending with completion of the movement of the motor switching shaft to the specified position. The switching was judged to have been normally performed if, after the completion of the switching, problem-free lateral motion of the steering rod by the sub motor was confirmed.

**Fig. 10** graphically illustrates the motor switching test. To determine switching reliability, three test runs were performed for each loading condition.

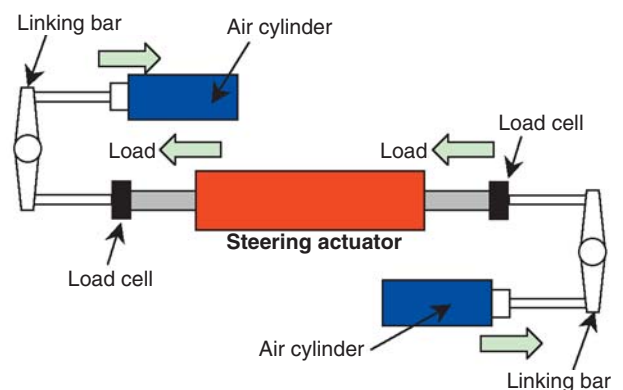


**Fig. 9** Bench assessment test rig

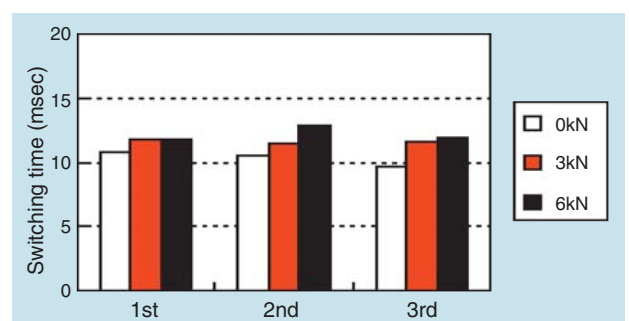


**Fig. 10** Time required to complete motor switching

From Fig. 10, the switching time falls in a range of 10–13 msec and normal switching occurred regardless of the load. As the load became larger, the motor switching action became slightly slower. The reason for this is that an increase in the torque applied on the key and spline on the motor switching shaft causes the slide resistance at the time of switching to increase.

For this test, the time needed to judge whether the main motor was normal was ignored. Even when this time is taken into account, the time elapsed from the failure of the main motor to the completion of the switching was 0.1 sec or less.

#### 4.2 Onboard assessment test

Next, we assessed the operation of the motor switching feature of the NTN-SBW on a test vehicle that had its EPS replaced with the NTN-SBW.

Table 3 shows the main specifications of the test vehicle. Fig. 11 shows a view of the NTN-SBW installed in the vehicle.

In the test, the vehicle was slalomed at 60 km/h, and a motor failure signal was sent to the controller to trip the motor switching mechanism.

Fig. 12 shows the test results. The upper chart shows the main motor failure signal and the axial position of the motor switching shaft, and the lower chart shows the steering wheel angle and the yaw angular velocity on the vehicle. From Fig. 12, it is

Table 3 Specifications of the test vehicle

Drive system	Front wheel drive
Total length	3765 mm
Total width	1690 mm
Total height	1510 mm



Fig. 11 View of NTN-SBW mounted in test vehicle

apparent that the time required for motor switching is 10 msec, which is about the same as the bench test result, and that the wheels could be steered normally after motor switching. The signs of disturbance in the steering before and after switching were due to the driver's steering action, rather than a malfunction of the switching mechanism.

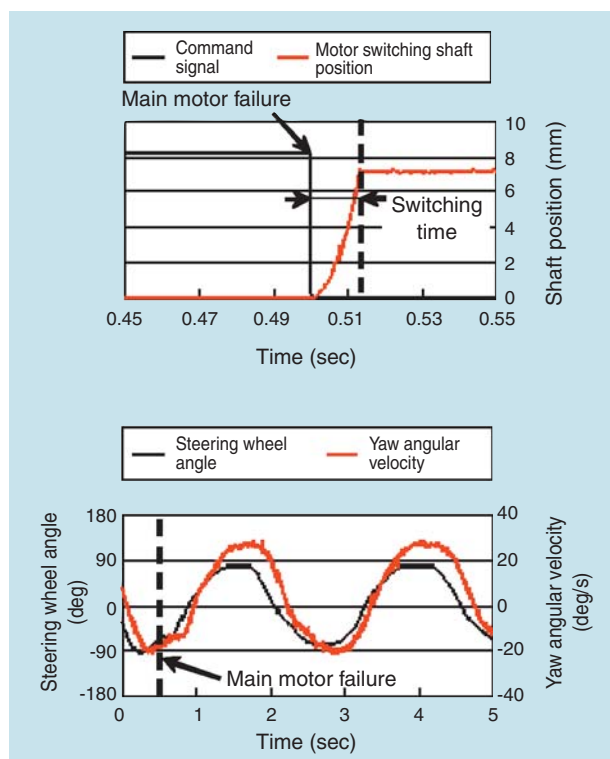


Fig. 12 Results of evaluation of motor switching system in test vehicle

### 5. Verification of Toe Angle Adjustment Mechanism

NTN's newly-developed steering actuator is equipped with a toe angle adjustment mechanism. Controlling the toe angle in accordance with the traveling state of the vehicle in cornering could help prevent slipping of the vehicle by appropriately varying the proportion of lateral force between the right and left wheels. As one of the basic tests for this control feature, a cornering test was conducted on the same vehicle as described previously.

In the test, five levels of toe angle—0 degs, ±1.0 deg and ± 1.8 degs—were applied to the front wheels. The vehicle was allowed to circle at 40 km/h at a radius of 30 m, and the lateral force acting on the front wheels was investigated. The toe angles applied to the front wheels were estimated using calculations based on the coordinate system of the link mechanism

consisting of the steering rod, tie rod and knuckle arm. The lateral force was measured by means of a load sensor built into the hub. For the toe angle, positive means toe-out and negative means toe-in.

Fig. 13 shows the lateral force on the right and left wheels during cornering. With the vehicle cornering at a constant speed, the lateral force is theoretically constant. Two cornering directions were used—clockwise (CW in Fig. 13) and counterclockwise (CCW in Fig. 13) with the vehicle as seen from above. The lateral force acting leftward with respect to the traveling direction was taken as positive.

As shown in Fig. 13, the inner lateral force on the tire increases (and the outer lateral force on the tire decreases) in the toe-out condition, while the inner lateral force on the tire decreases (and the outer lateral force on the tire increases) in the toe-in condition. It was confirmed that adjusting the toe angle causes the ratio of the lateral force on the left wheel to the lateral force on the right wheel to change.

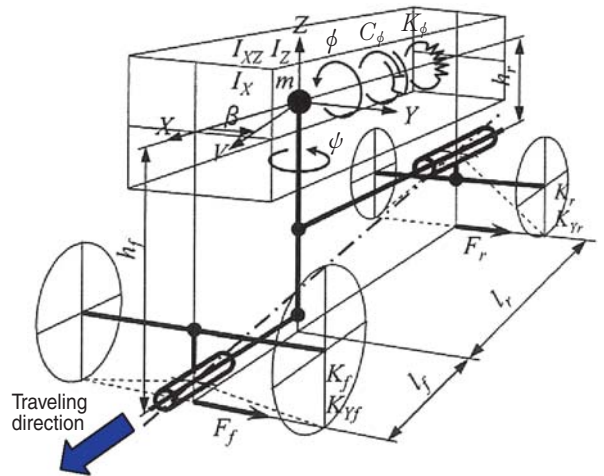


Fig. 14 Vehicle motion model<sup>4)</sup>

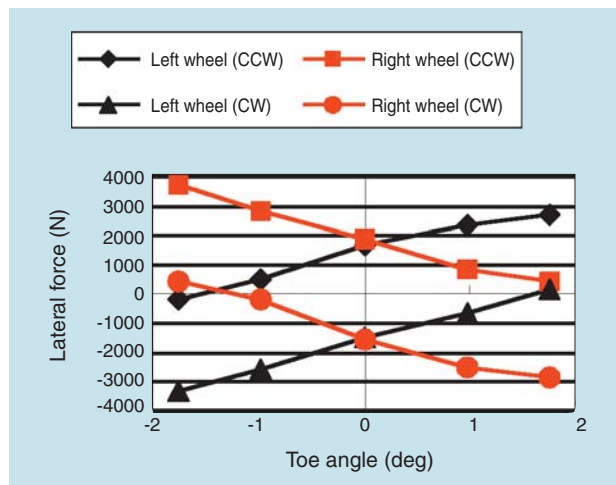


Fig. 13 Effect of toe angle on lateral tire forces

## 6. Theoretical Consideration

### 6.1 Vehicle motion model

As described earlier, it was confirmed in actual vehicle testing that the toe angle affects the balance in the lateral force in the steered wheel. In this section, the effect of toe angle adjustment on the vehicle motion is theoretically considered by means of a vehicle motion model.

This vehicle motion model is formed on the basis of Minakawa’s vehicle motion model<sup>3)</sup> shown in Fig. 14, with the following assumptions.<sup>4), 5)</sup>

- The model is one with three degrees of freedom describing the motion in the *y* axis, around the *z* axis

(yaw) and around the *x* axis (roll).

- The height of the roll center differs between the front and the rear of the vehicle.
- The model is based on a four-wheel vehicle in order to take differences between the lateral force acting on the right wheel and that acting on the left wheel into consideration.
- The lateral force on a tire corresponds with the direction of the *Y* axis.
- The vehicle advances in the *X*-axis direction (forward) at a constant speed *V*.

#### 6.1.1 Equation of motion

On the basis of the above assumptions, the equation of motion with respect to the parallel advancement in the *Y*-axis direction in this model is expressed by the following equation:

$$mV(\dot{\beta} + \dot{\psi}) = F_{fL} + F_{fR} + F_{rL} + F_{rR} \dots\dots\dots (1)$$

In equation (1), *m* denotes the vehicle mass and *F* is the lateral force acting on individual tires. In the suffixes to lateral force *F*, the first letter refers to the front or rear and the second to the left or right. For example, *F<sub>fL</sub>* refers to the lateral force acting on the front left wheel.

In the similar way, the equation of motion around the *Z* axis (yaw) is given by:

$$I_Z \ddot{\psi} + I_{XZ} \ddot{\phi} = l_f(F_{fL} + F_{fR}) - l_r(F_{rL} + F_{rR}) \dots\dots\dots (2)$$

In the equation, *I<sub>Z</sub>* denotes the yaw moment of inertia, *I<sub>XZ</sub>* the yaw-roll inertia product, *l<sub>f</sub>* and *l<sub>r</sub>* the distance from the vehicle center of gravity to the front axle and to the rear axle, respectively.

The equation of motion around the *X* axis (rolling) is given by:

$$I_X \ddot{\phi} + C_\phi \dot{\phi} + (K_\phi - mgh_c) \phi + I_{XZ} \ddot{\psi} = h_f(F_{fL} + F_{fR}) + h_r(F_{rL} + F_{rR}) \quad (3)$$

In the equation,  $I_X$  denotes the roll moment of inertia,  $C_\phi$  is the roll attenuation factor, and  $K_\phi$  is the roll rigidity. The roll moment arm length at the vehicle center of gravity  $h_c$  is expressed as shown below, using the roll moment arm lengths  $h_f$  and  $h_r$  at the front and rear axles.

$$h_c = \frac{h_f l_r + h_r l_f}{l_f + l_r} \quad (4)$$

By solving the three coupled equations of motion above and determining the angle of sideslip of the body  $\beta$ , the yaw angular velocity  $\dot{\psi}$ , and the roll angle  $\phi$ , the state of motion of a vehicle can be determined.

**6.1.2 Tire lateral force model**

The lateral force to the tire expressed in equations (1) to (3) is expanded in the following equations:

$$\begin{aligned} F_{fL} &= -K_{cfL} \beta_{fL} \\ F_{fR} &= -K_{cfR} \beta_{fR} \\ F_{rL} &= -K_{crL} \beta_{rL} \\ F_{rR} &= -K_{crR} \beta_{rR} \end{aligned} \quad (5)$$

In the above equations, signs such as  $\beta_{fL}$  denote the sideslip angle of each tire. As shown in Fig. 15, the sideslip angle of a tire refers to the angle formed by the traveling direction and the surface of revolution of the tire.  $K_c$  is the cornering power of the individual tires. The sideslip angle of a tire is expanded further by the following equations:

$$\begin{aligned} \beta_{fL} &= \beta + \frac{l_f \dot{\psi}}{V} - \delta - \delta_t + \frac{h_f \dot{\phi}}{V} - C_{sf} \dot{\phi} - C_{rff} \dot{\phi} \\ \beta_{fR} &= \beta + \frac{l_f \dot{\psi}}{V} - \delta + \delta_t + \frac{h_f \dot{\phi}}{V} - C_{sf} \dot{\phi} - C_{rff} \dot{\phi} \quad \dots (6) \\ \beta_{rL} &= \beta_{rL} = \beta - \frac{l_r \dot{\psi}}{V} + \frac{h_r \dot{\phi}}{V} - C_{sr} \dot{\phi} - C_{rrr} \dot{\phi} \end{aligned}$$

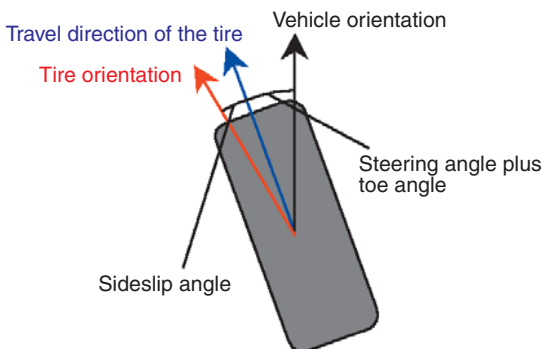


Fig. 15 Tire slip angle and steering angle

$\delta$  is the steering angle of the front wheel, formed by the orientation of the vehicle (X-axis) and the surface of revolution of the tire.  $\delta_t$  is the toe angle of the front wheel and, as in the previous chapter, toe-out is taken as positive.  $C_r$  denotes the roll steer coefficient and  $C_{rr}$  is the roll rate steer coefficient.

**6.1.3 Tire characteristics**

The cornering power  $K_c$  is expressed in the following equations using the lateral rigidity of the tire suspension  $K_Y$  and the steady cornering power  $K$ .

$$\begin{aligned} \dot{K}_{cf} + \left( \frac{1}{K_f} - C_{sff} \right) \left( \frac{1}{K_{Yf} V} - C_{sfff} \right)^{-1} K_{cf} &= \left( \frac{1}{K_{Yf} V} - C_{sfff} \right)^{-1} \dots (7) \\ \dot{K}_{cr} + \left( \frac{1}{K_r} - C_{sfr} \right) \left( \frac{1}{K_{Yr} V} - C_{sfrf} \right)^{-1} K_{cr} &= \left( \frac{1}{K_{Yr} V} - C_{sfrf} \right)^{-1} \end{aligned}$$

In the above equations,  $C_{sf}$  denotes the lateral force steering coefficient and  $C_{sfr}$  is the lateral force differential steering coefficient. The cornering power varies depending on the vertical force  $W$  acting on the tire. With rolling motion occurring on the vehicle, the vertical force acting on the tire increases or decreases by  $\Delta W$  as shown in the following equations:

$$\begin{aligned} \Delta W_f &= \left\{ \frac{K_\phi}{2} \phi + H_f (F_{fL} + F_{fR}) \right\} / d_f \dots (8) \\ \Delta W_r &= \left\{ \frac{K_\phi}{2} \phi + H_r (F_{rL} + F_{rR}) \right\} / d_r \end{aligned}$$

In the above equations,  $H$  denotes the height of the roll center of the front and the rear and  $d$  the track width of the front and the rear. On the basis of this, the cornering power is used in the corrected forms as in the following expressions.<sup>6)</sup>

$$\begin{aligned} K_{cfL} &= \left( \frac{W_{fL} - \Delta W_f}{W_{fL}} \right)^{2/3} K_{cf} \\ K_{cfR} &= \left( \frac{W_{fR} + \Delta W_f}{W_{fR}} \right)^{2/3} K_{cf} \dots (9) \\ K_{crL} &= \left( \frac{W_{rL} - \Delta W_r}{W_{rL}} \right)^{2/3} K_{cr} \\ K_{crR} &= \left( \frac{W_{rR} + \Delta W_r}{W_{rR}} \right)^{2/3} K_{cr} \end{aligned}$$

### 6.2 Conditions for analysis

Table 4 shows the main conditions. The main parameters in the table are values for the experimental vehicle determined on the basis of the results of the running test. For the experimental vehicle used this time, the effect of the inertia product  $I_{XZ}$  was so small that it was approximated as zero.

In the analysis, the steering angle was set as a constant and cornering on a static circle was assumed.

Table 4 Major conditions for analysis

Vehicle mass $m$	1400 kg
Distance from vehicle center of gravity to front wheel $l_f$	1.1 m
Distance from vehicle center of gravity to rear wheel $l_r$	1.29 m
Front wheel track width $d_f$	1.46 m
Rear wheel track width $d_r$	1.47 m
Roll inertia moment $I_X$	600 kg · m <sup>2</sup>
Yaw inertia moment $I_Z$	1900 kg · m <sup>2</sup>
Roll rigidity $K_\phi$	5.0 × 10 <sup>4</sup> Nm/rad
Roll attenuation coefficient $C_\phi$	5500 Nm · s/rad
Front wheel static cornering power $K_f$	4.3 × 10 <sup>4</sup> N/rad
Rear wheel static cornering power $K_r$	3.8 × 10 <sup>4</sup> N/rad
Tire suspension lateral rigidity $K_Y$	2.0 × 10 <sup>5</sup> N/m

### 6.3 Results of analysis

The results of the analysis were evaluated by the ratio of the resultant braking/driving force  $Q$  and the lateral force  $F$  to the tire vertical force  $W$ .

With the running speed taken as a constant in this analysis, the braking/driving force  $Q$  was ignored, with the result of the analysis evaluated by the ratio of  $F$  to  $W$  as shown in equation (10). This value does not exceed the coefficient of road surface friction  $\mu$ . If it did, the tire would slip.

$$\frac{\sqrt{Q^2 + F^2}}{W} \approx \frac{F}{W} \dots\dots\dots (10)$$

Fig. 16 shows some of the results of analysis. This analysis is based on a hypothetical situation in which a vehicle corners at a speed of 60 km/h on a circle with a radius of 50 m. The direction of cornering is counterclockwise based on the vehicle seen from above.

Fig. 16 shows that, with the coefficient of road surface friction  $\mu$  assumed to be 0.7, a toe-out setting causes the front left wheel to slip. A 2-deg. toe-in setting also causes the front right wheel to slip. If the front right wheel, which needs large lateral force slips, the driver becomes unable to control the vehicle, resulting in a very dangerous condition.

However, if the toe angle adjustment mechanism is

operated to provide a 1-deg. toe-in setting, the  $F/W$  on both sides becomes smaller than 0.7, preventing the front wheels from slipping. Furthermore, with a toe-in setting at the cross-section of the two straight lines, namely, at about 0.5 deg., the  $F/W$  values on both sides are equal, decreasing the risk of the front wheel losing traction. The optimum toe angle that equalizes the  $F/W$  values on both sides has a relationship with the vehicle speed as shown in Fig. 17. Using the NTN-SBW allows one to adjust to the optimum toe angle while running.

Provided with the characteristics described above, the toe angle adjustment mechanism, a feature of the product developed, is capable of providing an optimum toe angle that allows a vehicle to run safely, avoiding the danger of slipping even on road surface conditions that invite tire slipping.

Adjusting the toe angle to about zero degrees for straight-ahead driving allows the lateral force on the tire to decrease, with an improvement in fuel efficiency to be expected.

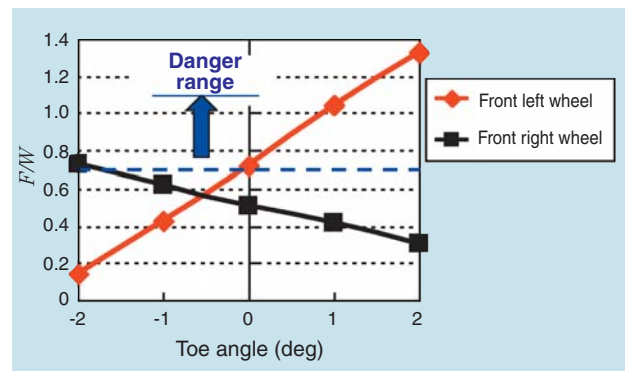


Fig. 16 Relationship between toe angle and  $F/W$  values

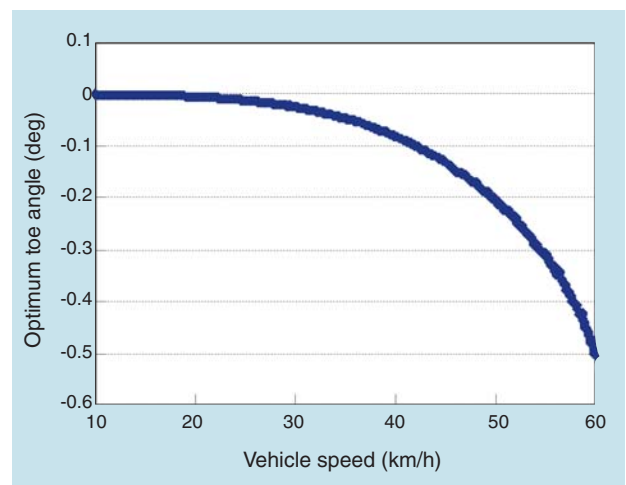


Fig. 17 Optimum toe angles for vehicle speeds

## 7. Conclusion

The NTN-SBW is equipped with a fail-safe mechanism that addresses failures of the system as a whole. As an example, a fail-safe demonstration test was conducted on the assumption that the main motor for steering failed. In addition, a bench test and an actual-vehicle test were conducted to demonstrate the effectiveness of the toe angle adjustment function. Furthermore, a vehicle motion model was created to theoretically assess the relationship between the toe angle and tire slip. The results obtained are summarized as follows:

- It was demonstrated in a fail-safe experiment that switching from the main motor for steering to the sub motor does not hinder continued steering capability.
- A running test on an actual vehicle showed that adjustments to the toe angle cause the balance in lateral force between the left and the right tires to change.
- A numerical analysis showed that even in a running condition in which the tire would lose traction, a toe angle adjustment could make it possible to avoid the loss of tire traction.

## Reference

- 1) Motoyama, S., Possibilities of Steer-by-wire on Vehicle Dynamics, Journal of Society of Automotive Engineers of Japan, Vol. 57, No. 2, pp. 39-43, 2003.
- 2) Yamamoto, M., Effect of Wheel Alignment on Handling and Stability, Journal of Society of Automotive Engineers of Japan, Vol. 54, No. 11, pp. 10-15, 2000.
- 3) Minakawa, M., Model Concept for a Simple 3DOF Vehicle Model with Considerations of the Effect of Body Roll, Transactions of the Society of Automotive Engineers of Japan, 20075786, 2007.
- 4) Abe, M., Vehicle Dynamics and Control, First edition, Tokyo Denki University Press, 5-180, 2008.
- 5) Sakai, H., Influence of Roll Characteristics on Vehicle Dynamic Behavior, Transactions of the Society of Automotive Engineers of Japan, 20055693, 2005.
- 6) Kobayashi, A., The Latest Automotive Engineering, Tosho Shuppan, 1975.

## Photo of authors



Katsutoshi MOGI  
EV System Division  
Chassis System  
Engineering Dept



Tomohiro SUGAI  
EV System Division  
Chassis System  
Engineering Dept



Ryo SAKURAI  
EV System Division  
Chassis System  
Engineering Dept



Nobuyuki SUZUKI  
EV System Division  
Chassis System  
Engineering Dept

## Development of Two-seat Electric Vehicles with In-Wheel Motors

Akira YAMAGATA\*  
Chinami ITOU\*  
Kayo SAKAI\*  
Kaori TOMODA\*

Aiko ISHIKAWA\*  
Tomomi GOTOU\*  
Yukiko TAKEKAWA\*  
Daisuke MATSUOKA\*\*



Compact electric vehicles are thought to be suitable as small models due to the advantages of quietness, low-heat generation and no exhaust gas. In particular, in-wheel motors realize smaller space requirements for power trains and drive trains. Moreover, in-wheel motors can achieve high-performance drive through independent steering mechanisms for all wheels. An NTN development team of young engineers has designed a two-seat electric vehicle that provides "pivot turning" and "lateral movement" capabilities with in-wheel motors. This paper introduces the features and structure of this electric vehicle.

### 1. Introduction

With automobile manufacturers having started mass-producing passenger car-type electric vehicles (EVs) recently, EVs are seeing rapid popularization. On the other hand, some automobile manufacturers have proposed small EVs with one or two seats and electric two-wheel vehicles that are intended for short-distance travel,<sup>1)-4)</sup> and some have already been brought to market.

Electrification is suitable for small vehicles as electric power is quiet, generates little heat, and has no exhaust gasses when compared to similar vehicles with internal combustion engines. Such compact vehicles are expected to be used as means of transportation not only on public roads but also in indoor spaces, such as hospitals and factories. In particular, the application of in-wheel motors as power sources offers the possibility of two great advantages. One of the advantages is freedom from the necessity of installing differentials and constant velocity joints (CVJ) for the drive wheels, so space is easily made between the drive wheels. The other is the wide steering angle range, which is not limited by CVJ operating angles.

Several EVs that are equipped with in-wheel motors and said to be capable of four-wheel independent wide-angle steering have been proposed thus far. For

example, the development of a city-commuter-type vehicle on which both the track width and the wheel base are variable as a result of adopting a four-wheel-driven, two-tier, four-wheel independent steering mechanism has been reported.<sup>5)</sup>

Having been engaged in the development of systems for EV use such as in-wheel motor drive systems<sup>6)</sup> and steer-by-wire systems,<sup>7)</sup> NTN has realized vehicles equipped with its EV-specific systems to demonstrate the features and advantages of such newly-developed systems.

Given these conditions, NTN has organized a development team consisting of young engineers to investigate, the uses for small EVs equipped with in-wheel-motor-driven systems. As a result, they have invented the "Electric Mobility," a small two-seat vehicle that makes the most of the features of in-wheel motors, is capable of four-wheel independent wide-angle steering, and is compact and excellent in small-radius turn performance.

This paper presents the concept of NTN's newly-developed two-seat Electric Mobility and the features of its mechanisms.

\*EV System Division Driveline System Engineering Dept.

\*\*EV System Division Control System Engineering Dept.

## 2. Vehicle Concept

The considerations of the development team have led to the conclusion that for the popularization of EVs it is important that NTN study the commercial usefulness of small vehicles. These vehicles excel in handling in an urban environment due to their compact bodies and feature sets that contain certain levels of road running performance and load-bearing capacity.

The two-seat Electric Mobility vehicle presented in this paper has a compact body that excels in the capability of turning in a small radius in a limited space. Furthermore, an advantage of in-wheel-motor-equipped vehicles is that the four-wheel independent wide-angle steering feature makes it possible to pivot-turn and to move laterally. Such compact electric vehicles will work not only as means of everyday transportation, they also have the potential to be used in other practical applications, such as medical services and tourism.

Fig. 1 shows the orientations of different wheels during pivot turns and lateral movements. A pivot turn is a rotational movement of a vehicle with the vehicle center as the center of rotation. The “vehicle center” here refers to the point of intersection of the bisector between the front and rear wheel axes and of the center line between the right and left wheels. When a vehicle pivot-turns, the number of drive wheels does not affect whether or not it is possible. In other words, if the rotation axes of all wheels are directed toward the turning center of the vehicle, a pivot-turn is possible regardless of whether the vehicle is in two-

wheel-drive, four-wheel-drive or even one-wheel-drive mode. The steering angle required to achieve a pivot-turn is determined by the wheelbase and the track width. For example, when the wheelbase equals the track width, the steering angle required is 45 degrees. When the wheelbase is longer than the track width as in common passenger automobiles, a steering angle of between 45 degrees and 90 degrees is required. For lateral movement, the four wheels are all turned to 90-degree angles.

Table 1 shows the rotation directions of individual wheels in different running modes.

The rotation directions of individual wheels during pivot-turning and lateral movement differ from those during normal running.

These movements cannot be achieved in ordinary four-wheeled vehicles equipped with differentials. They are achieved only by the combination of the in-wheel-motor drive system, which is characterized by independent drive for the right and left wheels, and a mechanism that steers the four wheels in wide angles independently.

Table 1 Rotational direction of wheels

Running mode	Front left wheel	Front right wheel	Rear left wheel	Rear right wheel
Normal running (forward)	CCW	CW	CCW	CW
Pivot-turning (right)	CCW	CCW	CCW	CCW
Lateral movement (rightward)	CCW	CCW	CW	CW

CW: Clockwise as seen from the outside of the vehicle  
 CCW: Counterclockwise as seen from the outside of the vehicle  
 Note: Rotation is reversed for backing up, left pivot turns and left lateral movements

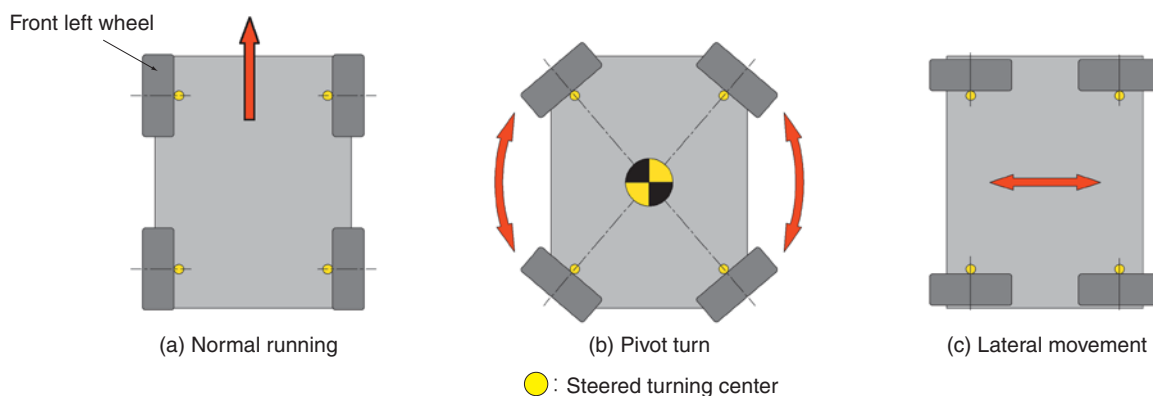


Fig. 1 Pivot turn and lateral movement

### 3. Test Vehicle

#### 3.1 Vehicle layout

**Fig. 2** shows the test vehicle. The vehicle is equipped with two rear wheels that have in-wheel motors. To enable four-wheel independent steering, all four wheels are equipped with steering actuators. Furthermore, in order to reduce space, the steering actuators are located near the wheels.

The major dimensions of the body are about 1700 mm in total length, about 1200 mm in total width and about 1900 mm in total height. Including space sufficient for two passenger seats, an inverter, a battery and other components, the vehicle was designed for maximum compactness. Since the battery is the heaviest component, it was installed in the lowest part at the center of the body, with the space above the battery serving as the passenger leg space.

Furthermore, by providing the seating space above the rear wheels and installing the inverter above the front wheels, the space needed for this vehicle is as small as the area occupied by two ordinary mopeds.

#### 3.2 Suspension

The steering mechanism for conventional vehicles is a tie rod system in which the thrust from the

steering gearbox is transmitted via a tie rod to the hub carrier to produce steering torque around the kingpin shaft. In this test vehicle, however, the steering range is wide, and moreover, it is necessary for the right and left wheels to be steered independently of each other. For this reason, a steering system with a tie rod scheme results in a very long operating stroke in the steering gearbox, requiring a large area. In this test vehicle, therefore, the four wheels are each equipped with a steering actuator with the aim of minimizing the area occupied by the steering system and thereby making full use of the space around each wheel.

**Fig. 3** shows the layout of an in-wheel motor and steering actuator. The suspension is structured on the basis of a four-wheel double wishbone system.

The in-wheel motors and the steering actuators are built into an integral structure, and the rotation around the kingpin shafts of the output members of the steering actuators connected to the upper arm joints is regulated. Thereby, this structural arrangement allows the upper arms to support the steering reaction force. This arrangement allows the steering actuator bodies to rotate around the kingpin shafts, allowing the in-wheel motors connected to the steering actuators and the wheels connected to the in-wheel motors to be steered.

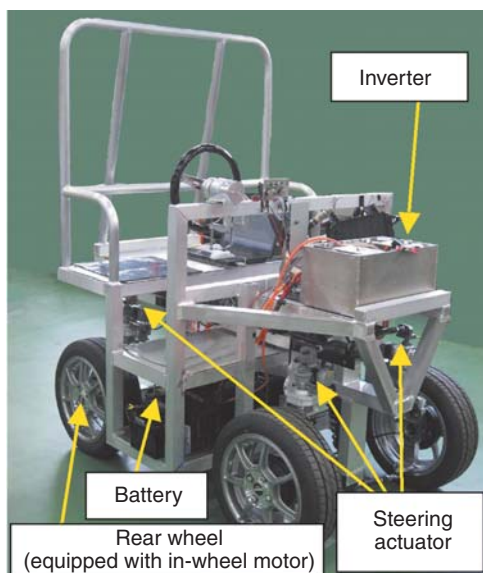


**Fig. 2** Test vehicle

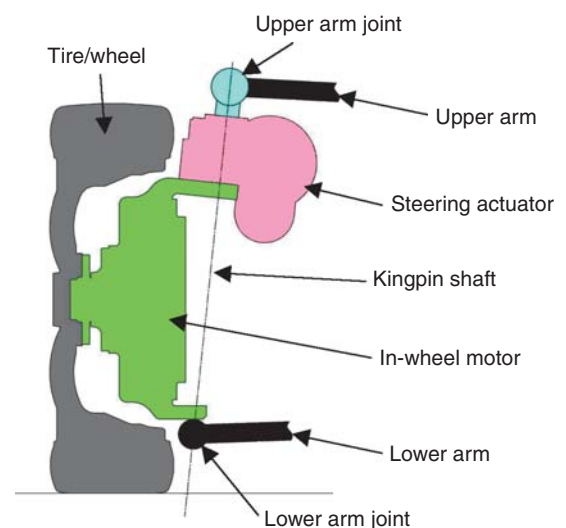


**Fig. 3** Suspension layout

### 3.3 Kingpin offset

**Fig. 4** schematically illustrates the kingpin offset. The kingpin offset refers to the distance between the intersection of the kingpin axis with the ground and the center of the tire tread. It is general practice to minimize the kingpin offset with the steering wheel. The offset is determined through comprehensive considerations around possibly conflicting factors such as straight running stability and minimum necessary steering wheel operation effort. To reduce the kingpin offset, the joint of the lower arm must be placed inside the wheel.

However, because the range of the steering angle on this vehicle exceeds 120 degrees, the location of the lower arm joint is greatly limited. For example, when the clearance between the outer circumference of the motor and the wheel bore surface is small and the lower arm joint is located in the bottom of the wheel in order to minimize the kingpin offset, if the steering handle is turned greatly, then the lower arm can interfere with the inside surface of the wheel.

In this test vehicle, the lower arm joint is situated outside the wheel (inside the vehicle) so that the lower arm does not interfere with the wheel when the steering wheel is turned at a large angle. The resulting greater kingpin offset can be one factor that contributes to an increase in steering torque. This effect is particularly apparent when the steering wheel is turned sharply while the vehicle is stationary and the brake is applied. For this reason, the tires on this vehicle are set free with the brakes not applied when steering in a wide angle to avoid an increase in the steering torque.

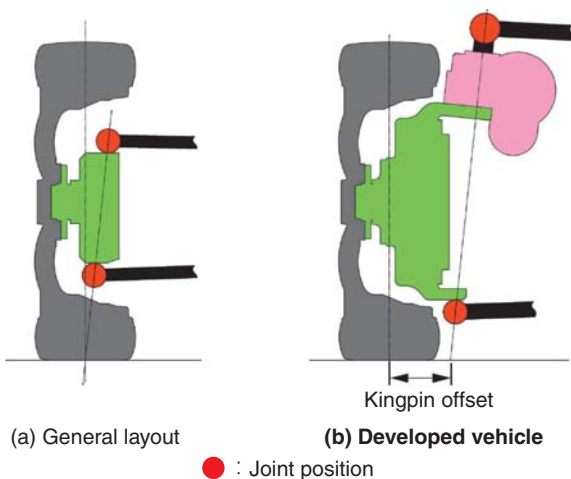


**Fig. 4** Kingpin offset and joint position

### 3.4 In-wheel motor unit

An in-wheel motor composed of a motor, a reducer and a hub is used for the drive wheels. With the condition that it is used with a wheel of 14-inch diameter or greater, this in-wheel motor was designed with emphasis placed on a greater reduction of the dimension in the axial direction than in the motor outside diameter.

### 3.5 Steering actuator

**Fig. 5** shows the structure of the steering actuator. In the steering actuator, the motor output speed is reduced by a worm gear to produce steering torque. With the shaft of the worm wheel forming part of the kingpin shaft, the worm wheel is fastened to the upper arm so that only the upper arm joint is free to pivot. This configuration restrains the rotation of the worm wheel. For this reason, as the motor built into the steering actuator rotates, the housing covering the part from the worm gear to the motor and the coupled in-wheel motor rotate around the kingpin shaft.

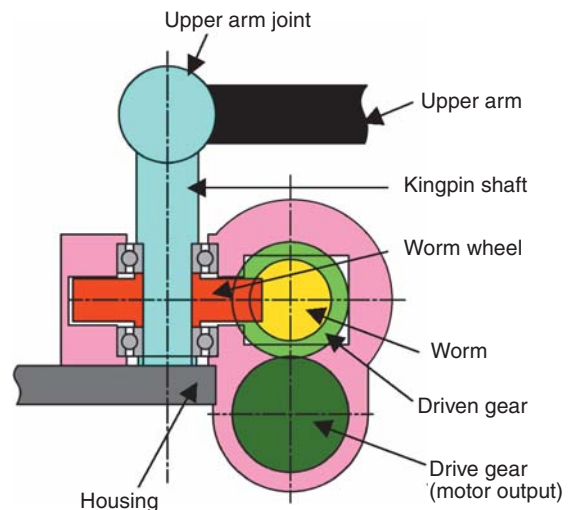


**Fig. 5** Structure of the steering actuator

## 4. Mode Operation Control

This test vehicle is equipped with steering mechanisms that are mechanically independent on the four wheels, and the four wheels are steered by electric signals transmitted through the steer-by-wire control system.

**Fig. 6** shows the basic control configuration in which the in-wheel motor is installed in all four wheels. The vehicle is integrally controlled by the vehicle control unit (VCU), which provides overall control of the in-wheel motors and the steering actuators according to the three running modes—normal running mode, pivot-turning mode, and lateral movement mode.

According to the running mode selected by the operator and the running commands, including the accelerator stroke, the VCU gives commands for the drive power and the rotational direction needed for individual in-wheel motors to the inverter. Based on these commands, the inverter generates the necessary AC outputs. At the same time, in response to the steering commands from the VCU, the steering drivers in turn control the steering actuators so that the target steering angle is achieved.

### 4.1 Control of drive wheels

When the vehicle advances (or backs up) in normal running mode, the drive wheels on both sides drive the vehicle forward (or backward) in a manner identical to that of the drive wheels of conventional vehicles. On the other hand, in pivot-turning mode and lateral movement mode, the drive wheels move in the directions necessary for these modes as shown in **Table 1**.

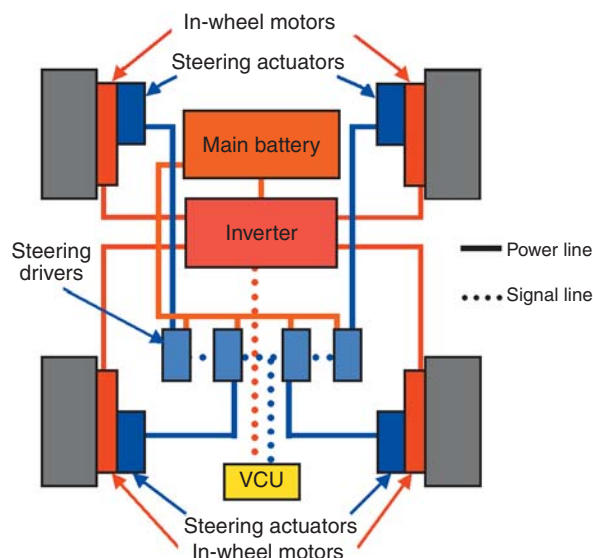


**Fig. 6** Control system configuration diagram

### 4.2 Steering control

The steering system of this vehicle is provided by a steer-by-wire scheme, with the individual wheels being capable of independent steering. In the normal running mode, however, only the front wheels are steered, as with conventional vehicles, according to the steering input. However, it is possible to reduce the turning radius by steering the front and the rear wheels in mutually opposite phases. In addition, in a situation such as a lane change, it is possible to reduce the yaw of the vehicle and improve road holding by steering the front and the rear wheels in the direction of the same phase.

In contrast, the pivot-turning mode enables all four wheels to be steered so that their axes are oriented toward the turning center of the vehicle. In lateral movement mode, the steering angle is increased beyond that used in pivot-turning mode, with all four wheels turned a full 90 degrees from normal mode.

**Figs. 7** and **8** show how the rear wheels of the test vehicle are steered in pivot-turning mode and lateral movement mode, respectively. The front wheels can be steered in the same way, and it is even possible for all four wheels to be turned by over 90 degrees within a limited vehicle space.



**Fig. 7** Steering in pivot-turning mode



**Fig. 8** Steering in lateral movement mode

## 5. Two-seat Electric Mobility

Fig. 9 shows an example of a vehicle design embodying the vehicle concept described in this paper, and Table 2 lists the major specifications for this design. This vehicle is equipped with in-wheel motors installed in all four wheels, is four-wheel-driven, and is steered using the four-wheel independent wide-angle steering principle. With a layout following that of the test vehicle, this vehicle was designed so as to locate the battery and the inverter below the floor to lower the center of gravity of the vehicle with the aim of improving the load-capacity and securing space for two seats.



Fig. 9 Two-seat Electric Mobility

Table 2 Main specifications of the vehicle

Battery	DC 96 V (Serving both the in-wheel motors and the steering actuator)	
In-wheel motors	Maximum output/shaft	2 kW
	Drive wheel	Four-wheel drive
Steering system	Four-wheel independent wide-angle steering mechanism	
Cooling system	In-wheel motor	Air-cooled
	Inverter	Water-cooled
Seating capacity	Two people	

## 6. Conclusion

A two-seat electric vehicle with a compact body was fabricated that uses a four-wheel, wide-angle steering mechanism and in-wheel motors, making it capable of both pivot-turning and lateral movement.

Equipping each wheel with a small-footprint steering actuator makes it possible to turn all four wheels over 90 degrees in a limited vehicle space.

In the future, this test vehicle will be used to confirm the function of EV systems.

## Reference

- 1) Society of Automotive Engineers of Japan, Hybrid Vehicles, Fuel Cell Electric Vehicles, Electric Vehicles, Journal of Society of Automotive Engineers of Japan, Vol. 61, No. 8, pp. 84-89, 2007.
- 2) Nunogaki, N. et al., Personal Mobility Design of Toyota, Journal of Society of Automotive Engineers of Japan, Vol. 64, No. 6, pp. 56-59, 2010.
- 3) Makiyama, T. et al., 41st Tokyo Motor Show: Nissan leads the way to zero-emission, Nissan Technical Review, No. 66, pp. 73-81, 2010.
- 4) Nishiyama, M., Development of the electric commuter model EC-03, 1st International Electric Vehicle Technology Conference 2011 (EVTec'11), No. 20117222, 2011.
- 5) Fukui, A. et al., 40th Tokyo Motor Show, Nissan Technical Review, No. 62, pp. 66-75, 2008.
- 6) Suzuki, M. et al., Development of an In-Wheel Motor Axle Unit, NTN Technical Review, 75, pp. 46-52, 2007.
- 7) Mogi, K. et al., Development of Steer-by-wire System with an Adjustable Toe Angle Mechanism, Transactions of the Society of Automotive Engineers of Japan, No. 146-11-257, 2011.

Photo of authors

---



**AKIRA YAMAGATA**  
EV System Division  
Driveline System  
Engineering Dept.



**Aiko ISHIKAWA**  
EV System Division  
Driveline System  
Engineering Dept.



**Chinami ITOU**  
EV System Division  
Driveline System  
Engineering Dept.



**Tomomi GOTOU**  
EV System Division  
Driveline System  
Engineering Dept.



**Kayo SAKAI**  
EV System Division  
Driveline System  
Engineering Dept.



**Yukiko TAKEKAWA**  
EV System Division  
Driveline System  
Engineering Dept.



**Kaori TOMODA**  
EV System Division  
Driveline System  
Engineering Dept.



**Daisuke MATSUOKA**  
EV System Division  
Control System  
Engineering Dept.

## Hub Bearing with Integrated Multi-axis Load Sensor

Kentaro NISHIKAWA\*



Cars have advanced vehicle control systems to ensure safety and various sensors installed to sense and control vehicle conditions. However, the control responses of conventional yaw and G sensors installed in vehicles are delayed because they begin to detect after the vehicle position changes. To further improve vehicle control, a hub bearing with an integrated multi-axis load sensor has been developed that can detect the frictional force change of a tire at a position near the road surface in real time.

### 1. Introduction

To ensure safety, recent automobiles have highly sophisticated vehicle control systems that include various onboard sensors for helping estimate and control the current states of the vehicle. A typical control system for this purpose receives signals from the yaw rate sensors and accelerometers installed in the car body (onboard sensors), and from velocity sensors (ABS sensors) and steering angle sensors on the axle side; on the basis of information from these sensors, the control system estimates the current state of the vehicle. Note that the onboard sensors begin detecting changes in the vehicle after a change in the vehicle dynamics has occurred; consequently, a vehicle control sequence begins after a certain delay<sup>1)</sup>.

For further sophistication of vehicle control systems, NTN believes that frictional force between tire tread and road surface should be detected on a real time basis at a location nearest to the road surface in order to promptly determine current state of the vehicle relative to the ground. In this paper, "Multi Axis Load Sensor-Integrated Hub Bearing" NTN has developed a new bearing to address this challenge and it is described hereunder.

### 2. Development Concept and Structure

#### 2.1 Development concept

There are two approaches for ensuring safety during operation of automobiles: active safety, where a symptom of an abnormal situation is detected and the possible hazard is avoided, and passive safety, that helps protect human bodies in case of collision and other accidents. Typical means for active safety include ABS (anti-lock braking system) and ESC (anti-skidding system); and those for passive safety include seat-belts and air-bags. Focusing on improvements in active safety functions, NTN determined the concept for this development project, which is, detecting changes in frictional force on tires based on information from sensors situated nearest to the road surface (the sensors are integrated in the hub bearings). Vehicle information that is utilized for active safety is summarized in [Table 1](#).

#### 2.2 Structure

[Fig. 1](#) shows the appearance of the new hub bearing NTN has developed for the above-mentioned purpose. The detection principle of this new bearing product is schematically illustrated in [Fig. 2](#). A strain sensor is installed to the outer ring (fixed ring) of a hub bearing: when the car is travelling, a strain occurs on the outer ring, and the strain sensor detects the strain, thereby the active safety system can detect longitudinal force (Fx), lateral force (Fy) and vertical

\* Automotive Business HQ. Axle Unit Engineering Dept.

force ( $F_z$ ) working between the road surface and tire; independent of the motion of the suspension.

When a load is applied to the hub bearing, infinitesimal deformation occurs on the outer ring of the hub bearing, wherein the pattern of the deformation can vary depending on the direction of loading. This infinitesimal deformation is detected by four sensors (situated in upper, lower, right and left locations), and then the resultant sensor signals are subjected to arithmetic operations in order to determine the magnitude of the loads in three directions. Also, since the load-induced deformation

on outer ring is detected, the load can be detected based on the weight of vehicle even when the tires are at a standstill (locked).

### 2.3 Bearing types for load sensor-integrated hub bearing

Fig. 3 illustrates the types of load sensor-integrated hub bearings. Installed to the fixed outer ring of GEN2 and GEN3 flanged hub bearings whose inner ring can freely rotate, the load sensor detects the load acting on the bearing.

Table 1 Vehicle information applicable to active safety system

Characteristic to be detected	Sensor	Mounting location	Response for change detection
Vehicle velocity detection	ABS (wheel speed) sensor	Hub bearing (axle)	Real time
Steering angle detection	Angle sensor	Steering system	Real time
Angular velocity detection	Yaw rate sensor	Onboard (sprung)	Minor delay
Acceleration detection	G sensor	Onboard (sprung)	Minor delay
Tire load (change in $\mu$ ) detection	Multi axis load sensor	Hub bearing (unsprung)	Real time



Fig. 1 Load sensor-integrated hub bearing

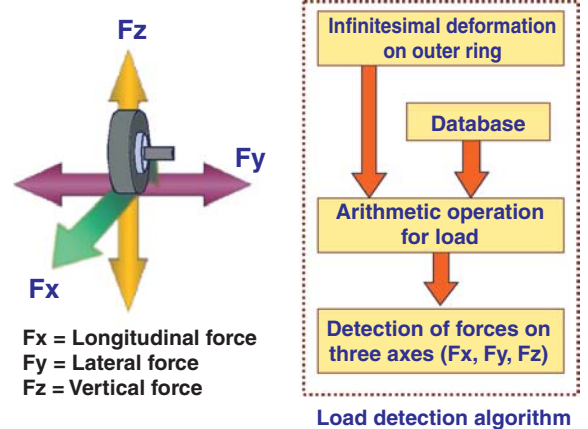


Fig. 2 Load detection scheme

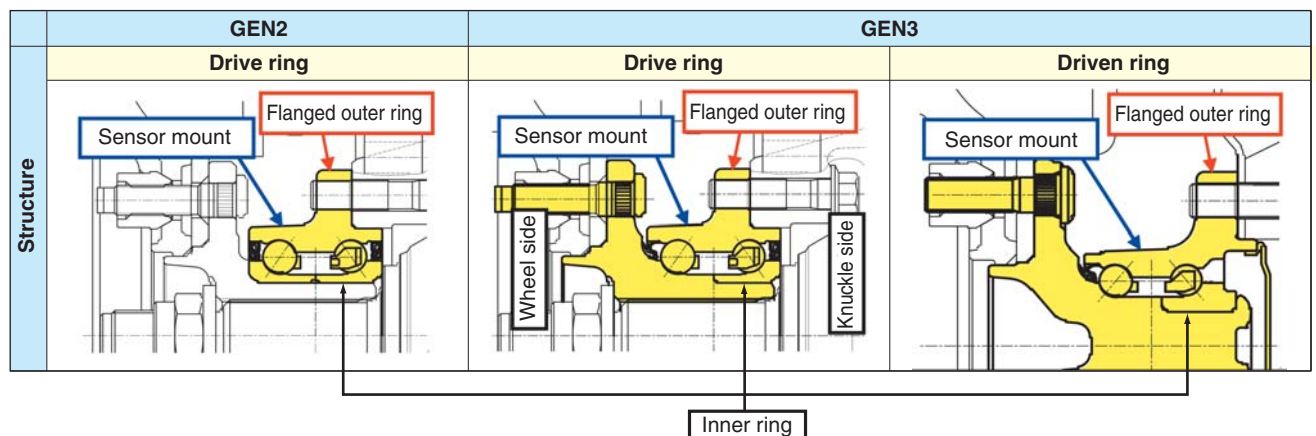


Fig. 3 Bearing types for load sensor-integrated hub bearing

### 3. Load Detection Algorithm

#### 3.1 Strain detection system

When a load acts on the outer ring, the magnitude of strain at a given location on the outer ring varies depending on the magnitude of external load, and at the same time, is affected by passing rolling elements. The magnitude of strain on a running bearing that is being affected by external load varies when rolling elements pass by, and is maximized at the very moment where a rolling element passes by a given strain detection point and is minimized at a moment where the same strain detection point is situated at midpoint between the two neighboring rolling elements (Fig. 4). In other words, even if the magnitude of external load remains unchanged, the magnitude of strain will vary depending on the positional relationship between a strain detection point and the rolling elements.

As can be understood from the discussion above, strain occurring at a given detection point under a load of certain magnitude essentially consists of a constant component from external load and a varying component from passing rolling elements (Fig. 5). Incidentally, strain at a given detection point on the outer circumference of the outer ring, derived from an external load, can be detected regardless of the axial location of that detection point. However, variation in the magnitude of strain at a particular strain detection

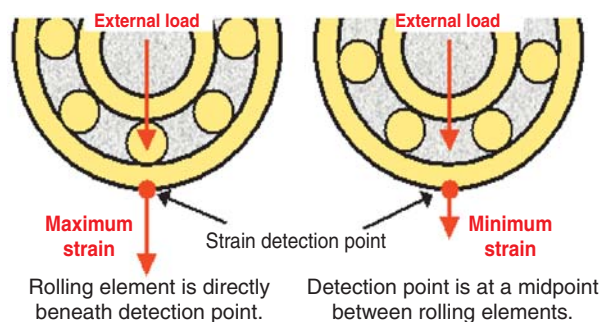


Fig. 4 Influence of location of rolling elements

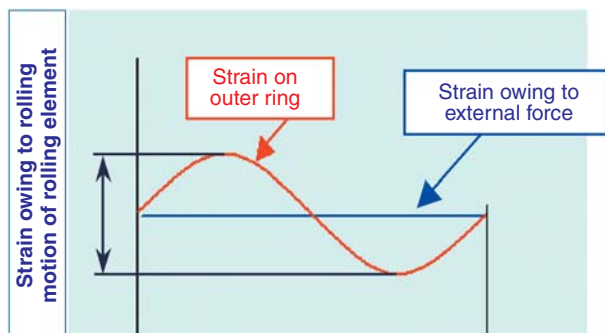


Fig. 5 Strain occurring on outer ring

point is nearly impossible when the detection point is axially deviated from a location where the rolling surface is situated directly beneath it or the detection point is situated on the non-load side on outer circumference and if this variation in strain derives from this location and passage of rolling elements. Additionally, the two types of strain in Fig. 5 each exhibit unique characteristics depending on the magnitude and direction of loading.

Therefore, a plurality of strain sensors capable of detecting these two types of strain are installed on the outer circumference of the outer ring in order to allow the load on outer ring to be accurately estimated.

#### 3.2 Shape of sensor and signal processing system

To be able to amplify infinitesimal deformation on an outer ring, the strain sensor used is a plate type sufficiently thin relative to the outer ring. The strain detection area of the sensor includes necks (Fig. 6) while the mount for the sensor has slots so that deformation around these slots concentrates on the strain detection area to improve detection sensitivity of the sensor.

As previously described in Sec. 3.1, the strain sensor also detects strain from the rolling motion of the rolling elements; consequently, even when a constant load is applied to the outer ring, the level of sensor output signal can vary depending on the location of rolling elements. For example, when the bearing is running, variation in strain within one cycle owing to passing rolling elements can be determined by arithmetic operation to calculate the magnitude of strain (strain from external force) corresponding to the magnitude of external force. In contrast, when the bearing is at a standstill, the strain component of the external force cannot be readily separated from the magnitude of strain detected by one strain gage alone. To address this issue, NTN has adopted a unique sensor structure characterized in that one strain sensor has two detection areas as shown in Figs. 6 and 7. These detection areas are situated with a space 1/2 as large as the pitch between adjacent rolling elements (balls), and two outputs from these detection areas are summed up in order to compensate for variation in the output that is governed by the location of rolling elements. Consequently, it is now possible without adopting an outside sensor or the like to estimate the load on the outer ring even when the tire is at a standstill.

#### 3.3 Load estimation method

First, sensor output and input loads under expecting driving conditions for both simulator testing and road testing are measured; thereby, a database for the load

estimation matrix is developed. An arithmetic operation for matrix input conditions includes various scenarios and combinations for various driving conditions estimated from sensor output rather than simple sensor outputs themselves. Thus, adoption of NTN's unique calculation technique helps offer a load estimation approach that boasts higher accuracy compared with conventional techniques.

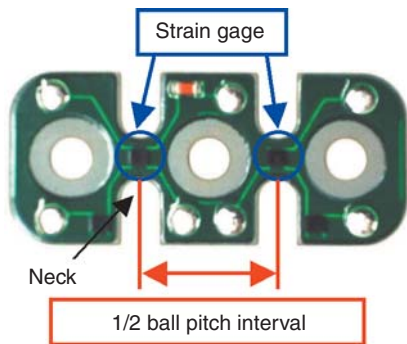


Fig. 6 Strain sensor

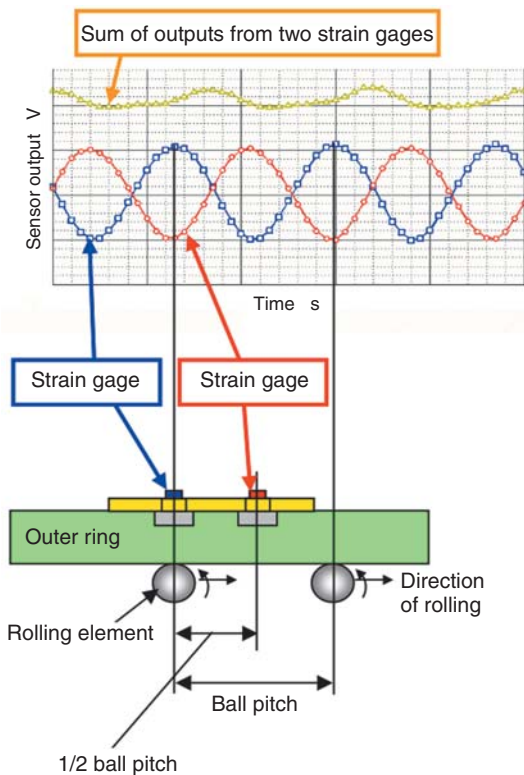


Fig. 7 Signal processing scheme

## 4. Result Assessment by Road Test

### 4.1 Test conditions

NTN's multi axis load sensor-integrated hub bearings were incorporated in the four wheels on the test vehicle that was subjected to road testing; thereby load detection accuracy and response of these sensors were assessed. For assessing load detection accuracy, output of a six-component force transducer installed in the tire was taken as "tire-to-road surface" load, and was compared with the output of a multi-axis load sensor. For assessing sensor response, output of the onboard yaw rate sensor was compared with output of the multi-axis load sensor. **Table 2** summarizes the specification of the sensors mounted on the test vehicle.

Table 2 Load sensor specification

Characteristic	Value
Detection load	Longitudinal force: Fx
	Lateral force: Fy
	Vertical force: Fz
Detectable load range	Fx $\pm 10\text{kN}$
	Fy $-4\text{kN} \sim 10\text{kN}$
	Fz $0 \sim 10\text{kN}$
Targeted estimation accuracy	Fx $\pm 5\%FS (\pm 1\text{kN})$
	Fy $\pm 5\%FS (\pm 0.7\text{kN})$
	Fz $\pm 5\%FS (\pm 0.5\text{kN})$
Sampling frequency	300Hz
Response	30 ms max.
Subject of comparison for accuracy	Six-component force transducer

\* FS: Full Scale

### 4.2 Assessment of the load detection accuracy

Road testing was performed using a slalom mode, lane change mode and acceleration/deceleration mode; thereby the load detection accuracy of the sensor in each road mode was determined. As representative examples, road test results of the slalom mode and lane change mode are graphically plotted in **Figs. 8** and **9**. These graphs show variation in the outputs from the six-component force transducer and multi-axis load sensor. At each time point, output error of multi-axis load sensor relative to the output of the six-component force transducer was determined.

In the slalom test whose result is graphically plotted in **Fig. 8**, the error in component forces in three directions (Fx, Fy, Fz) each fall in the targeted range ( $\pm 5\%FS$ ) relative to the outputs from the six-component force transducer.

In quick acceleration and lane change testing, results in **Fig. 9**, the change in three component

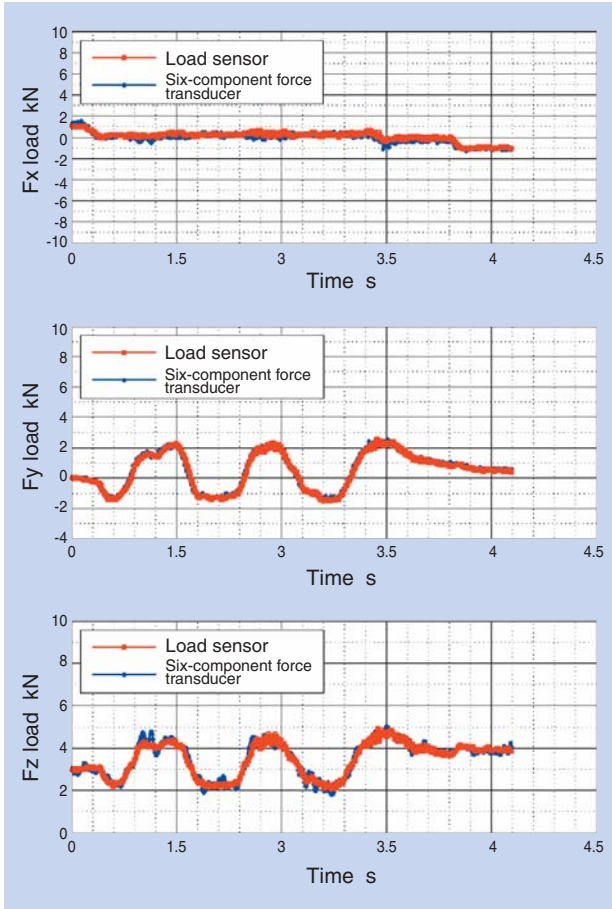


Fig. 8 Result of slalom test

forces and output from the multi-axis load sensor is similar to that of the output from the six-component force transducer: it has been proven that the multi-axis load sensor positively detects a quick change in load that can result from quick acceleration/deceleration or violent lane change.

### 4.3 Assessment of response

In Sec. 4.2, the load detection accuracy and response capability for variation in load was verified for the six-component force transducer built into the wheel. In this section, output from the onboard yaw rate sensor is compared with output from the multi-axis load sensor in the hub bearing in order to verify response of the load sensor. The graphical plotting in Fig. 10 illustrates changes in outputs of the yaw rate sensor and the multi-axis load sensor that occur when the steering wheel on a car running straight is turned quickly. It should be understood that compared with the response of the yaw rate sensor, the response of the multi-axis load sensor is approximately 10 ms quicker. This difference appears to coincide with a time span from the occurrence of lateral force on the tire to detection of this force by the onboard yaw rate

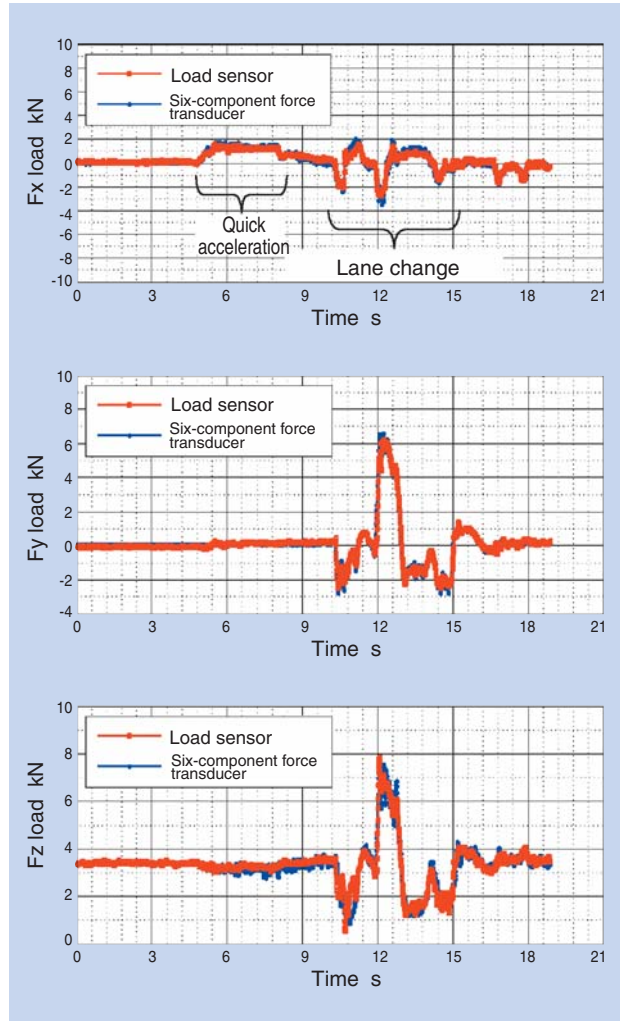


Fig. 9 Result of quick acceleration/deceleration and lane change tests

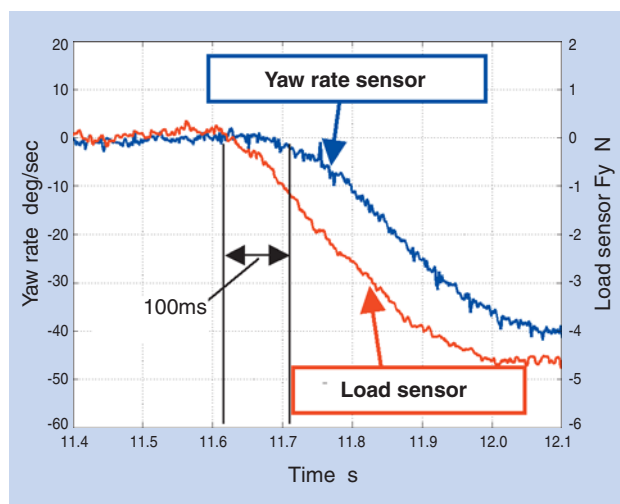


Fig. 10 Comparison of responses

sensor included in the sprung mass. In other words, if the car is traveling at 100 km/h, this time difference coincides with a thinking distance of approximately 3 m.

On the basis of these findings, **NTN** believes that the ability to estimate tire-to-road status with a multi-axis load sensor will help ensure driver safety during situations including hazard avoidance, and that this arrangement will provide useful vehicle information while improving ride comfort by controlling the behavior of the vehicle before the driver feels uncomfortable motion of the vehicle.

## 5. Conclusion

To help assist in further sophistication of the vehicle control technique, **NTN** has developed a “multi-axis load sensor-integrated hub bearing” that can detect variation in frictional force on the tire in a real time bases at a location the near road surface.

In the presented road test, it has been verified that the **NTN**'s multi-axis load sensor provides output equivalent to that obtained from a six-component force transducer, and boasts better response compared with onboard sensors included in the sprung mass such as a yaw rate sensor. **NTN** will seek the possibility of vehicle control using an intelligent corner module that comprises a load sensor alone or a load sensor in conjunction with a “high resolution sensor<sup>2)</sup>” or the like, in an attempt to adopt improved vehicle control systems to further enhance vehicle stability.

## Reference

- 1) Norimatsu, T., Nishikawa, K., "Development of Multi Axis Load Sensor Integrated Hub Bearing," Journal of the Society of Automotive Engineers of Japan, Vol. 64, pp. 104-105, 2010.
- 2) Norimatsu, T., "Technical trends in hub bearings with integrated sensors," The Tribology, No. 280, Shinjusha Co., Ltd., pp. 42-43, 2010.

Photo of author

---



Kentaro NISHIKAWA

Automotive Business HQ  
Axle Unit Engineering Dept.

# Hub Bearing for Severe Environments

Yasushi SHIBATA\*



With the increase of automobile demand in emerging markets, the number of cars driven in severe environments, such as on unpaved roads or in cold and snowy weather, is increasing.  
 A hub bearing for use in such severe conditions is introduced in this report.

## 1. Introduction

Recently, demands for cars have been ever increasing in many emerging countries and many of these cars are traveling on poor roads including unpaved roads. In this context, automotive hub bearings are expected to meet increased muddy water resistance and load bearing capacity.

During long distance transportation of automobiles on railway freight cars in cold weather, raceway surfaces on automotive hub bearings can develop fretting owing to shocks that occur when freight cars pass rail joints: as a result, the hub bearings can develop abnormal noise and premature failure.

This paper hereunder describes NTN's unique "hub bearing for severe environment (or, severe environment-capable hub bearing)" that helps solve the above-mentioned problem and contributes to reliability of automobiles.

## 2. Development Concept and Structure

Typical severe environments which automotive hub bearings can experience include:

- Ingress of muddy water into hub bearing as cars more frequently travel on muddy road.
- Excessive loading onto the hub bearings as cars travel on poor roads and/or carry excessively heavy cargos.
- Possible fretting wear resulting from long distance railway transportation on freight cars in cold weather.

Focusing on a design concept for hub bearing design that can withstand these severe environments and promised designed bearing life, NTN has executed the following development projects:

- Development of an improved seal for muddy water resistance
- Development of bearing internal structure for improved load capacity (impact resistance)
- Development of grease that helps improve fretting resistance of bearing components

A typical example of the structure of a hub bearing –topic of this report – is shown in Fig. 1.

Note that the new development (severe environment-capable hub bearing) is equivalent with NTN's conventional product in terms of bearing life and torque.

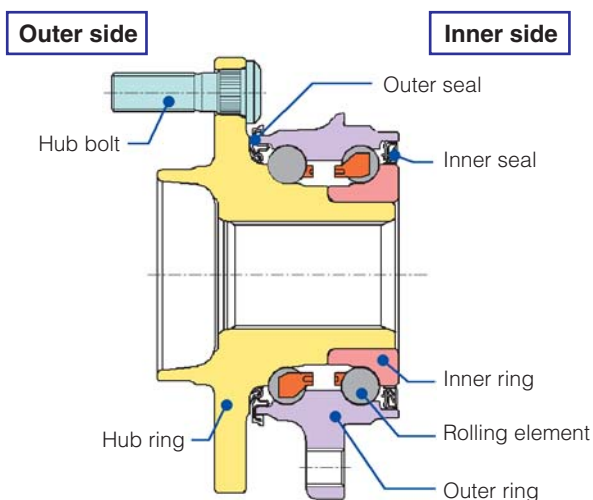


Fig. 1 Typical structure of hub bearing

\* Automotive Business HQ. Axle Unit Engineering Dept.

### 3. Development Specification

#### 3.1 Improved muddy water resistance

As illustrated in Fig. 1, there is an unavoidable difference in structure between the inner seal of a hub bearing and outer seal. Therefore, to be able to improve muddy water resistance of a hub bearing, the structures of the inner seal and outer seal have each been optimized.

##### (1) Inner seal

As shown in Fig. 2, the structure of a conventional inner seal consists of a side lip and radial lip A each intended to block ingress of muddy water from outside, and a radial lip B for containing grease prefilled in the hub bearing.

To improve muddy water resistance, the newly developed inner seal shown in Fig. 3 has side lip B in place of conventional radial lip A, and at the same time, contact width and bearing pressure between the seal lip and slinger have been optimized.

##### (2) Outer seal

As shown in Fig. 4, the structure of a conventional outer seal consists of a side lip and intermediate lip each intended to prevent ingress of muddy water from outside, and a radial lip for containing the prefilled grease.

To improve muddy water resistance, NTN's newly developed outer seal shown in Fig. 5 featuring

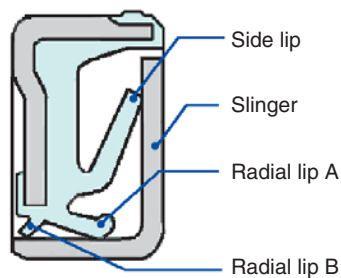


Fig. 2 Structure of a conventional inner seal

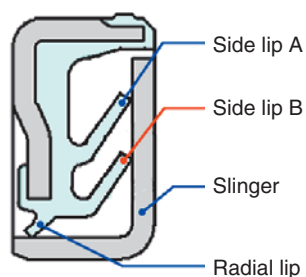


Fig. 3 Structure of the newly developed inner seal

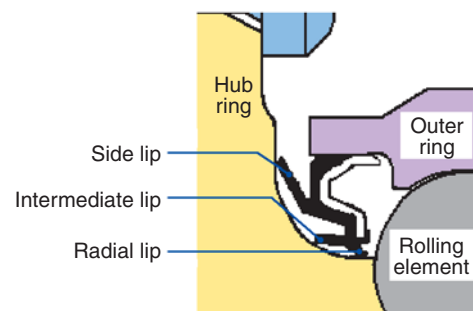


Fig. 4 Structure of a conventional outer seal

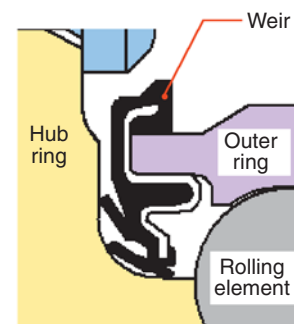


Fig. 5 Structure of the newly developed outer seal

optimized contact width and bearing pressure between the seal lip and hub ring. Similar improvements were made to the inner seal as well for blocking muddy water that possibly runs along the outer ring and penetrates the seal.

#### 3.2 Improved load capacity

When automotive tires roll on unpaved road or ride on a curb, an abnormally large load will momentarily act on the hub bearings. When greater load acts on a hub bearing, the contact area between the raceway surface and rolling element shifts toward the shoulder edge of the raceway as shown in Fig. 6; thereby causing the rolling elements to ride on the raceway shoulder edge. Consequently, stress concentration can occur on the shoulder edge of the raceway and impact dents tend to occur in this area.

Consequently, when rolling elements roll over the so-formed fretting marks, abnormal noise and vibration can occur as schematically illustrated in Fig. 7.

To inhibit the occurrence of impact denting, a straight section has been added as shown in Fig. 8 toward the tangential direction from a conventional raceway shoulder so that the height of raceway shoulder is increased. With this arrangement, the tendency of the rolling elements riding onto raceway shoulder is limited to help reduce stress concentration at raceway shoulder.

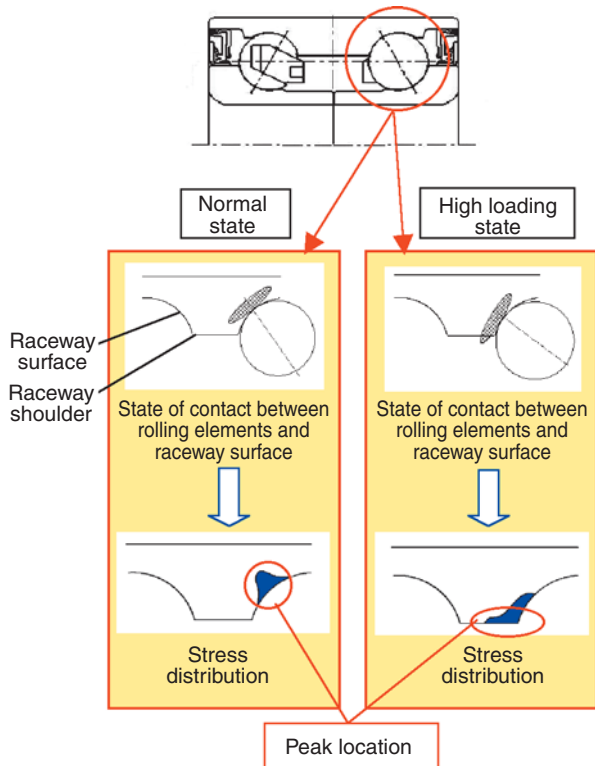


Fig. 6 State of raceway shoulder

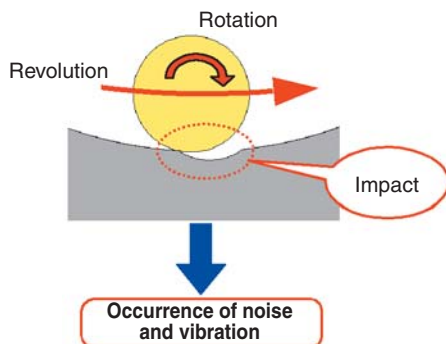


Fig. 7 Mechanism of occurrence of noise and vibration

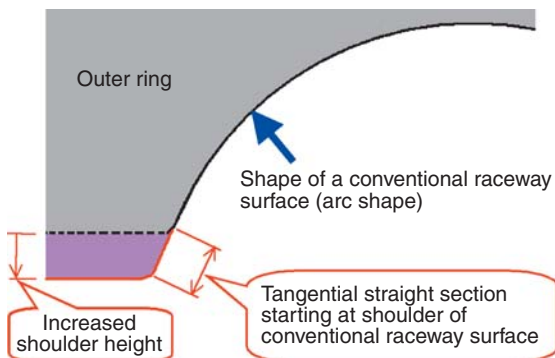


Fig. 8 New raceway design

### 3.3 Fretting resistance enhancing grease

During long distance transportation of automobiles on railway freight cars, minor oscillations will occur between the raceway surfaces and the rolling elements in automotive hub bearings; thereby fretting wear can result as schematically illustrated in Fig. 9.

In minor oscillation mode, a portion of grease between the raceway surface and rolling elements will be pushed out of the contact path; consequently, metal-to-metal contact will occur, possibly leading to fretting wear. In a cold weather situation, the fluidity of grease will be further deteriorated; thereby fretting wear can occur more frequently.

To address this problem, NTN has adopted improved grease additives to help generate a reactionary film between the raceway surface and rolling elements in addition to an oil film in order to inhibit the occurrence of metal-to-metal contact situation.

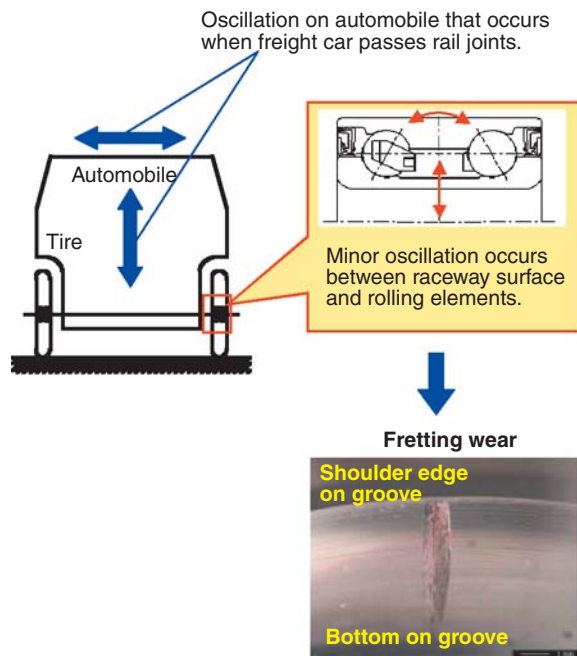


Fig. 9 Mechanism of occurrence of fretting wear

## 4. Assessment Test

To verify the advantages of NTN's "severe environment capable hub bearing", in terms of muddy water resistance, load capacity and fretting resistance, this bearing type has been subjected to rig assessment tests (1) through (3) summarized below:

- (1) Muddy water resistance: Muddy water resistance test for seal
- (2) Load capacity (impact resistance): Static high-load bearing test
- (3) Fretting resistance: Fretting wear test with newly developed grease

### 4.1 Muddy water resistance

To assess the muddy water resistance of NTN's severe environment-capable hub bearing, the bearing samples were repeatedly run and stopped with their seals submerged in muddy water up to their axial center.

The degree of mud water resistance for each hub bearing sample has been determined based on the number of cycles run at which muddy water has overcome the seal.

As shown in Fig. 10, it has been verified that both the newly developed inner seal and outer seal feature muddy water resistance twice as great compared with conventional seals.

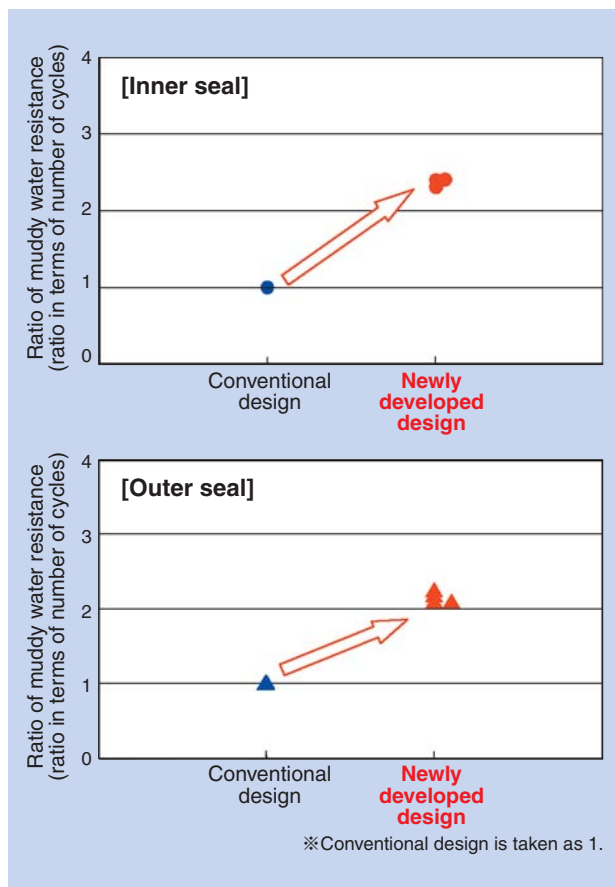


Fig. 10 Muddy water test result

### 4.2 Improved load capacity

To assess load capacity (impact resistance) of NTN's newly developed hub bearing, bearing samples were subjected to a static load equivalent to a cornering force of 2G or greater on a vehicle to simulate lateral collision to curb. Thereby, stress distribution was analyzed and impact testing was performed for the newly developed hub bearing.

As illustrated in Fig. 11, the analysis result shows that the newly developed shape of the raceway surface positively reduces stress occurring on the raceway shoulder.

In addition, as a result of the impact test, it has been learned that the depth of impact dents on the raceway shoulder using the improved shape is approximately 1/4 as deep compared with the conventional raceway shape as shown in Fig. 12.

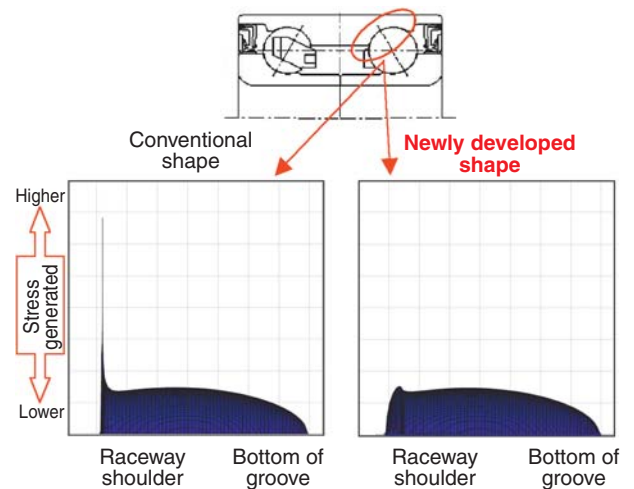


Fig. 11 Result of stress distribution analysis on raceway surface

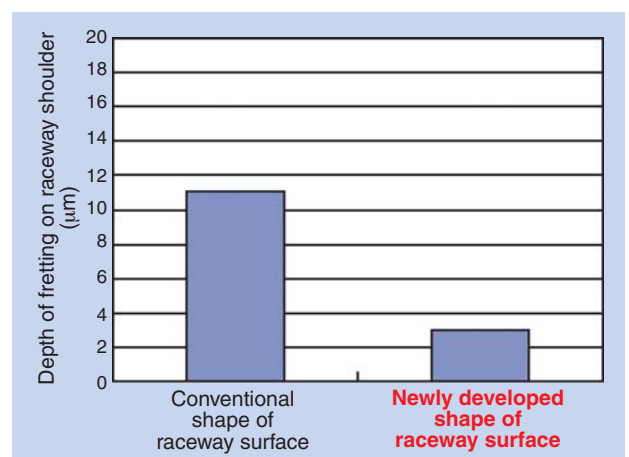


Fig. 12 Typical result of fretting test

### 4.3 Fretting resistance

A fretting wear test was performed by alternately applying lateral load and longitudinal load to the hub bearing samples, simulating a vibration pattern occurring in automobiles transported by railway.

As shown in Fig. 13, depth of fretting wear on raceway surface lubricated with conventional grease under unusually low temperature is as great as 10 times or more compared to when the bearing is at operating temperature. In contrast, since the additive in the newly developed grease helps generate a reactionary film between the steel balls and raceway surface, severity of fretting on the raceway surface lubricated with the improved grease under lower temperature is equivalent to raceway surface lubricated with the same grease under operating temperatures.

Additionally, NTN has executed test requirements the bearing needs to meet, other than fretting resistance, which include bearing life, high speed grease life, and running torque, thereby NTN has found that the performance of NTN's newly developed grease is equivalent to or better than conventional grease.

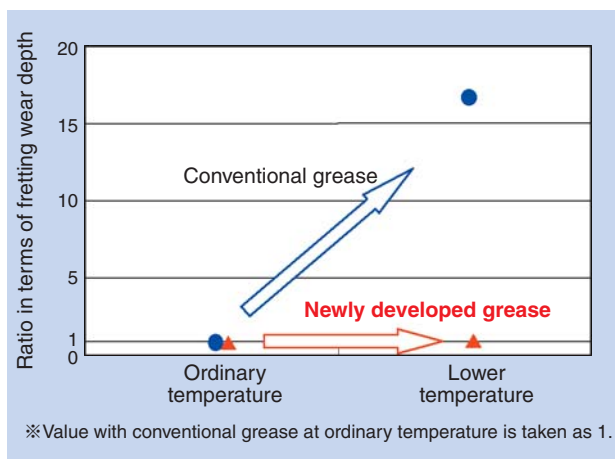


Fig. 13 Result of fretting wear test

### 5. Conclusion

NTN has developed a unique “severe environment-capable hub bearing” that boasts improved muddy water resistance, improved load capacity, and improved cold weather fretting resistance. These improvements allow for increased performance in severe environments where the road conditions are poor and vehicles are transported by rail over extended distances. As the demand for automobiles continues to increase in emerging countries, automobiles are expected to be used in increasingly demanding environments. To address this situation, NTN will further improve its technology described in this report.

### Reference

- 1) Shibata, K., Norimatsu, T., NTN Technical Review No. 75, p. 31, 2007.
- 2) Nagatani, H. and Imou, A., "Contact Pressure and Shear Stress Analysis on Conforming Contact Problem," Journal of Advanced Mechanical Design, Systems, and Manufacturing, Vol. 2, No. 6, pp. 1055-1066, 2008.

Photo of author



Yasushi SHIBATA  
Automotive Business HQ  
Axle Unit Engineering Dept.

## Lightweight and High-efficiency Drive Shafts for Rear-wheel-drive Cars



Tatsuro SUGIYAMA\*  
Yuichi ASANO\*

A lightweight and high-efficiency drive shaft designed exclusively for rear-wheel-drive cars with a mass reduction by 16% and a torque loss rate reduced by 40% in comparison with conventional products.

### 1. Introduction

Constant velocity joints (hereinafter referred to as CVJ) are often used for automotive drive shafts. Front-wheel-drive (FWD) cars such as a one shown in Fig. 1 use fixed CVJ (for example, NTN's EBJ) on the tire side because of greater operating angle. In the engine side, the CVJ must be capable of sliding in axial direction to compensate for suspension movement (for example, NTN's ETJ) is used.

On the other hand, rear-wheel-drive (RWD) cars can use a tire-side CVJ whose operating angle is not greater than 23°. Thus, RWD cars can adopt mounting procedure for fixed and plunging CVJs reverse to that of FWD cars, or may utilize drive shafts whose both sides are capable of plunging.

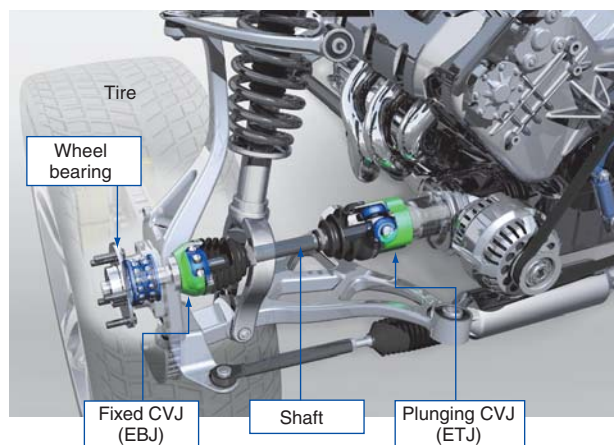


Fig. 1 Construction of drive shaft for FWD cars

Recently, needs for more compact, lighter, more efficient drive components have been mounting to reduce fuel consumption in addressing environmental conservation. This trend is also true with luxury cars of larger engine displacement.

Generally, RWD cars use CVJs whose design specification is identical to that of CVJs for FWD cars. Nevertheless, NTN has newly developed high performance drive shaft dedicated to RWD cars. This drive shaft is intended for luxury RWD cars that require an amply sized (high load capacity) drive shaft: this product is compact, light-weight, much more efficient rear wheel-dedicated drive shaft that contributes to lighter car design and improved fuel economy.

This special rear wheel drive shaft consists of two sets of newly developed compact, light-weight, highly efficient cross groove type plunging CVJs that are coupled with each other via a light-weight hollow shaft. The structure and features of this new product are hereunder described.

### 2. Structure of Newly Developed Driveshaft

The structure of NTN's newly developed drive shaft is shown in Fig. 2

Both ends of this drive shaft are each equipped with a cross groove type plunging CVJ featuring improved efficiency and smaller size through increasing the number of balls as compared with conventional cross groove CVJ's, wherein both CVJ's are linked with a light-weight hollow shaft not undergoing any drawing processes.

\* Automotive Business HQ. C.V. Joint Engineering Dept.

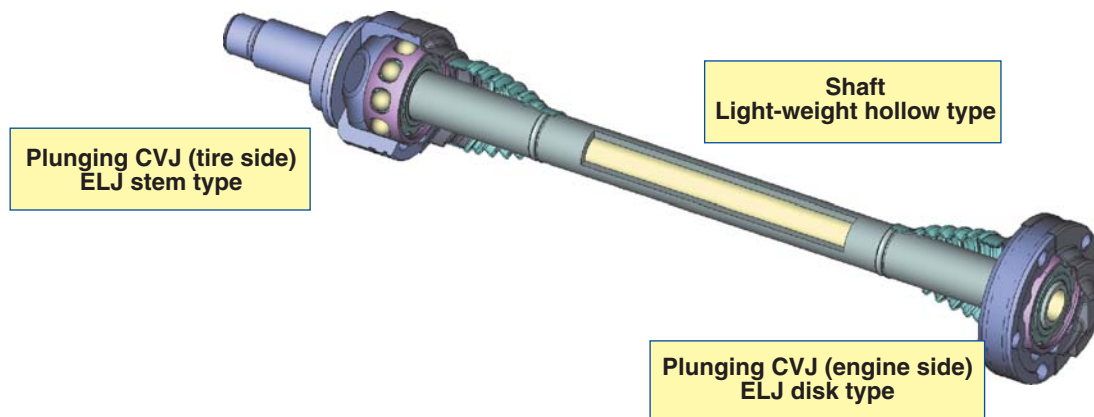


Fig. 2 Newly developed construction of drive shaft for RWD cars

Various structures are available for installing CVJ to car bodies. On an example in Fig. 2, the mount system in tire side of CVJ is stem mount system where the splined shaft end of CVJ is fitted into the counterpart (hub) and the mounting system in the differential side of CVJ is a disk mount system where the shaft end of differential side is bolted down to the companion flange; thereby, stem specification may be applied to both drive shaft ends.

The two CVJs on both ends of drive shaft may be identical in terms of their internal structure; thereby, the plunging CVJs at both ends of drive shaft can both accommodate axial displacement.

Compared with conventional cross groove CVJ (NTN's LJ), the NTN's newly developed CVJ has an increased number of balls of smaller diameter. This new CVJ design has contributed to higher efficiency and much compact size of drive shaft.

This unique CVJ has been designated "ELJ" that constitutes a part of NTN's E series constant velocity joint products boasting light weight, compact size and higher efficiency.

In addition, the light-weight hollow shaft for coupling the two ELJ CVJs is joined to the inner rings by amply sized splines; thereby, the thin-walled shaft having near-uniform bore diameter and outside diameter over the entire shaft length can be designed, and this feature contributes to realization of light-weight drive shaft. This drive shaft is very unique in that it does not require drawing at the shaft ends that is necessary for standard splined joint on a conventional hollow shaft (refer to Figs. 2 and 8).

### 3. High-Efficiency Plunging CVJ (ELJ)

#### 3.1 Construction and features of newly developed CVJ

NTN's conventional cross groove plunging CVJ "LJ" has six cross grooves for rolling balls on the inner ring and outer ring; wherein, these grooves are oriented inclined toward the circumferential direction and two adjacent grooves are inclined in reverse directions (refer to Figs. 4 and 5). The balls are held at the intersection points between cross grooves on inner ring and outer grooves (grooves on the inner ring are inclined in the direction opposite to that of grooves on outer ring), all the balls are situated on a common plane in a bisector with the cage; thereby, the CVJ can run at constant speed while the inner ring can slide in the axial direction.

Fig. 3 shows an exploded view of NTN's newly developed cross groove CVJ "ELJ", and Fig. 4 gives an exploded view of conventional cross groove CVJ "LJ". Compared with "LJ", "ELJ" features increased number of balls of smaller diameter, and inclination of cross grooves on inner ring and outer ring is smaller; thereby the ELJ CVJ is capable of maximum operating angle equivalent to that of conventional CVJ "LJ" while achieving compact size, lighter weight and more efficient torque transmission.

Table 1 summarizes characteristics of NTN's newly developed cross groove plunging CVJ "ELJ" as compared with those of conventional cross groove CVJ "LJ". Fig. 5 schematically illustrates difference between the newly developed cross groove CVJ and conventional cross groove CVJ in terms of inclination of their cross grooves by referring to cutaways of their disk type outer rings.

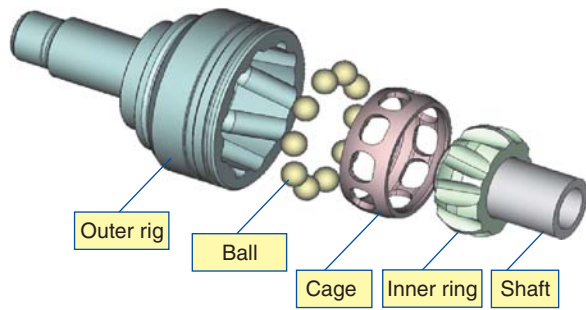


Fig. 3 Newly developed cross groove type CVJ "ELJ"

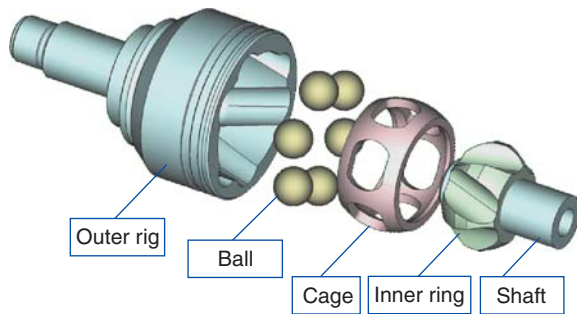


Fig. 4 Conventional cross groove type CVJ "LJ"

Table 1 Comparison of characteristics of ELJ with those of LJ

	Newly developed ELJ	Conventional LJ
Number of balls	10	6
Inclination of cross groove	Low	High
Max. operating angle	23 deg	23 deg

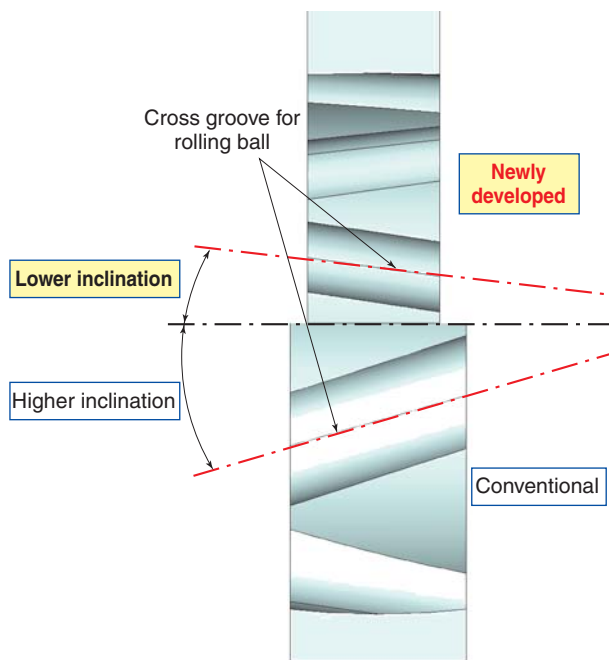


Fig. 5 Schematic illustration of inclination of cross groove for rolling balls

### 3.2 Reduced size and weight with "ELJ"

As previously mentioned, "ELJ" has achieved smaller size through size reduction and increase in number of balls and decrease in inclination of cross grooves for rolling balls. At the same time, smaller ball size allows the wall thickness of the inner ring to be greater; consequently, the diameter of splined bore of inner ring to be joined to the splined shaft end can be greater. As a result, the axial dimension of inner ring can be further reduced; thus the weight of inner ring has been much reduced.

In Fig. 6, a cutaway of the newly developed stem outer ring type ELJ109 (109 is designation of NTN's drive shaft) is compared with that of conventional design. Compared with conventional design, the outside diameter of ELJ 109 is approximately 9% smaller and weight reduction with the joint alone has amounted to approximately 22% (2.63 kg to 2.05 kg).

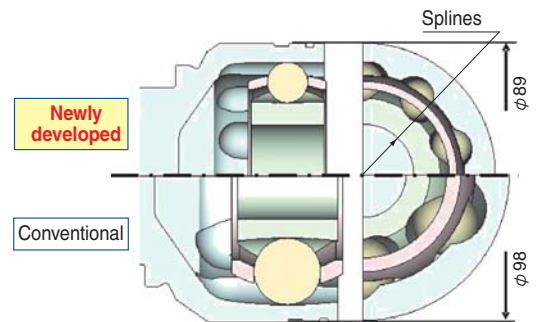


Fig. 6 Comparison of cutaway of ELJ with that of conventional cross groove type CVJ

### 3.3 Efficiency enhancement for ELJ

Smaller ball size, increased number of balls, and reduction in inclination of cross grooves on inner ring and outer ring each help improve efficiency of CVJ.

Reduction in inclination of cross grooves helps reduce axial sliding friction on the balls, and decrease the shift of balls; consequently, torque loss is much decreased.

Fig. 7 shows the result of torque loss reduction ratio with ELJ with the operating angle of CVJ kept at 5 degrees. Compared with conventional "LJ", the torque loss with the newly developed "ELJ" is approximately 40% smaller.

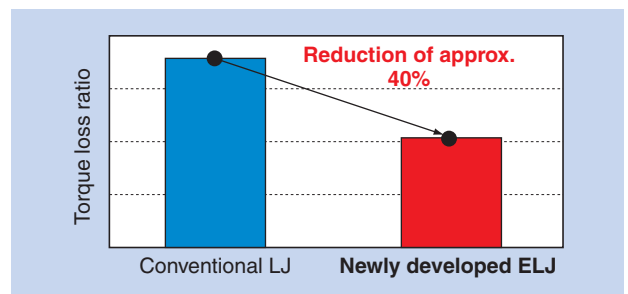


Fig. 7 Torque loss reduction ratio with ELJ

#### 4. Light-weight hollow shaft

Conventional hollow shafts used in drive shafts have limitation in size of splined section because as shown by the lower example in Fig. 8, a smaller diameter is adopted for shaft end while maintaining sufficient wall thickness for the inner ring. Since necessary strength needs to be maintained for shaft end even with a smaller diameter, the shaft end is subjected to drawing to provide greater wall thickness for this area.

The newly developed drive shaft is dedicated to RWD applications, and will not be operated at greater operating angle. Furthermore, adoption of the newly developed "ELJ" helps enlarge the splined section for joining to the inner ring as previously explained in Sec. 3.2; consequently, as shown by the upper example in Fig. 8, the newly developed hollow shaft does not need drawing on either end. This is because the NTN's newly developed drive shaft technology allows the diameter of splined section on shaft end to be larger; consequently, sufficient mechanical strength can be provided for both ends of the hollow shaft without modification of both ends to increase wall thickness.

NTN's new hollow drive shaft features thinner wall thickness, with its bore diameter and outside diameter remaining uniform over nearly entire longitudinal dimension. This feature helps to further reduce the weight of drive shaft. For comparison purpose, a hollow shaft whose outside diameter at its midpoint is equal to the newly developed drive shaft, with both ends subjected to a drawing process such that its both ends have strength equivalent to the newly developed drive shaft; then the weight of this comparison hollow shaft was compared with the new drive shaft. Consequently, it has been found that the NTN's new

hollow shaft achieved weight reduction of approximately 18%. Thanks to this weight reduction, hollow drive shaft may have greater wall thickness to enhance rigidity of the hollow shaft provided that increase in wall thickness does not lead to weight of drive shaft greater than that of conventional design.

#### 5. Conclusion

- (1) NTN's newly developed rear wheel drive shaft achieves approximately 16% of weight reduction\*1 by adoption of "ELJ" + thin-walled hollow shaft + "ELJ".
- (2) Adoption of "ELJ" realizes approximately 40% reduction in torque loss\*2 (higher efficiency)
- (3) Adoption of "ELJ" realizes approximately 9% of reduction in outside diameter\*2 (outside diameter of stem outer ring type).
- (4) Adoption of thin-walled hollow shaft that has not undergone the drawing process on either end leads to further weight reduction.

\*1 Comparison in weight of drive shaft assembly with conventional design LJ + hollow shaft (drawn shaft ends).

Total of approximately 16% weight reduction by stem outer ring type CVJ (Sec. 3.2, approximately 22% weight reduction) + hollow shaft (Sec. 4, 18% weight reduction) + disk outer ring type CVJ.

\*2 Comparison with conventional LJ.

Compared with conventional LJ, NTN's newly developed drive shaft (ELJ) dedicated to rear wheel drive cars has achieved size reduction, lighter weight and higher transmission efficiency. As people are going to be more eco-conscious, NTN will apply its improved drive shaft technology to automobiles that need higher efficiency in transmitting driving power.

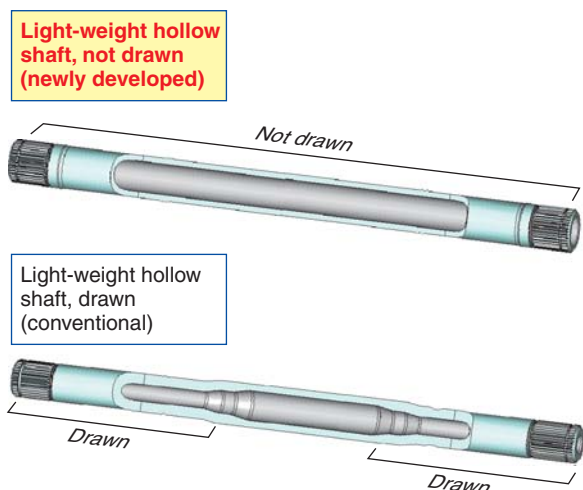


Fig. 8 Comparison of hollow shafts in terms of shape

#### Photo of authors



Tatsuro SUGIYAMA  
Automotive Business HQ  
C.V. Joint Engineering Dept.



Yuichi ASANO  
Automotive Business HQ  
C.V. Joint Engineering Dept.

## Ball Screw Unit for Automotive Electro-actuation

Koji TATEISHI\*



In the automotive market, numerous new hybrid cars and engines with low fuel consumption and low emissions have been developed to reduce CO<sub>2</sub> emissions and to make their exhaust cleaner. At the same time, many projects are being undertaken to achieve greater car amenities and safer driving by applying quick and reliable electric motor drives utilizing ball screws.

NTN started to develop new ball screw units and actuators in the 1990s. Now there are some ball screw products that are modularized with peripheral parts. This article introduces the results of development and the features of these ball screw and actuator units.

### 1. Introduction

Fuel economy of automobiles was dramatically improved when hydraulic pumps for auxiliary engine systems were superseded by electromechanical actuation system (adoption of driving system that are based on electric motors) that run only when the auxiliary engine systems need to operate. Control-by-wire systems for controlling automobiles, such as shift-by-wire or throttle-by-wire, have recently become more commonly commercialized. In the present day European car markets, brake-by-wire control technology is being commercialized.

NTN has developed and is currently marketing unique quick-response, high-thrust automotive electromechanical ball screw units that can be used in electromechanical control-by-wire actuators for the above-mentioned automotive applications.

This paper hereunder describes automotive electromechanical ball screw unit and electromechanical ball screw actuator (hereinafter referred to as "actuator unit" ) NTN has developed.

### 2. Structure and Features of Automotive Electromechanical Ball Screw

Being common with any rolling bearings, ball screw units include rolling mechanism involving balls. Thus, ball screw units have been often used on industrial machines as machine elements that can efficiently convert rotary motion into linear motion.

However, this useful mechanical component has failed to achieve wider support in the automotive component market because the conventional ball screw unit design does not meet productivity needed for mass production and at the same time the ball circulator—a key mechanism in ball screw— may fail to satisfy durability requirement of 10 operating years or 0.30 million km of distance traveled. So that ball screw units can be applied to automotive applications, NTN has begun development activities that are to be described in the following sections.

#### 2.1 Improved reliability for ball circulator

Previously, a return tube type ball circulator has been widely used because of the relative ease of design and manufacture. Fig. 1 illustrates a typical example of a return tube type ball circulator.

Because this type of ball circulator uses a ball picker it needs improved mechanical strength, NTN adopted a deflector type ball circulator for automotive

\* Automotive Business HQ. Axle Unit Engineering Dept.

applications. **Fig. 2** illustrates a typical example of deflector type ball circulator.

NTN's deflector is first inserted into the bore side of the nut and then fixed to the nut by a staking technique, thereby the deflector boasts improved reliability and compact size.

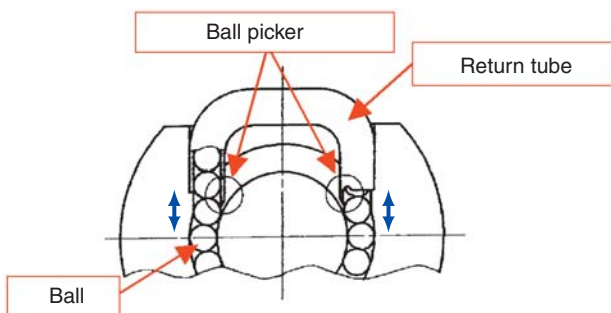


**Fig. 1** Return tube type ball circulator

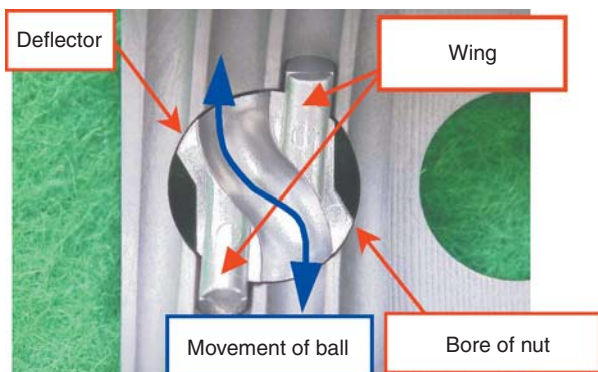


**Fig. 2** Deflector type ball circulator

## 2.2 Improved productivity

Previously, the threaded groove of the ball screw had been formed by grinding with a grinding wheel. To be able to reduce consumption of grinding wheels and decrease machining energy used through size reduction of machining equipment, NTN has developed a ball screw machining technique that does not involve a grinding operation.

To generate the thread groove on a screw shaft, a precision thread rolling process that uses roller dies is adopted to form thread grooves in one pass. Then, the screw shaft is subjected to a newly adopted induction hardening process that does not generate scale, thereby machine cycle time has been reduced. **Fig. 3** shows the appearance of the thread grooves on the screw shafts: one example having undergone the conventional induction hardening process and the other example having undergone NTN's newly developed induction hardening process.

Generation of the thread groove on the bore surface

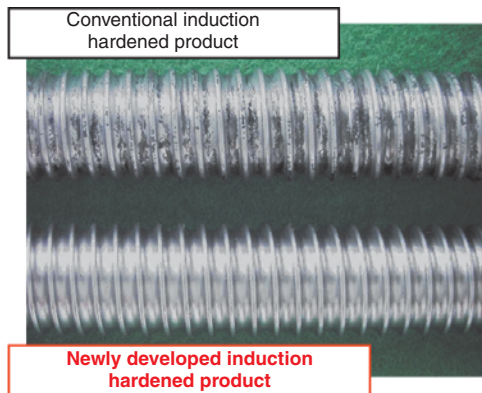


**Fig. 3** Appearance of thread groove on screw shaft



**Fig. 4** Appearance of thread groove on nut

of the nut was a challenge in particular when seeking high precision finish. By adoption of a CNC-controlled high-precision cutting technique, NTN has successfully formed thread grooves on the bore surface of the nut without involving grinding operation, wherein the so-formed thread groove boasts sufficient durability and operability. **Fig. 4** shows the appearance of thread grooves on the bore surface of a nut achieved by NTN's unique high-precision cutting process.

## 3. Application of Electromechanical Ball Screw Unit to Electromechanical Actuator

NTN's experience in the development work for electromechanical ball screw units and actuator units that NTN has already marketed is hereunder described.

### 3.1 Ball screw unit for automotive automated manual transmission

Automated manual transmission (AMT), which automates manual transmission to improve fuel economy and driver's comfort, are seeing increased use.

Conventional AMT's have typically been hydraulically or pneumatically operated, but they have drawbacks in that hydraulic or pneumatic actuation systems involve a lot of components. This large

number of components leads to relatively large friction which in turn leads to poor efficiency and the inability to achieve greater thrust; or slow response.

To be able to solve these problems, NTN has adopted a ball screw driving system for a gearshift actuator for automated manual transmission on compact trucks.

### 3.1.1 Appearance of AMT

Fig. 5 shows the typical appearance of an AMT that incorporates a gear shift actuator. A gearshift actuator is mounted on top of the transmission that is originally designed for manual gearshift operation to automate the transmission without much modification to the structure of transmission.

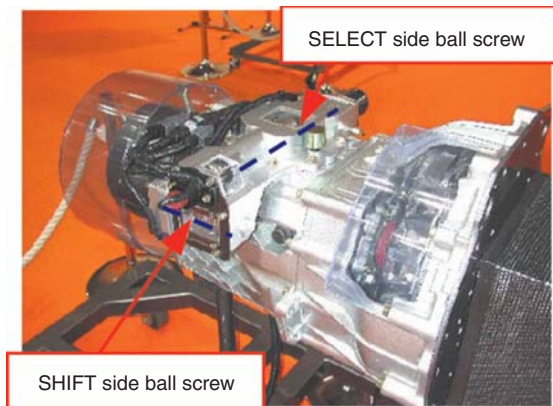


Fig. 5 Appearance of AMT

### 3.1.2 Features of ball screw for AMT

The ball screw unit adopted for this mechanism has the functionality and durability sufficient enough for automotive applications. Fig. 6 shows the appearance of the newly developed ball screws.

The ball screw converts rotary motion into linear motion at higher efficiency, and develops higher thrust. For this reason, an AMT can be used while maintaining the existing basic structure that was originally intended for manual gearshift operation.

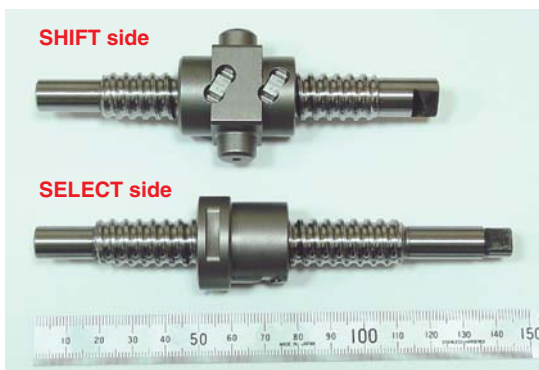


Fig. 6 Ball screw for AMT

### 3.2 Ball screw unit for variable valve system

Most automotive gasoline engines are four-stroke engines that feature four steps of operation—intake of an air-gasoline mixture into the engine, compression and combustion in the engine, and exhaust from the engine.

The very mechanical component that governs this cyclic operation is the intake & exhaust valves in the engine. It is possible to improve fuel economy or power of a given automobile by varying the timing for the opening/closing of these valves, or their vertical stroke (lift).

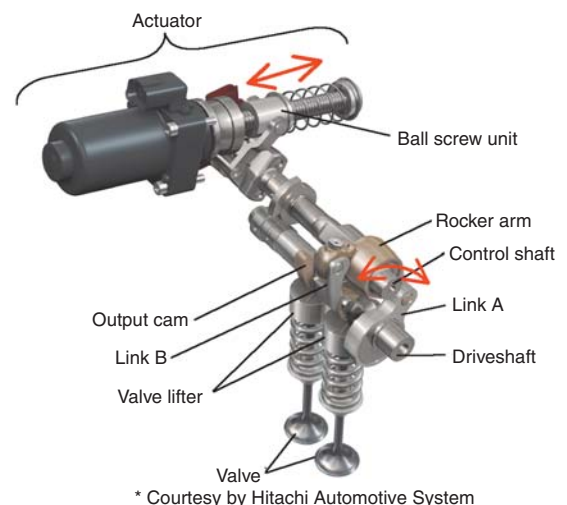
Recently, the need to reduce CO<sub>2</sub> emissions within the automotive industry has been mounting in order to help improve the global environment. In this context, development activities are in progress in the automotive industry for a stepless-variable valve mechanism that is capable of more delicate valve control. In the EU market, marketing of a worm gear-based mechanism for this purpose began several years ago. Opposite the worm-gear based valve control system there is the ball screw design, that offers low friction and high efficiency. NTN has developed a unique ball screw unit that boasts a compact mechanism, higher reliability (safety) and quick response.

#### 3.2.1 Structure of variable valve system

Fig. 7 shows the layout of a variable valve system NTN has adopted.

On this mechanism, rotary motion on the driveshaft having an eccentric cam is translated into vertical motion on the valve lifter via a plurality of links (link A, rocker arm, link B, and output cam).

During this course, the relation between the phase of the actuator and the control shaft coupled to the actuator is changed to alter the positional relation



\* Courtesy by Hitachi Automotive System

Fig. 7 Appearance of variable valve system

among the links to invariably control the lift and operating angle of a valve in the valve system.

When mounted to an automobile, this variable valve system helps improve output and response of the engine: consequently, improvements will be achieved not only in fuel economy but also in cleanness of emissions. In particular, fuel economy is said to be improved by approximately 10%.

### 3.2.2 Features of ball screw unit for variable valve system

The ball screw unit adopted for the variable valve system has sufficient durability for withstanding loading from the valve.

In particular, to axially locate the bearing on the ball screw shaft, a lock nut and retaining ring are usually used. In contrast, a bearing is fixed to NTN's newly developed screw shaft by a staking technique with which a part of the shaft is allowed to develop plastic deformation by staking to lock the bearing. The force needed to extract the bearing, which has been fixed to the ball screw shaft by staking technique, is at least 10 times as great as the maximum axial load acting on the ball screw shaft.

### 3.3 Actuator unit

To be able to further reduce the size and weight of the previously mentioned ball screw unit, NTN has

proceeded with unitization that covers auxiliaries and developed an automotive actuator unit that boasts quicker response and greater thrust.

#### 3.3.1 Structure of actuator unit

Fig. 9 shows the appearance of NTN's actuator unit, and Fig. 10 schematically illustrates a cutaway of this actuator unit.

According to the design specification of the actuator unit, the efficiency for converting forward/reverse rotary motion into linear motion with the ball screw has to be 90% or higher.

The operating shaft is supported by a liner ball bearing in a rolling contact mode; thereby friction on the screw shaft is low and the ball screw runs smoothly.

#### 3.3.2 Features of actuator unit

##### (1) Higher thrust

Higher efficiency with the ball screw helps the actuator unit to develop higher thrust.

Fig. 11 shows thrust measurements with NTN's newly developed actuator unit. NTN's actuator unit develops thrust nearly equivalent to that found via theoretical calculations (1200 N): also, the actuator unit has been earning a good reputation from its users. Note that a sliding screw unit of the same size develops thrust as low as approximately 1/3 that of NTN's actuator unit because of greater frictional forces occurring on it.

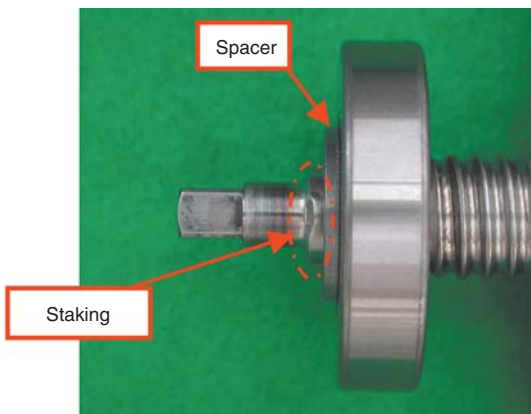


Fig. 8 Appearance of bearing staking



Fig. 9 Ball screw actuator unit

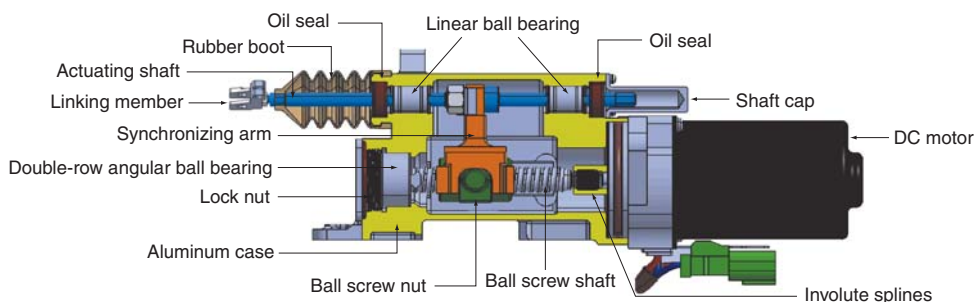


Fig. 10 Structure of actuator unit

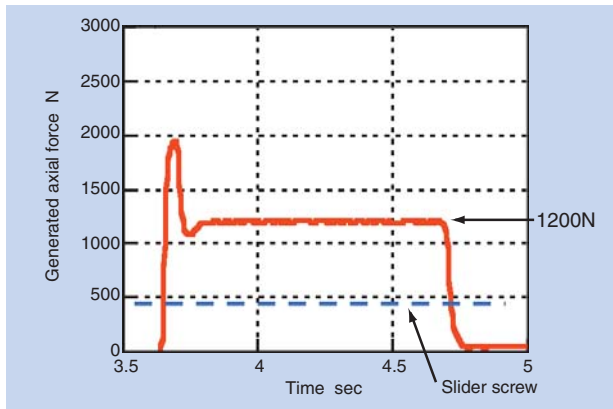


Fig. 11 Thrust force measurements

**(2) High reliability**

For proving immunity to severe environment, NTN's actuator unit has been subjected to durability tests under a specified load within high-temperature atmosphere. To assess performance of the actuator unit having undergone durability test, the actuator unit has been further subjected to response testing by checking operating time measurements.

Even after testing, the actuator unit has maintained its high response capability: no deterioration is found even after durability testing as can be seen in Fig. 12.

Aiming principally at shift-by-wire control system, NTN has developed a novel actuator unit that boasts compact structure with a built-in position sensor, and has already been marketing this novel product. Fig. 13 shows appearance of this actuator unit.

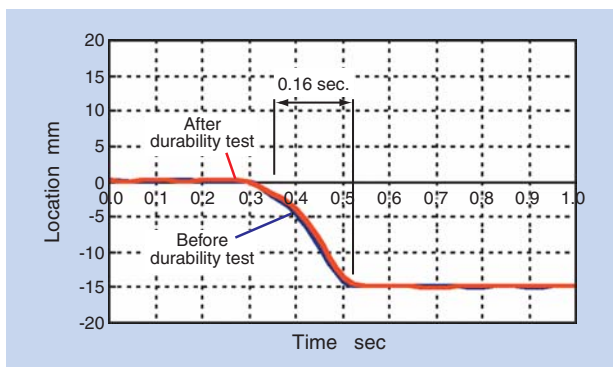


Fig. 12 Operating time measurements



Fig. 13 Shift-by-wire electromechanical actuator unit

**4. Conclusion**

This paper has thus described NTN's newly developed electromechanical ball screw unit that is applied to electromechanical automotive mechanisms.

In electromechanical applications for automotive components, there have been examples of adoption of a planetary roller screw as a novel mechanism. Nevertheless, because ball screw units consist of a smaller number of components and feature simplicity in structure, car designers will increasingly consider adoption of ball screw drive systems in their designs.

In addition to development of ball screw materials of higher reliability and improvements in heat treatment and machining techniques, NTN is also committed to development for further improvement in efficiency of ball screws, which is an outstanding advantage of the ball screw actuator.

At the same time, NTN is attempting to realize higher functionality, a reduction in size and weight with the actuator unit, and will remain committed to the further expansion of the scope of applicability of its actuator unit products.

**Reference**

- 1) Tateishi, K., et al., "Ballscrew for Automated Manual Transmission," NTN Technical Review, No. 73, pp. 72-75, 2005.
- 2) Kazuno, K., "Ball-screw Unit for Variable Valve Event and Lift System," NTN Technical Review, No. 75, pp. 72-77, 2007.
- 3) Ikeda, Y., et al., "Electric Ball Screw Actuators for Automobiles," NTN Technical Review, No. 77, pp. 45-48, 2009.
- 4) Hamamura, Y., et al., "Developing a New 2.0L Gasoline Engine with a Continuous Variable Valve Train" Transactions of the 2007 (Autumn) Congress of the Society of Automotive Engineers of Japan, pp. 17-22, 2007.

Photo of author



Koji TATEISHI

Automotive Business HQ  
Axle Unit Engineering Dept.

# Low-torque Deep-groove Ball Bearings for Transmissions

Katsuaki SASAKI\*



To achieve low fuel consumption in response to environmental concerns, we have focused on reducing the friction of tapered roller bearings.

NTN has expanded to focus on ball bearings by analyzing friction in oil lubrication and developing low-torque deep-groove ball bearings for transmissions. This paper introduces the structure and performance of these bearings.

## 1. Introduction

In addressing global environmental issues, the need for reduced running torque has been increasing for transmission bearings in order to help improve fuel economy for automobiles. As discussed in “Market and Technology Trends in the Automotive Industry” in this issue of the NTN Technical Review, there have long been active development efforts about tapered roller bearings, in which rolling elements are in line contact with the raceway surface, to reduce friction loss on automotive transmissions.



Fig. 1 Low torque deep groove ball bearing

The running torque on deep groove ball bearings, in which rolling elements roll on the raceway surface in point contact, is fairly low. Therefore, further reduction in running torque with this bearing type was believed to be near impossible. However, NTN has succeeded in reducing running torque on this bearing type by optimizing the shape of the cage.

Fig. 1 shows NTN's low torque deep groove ball bearing. This bearing type does not require installation of new production equipment.

## 2. Low Torque Deep Groove Ball Bearing

### 2.1 Structure and features

NTN's newly developed low torque deep groove ball bearing is unique in that the contact area between ball and cage is decreased by providing a recess in the pocket of the cage (guide surface for guiding balls) as shown in Fig. 2 in order to reduce oil shear occurring in this area.

Consequently, the newly developed deep groove bearing boasts approximately 25% torque reduction compared with the conventional product.

### 2.2 About torque-generating factors

As summarized in Fig. 3, there are six factors that can be responsible for torque generated on deep groove ball bearing.

Factors (1) through (4) are governed by the specification for internal design of bearing and their magnitudes can be determined by calculation.

\* Automotive Business HQ. Automotive Engineering Dept.

Magnitude of factor (5) "Shear torque on oil between cage and balls" is determined by the specification for cage, while magnitude of factor (6) "Agitation torque owing to viscosity of lubricating oil" is much affected by physical properties and amount supplied of the lubricating oil used.

In recent years, to help reduce fuel consumption of automobile, oil flow rates in automotive transmissions has been decreasing. Automotive transmissions have been increasingly lubricated with oil mist or near-

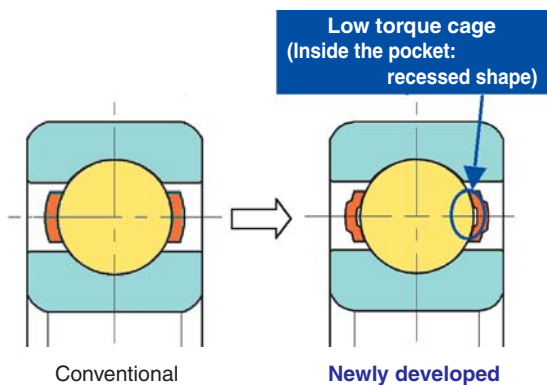


Fig. 2 Structure and features

**(1) Rolling viscosity torque on rolling surface**

Torque occurring from reactive force on the oil film that exists between the rolling surfaces and the balls.

**(2) Elastic deformation torque on balls**

Torque loss resulting from repeated elastic deformation on balls.

**(3) Torque from differential slipping**

**(4) Torque from spin slipping**

Slip torque resulting from difference in circumferential velocity between the raceway surface and the balls.

**(5) Shear torque on oil between cage and balls**

Torque resulting from shear resistance occurring on the oil between the ball guide surface and balls in the cage.

**(6) Agitation torque from viscosity of lubricating oil**

Scrape-up torque and scrape-through torque on oil resulting from actions of balls and cage.

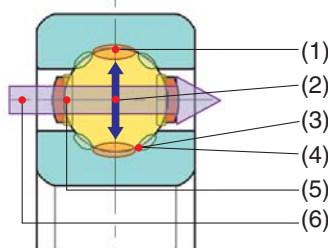


Fig. 3 Possible torque-developing factors on deep groove ball bearing

splash lubrication technique rather than oil bath system. Focusing on factor (5) that accounts for a larger percentage in torque occurred under these operating conditions with NTN's deep groove ball bearing products, NTN has attempted to develop low torque variant of the cage.

**2.3 Technique for reducing torque**

Fig. 4 illustrates share breakdown by torque-generating factors, where this data has been obtained by running NTN's deep groove ball bearing 6207 under high speed, low load conditions. Under lubrication conditions that assumes mist or splash lubrication, torque resulting from "agitation resistance with oil" is very small. Therefore, NTN has ignored this factor from its consideration about torque reduction. Factors "rolling viscosity", "differential slipping" and "elastic hysteresis loss on balls" are governed by the internal design specifications of bearing and bearing operating conditions. In other words, these factors can affect life and rigidity of the bearing.

By focusing on "shear resistance on lubricating oil in cage" that accounts for approximately 70% of share in torque generation, NTN has successfully reduced torque on deep groove ball bearing through improvement in cage design.

As can be understood from Fig. 5 and formula (1), reduction in slip area is effective to reduce shear resistance on oil in the cage. For this reason, a recess has been added inside the pockets in cages made of shaped sheet steel shown in Fig. 6 in order to reduce slip area. Consequently, the size of the contact area between the balls and cage has been reduced, thereby decreasing shear resistance from the lubricating oil.

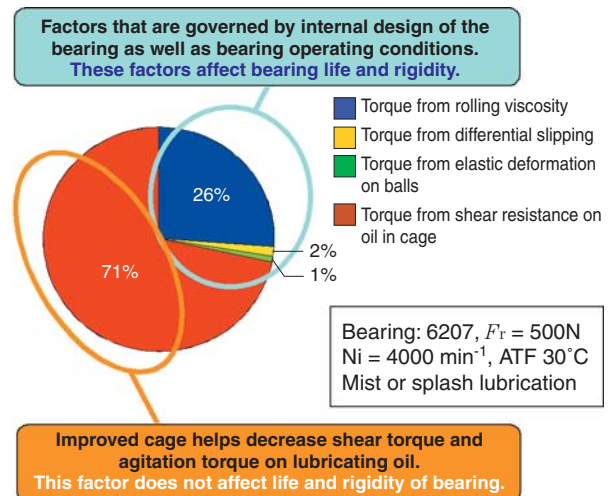


Fig. 4 Share breakdown of effects of torque-generating factors

Shear resistance  $F = \eta \frac{u}{h} s$  .....Formula (1)

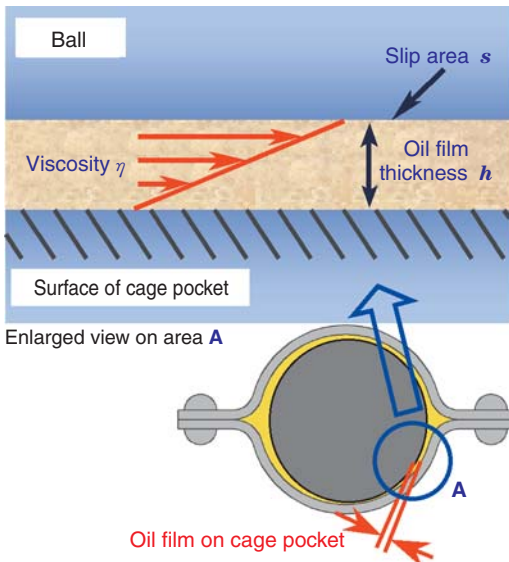


Fig. 5 Cutaway of cage pocket



Fig. 6 Low torque cage (inside of pocket)

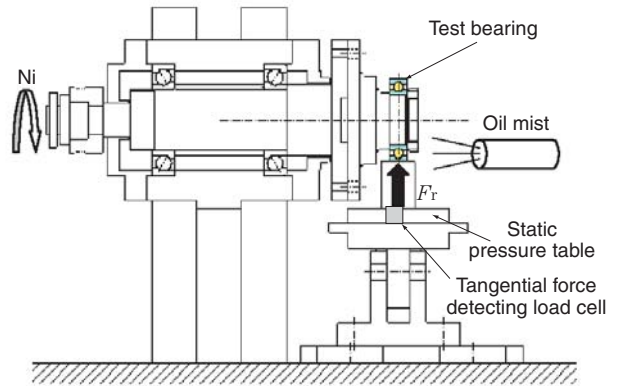


Fig. 7 Torque test rig

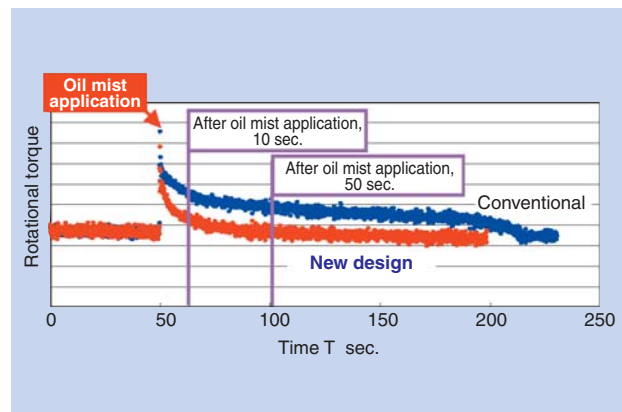


Fig. 8 Result of torque comparison test on 6207 ball bearing

## 2.4 Performance assessment

The performance of unsealed low-torque ball bearings has been tested with NTN's bearing type 6207 which is a typical bearing for automotive transmissions.

### 2.4.1 Result of torque measurement

Bearing samples were tested under the following test conditions, on the test rig and by the method summarized in Fig. 7. Fig. 8 graphically shows the result of the torque comparison test with the 6207 bearing. Due to the effect of the recess in the cage, the newly developed design shows reduced shear resistance on the oil film. The torque reduction reached as much as 25% compared with conventional design. Also, it has been verified that reduction in area of the cage pocket corresponds with the theoretical reduction in shear resistance of oil in the bearing.

- Test bearing: 6207
- Bearing dimensions:  $\phi 35 \times \phi 27 \times 17$
- Radial load: 500 N
- Bearing speed: 4,000 min<sup>-1</sup>
- Lubricating oil: ATF, 30°C, mist lubrication system

### 2.4.2 Strength of cage

For mechanical strength of the cage, the newly developed design and conventional design in Fig. 9 were compared by FEM analysis and strength testing.

- Test bearing: 6207
- Bearing dimensions:  $\phi 35 \times \phi 72 \times 17$



Fig. 9 Bearings tested

**(1) Stress analysis**

The conventional cage and the newly developed cage were subjected to loading under same conditions. The resulting stresses in these samples were compared by FEM analysis technique.

- Ball position (4): Circumferential loading of 49N\*1
- Ball position (1) to (5): (other than (4)): restrained

\*1 Equivalent to loading when 50% load torque from the engine at 2nd speed is acting on the differential-side bearing on transmission of small-displacement FF car.

Fig. 10 shows a half model of the cage, and Fig. 11 (stress distribution diagram) schematically illustrates

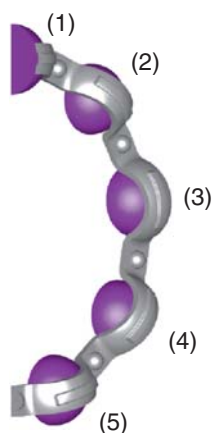


Fig. 10 Cage analysis model

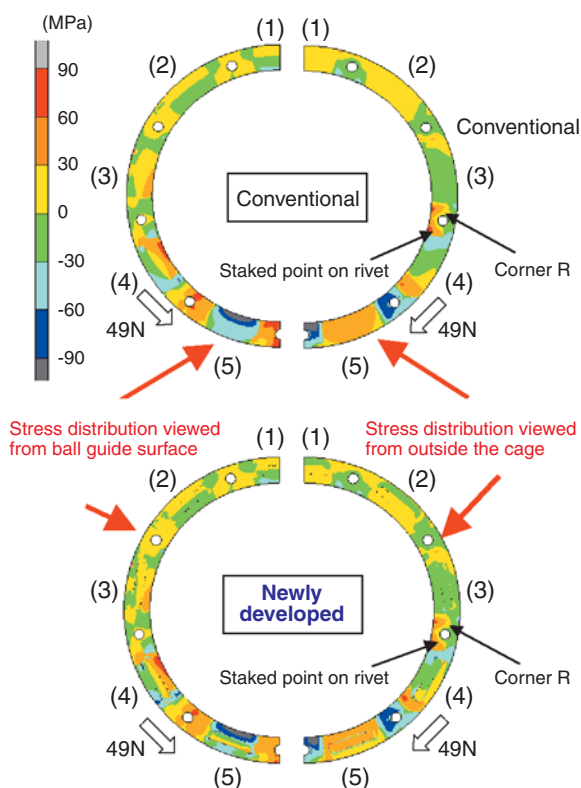


Fig. 11 Result from stress analysis

the result of analysis of the cage model. For either conventional design or newly developed design, the diagrams in the left are stress distributions viewed from the ball guide surface, and those in the right are stress distributions viewed from outside the cage.

As a result of stress analysis, it has been learned that the greatest tensile stress occurs at corner R area in the vicinity of rivet, and the magnitude of stress generated is same with both the conventional design and newly developed design. Note that stress occurs on the recess in pocket of low torque cage; however, this stress is much smaller compared to that occurring at the corner R area and does not adversely affect mechanical strength of cage.

**(2) Strength verification test**

The most frequent cause of damaged cage is excessive loading on the cage that results from delay in travel of the balls when an excessively large moment acts on the balls. To simulate this situation, excessive load was exerted on the bearing, thereby testing cage strength. Table 1 summarizes the test conditions for testing mechanical strength of the newly developed cage and conventional cage, while Fig. 12 graphically shows the test result.

Accumulated failure time and mode of failure are identical in both the newly developed cage and the conventional cage. The failure that occurred was fracture that started at corner R area and staked point on the rivet shown in Fig. 13, and correlates with the result of FEM analysis in Fig. 11. In summary, it has been positively verified that the cage of the newly developed deep groove bearing, featuring a recessed cage, has equivalent mechanical strength to the conventional product.

Table 1 Test conditions

Momental load	13.7 Nm
Bearing speed	1800 min <sup>-1</sup>
Run time	Until failure occurs.

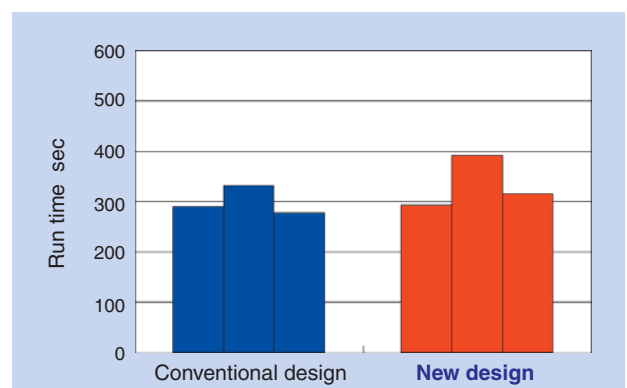
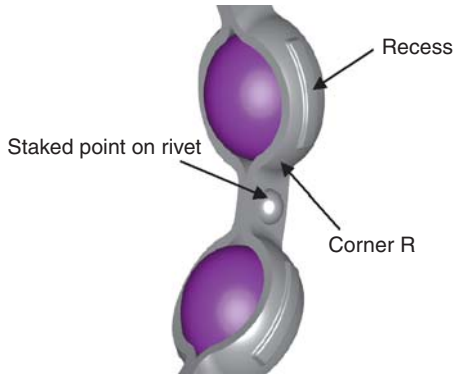


Fig. 12 Result of cage strength test



**Fig. 13** Names of areas on cage

### 3. Conclusion

This paper has described the NTN's new low torque deep groove ball bearing technology for automotive transmissions. This bearing technology boasts significantly reduced torque without loss in bearing life and rigidity. Regarding bearing production, this new technology helps realize production of improved bearing product without the need for introduction of new purpose-specific production machines. As such, NTN will market this new bearing as a major bearing product series.

### Reference

- 1) "Agitation torque that occurs with bath lubrication of rolling bearings" (reports 1 and 2), 2001 Japan Society for Precision Engineering Autumn Meeting Academic Lecture Proceedings.
- 2) NTN Technical Review, Vol. 6-1, pp. 784-792, 1957.

Photo of author



Katsuaki SASAKI

Automotive Business HQ  
Axle Unit Engineering Dept.

## Technology Trends in Auto Tensioners

Seiji SATO\*



With the trend toward high-performance automobile engines, auto tensioners have been widely adopted for automobile engines since the 1980s in order to improve durability and to reduce noise from timing belts which are used to drive camshafts. In recent years, demands for further engine downsizing and improved reliability have become strong, and major trends include a change from timing belts to timing chains and the use of serpentine drives with single accessory drive belts. Furthermore, as concern about global warming and other environmental issues becomes strong, the development of technologies to reduce fuel

consumption have sped up, and demands that auto tensioners be made more compact, lighter in weight and lower friction have increased.

NTN supplies various types of hydraulic auto tensioners for camshaft drive systems and accessory drive systems. This article introduces the current technologies used in these auto tensioners.

### 1. Introduction

On automotive engines, a drive belt and/or chain is used to transmit the rotary motion of crankshaft to the camshaft and auxiliaries. The auto tensioner keeps correct tension on drive belt and chain.

Recently, people have been increasingly conscious about environmental issues such as global warming and needs have been mounting for a reduction in environmental impacts associated with automobiles. Various nations have imposed regulations for reduction in fuel consumption with targeted values. To address this situation, engineers in these nations have been developing low fuel consumption technologies that contribute to the reduction of CO<sub>2</sub> emissions and increase energy saving.

In this context, the auto tensioner needs to assist in the reduction of size and weight of the engine in order to help improve the fuel economy of the automobile. At the same time, the auto tensioner incorporated into camshaft drive & auxiliaries drive systems has been increasingly expected to contribute to improvements in fuel economy and reduction in friction.

This article describes information about NTN's auto tensioner products that are intended to meet current emissions and energy savings market needs.

### 2. Engineering Trend in Engine Drive Systems

The camshaft drive system on automotive engines has to incorporate a meshed transmission-capable timing belt or chain system in order to synchronize the motion of engine pistons with the cams that govern air intake and exhaust emission. **Fig. 1** shows typical layout of a timing belt, while **Fig. 2** illustrates a timing chain. **Fig. 3** illustrates change in market shares with different camshaft drive systems.

NTN offers a full lineup of auto tensioner products for both camshaft drive types.

Previously, chain drive systems have been said to develop friction loss whose level is greater than that of belt drive systems (note that friction loss can significantly affect the fuel economy of an automobile). Nevertheless, as silent chain systems boasting quiet operation have been more commonly employed, the chain drive has gradually superseded the belt drive. Consequently, the market share of chain drive systems for camshaft drives has been increasing.

Historically, the chain drive system was not commonly used for diesel engines because it operates using engine oil as lubricating oil which is adversely affected by deterioration of oil by contamination with

\* Automotive Business HQ. Automotive Engineering Dept

soot. However, mechanical strength of drive chains have been much improved thanks to the improvement in surface treatment technique; thus, chain drive is currently more often applied to automotive diesel engines.

The auxiliary drive systems drive a lot of automotive auxiliaries using frictional transmission technology based on V-ribbed belts, etc. Belt drive systems for the automobile began as a multi-belt configuration where multiple drive belts are commonly engaged with the crankshaft and the drive belts respectively transmit driving power to assigned auxiliaries. The belt drive system has further evolved into a serpentine drive system such as a one illustrated in Fig. 4 where multiple auxiliaries are driven by one drive belt. This allowed the length of entire engine system to be

reduced. In the present-day auto industry in Japan, serpentine camshaft drive systems are used on approximately 80% of cars newly manufactured in Japan.

The idling stop system, a system that stops the engine during idle, appears to be a useful fuel consumption reduction technology. For this system, a unique mechanism has been commercialized where the engine is restarted by power transmitted from the alternator via the auxiliaries belt rather than activating the starter. For this system, a variety of different auto tensioner types are arranged within the layout of the auxiliaries belt, wherein each auto tensioner has to meet requirements for system functionality. This arrangement can now be seen in new applications.

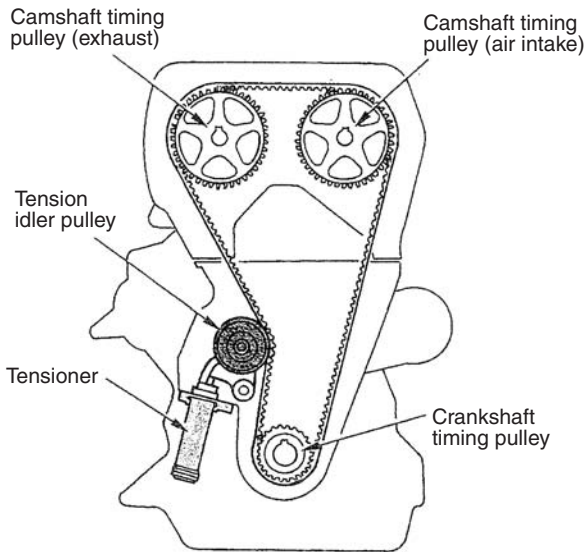


Fig. 1 Typical layout of timing belt

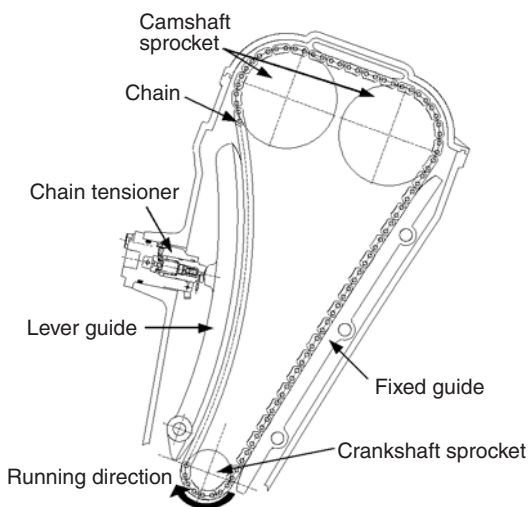


Fig. 2 Typical layout of timing chain

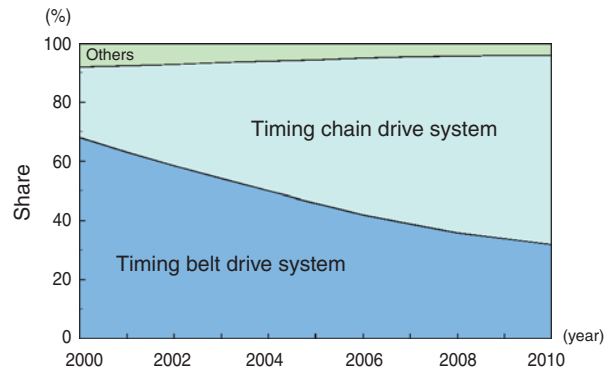


Fig. 3 Transition in market shares of camshaft drive systems

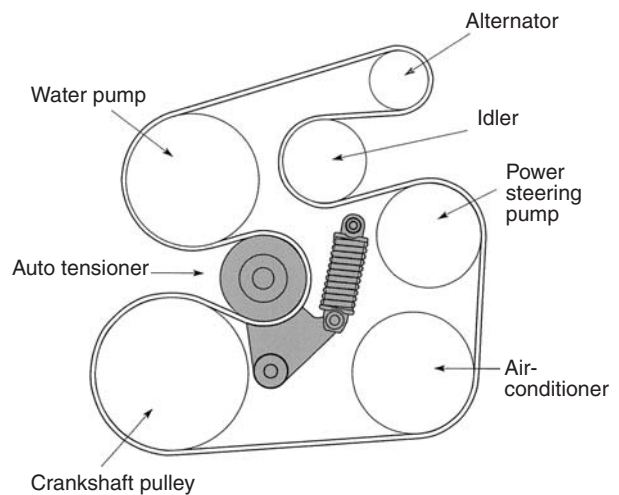


Fig. 4 Typical example of auxiliaries drive belt

### 3. Types and Structures of Auto Tensioners

#### 3.1 Timing belt auto tensioner

Two scenarios are possible to provide correct tensioning of the timing belt. In one scenario, the amount of tension is determined when the pulley is installed. In the other scenario, an auto tensioner that is capable of tension adjustment is incorporated into the timing belt system. The types of auto tensioners can be categorized on the basis of damping structure into frictional systems and hydraulically operated systems. NTN's auto tensioner is a hydraulically operated type which offers the benefit of reduced friction by reducing the initial belt tension.

**Fig. 5** schematically illustrates the basic structure of NTN's auto tensioner for timing belts.

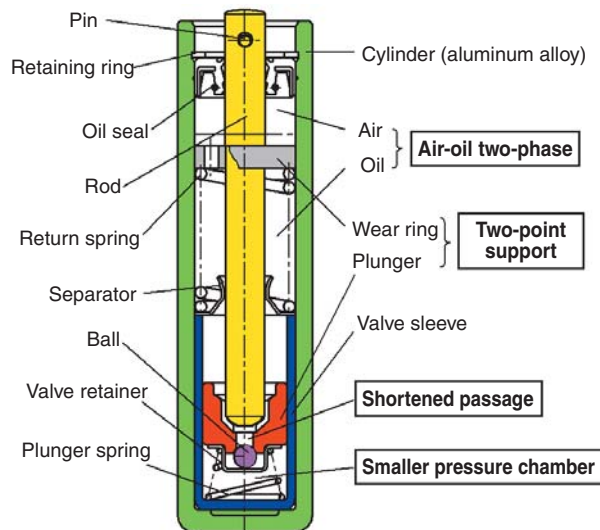


**Fig. 5** Basic structure of auto tensioner

A hydraulically operated auto tensioner has a damping structure that utilizes hydraulic oil prefilled in the interior of its cylinder. To be able to absorb expansion of oil at higher temperature and maintaining an adequate seal, NTN employs air-oil two phase structures and oil seals to contain hydraulic oil. The change in belt length caused by temperature change and aging is accommodated by the operation of the spring in the cylinder; thereby the tension of the timing belt can be adjusted accordingly. Thus, even though the belt will inevitably develop wear and elongation, virtually no change will occur with the tension setting. Consequently, after the initial setting, the NTN's auto tensioner will maintain appropriate belt tension until the timing belt reaches the end of its useful life.

**Fig. 6** shows NTN's auto tensioner types intended for various timing belt types.

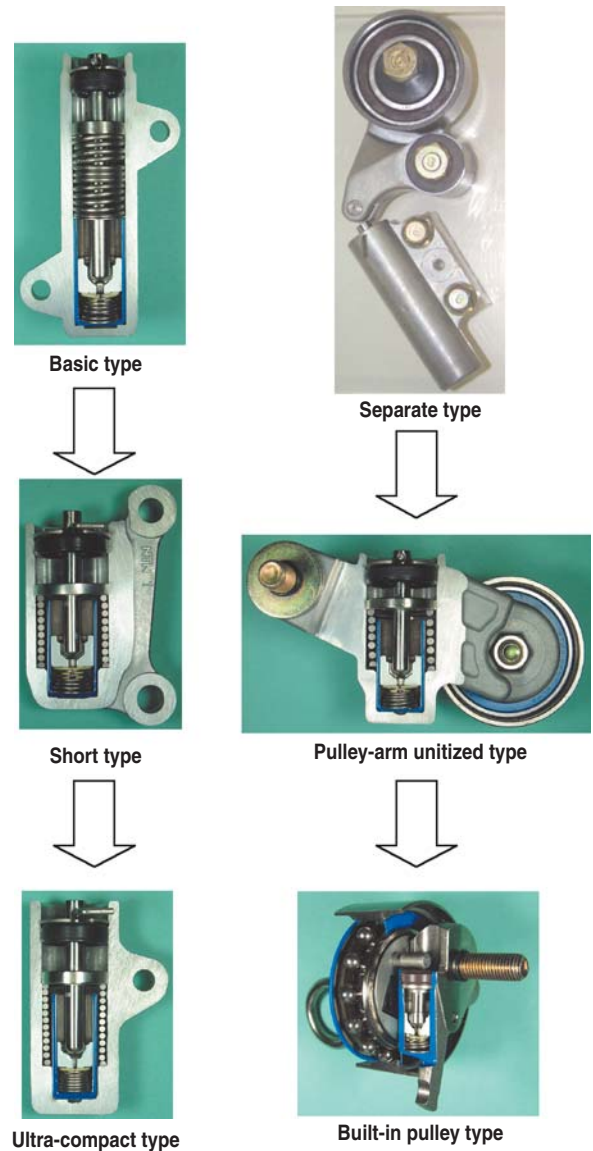


**Fig. 6** Various timing belt auto tensioners

NTN's aluminum cylinder design addresses the need for lighter weights while the smaller size requirement is met by NTN's "short type" featuring shorter axial dimension and "ultra-compact type" featuring size reduction in all dimensions.

The "pulley-arm unitized" type is essentially a unit comprised of a hydraulic damper and a pulley arm, which will lead to lower cost and space saving. The built-in pulley type helps achieve space saving because the hydraulic damper is housed within the pulley; thus this auto tensioner can supersede the fixed type tensioner.

### 3.2 Timing chain auto tensioner

On chain drive system, the drive chain between the camshaft and crankshaft is guided with various sliding guides; sliding resistance between the chain and guides develops friction loss that can vary depending on the level of chain tension. For this reason, optimization of the auto tensioner for timing chain systems is more important than that for timing belt systems.

Optimal design of an auto tensioner is generally determined through tuning on the intended engine type. Depending on an engine type, control of the chain tension may be necessary by adopting special damping mechanisms such as a relief valve mechanism that regulates the internal pressure of the auto tensioner.

Fig. 7 illustrates a typical example of measuring operation for tuning an engine.

Previously, mechanical tensioners were used for motorcycle engines. Now, hydraulically operated auto tensioners having built-in compact relief valve mechanisms are available for high-speed motorcycle engines. Consequently, many big sport motorcycles adopt NTN's hydraulically operated auto tensioners, and this product enjoys a larger share in Japan's motorcycle auxiliaries market.

Incidentally, in optimizing an auto tensioner for a chain drive, considerations must be given to the behavior of the chain at engine startup. At engine start up, oil supply to the auto tensioner will be insufficient for a short period of time due to a delay in oil supply from the oil pump during start up. Consequently, the chain can develop wobbling. To prevent this, a "no-back" mechanism is needed which prevents "push-in" of the auto tensioner while the engine is being shut down. To address this problem, NTN employs a ring that features a simplified ratchet

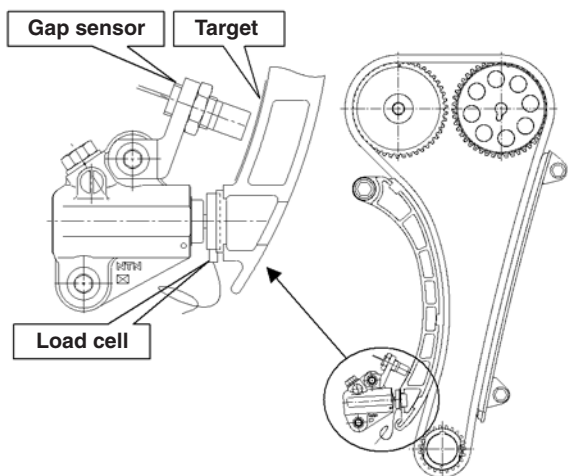


Fig. 7 Example of measuring operation for engine tuning

mechanism as well as a serrated screw type that utilizes a stepless "no-back" mechanism for controlling frictional resistance on the screw.

The ring type has a "no-back" mechanism that while permitting "push-in" of the actuator by a preset amount of axial shift, prevents "push-in" of the actuator in steps. This mechanism is a compact system that utilizes the elasticity of the ring arranged concentrically relative to the axial center of auto tensioner.

The serrated screw type is NTN's unique "no-back" mechanism, and can accommodate vibration on the chain through high-speed ranges. It can also maintain the smallest possible "push-in" when the engine is shut down regardless of its position. Thereby it contributes to noise damping at engine startup.

Fig. 8 shows the typical shapes of NTN's timing chain auto tensioners.

To create a light-weight auto tensioner design, NTN has long been attempting to employ an aluminum cylinder. For the ring type, the ratchet mechanism has been superseded with a register ring formed with wire material to create a "no-back" function and simplify the structure. Consequently, a new auto tensioner boasting much reduced size and weight has been successfully developed.

As for the serrated screw type, the technical data of the conventional serrated screw has been reconsidered. Next, the effective diameter of the screw component has been reduced without a reduction in load capacity in order to further reduce the weight of the auto tensioner. Note that this alteration has helped improve the ability to form the thread on the serrated screw resulting in the production process being drastically shortened. At the same time, the amount of material scrapped has been significantly reduced because the mass-removal machining process has been deleted.

To be able to reduce running friction on the timing chain, it is necessary to accommodate a variation in engine torque during continuous engine operation and at engine startup.

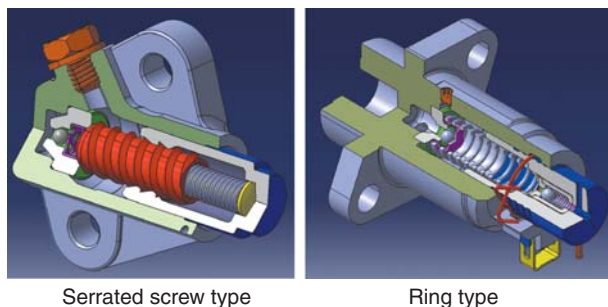


Fig. 8 Examples of NTN's timing chain auto tensioner

The serrated screw type auto tensioner is better at accommodating this variation. With the serrated screw type, “push-in” distance for the auto tensioner before the “no-back” function becomes enabled corresponds with the dimension of the backlash on the screw and therefore can be set to a much smaller distance. The serrated screw type is very convenient as this function is active regardless of position on the serrated screw, and thereby the “push-in” distance can be invariably adjusted. Consequently, this auto tensioner type boasts a low noise emission level. Also, thrust occurring from the spring load within the tensioner is minimized therefore chain tension and frictional losses are decreased.

Fig. 9 summarizes the results of the friction reduction effect of NTN’s auto tensioners on an automotive engine. It should be understood from this diagram that the ratchet type (ring type) does not generate noise when the engine is started and leads to greater plunger thrust. In contrast, the serrated

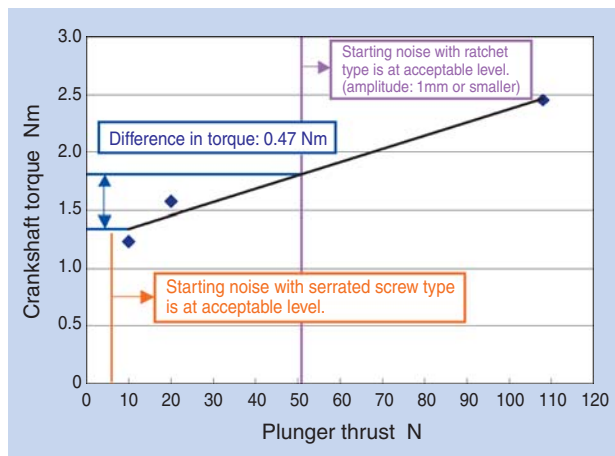


Fig. 9 Result of assessment about reduction in crankshaft drive torque

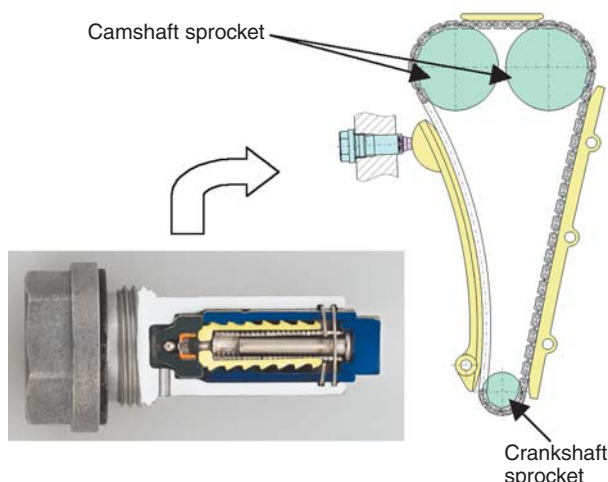


Fig. 10 Self-mounting auto tensioner

screw type does not emit noise even at low plunger thrust and the resultant crankshaft drive torque is low.

Additionally, NTN has been committed to weight reduction by an improvement in the method used for mounting to the engine. Compared with the conventional method for mounting, NTN’s newly developed self-mounting auto tensioner is unique in that the threading is formed on the tensioner body so that the tensioner is directly fastened to the engine. Thereby any previously needed mounting screws are removed which positively contributes to a weight reduction for the automotive engine.

Fig. 10 shows an example of NTN’s self-mounting auto tensioner.

### 3.3 Auxiliaries drive belt auto tensioner

Previously, multiple belt type drive belt systems were commonly used to drive engine auxiliaries on automobiles. Recently, serpentine drive systems that drive all of the associated engine auxiliaries with one belt have been more commonly adopted in order to reduce the overall length and weight of the engine auxiliaries system, promote a maintenance-free feature and simplify the belt mounting procedure.

Two types of auto tensioners for auxiliaries drive belts are available. One type is a friction-based type that directly utilizes frictional resistance as a damping force: the other type is hydraulically operated type that utilizes an amount of prefilled oil in the auto tensioner as a hydraulic damper. NTN uses the hydraulically operated type since this type is relatively immune to changes in the characteristics of the belt possibly resulting from aging and temperature change as well as stably maintaining belt tension at a predetermined level.

Fig. 11 shows NTN’s auxiliaries drive belt auto tensioner.

NTN offers unitized assemblies that include pulleys and pulley brackets. By using 3D models, NTN

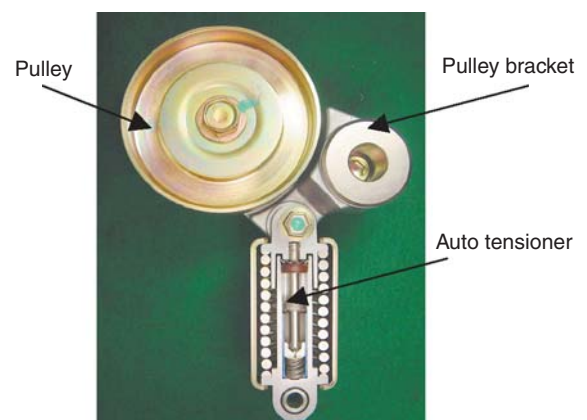


Fig. 11 NTN's auxiliaries drive belt auto tensioner

investigates possible interference with engine-related components as well as FEM analysis. This has helped NTN achieve lighter, yet still highly rigid auto tensioner design.

NTN's hydraulically operated auto tensioner is unique in that it has a spring function for obtaining the minimum necessary tension for the drive belt which can be set up independent of the hydraulic damper function. This feature is advantageous because the auto tensioner damper function can be tuned up without increasing the minimum belt tension even when it has to develop greater damping force. Consequently, frictional losses on the auxiliaries drive belt are mitigated.

Recently, in an effort to improve fuel economy of automobiles and to help assist in the push for global energy conservation, idling stop (no idling) systems in the form of ISG (Integrated Starter Generator) or BSG (Belt Starter Generators) have been increasingly commercialized. Fig. 12 shows a typical layout of an auxiliaries drive belt employing ISG system.

In restarting the previously inactive engine, the ISG system activates the starter and alternator to transmit

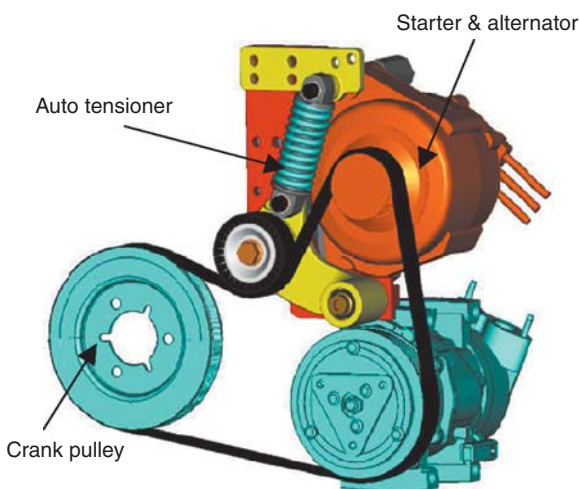


Fig. 12 Belt layout of ISG system

rotary power to the crankshaft via the auxiliaries belt to start the engine.

The auto tensioner must generate damping force that prevents the drive belt from slipping even when subjected to higher torques seen in the restarting operation of the engine.

When the engine is started by the starter and alternator, the crankshaft (whose inertia is large) is rotated resulting in higher tension on the belt. To address this situation, NTN has adopted its unique hydraulically operated auto tensioner which is capable of greater damping effects because of the previously

mentioned advantages.

Recently, these "idling stop" (no idling) systems have been increasingly applied to hybrid electric vehicles and large displacement engines. Fig. 13 illustrates a typical layout of NTN's hydraulically operated auto tensioner with the addition of the frictional auto tensioner.

Once an automotive engine has been started, greater drive torque acts on the auxiliaries drive belt system. Therefore, to prevent the belt from slipping and improve reliability of the belt drive, a frictional auto tensioner is added immediately downstream of the starter and alternator so that the frictional auto tensioner can operate in conjunction with the hydraulically operated auto tensioner. To cope with the trend of increased popularity of "idling stop" systems, NTN has developed a shortened auxiliaries auto tensioner aimed at a reduction in weight and size of the auto tensioner.

Fig. 14 shows NTN's short type auxiliaries auto

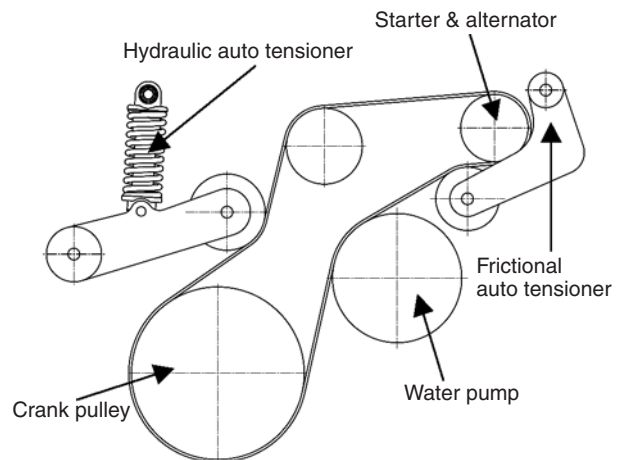


Fig. 13 Layout of NTN's hydraulically operated auto tensioner with addition of frictional auto tensioner

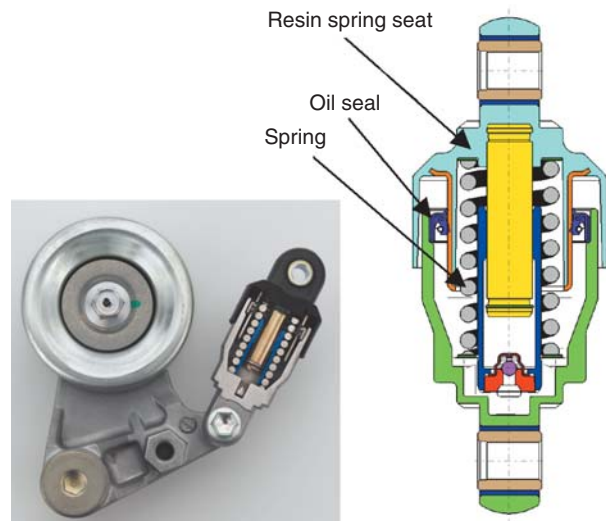


Fig. 14 Short-type auxiliaries drive auto tensioner

tensioner. In this auto tensioner, the oil line to the high pressure chamber has been relocated to below the high pressure chamber in order to provide sufficiently large oil prefill space. At the same time, the spring is now housed in the casing. Consequently, a 15% size reduction has been achieved. In addition, a resin made seat for the spring is used in this new auto tensioner leading to 10% weight reduction.

#### 4. Future of Auto Tensioner

In the automotive market, concept development has already begun for a system that places top priority on a reduction of frictional loss intending to further reduce fuel consumption. As already described, a reduction of tension on belt or chain is effective in reducing frictional loss. For this reason the auto tensioner needs to develop the minimum necessary damping force for stability.

Additionally, it will be necessary to optimize the comprehensive scope of the system. This will include the adoption of friction reduction technologies NTN has been developed for peripheral components such as pulley bearings and chain guides as well as incorporating other fuel consumption reduction technologies that will become more increasingly used, such as no idling system.

#### 5. Conclusion

This article has reported the engineering trend seen in camshaft drive and auxiliaries drive systems for automotive engines as well as the functions needed for auto tensioners that are used together with the above-mentioned systems. Also shown was NTN's engineering commitment to its newly developed auto tensioners.

The need for better fuel economy in automotive engines appears to be growing in an effort to help alleviate possible environmental impacts.

NTN will remain committed to the development of its auto tensioner products by ensuring that ever diversifying market needs are met using improvements in the entire auto tensioner system including peripheral components.

#### Reference

- 1) Koji, A., et al., The Tribology, No. 10, pp. 28-30, October 2009.
- 2) Kita, H., The Tribology, No. 5, pp. 35-37, May 2005.
- 3) Kitano, S., et al., The Tribology, No. 10, pp. 24-26, October 2004.
- 4) Kitano, S., et al., NTN Technical Review, No. 73, pp. 110-117, 2005.
- 5) Society of Belt Transmission Engineers, Practical Designs for Belt Transmissions and Precision Conveyances, New Edition, Yokendo Co., Ltd., 2006.

Photo of author



Seiji SATO

Automotive Business HQ  
Axle Unit Engineering Dept.

# NTN-SNR Low-torque Strut Bearing for Severe Environments

NTN-SNR    Gérald MIRABEL\*  
 NTN        Susumu YAMAJI\*\*



Sealing reliability is a significant issue for automobile strut bearings, because they must be protected from severe environmental conditions, such as muddy water intrusion. Based on its knowledge and experience, NTN-SNR has developed a second-generation strut bearing.

This article introduces the features and performance of the bearing's floating seal.

## 1. Introduction

Automotive strut bearings are used in the upper section of the McPherson suspension system, and allow the strut to smoothly oscillate when the front wheels are turned.

Recently, demand for cars has been increasing in regions where automobiles encounter severe muddy water environments. Therefore, improved sealing performance is needed for these bearings. However, improved sealing performance is typically accompanied by increased torque on the seal, which can adversely affect stability in steering. Thus, avoiding an excessive increase in torque on the seal poses an engineering challenge.

Recently, NTN has developed a unique sealed strut bearing that boasts both good sealing performance and low running torque. The following article describes this unique bearing.

## 2. Structure of McPherson Suspension System

Fig. 1 illustrates structure of a typical McPherson suspension, and Fig. 2 shows the structure surrounding the bearing. This suspension structure is used in about 70% of passenger cars around the world.

The upper section that includes the strut bearing is situated within the tire housing, and has to function in severe environment where it is directly subjected to splashes of muddy water from the road surface.

NTN-SNR's strut bearings are designed to accommodate both car type and the structural surroundings of the bearing. The main product line within NTN-SNR's strut bearing products to date has been the GEN2 strut bearing shown in Fig. 3, which comprises a press-formed bearing race and resin case.

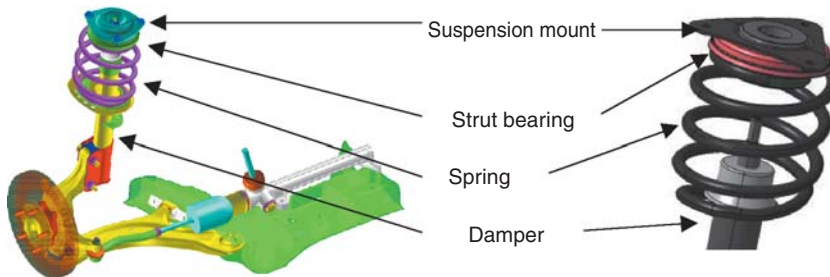


Fig. 1 Structure of McPherson suspension

\*NTN-SNR ROULEMENT Automotive Equipment Engineering

\*\*Automotive Business HQ. Automotive Engineering Dept.

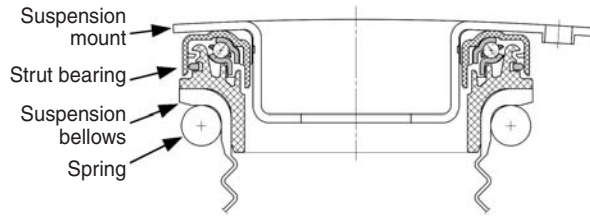


Fig. 2 Strut bearing and surrounding structure



Fig. 3 Structure of GEN2 strut bearing with floating seal

### 3. Structure and Features of GEN2 Strut Bearing

Fig. 3 shows exploded view of structure of GEN2 strut bearing.

- Resin moldings (01 and 02) contain bearing

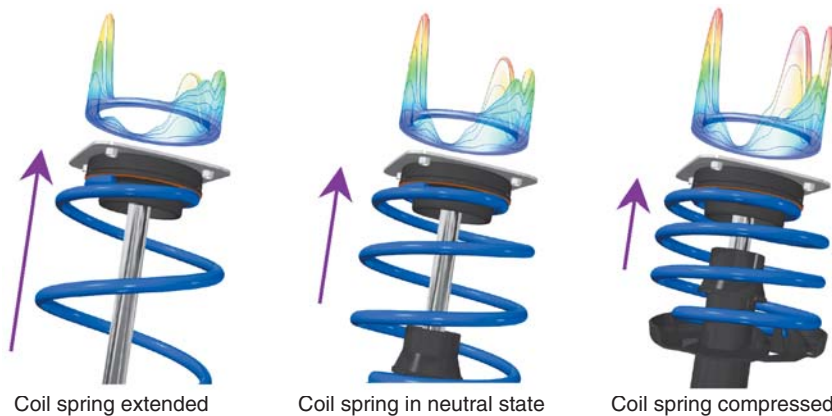


Fig. 4 Load distribution patterns by state of coil spring

components; the strut bearing is mounted to surrounding parts such as the suspension mount and the spring.

- Floating seal (03)
- Press-formed bearing race (04, 06)
- Retainer and balls (05)
- Grease

The GEN2 strut bearing includes the top cover and spring seat, each made of resin: consequently, when the spring is loaded, the entire bearing will be deformed. Fig. 4 shows examples of load distribution patterns on the strut bearing being subjected to a spring load. The length of the coil spring changes depending on the length of suspension stroke; therefore, the magnitude of load acting on the strut bearing will vary greatly. The resulting non-uniform circumferential load at the end face of the spring leads to deformation of the strut bearing proper.

This type of deformation occurring on the GEN2 strut bearing may enlarge the size of the passage in the labyrinth formed between the resin components (that is, top cover and spring seat) on the strut bearing as shown in Fig. 5; as a result, water can more easily reach the interior of the bearing.

If water enters the bearing, the bearing race will corrode and the suspension spring, which oscillates owing to varying load amplitude, will cause the bearing race to develop fretting wear (FBE: False Brinelling Effect). While traveling in a car, or in particular, parking a car in a garage, the car driver will feel uncomfortable noise and vibration through the steering wheel. To address this problem, the strut bearing must incorporate a structure that blocks water ingress.

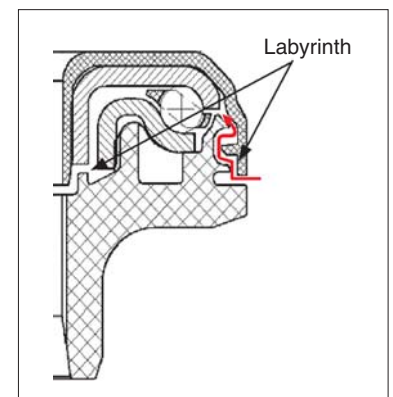


Fig. 5 Labyrinth structure and water ingress route in strut bearing

## 4. Features of Floating Seal

Strut bearings used in severe muddy water environments are directly subjected to large amounts of water and dust in addition to muddy water. To address this situation, NTN-SNR has recently developed the unique strut bearing with a floating seal, shown in Fig. 3. This strut bearing simultaneously meets both the required sealing performance and the desired low running torque.

Fig. 6 provides a concept view of the operation of the floating seal. The seal (03) is in contact with the resin top cover (01) situated above it; thereby it maintains an appropriate labyrinth in relation to the resin spring seat (02), regardless of its position.

The floating seal can move freely within the slot formed in the spring seat, independent of radial and axial displacement between the resin components; thereby positive contact remains between the floating seal and top cover. This floating seal not only prevents ingress of water, dust and muddy water into the bearing but also helps realize low running torque.

The seal material is an important factor for bearing performance. NTN-SNR employs polyacetal (POM) as a standard seal material for its strut bearing. This is because this material not only boasts excellent wear resistance but also features elasticity that helps to simplify mounting the seal into the bearing.

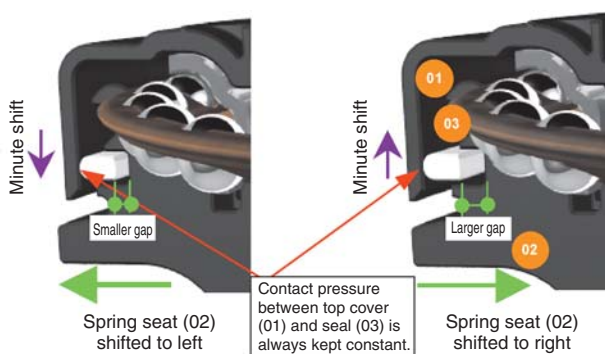


Fig. 6 Contact between floating seal and top cover

## 5. Performance Assessment for Floating Seal

To meet the diverse requirements of various car makers, NTN-SNR is executing various performance assessment tests. In particular, NTN-SNR is assessing the sealing performance of various floating seal designs on actual suspension assemblies so that floating seal samples are tested in situations that realistically simulate environments automobiles will experience. Fig. 7 shows the muddy water resistance test rig that NTN-SNR has used for this test.

The standard test conditions applied are as summarized below:

- Oscillation angle:  $\pm 40^\circ$
- Loading: 6490 N (typical)
- Muddy water nozzle: 2 pos.
- Muddy water flow rate: 3 L/min (per nozzle)
- Run cycle: 8 hours (6 hours of spraying, 2 hours of drying)
- Test temperature: room temperature

Figs. 8 through 10 show structures of NTN-SNR's conventional design, NTN-SNR's floating seal and a competitor's molded lip seal; Fig. 11 shows the results of the muddy water resistance test for these seals.

NTN-SNR's floating seal design (Fig. 9) boasts excellent prevention of water ingress (as much as 90%) into the bearing compared with the conventional design (Fig. 8).

Note that the competitor's spring cover structure shown in Fig. 10, having a molded seal lip, boasts excellent sealing performance during the early stage of use. NTN-SNR has demonstrated that muddy water

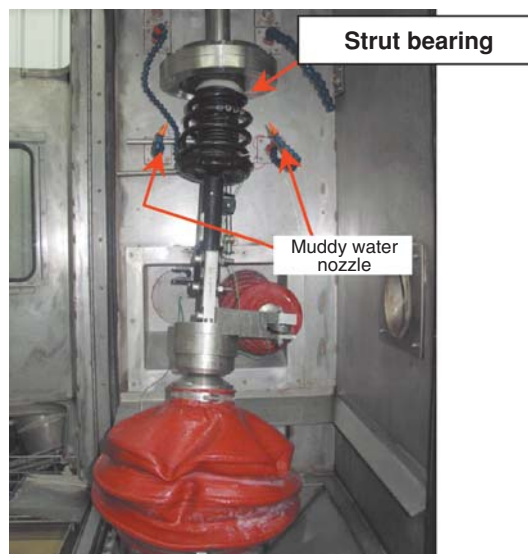
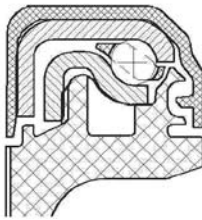
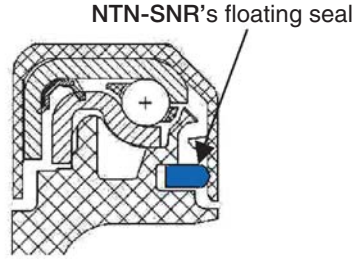


Fig. 7 Muddy water test rig for McPherson suspension



**Fig. 8**

NTN-SNR's conventional design



**Fig. 9**

NTN-SNR's floating seal design

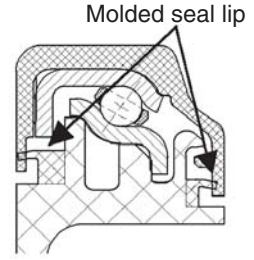


**Fig. 10**

Competitor design: molded seal lip

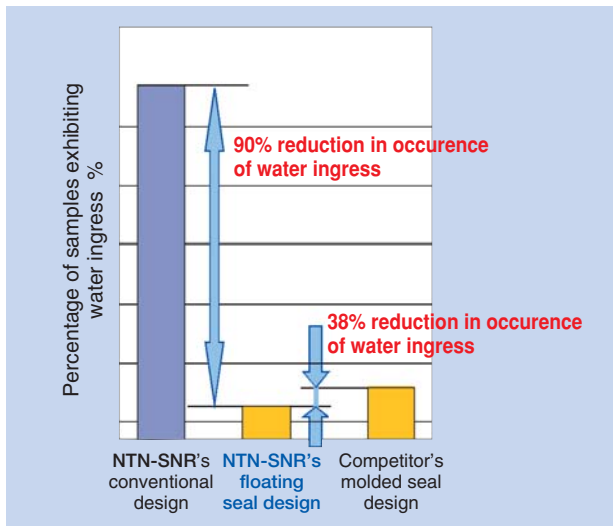


**Fig. 11** Muddy water test results

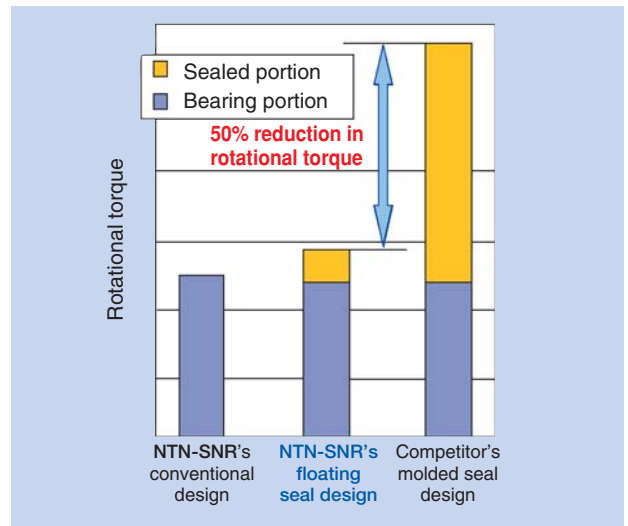


**Fig. 12** Torque test results

sealing performance with this molded seal design is 38% less effective than NTN-SNR's floating seal design because the molded seal develops localized wear owing to unbalanced loading resulting from deformation on the resin component.

In addition, **Fig. 12** graphically summarizes shares of contributing factors of seal types to rotational torque on strut bearing. NTN-SNR's floating seal design boasts 50% lower torque versus the competitor's design.

## 6. Conclusion

NTN-SNR has developed and standardized this proprietary seal concept that will positively improve reliability of its strut bearings.

At present, NTN-SNR's strut bearings with floating seal have been finding an increasing number of applications in newly developed automobiles. NTN-SNR hopes to supply its strut bearing products to more diverse automakers around the world to help improve reliability of automobiles in travel.

Photo of authors



Gérald MIRABEL

NTN-SNR ROULEMENT  
Automotive Equipment  
Engineering



Susumu YAMAJI

Automotive Business HQ  
Axle Unit Engineering Dept.

# NTN-SNR Low-torque High-capacity Pulley Bearing Unit for Water Pumps

NTN-SNR    Sebastien BRISSON\*



Water pumps used on automobile engines are used to circulate the coolant between the engine and heat exchangers. Water pumps are very important to the operation of the engine and require a high level of reliability. The seals and bearings inside the water pump are critical components and require the same high level of reliability.

As engine technology advances, additional functions of the timing and accessory belts have increased the load applied to the water pump pulley bearing and also increased the temperature the water pump pulley bearing is exposed to. The internal design of the bearing must take into account the higher loads and increased temperatures of today's water pump pulley bearings.

This paper introduces the structure and performance of a pulley bearing unit developed for water pumps.

## 1. Introduction

There has been an increasing requirement for reducing CO<sub>2</sub> emissions/fuel consumption as well as improved reliability with industrial products. This trend is same with a pulley bearing unit for water pumps in an automotive engine system. To address these market needs, functionality of bearings has to be improved.

NTN-SNR has recently developed unique, easy-to-use, compact, high-performance pulley bearing unit for water pump (hereinafter referred to as newly developed bearing unit). The bearing unit employs a coupling system where its outer ring is coupled with the shaft via a newly developed flange.

## 2. Structure

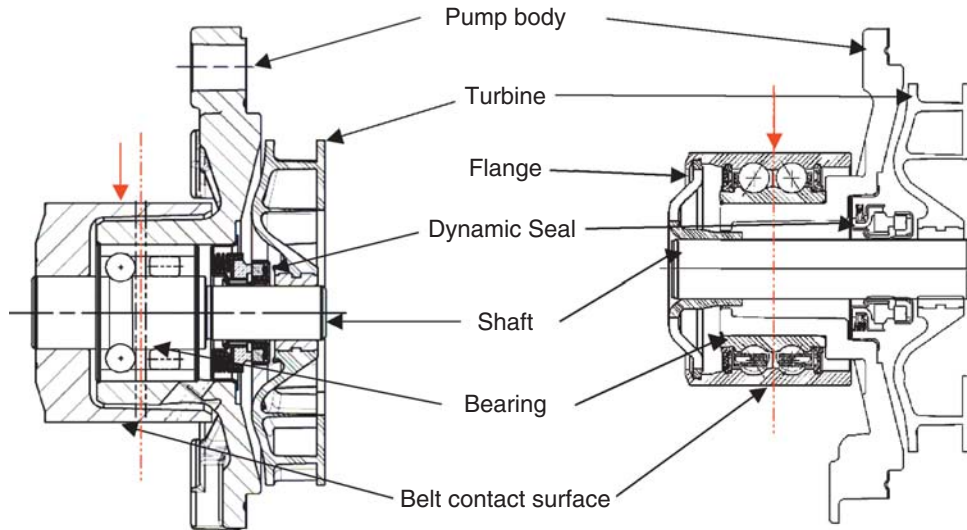
**Fig. 1** shows an area on the automotive engine where the water pump is installed. **Fig. 2** illustrates the structure of bearing unit for water pumps. The primary function of the water pump is to translate rotary motion of drive belt into rotation of the turbine. On the conventional bearing unit for water pumps (**Fig. 2** left), the bearing outer ring is fixed while the shaft (which doubles as the bearing inner ring) can rotate. To prevent outward leakage of coolant, a dynamic seal is provided to isolate the bearing interior from the outside environment. To ensure sufficient

durability of the seal, even when the bearing unit is running at higher speed, the sealing system needs to allow a minimal amounts of coolant to flow from the seal lip.

In contrast, the newly developed bearing unit for water pumps (**Fig. 2** right) differs from the conventional bearing unit. Two main differences are that the bearing inner ring is fixed and the bearing outer ring forms the outer circumference of the bearing unit; which turns together with the pulley. This novel structure is realized by the newly developed flange which helps the bearing outer ring be coupled with the pump shaft. This flange not only transmits torque from the outer ring to the pump shaft but also accommodates possible misalignment with the pump



**Fig. 1** Applicable area on automotive engine



Structure of conventional water pump

Structure of newly developed water pump

**Fig. 2** Structure of bearing unit for water pump

shaft. With a bearing unit size unchanged, this novel structure helps accommodate a bearing of larger outside diameter. Because the bearing is larger, the bearing unit can use a larger number of balls and carry a greater bearing load. Furthermore, the NTN-SNR's newly developed bearing unit allows the loading point from the drive belt to be situated at the midpoint in bearing width. Consequently, bearing stress within the bearing is alleviated; thereby the bearing can enjoy longer life. **Fig. 3** shows cutaway of the newly developed bearing unit.

Additionally, as shown in **Fig. 4**, the outer ring of the newly developed bearing unit for water pumps can be fitted with a V-ribbed pulley or timing pulley. In other words, a bearing unit of a given size for water pumps may be used in conjunction with various pulley shapes.

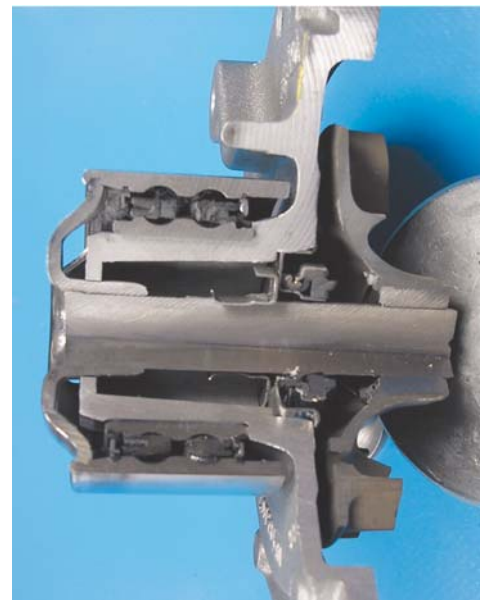


**Fig. 3** Cutaway of newly developed bearing unit

### 3. Features

There are two operating modes which are possible with a bearing unit whose outer ring can rotate. In one mode, a pulley member is simply fitted onto the bearing outer ring like on a bearing for compressors. In the other mode, the bearing outer ring itself functions as a pulley member. As with the newly developed bearing unit, the bearing outer ring is coupled with the shaft of water pump via a special flange. The features of this bearing unit can be summarized as follows:

1. With a given bearing unit the size is the same as that of conventional design. The bearing outer diameter of the newly developed bearing unit can be larger; thereby larger balls can be adopted,

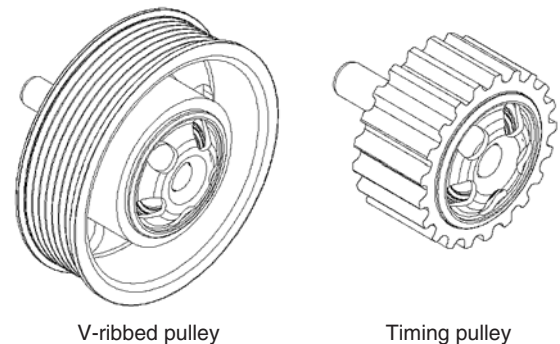


**Fig. 4** Pulleys applicable to newly developed bearing unit

helping the bearing unit to be capable of higher load carrying capacity and longer service life.

2. Possible misalignment from mounting of bearing to the water pump is reduced.
3. Weight is reduced in the water pump assembly.
4. Standard bearing unit of a given size can be equipped with a wide variety of sizes and types of pulleys.

Fig. 5 provides a cutaway of coupling between the bearing outer ring and flange as well as a photo that illustrates a swaged portion on the outer ring. As can be viewed from the photo in Fig. 5, the outer rim of the outer ring is fitted over the entire outer circumference of the flange by swaging technique. Fig. 6 shows the outer ring swaging process for joining the outer ring to the flange.

Fig. 7 shows appearance of the NTN-SNR's

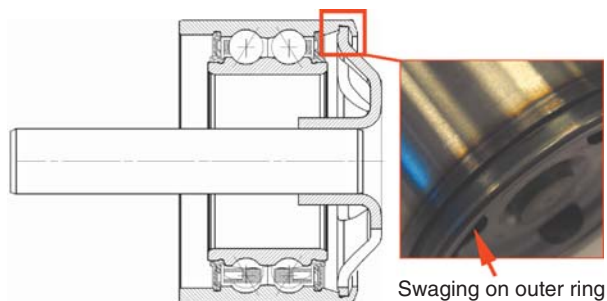


Fig. 5 Coupling between outer ring and flange

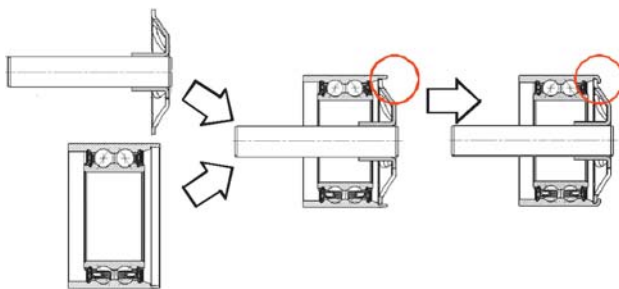


Fig. 6 Swaging process for outer ring

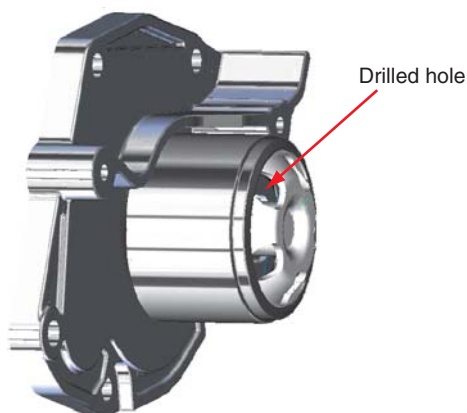


Fig. 7 Appearance of newly developed bearing unit

bearing unit. The side face of the flange has drilled holes which help simplify installation of the bearing unit to the water pump casing because the inner ring can be press-fitted by applying force through these holes.

Furthermore, to ensure durability, the dynamic seal described in the previous section needs to allow minimal amount of coolant away from the seal lip. Owing to the structure of conventional bearing unit, coolant flowing from the seal lip can reach the interior of the bearing; possibly shorten useful life of the bearing.

In contrast, on the newly developed bearing unit, coolant is drained away through the drilled holes; thereby reducing the likely hood of coolant ingress into the bearing.

## 4. Performance

### 4.1 Seal torque

On the conventional bearing unit, a trace amount of coolant is allowed to flow from the dynamic seal. For this purpose, the structure of this seal is very unique, having triplex seal lip. However, this seal structure leads to higher seal torque. Remember that the outer ring of the newly developed bearing unit can rotate: therefore, even when a trace amount of coolant is allowed to flow from the dynamic seal (as in the case of conventional bearing design described previously), bearing life is not adversely affected. Thus, a standard seal such as one having cross-sectional profile in Fig. 8 may be used, leading to lower seal torque. Results of bearing torque measurement are given below:

- Entire water pump: 0.05 N·m
- Bearing unit alone: 0.03 N·m

### 4.2 Coupling torque

On the newly developed bearing unit, the addition of a newly developed flange allows the outer ring to rotate. To verify that there is sufficiently high coupling strength between the flange and shaft and outer ring, the following assessment tests have been performed.

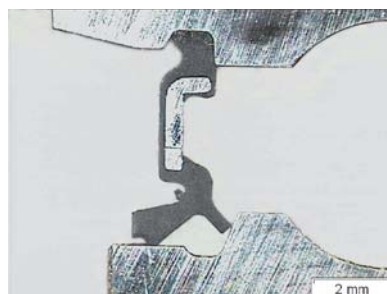


Fig. 8 Cross-sectional profile of standard seal

#### 4.2.1 Coupling torque between shaft and flange

Fig. 9 graphically shows relationship between interference and coupling torque between the pump shaft and bearing flange. The coupling torque between the shaft and flange is governed by the interference between these members: appropriate adjustment of the interference helps maintain optimal coupling torque. When the interference between the shaft and flange falls in a range of 0.035 to 0.085 mm, variation in the coupling torque falls in a range of  $\pm 10$  N·m.

When the interference between the shaft and flange falls in a smaller range of 0.025 to 0.075 mm, the coupling torque can vary by 17 N·m at maximum. NTN-SNR controls the interference on mass-produced products of its newly developed bearing unit design so that the coupling torque with mass-produced products falls in a range of 42 to 51 N·m. More specifically, the mass-produced bearing units meet the design requirement for coupling torque which is 20 N·m or greater.

#### 4.2.2 Coupling torque between outer ring and flange

Fig. 10 graphically plots the result of actual measurements of coupling torque between the outer ring and flange on mass-produced bearing units. Note that the minimum coupling torque requirement (design

specification) is 20 N·m for the coupling between the outer ring and flange on the bearing unit for water pumps. The measurements of coupling torque on mass-produced bearing units are at around 80 N·m. In other words, in spite of possible dimensional variation, the mass-produced products positively satisfy the design requirement of 20 N·m.

#### 4.3 Durability test

The newly developed bearing unit has been subjected to a durability test under the following test conditions:

##### (1) High-speed durability test conditions

- Bearing speed: 7500 min<sup>-1</sup>
- Radial load: 2000 N
- Ambient temperature: 110°C ± 10°C
- Test duration: 1000 h

##### (2) High-load durability test conditions

- Bearing speed: 2250 min<sup>-1</sup>
- Radial load: 3500 N
- Ambient temperature: 110°C ± 10°C
- Test duration: 1000 h

No bearing failure occurred during a series of tests within NTN-SNR under the above-mentioned test conditions. Also, no failure has occurred in the customer's bench test.

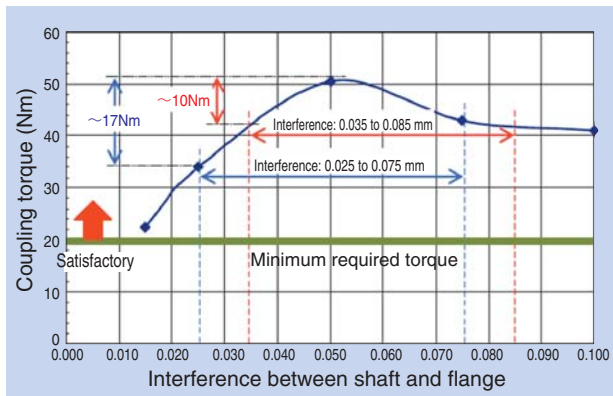


Fig. 9 Relationship between interference and coupling torque between shaft and flange

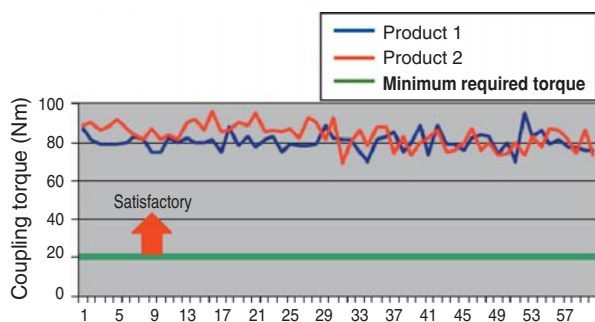


Fig. 10 Creep torque between outer ring and flange

## 5. Conclusion

This article has presented NTN-SNR's newly developed pulley bearing unit for automotive water pumps, which features a novel bearing structure with a rotating outer ring. In cooperation with the water pump manufacturer, NTN-SNR will further expand the scope of bearing users, in particular, automakers, and will contribute to reduction in CO<sub>2</sub> emissions and improvement in fuel economy.

Photo of author



Sebastien BRISSON  
NTN-SNR ROULEMENT  
Automotive Equipment  
Engineering

## Development of a System for Rolling Bearing Design Optimization

Daisuke IMADA\*  
Tsuyoshi NIWA\*  
Takashi UENO\*\*  
Tomohisa UOZUMI\*\*



There are demands to improve the torque, size, weight, life and rigidity of rolling bearings used in automotive transmissions and differentials.

In order to meet those demands, a system for rolling bearing design optimization has been developed. This paper introduces this system with application examples.

### 1. Introduction

People have been increasingly conscious about the global environment, and, car users are demanding improved fuel economy for their cars. Needs have been mounting for reduced running torque, size and weight for rolling bearings used in automotive transmissions and differentials (such bearings may be hereunder simply referred to as “bearings”). Bearing manufacturers have been committed to improvements to bearing design techniques for this purpose <sup>1)</sup>.

Bearings used in transmissions and differentials need to meet various requirements including bearing life, rigidity and safety factors. For improved automobile fuel economy, bearings need to satisfy these requirements while also achieving lower torque and decreased size and weight <sup>2)</sup>. To develop a bearing design that satisfies all of the required characteristics, a sequence of trial and error needs to be repeated; in each sequence, a bearing design is developed and then checked for whether the design satisfies each requirement. This procedure takes a lot of man-hours. There may be cases where requirements specification is not satisfied under a specified condition (size). In particular, tapered roller bearings and angular ball bearings involve many

design factors that can affect required characteristics. Consequently, it is very difficult to establish a bearing design that satisfies all required characteristics under a combination of different loading conditions.

In recent years, optimization analysis has been more commonly used in the field of CAE <sup>3)</sup>. When applying optimization analysis to the previously mentioned bearing design problem, various required characteristics are set as constraint conditions and characteristics including minimum torque, minimum size, long life and high rigidity are set as objective functions.

NTN has developed a unique bearing design optimization system that combines a design variables optimization routine for improving bearing torque or life and a detailed design routine for realizing the functionality of the design variables optimization routine. This unique design optimization system is hereunder described.

NTN has used a unique design optimization system for tapered roller bearings commercially since autumn of 2008. NTN believes this is a pioneering example of similar systems that are currently used throughout the world.

\* Automotive Business HQ. CAE Dept.

\*\* Automotive Business HQ. Automotive Engineering Dept.

## 2. NTN's Bearing Design Optimization System

### 2.1 Scope of applicability

Fig. 1 shows an example where tapered roller bearings are used in a rear differential. NTN's newly developed bearing design optimization system adopts a calculation model as illustrated in this example, wherein two bearings support one shaft; thus, this optimization system is capable of automatic design optimization for two bearings simultaneously. Thanks to this capability, a combination of two bearings each having a contact angle (such as tapered roller bearing and angular ball bearing) may be optimized while considering the balance between the contact angles of the two bearings. NTN's newly developed bearing

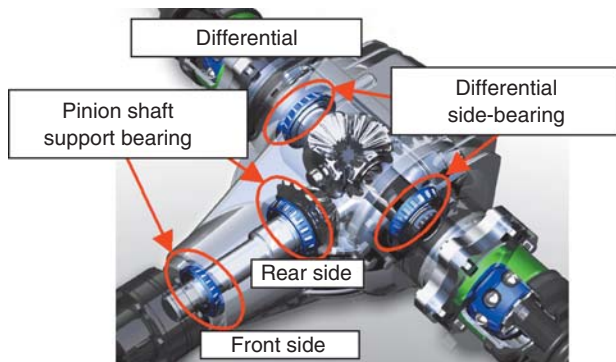


Fig. 1 Typical application to tapered roller bearing

Table 1 Possible combinations of bearings

	Deep groove ball bearing	Angular ball bearing	Tapered roller bearing
Deep groove ball bearing	○	○	—
Angular ball bearing	○	○	—
Tapered roller bearing	—	—	○

design optimization system can be used to optimize the design of ball bearings (deep groove ball bearings and angular ball bearings) and tapered roller bearings. Table 1 summarizes the bearing combinations whose design can be evaluated with this system. The combinations in Table 1 account for approximately 90% of automotive transmission bearings.

### 2.2 Description of functions of design optimization system

Fig. 2 summarizes calculation process flow for bearing design optimization with NTN's bearing design optimization system. First, the operator determines the intended bearing combination, and then inputs the bearing bore diameter, outside diameter, width and loading conditions and other factors, and next sets variables (such as number of rolling elements); then, the operator executes calculation. The past performance record-based database may be referred to for data about existing rolling elements and cages to help unify bearing designs.

Detail of the calculation sequence can be described as follows. First, bearing specifications are determined on the basis of initial values, and bearing life and bearing stress, etc. are calculated and the calculation result is analyzed. Next, the NTN's optimization program reads in the result of analysis: then, while considering the objective functions and constraint conditions, the program defines variables that lead to a more relevant solution to meet the requirements specification; and based on the so-obtained technical data, the program repeats calculation until optimal solution is reached. For searching the best solution, response surface methodology<sup>4)</sup> is used. Additionally, detailed rigidity data about housing, if available, can help realize bearing design that reflects housing rigidity.

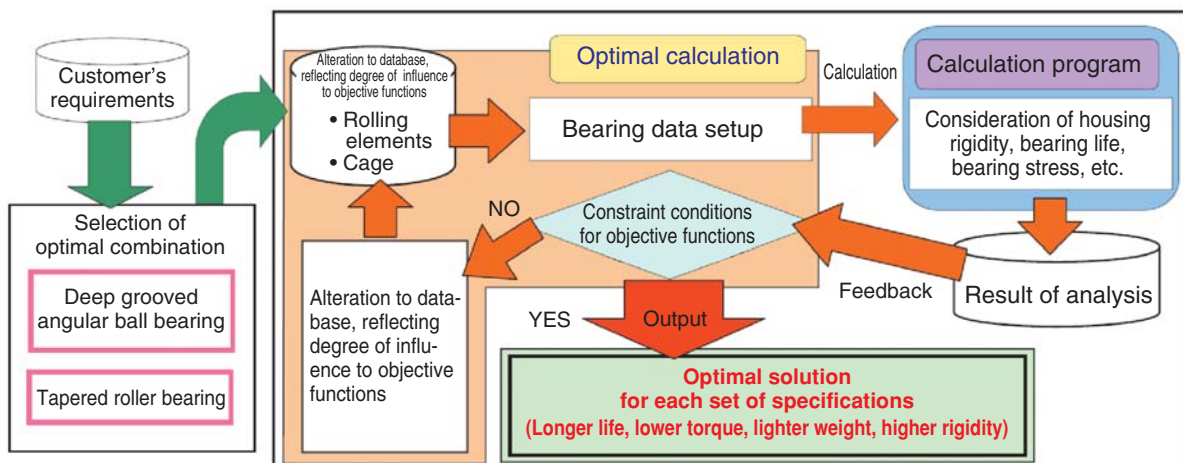


Fig. 2 Calculation process on NTN's bearing design optimization system

Typical examples of a “calculation program” as found at the upper right corner of Fig. 2 are as follows:

- [1] Program for determining bearing load on the basis of load acting on the shaft system.
- [2] Program for calculating loading on rolling elements of the bearing and contact bearing stress on rolling surface.
- [3] Program for calculating dimensions of relevant crowning.
- [4] Program for calculating bearing load capacity.
- [5] Program for calculating bearing torque.
- [6] Bearing life calculation program.
- [7] Bearing mass calculation program.

NTN's bearing design optimization system is capable of the following settings for objective functions:

- Calculated life
- Torque
- Mass
- Bearing rigidity

The bearing design optimization system is also capable of the following settings for constraint conditions, as well as settings for upper and lower limits:

- Calculated life
- Safety factor
- Bearing stress
- Bearing rigidity
- Torque
- PV value on rib (only for tapered roller bearing)
- Bearing dimensions (design dimensions); etc.

### 2.3 Effects of bearing design optimization system

By adoption of this unique system, NTN has succeeded in significantly reducing the time of the design study phase compared with the design conventional system.

Fig. 3 shows a comparison in terms of days needed for design (design study only). The effect of this system is particularly apparent for shortening the design phase associated with tapered roller bearings.

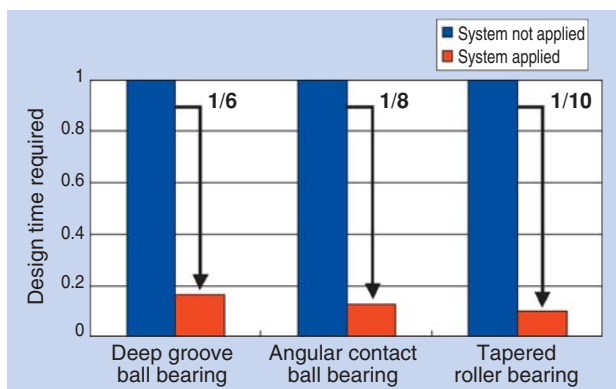


Fig. 3 Comparison in terms of design study time

## 3. Examples of Design Study Activities

### 3.1 Overview of optimization

Using this newly developed bearing design optimization system, NTN has studied optimization of tapered roller bearing, with lower torque as the objective function, under constraint conditions aimed at reducing the bearing width. This design study is described below.

The subject of this design study was the pinion shaft support bearings for the automotive differential as shown in Fig. 1. Fig. 4 illustrates the results of NTN's bearing optimization study.

Before the design study, the bearing design satisfies life requirement with a certain margin. The design of the bearing internal geometry is determined, wherein lower torque is taken as the objective function and the life requirement is the constraint in order to optimize the bearing design so to satisfy the life requirements and minimize the bearing torque.

Through this design optimization, the resultant

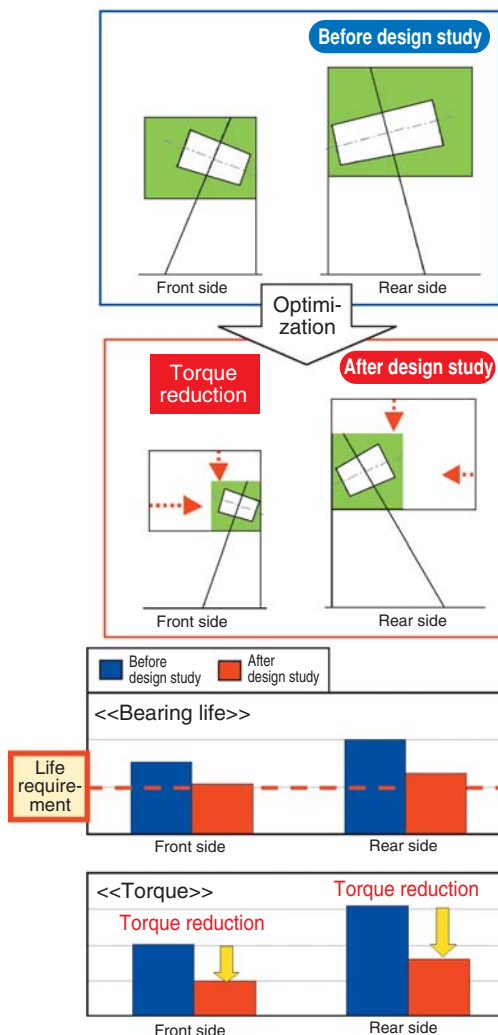


Fig. 4 Optimization activities for pinion shaft support bearings

bearing design will satisfy functional requirements including life and dimensions, while featuring minimized torque.

### 3.2 Typical example of optimization

Another example of a design optimization study for tapered roller bearings using this system is described below. The bearings in this design study are tapered roller bearings for the differential on a CVT as shown in Fig. 5.

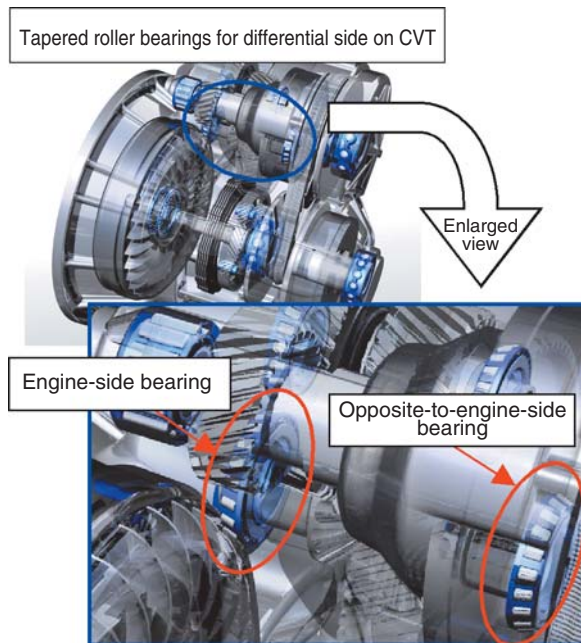


Fig. 5 Structure of differential on CVT

### <<Example of optimization study 1>> Optimization study for maximum bearing life

#### <Objective function>

Life: maximized

#### <Constraint conditions>

Torque: Not greater than conventional bearing design

Bearing stress: Not greater than conventional bearing design

Bearing dimensions: Same as conventional bearing design

Using the test bearings, optimization to maximize bearing life has been executed. Fig. 6 summarizes the results of comparison in terms of bearing specifications and bearing performance.

Generally, a increasing the contact angle ( $\alpha$ ) of a tapered roller bearing leads to a drop in the load rating, while bearing stress and torque also decrease. This is because the engine-side bearing in particular carries greater stress load, and an increased contact angle leads to improvement in bearing thrust load capacity.

The present bearing design optimization was intended to attain balance between the contact angles of the right-and left-bearings, which helps maximize the calculated bearing life; at the same time, the bearing stress and torque have been reduced.

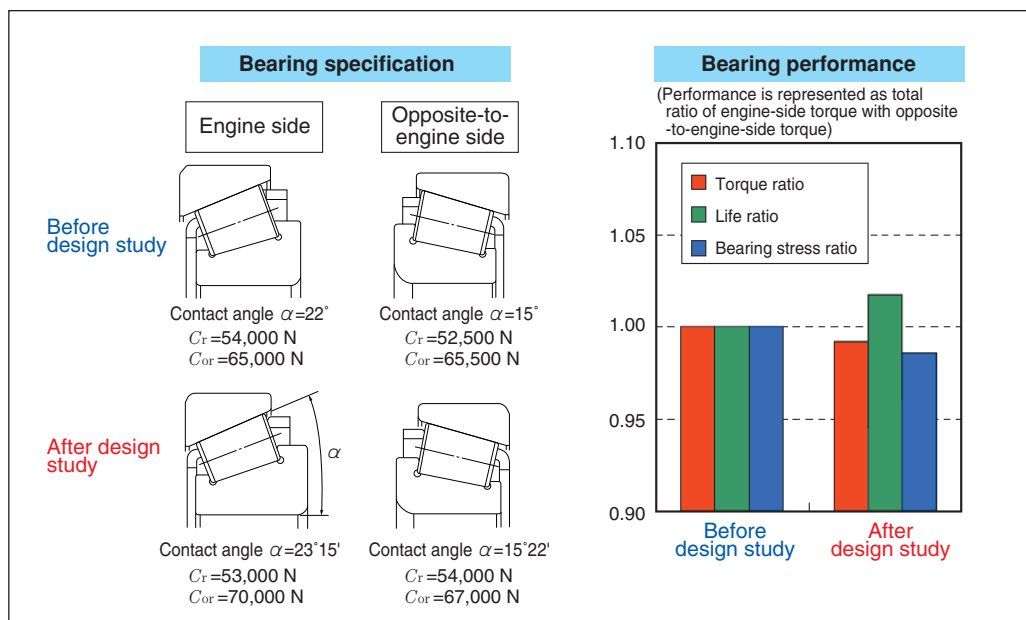


Fig. 6 Optimization result 1

<Example of optimization study 2>  
 Optimization study for minimum torque

<Objective function>

Torque: minimized

<Constraint conditions>

Life: Greater than conventional bearing design

Bearing stress: Not greater than conventional bearing design

Bearing dimensions: Same as conventional bearing design

Using the same test bearings, optimization to minimize bearing torque has been executed. Fig. 7 summarizes the results of comparison in terms of bearing specifications and bearing performance.

In this optimization study, increased contact angle and shorter roller length were selected in order to reduce bearing torque, resulting in a smaller load rating. Nevertheless, because the balance between contact angles of the right and left bearings has been optimized, the calculated life of the optimized bearing system is equivalent to that of the conventional design, and bearing stress on optimized bearings is smaller.

4. Conclusion

The bearing design optimization system described above boasts the following features:

<Features of rolling bearing design optimization system>

- Bearing design can maximize or minimize objective functions (life, torque, mass, bearing rigidity) while meeting constraint conditions.
- For bearings with contact angles such as tapered roller bearings and angular contact ball bearings, which are used in pairs to support a single shaft, the bearings can be designed so that good balance is achieved between the contact angles of right and left-bearings.
- Unification of bearing types is possible by referring to the database of past designs for rolling elements, cages and other bearing components.
- Time required for design study has been reduced compared with conventional design system.
- Less experienced designers can design bearing with competence of experienced designers.

Use of this bearing design optimization system helps shorten the time required to design bearings optimized for requirements such as reduction in torque, or reduction in size and weight. Consequently, NTN can now more promptly present optimal bearing designs to its customers.

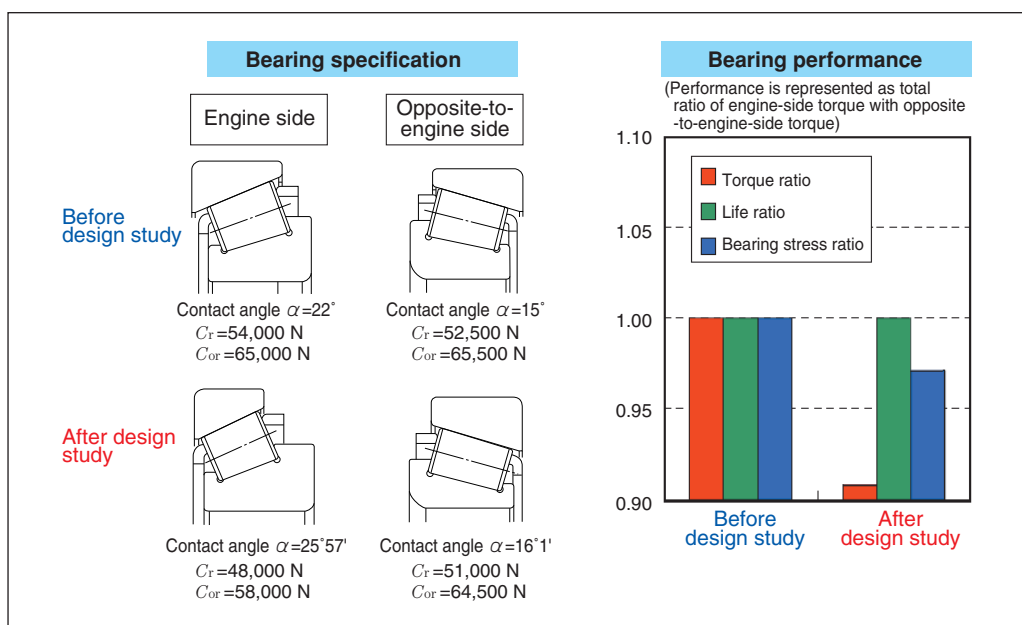


Fig. 7 Optimization result 2

## Reference

- 1) Tsujimoto, T., Mochizuki, J., "High Capacity Tapered Roller Bearings-Super Low Torque, High Rigidity Tapered Roller Bearings," NTN Technical Review, No. 73, 2005.
- 2) Kanamoto, T., Ueno, T., Katayama, A., Satou, M., "Transmission Technology Trends and Product Developments," NTN Technical Review, No. 75, 2007.
- 3) Nagatani, H., Niwa, T., "Application of Topology Optimization and Shape Optimization for Development of Hub-Bearing Lightening," NTN Technical Review, No. 73, 2005.
- 4) Yamakawa, H., ed., Optimal Design Handbook, Asakura Publishing Co., Ltd., 2003.

## Photo of authors

---



Daisuke IMADA  
Automotive Business HQ  
CAE Dept.



Tsuyoshi NIWA  
Automotive Business HQ  
CAE Dept.



Takashi UENO  
Automotive Business HQ  
Axle Unit Engineering Dept.



Tomohisa UOZUMI  
Automotive Business HQ  
Axle Unit Engineering Dept.

# Rapid Evaluation of Shear Fatigue Properties of Rolling Bearing Steels for Lifespans Up to the Gigacycle Range



**Noriaki SAKANAKA\***  
**Yukio MATSUBARA\***  
**Yoshinobu SHIMAMURA\*\***  
**Hitoshi ISHII\*\*\***

In rolling bearings, subsurface flaking failures occur under pure rolling contact fatigue conditions. In such failures, one of the crack initiation factors is believed to be repetitive orthogonal shear stress. The shear fatigue properties can be obtained by torsional fatigue testing. However, up until now, it has been all but impossible to establish the shear fatigue properties in the gigacycle range because of the limits of conventional low-loading-frequency torsional fatigue testers. In contrast, we employed ultrasonic fatigue testing to assure high loading speeds.

We have developed an ultrasonic torsional fatigue tester that enables the rapid evaluation of shear fatigue properties. The loading frequency of 20,000 Hz is quite high, resulting in a radical reduction of testing duration. For example, when loading cycles of  $10^{10}$  are applied, a conventional tester (with a loading frequency of 10 Hz) requires over 32 years to complete testing. In comparison the ultrasonic torsional fatigue tester requires only 7 days. This tester is effective for evaluating the properties of rolling bearing steels.

## 1. Introduction

One of the stresses that can trigger crack initiation prior to subsurface flaking failure in rolling bearing is repetitive orthogonal shear stress (near-purely alternating) that repeatedly acts on the surface of bearing<sup>1)</sup>. Shear fatigue characteristics of a given bearing steel can be determined by torsional fatigue testing. For tension-compression fatigue testing (axial load fatigue test and rotating bending test), so far, it has been a generally accepted practice to take the fatigue strength of steel having undergone  $10^7$  loading cycles as the fatigue limit of the material. However, even under heavy loading conditions, adequately lubricated rolling bearings do not develop subsurface flaking failures within  $10^7$  loading cycles. Therefore, in order to determine the shear failure properties of a given bearing steel, it is necessary to extend the duration of evaluation up to the gigacycle range. Incidentally, conventional torsional fatigue testers apply low frequency loading. For example, with a loading frequency of 10 Hz, it will take more than 32 years to apply  $10^{10}$  loading cycles. This means evaluation for bearing steel in the gigacycle range is virtually impossible.

One example of a rapid evaluation method for shear fatigue properties of rolling bearing steel is ultrasonic axial load fatigue testing. Many examples of evaluation results from this technique are available. In contrast, very little research of ultrasonic torsional fatigue test had been reported by the end of 2007, wherein the materials tested were Al alloy<sup>2-4)</sup> and mild steel<sup>5)</sup> and the maximum amplitude of shear stress applied was approximately 260 MPa. In 2008 and beyond, two results of evaluation for high strength steel have been published; one for spring steel of 598HV<sup>6)</sup> and the other for carburized steel of 817HV<sup>7)</sup>. According to these results, the maximum shear stress amplitude of the former material is approximately 600 MPa, and that of the latter material is approximately 800 MPa.

Conventional ultrasonic torsional fatigue testers were not capable of rapid analysis of high-strength steel materials under a wider loading range. To address this problem, NTN has developed a novel ultrasonic torsional fatigue tester (loading frequency; 200,000 Hz, alternating) for rapid evaluation of shear fatigue properties of high-strength rolling bearing steels under a wider loading range. This paper describes NTN's development work with its unique

\*Advanced Technology R&D Center

\*\*Department of Mechanical Engineering, Faculty of Engineering, Shizuoka University

\*\*\*Emeritus Professor of Shizuoka University

ultrasonic torsional fatigue tester and evaluation of shear fatigue properties of bearing steel JIS-SUJ2.

## 2. Ultrasonic Torsional Fatigue Tester

### 2.1 Constitution of NTN's ultrasonic torsional fatigue tester

Fig. 1 schematically shows the constitution of the tester. The major components of the tester are a torsional vibration converter (loading frequency range: 20,000 ± 500 Hz), amplifier and torsional vibration magnifying horn. Though having a relatively low rated output of 300 W, the torsional vibration converter is capable of applying a stable, high shear stress to the specimen by optimizing the configuration of the specimen and torsional amplitude magnifying horn.

As a result of repeated application of the shear stress onto a specimen of rolling bearing steel, a crack will eventually occur on the specimen. When the severity of the crack reaches a particular level, the resonance frequency of the specimen will drop. Based on this knowledge, we have developed a test procedure; according to which, when the resonance frequency of the specimen exceeds a preset variation, the specimen is regarded as failed and the test is terminated.

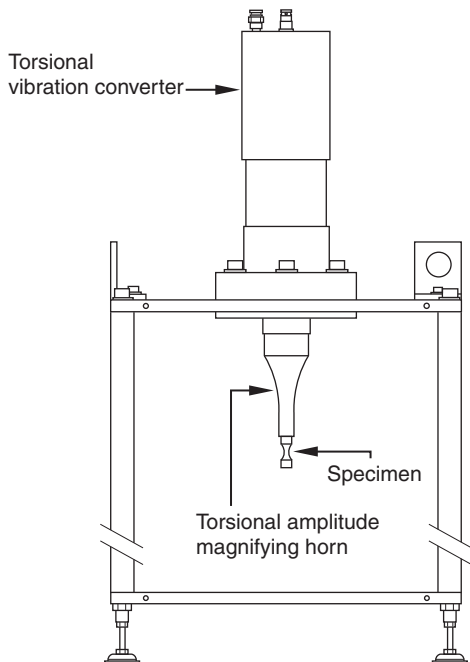


Fig. 1 Schematic of ultrasonic torsional fatigue tester

### 2.2 Design of specimen

Fig. 2 schematically shows the test specimen. The specimen is a dumbbell type that is defined with shoulder length  $L_1$ , half chord length  $L_2$ , shoulder radius  $R_2$ , minimum radius  $R_1$  and arc radius  $R$ . In designing the specimen, arbitrary  $L_2$ ,  $R_2$  and  $R_1$  are first chosen, and substituted into Expressions (1) through (6) along with resonant frequency = 20,000 Hz,  $E = 204$  GPa,  $\nu = 0.29$ ,  $\rho = 7,800$  kg/m<sup>3</sup> ( $E$ ,  $\nu$  and  $\rho$  are actual measurements taken on SUJ2) Thereby, a theoretical solution  $L_1$  is determined<sup>5)</sup>. Arc radius  $R$  can be determined with  $R_1$ ,  $R_2$  and  $L_2$ . At first, a test piece was prepared whose length satisfies the theoretical solution  $L_1$ ; however, this specimen did not develop resonance.

$$G = \frac{E}{2(1+\nu)} \dots\dots\dots (1)$$

$$\omega = 2\pi f \dots\dots\dots (2)$$

$$\alpha = \frac{1}{L_2} \operatorname{arccos} h \left( \frac{R_2^2}{R_1^2} \right) \dots\dots\dots (3)$$

$$k = \omega \sqrt{\frac{\rho}{G}} \dots\dots\dots (4)$$

$$\beta = \sqrt{\alpha^2 - k^2} \dots\dots\dots (5)$$

$$L_1 = \frac{1}{k} \operatorname{arctan} \left[ \frac{1}{k} \{ \beta \coth(\beta L_2) - \alpha \tanh(\alpha L_2) \} \right] \dots\dots (6)$$

Then, eigenvalue analysis for free torsional resonance was executed on the basis of FEM. Consequently, the resonance frequency of the specimen FEM model whose theoretical solution was  $L_1$  was 19,025 Hz, which did not fall in the loading frequency range of the torsional vibration converter (20,000 ± 500 Hz). Through eigenvalue analysis,  $L_1$  value that results in a resonant frequency of 20,000 Hz was determined.

Fig. 3 graphically plots the axial distribution of angle  $\theta$  and shear stress  $\tau$  on surface of specimen determined by eigenvalue analysis on free torsional resonance on the specimen FEM model. The torsional angle at the end face of the specimen was assumed to be  $\theta_{\text{end}} = 0.01$  rad, wherein the maximum shear stress acting on the surface of minimum diameter section of the specimen was  $\tau_{\text{max}} = 526$  MPa. Consequently, the relationship between  $\theta_{\text{end}}$  and  $\tau_{\text{max}}$  in the linear elasticity region can be shown by Expression (7) as follows:

$$\tau_{\text{max}} = 5.26 \times 10^4 \theta_{\text{end}} \dots\dots\dots (7)$$

Incidentally, the specimen in Fig. 2 lacks a parallel section. Thus, minor stress concentration occurs at the minimum diameter area. Nevertheless, the stress concentration coefficient is  $\alpha = 1.054$ <sup>8)</sup>, and is not a great value. Note that the possible values  $\alpha$  determined by Expression (7) include  $\alpha = 1.054$ .

**2.3 Optimized relationship in shape between specimen and torsional amplitude magnifying horn**

The magnitude of the maximum shear stress acting on the surface of the specimen's minimum diameter section is greater with a larger specimen size. However, a larger specimen size resulted in unstable resonance, and unwanted stoppage of the test. Therefore, the specimen size was determined so that the specimen can stably develop resonance up to 90% of the amplifier output and at the same time the magnifying power of the torsional amplitude magnifying horn was increased.

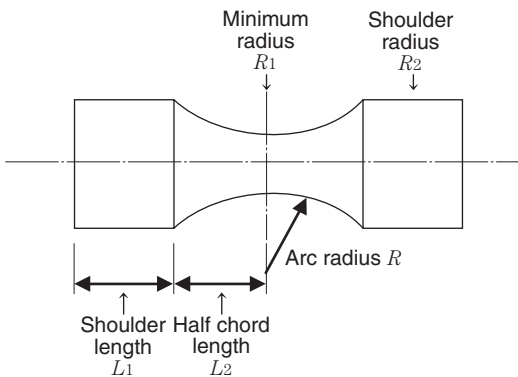


Fig. 2 Schematic of specimen

Fig. 4 shows the shape of a highly efficient torsional amplitude magnifying horn as well as graphical plotting of the axial distribution of the torsional angle obtained from eigenvalue analysis for free torsional resonance on the FEM model. The amplitude magnifying horn was designed and adjusted so that it develops resonance at around 20,000 Hz. The specimen material is Ti alloy ( $E = 116$  GPa,  $\nu = 0.27$ ,  $\rho = 4.460$  kg/m<sup>3</sup>). When the torsional angle at the large end face is  $\theta_{end,L} = 0.000418$  rad, the torsional angle at the small end face is  $\theta_{end,S} = 0.018$  rad. This means the torsional angle magnifying power is 43.1.

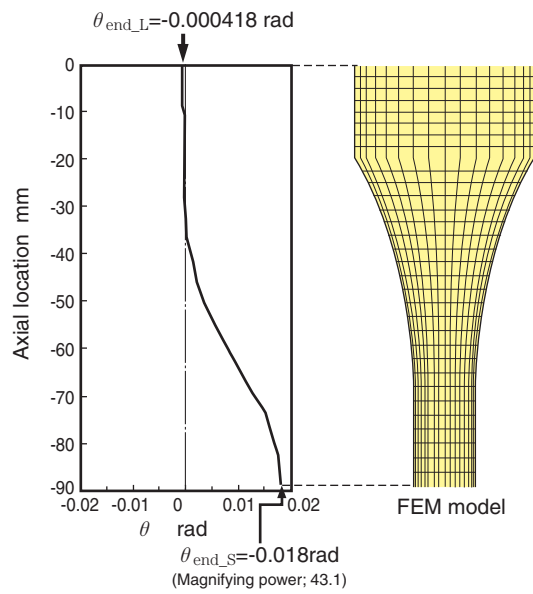


Fig. 4 Shape of a highly efficient torsional amplitude magnifying horn and the axial distribution of torsional angle distribution

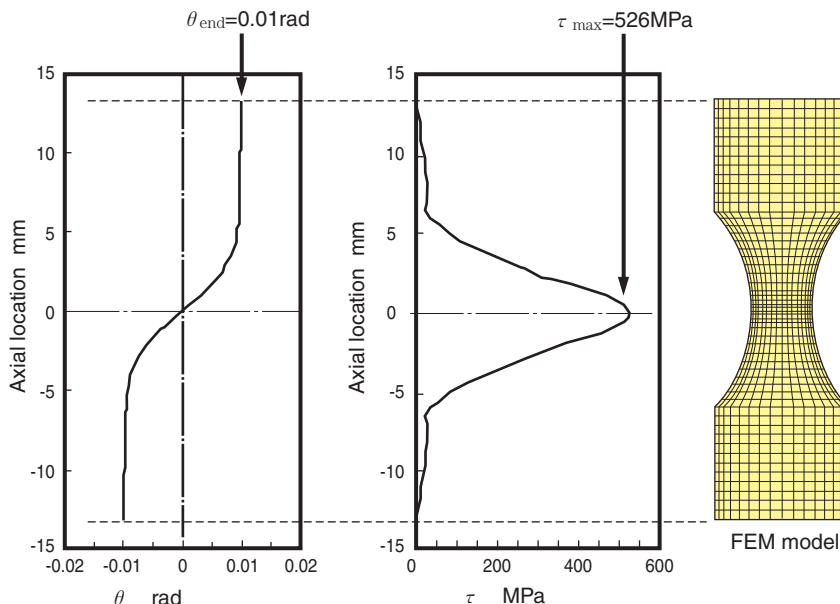


Fig. 3 Axial distribution of angle  $\theta$  and shear stress  $\tau$  on the surface of the specimen determined by eigenvalue analysis on free torsional resonance (When torsional angle  $\theta_{end} = 0.01$  rad at end face of specimen)

### 2.4 Amplitude measurements of maximum shear stress acting on the surface of the specimen's minimum diameter section

**Table 1** summarizes chemical components in high-carbon chromium bearing steel JIS-SUJ2 used to fabricate the specimen. The specimen was prepared through turning, heat treatment and finish by grinding. The heat treatment process consisted of heating (830°C for 80 min.), oil hardening (80°C), and tempering (180°C for 180 min.).

Using three pieces of the specimen, the torsional angle  $\theta_{end}$  (rad) on the end face of the specimen was measured with varied amplifier output  $P$  (%). The amplifier output  $P$  was varied from 10% to 90% in 5% increments. Thereby, the torsional width at the end face  $2a$  was measured and torsional angle  $\theta_{end}$  was determined on the basis of the relationship illustrated in **Fig. 5**. Consequently, a linear relationship has been

**Table 1** Chemical components in SUJ tested (in wt%; ppm for O)

C	Si	Mn	P	S	Ni	Cr	Mo	Cu	O
1.02	0.27	0.43	0.014	0.007	0.05	1.48	0.04	0.09	6

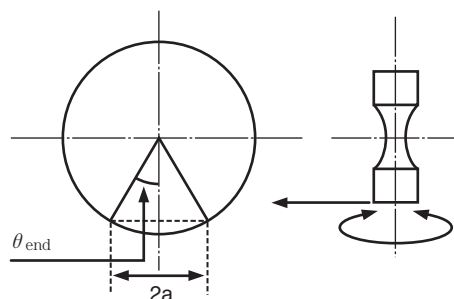


**Fig. 5** Relationship between torsional width  $2a$  and torsional angle  $\theta_{end}$  at the end face of specimen

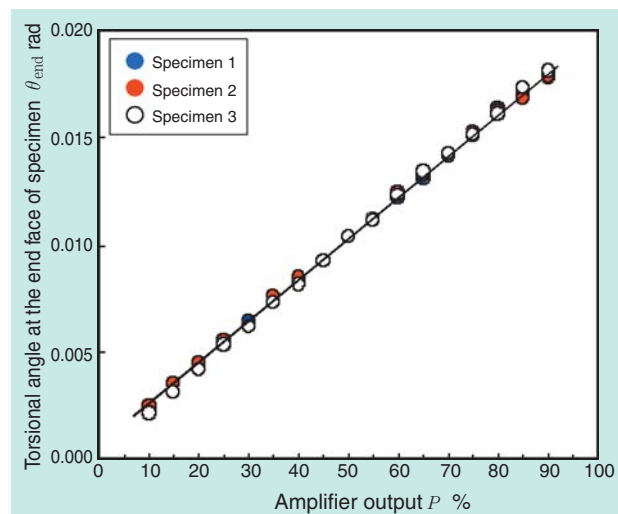


**Fig. 6** Relationship between amplifier output  $P$  and torsional angle at the end face of specimen  $\theta_{end}$

established between  $P$  and  $\theta_{end}$  as shown in **Fig. 6**. Thereby Expression (8) was obtained which represents a regenerative line. Expression (9) was developed using (7) and (8), defining the relationship between the amplifier output  $P$  and the maximum torsional stress amplitude  $\tau_{max}$  acting on the surface of the specimen's minimum diameter section. From Expression (9), when  $P = 90\%$ ,  $\tau_{max} = 951$  MPa. Thus, it has been found that this amplitude is great enough to cause high-strength rolling bearing steel to develop shear fatigue fracture.

$$\theta_{end} = (1.96 \times 10^{-4})P + 4.35 \times 10^{-4} \dots\dots\dots (8)$$

$$\tau_{max} = 5.26 \times 10^4 \theta_{end} = 10.3 P + 22.9 \dots\dots\dots (9)$$

### 2.5 Effective loading frequency in intermittent loading mode

**Fig. 7** shows the scheme of intermittent loading<sup>9)</sup>. A period of 0.01 s is needed before the specified amplifier output is reached. This period is designated rise time  $t_s$ . The number of loading cycles in this period is not included in the count of loading cycles. Also, when the predetermined loading time  $t_d$  has elapsed and the amplifier output has dropped to zero, vibration will gradually subside, rather than stopping immediately: loading cycles during this attenuation period are not counted, but the time is included in the non-loading time  $t_p$ . Therefore, when loading frequency is taken as  $f$ , then effective loading frequency  $f_e$  can be determined by Expression (10) below:

$$f_e = \frac{f \cdot t_d}{(t_s + t_d + t_p)} \dots\dots\dots (10)$$

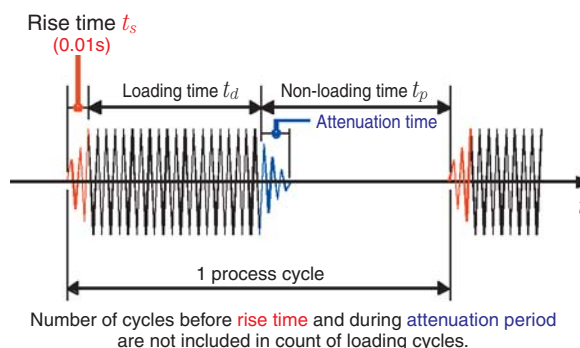


**Fig. 7** Scheme of intermittent loading

### 3. Evaluation of Shear Fatigue Properties of SUJ2 by Ultrasonic Torsional Fatigue Test

Shear fatigue properties of the SUJ specimen—the same specimen type previously described in Sec. 2.4 was tested. In order to eliminate possible effect of surface roughness, the nodes on the specimen were mirror-finished by subjecting these nodes to polishing with emery paper (#500 and then #2000) and lapping with diamond powder (grain size 1 μm) while turning the specimen.

To avoid heat buildup on the specimen, dry air was blown to the nodes for force-cooling. During testing, the temperature on the minimum diameter section was measured with a radiation thermometer; as a result, it was determined that significant heat is generated at a shear stress amplitude of 700 MPa or greater. Virtually no heat generation was found at an amplitude less than 700 MPa. For this reason, one phase of up to 10<sup>7</sup> cycles was designed to consist of 0.11 s of loading and 1.1 s of non-loading. If the specimen did not fail before the completion of this phase the test was temporarily suspended, and then resumed with a loading cycle consisting of 1 s of loading and 0.2 s of non-loading. If the specimen did not develop failure before 10<sup>10</sup> cycles, the test was terminated. If the loading frequency is set to 20,000 Hz, then by calculation with Expression (10) given in Sec. 2.5, the effective loading frequency is 1,803 Hz with each cycle consisting of 0.11 s of loading and 1.1 s of non-loading, and is 16,529 Hz with each cycle consisting of 1 s of loading and 0.2 s of non-loading.

Fig. 8 graphically plots the shear fatigue properties of SUJ2 obtained from evaluation by intermittent

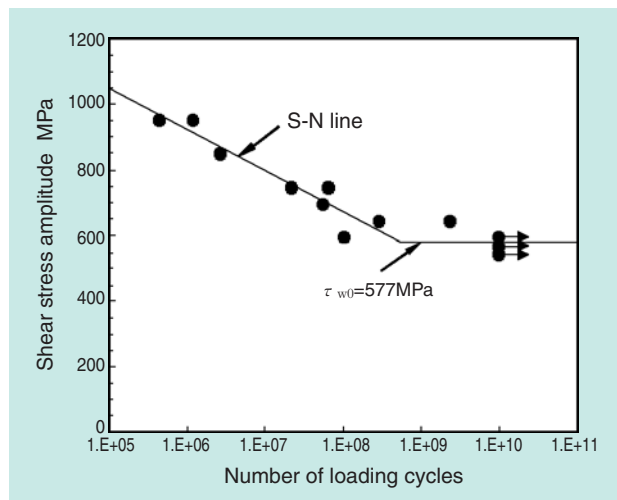


Fig. 8 Shear fatigue properties of SUJ2 evaluated by ultrasonic torsional fatigue test

operation of the ultrasonic torsional fatigue tester. The solid line in Fig. 8 is an S-N line fitted to the fatigue limit polygonal line model per metal material fatigue reliability evaluation standard JSMS-SD-6-02 of The Society of Materials Science, Japan where the shear fatigue limit is  $\tau_{w0} = 577$  MPa.

Observation of a particular area on the surface of each failed specimen, to which the maximum stress acts, reveals that initial shear-mode crack in the axial direction as shown in Fig. 9 appears on all the specimens.

### 4. Discussion

NTN's supersonic torsional fatigue tester (alternating) not only functions as a rapid torsional fatigue tester but also appears to provide the ability to estimate fatigue limit contact pressure of rolling bearing steel by evaluating shear fatigue properties up to giga-cycles range (e.g. 10<sup>10</sup> loading cycles). Rolling bearings have recently been used for greatly prolonged service periods. To address this situation, fatigue limit contact pressure has been used in the life calculation formula in the relevant ISO standard<sup>10)</sup>. Practice for estimating fatigue limit contact pressure is discussed below. Incidentally, there is a report about evaluation of fatigue properties of SUJ2 in a manner similar to that in this paper, with a conventional torsional fatigue tester. This report states that there is no shear fatigue limit with SUJ2 because all the specimens failed within 10<sup>10</sup> loading cycles<sup>11)</sup>. From Fig. 8, it appears that 10<sup>8</sup> loading cycles are in the time-strength regime, and more loading cycles are necessary to be able to determine the shear fatigue limit of SUJ2.

From Fig. 8, it is apparent that the shear fatigue limit of SUJ2 is  $\tau_{w0} = 577$  MPa. In line contact scenario, the maximum contact pressure  $P_{max}$  is four

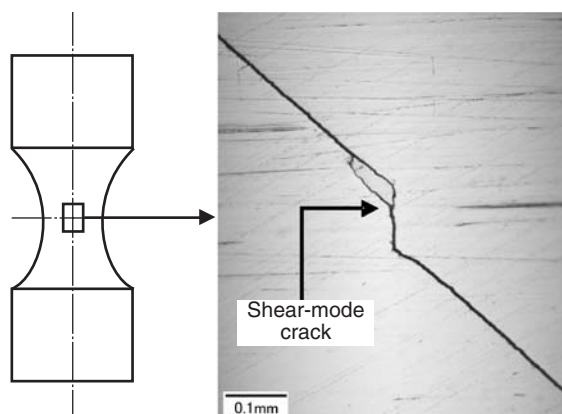


Fig. 9 Magnified view of initial shear-mode crack

times as great as the repetitive orthogonal shear stress amplitude  $t_0$ , as described in Sec. 4.3. To be able to estimate the fatigue limit contact pressure, we believe the following two modifications are necessary.

**Fig. 10** graphically plots the shear fatigue limit  $\tau_{w0}$  that reflects the following modifications:

- (1) Modification for failure probability (see Sec. 4.1)
- (2) Modification for size effect (see Sec. 4.2)

#### 4.1 About modification for failure probability

Results of fatigue testing include variation. Therefore, it is preferable that fatigue properties be determined through statistical techniques. For this purpose, a P-S-N line may be developed by evaluating several specimens at various stress levels. However, implementing this technique will be difficult in many cases due to limited time. The metal material fatigue reliability evaluation standard JSMS-SD-6-02 of The Society of Materials Science, Japan was applied to determine the shear fatigue limit  $\tau_{w0}$  from the shear fatigue properties in **Fig. 8**. This standard provides the ability to develop a P-S-N line from a smaller number of data sets. The broken line in **Fig. 10** shows the resultant P-S-N line at 10% failure probability, wherein the shear fatigue limit is  $\tau_{w0} = 515$  MPa.

#### 4.2 About modification for size effect

In the torsional fatigue test the specimen exhibits a shear stress gradient that is highest at the surface of specimen and lowest at the center of specimen. It is known that in various tension-compression fatigue tests, the vertical stress is uniform within the specimen cross-section at the parallel section, and has a particular fatigue limit regardless of the diameter. In contrast, rotary bending fatigue testing has a stress gradient. It is known that the specimen exhibits a size

effect, where the fatigue limit is lower at the larger diameter on the parallel section and gradually nears the fatigue limit found in axial load fatigue test<sup>12)</sup>. In NTN's test method, three different steels each having unique tensile strengths have been subjected to axial load fatigue testing and rotary bending fatigue testing (with varied diameters on parallel section) to determine the fatigue limit for each steel type. As a result, it has been learned that the fatigue life in axial load fatigue testing, regardless of the steel type, is approximately 80% that of the fatigue limit resulting from rotary bending testing on the parallel section of diameter 4 mm.

In summary, the fatigue limit in the axial load fatigue test, not having a stress gradient, makes the standard safe in tension-compression fatigue testing. On the other hand, because not having a stress gradient, the torsional fatigue test does not provide such a standard, even when the diameter of the parallel section is enlarged as much as possible. As long as there is a stress gradient, torsional fatigue testing cannot be free from size effects. To address this issue, it was assumed in **Fig. 10** that the standard for tension-compression fatigue testing can be applied without any modification to torsional fatigue testing. In other words, because the minimum diameter of the ultrasonic torsional fatigue specimen measures 4 mm, shear fatigue limit  $\tau_{w0}$  is multiplied by factor 0.8, resulting in  $\tau_{w0} = 412$  MPa.

#### 4.3 Estimation for fatigue limit contact pressure in line-contact mode

The relationship between the ratio of the major axis radius ( $a$ ) to the minor axis radius ( $b$ ) of contact ellipse ( $b/a$ ) and  $2\tau_0/P_{max}$  can be approximately defined by Expression (11)<sup>13)</sup>. The fatigue limit contact pressure can be estimated by substituting value of  $b/a$  in Expression (11). In the case of line contact mode, that is,  $b/a \rightarrow 0$ ,  $P_{max}$  is 4 times as great as  $\tau_{w0}$  from Expression (11):

$$\frac{2\tau_0}{P_{max}} = -1.00 \times 10^{-3} \left(\frac{b}{a}\right)^4 + 4.86 \times 10^{-2} \left(\frac{b}{a}\right)^3 - 1.12 \times 10^{-1} \left(\frac{b}{a}\right)^2 - 7.44 \times 10^{-3} \left(\frac{b}{a}\right) + 5.00 \times 10^{-1} \dots (11)$$

The shear fatigue limit having undergone modification for failure probability and size effects is  $\tau_{w0} = 412$  MPa. Accordingly, the fatigue limit contact pressure is estimated at  $P_{max\ lim} = 4\tau_{w0} = 1,648$  MPa. Incidentally, the latest ISO standard (2007 revision)<sup>10)</sup> specifies the fatigue limit contact pressure of 1,500

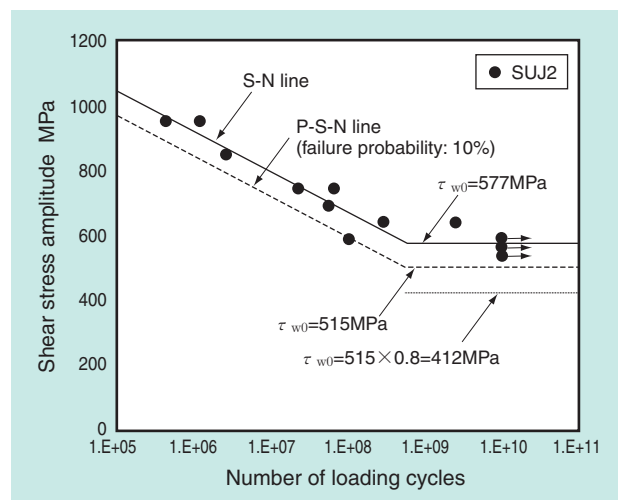


**Fig. 10** Shear fatigue limit  $\tau_{w0}$  with modification for failure probability and size effect

MPa. Our experimentally obtained fatigue limit contact pressure, mentioned above, is virtually same as the value in the ISO standard.

## 5. Conclusion

A typical example of stress among those governing occurrence of initial shear-mode crack prior to subsurface flaking failure on rolling bearings due to rolling fatigue is repetitive orthogonal shear stress (near-purely alternating) that repeatedly acts on the surface of the bearing. However, even if a rolling bearing is tested under low loading conditions, a subsurface flaking failure will not occur during a limited practical time frame. Though shear fatigue properties of rolling bearing steel can be evaluated through torsional fatigue testing, conventional fatigue testers are only capable of applying low frequency loading to specimens, and are virtually incapable of property evaluation up to giga-cycles ranges.

To be able to quickly evaluate shear fatigue properties of high-strength rolling bearing steels, **NTN** has attempted to develop a unique ultrasonic torsional fatigue tester (loading frequency 20,000 Hz, alternating), which is capable of exerting shear stress amplitudes of up to approximately 950 MPa to specimens. With this tester, **NTN** has successfully obtained shear fatigue properties of high-carbon chromium bearing steel JIS-SUJ2 from low cycle to high cycle regimes.

## Reference

- 1) Lundberg, G. and Palmgren, A., Acta Polytechnica, Mech. Eng. Series, 1-3, 5-58, 1947.
- 2) Stanzl-Tschegg, S., Mayer, H., and Tschegg, E. Ultrasonic, 31, 275-280, 1993.
- 3) Iijima, J., Ishii, H., Araki, H., Tohgo, K., High cycle torsion fatigue characteristic by ultrasonic fatigue testing method, Proceedings of the 54th Tokai Branch Regular Meeting of the Japan Society of Mechanical Engineers, 131-132, 2005.
- 4) Mayer, H., Int. J. Fatigue, 28, 1446-1455, 2006.
- 5) Garcia, I.M., Doucet, J.P. and Bathias, C., Int. J. Fatigue, 29, 2094-2101, 2007.
- 6) Akiniwa, Y., Stanzl-Tschegg, S., Mayer, H., Wakita, M. and Tanaka, K., Int. J. Fatigue, 30, 2057-2063, 2008.
- 7) Shimamura, Y., Narita, K., Ishii, H., Tohgo, K., Fujii, T., Yagasaki, T., Harada, M., Very High Cycle Fatigue Properties of Carburized Steel by Ultrasonic Torsional Fatigue Testing, 59, 938-943, 2010.
- 8) Pilkey, W.D., Peterson's Stress Concentration Factors (2nd Ed.), John Wiley & Sons, 128, 1997.
- 9) Ishii, H., Yamanaka, K. and Tohgo, K., Material Science Research International, Special Technical Publication 1, 59-63, 2001.
- 10) ISO 281, Rolling Bearings—Dynamic Load Ratings and Rating Life, 2nd Ed., 2007-02-15, Ref. No. ISO 281(E), 2007.
- 11) Shimizu, S., Tsuchiya, K. and Tosha, K., Tribol. Trans. 52, 807-816, 2009.
- 12) Ouchida K., Journal of the Japan Society of Mechanical Engineers, 64, 263-272, 1961.
- 13) Harris, T. A., Rolling Bearing Analysis, 3rd Ed., Wiley-Interscience, 147, 1991.

## Photo of authors



Noriaki SAKANAKA  
Advanced Technology  
R&D Center



Yukio MATSUBARA  
Advanced Technology  
R&D Center

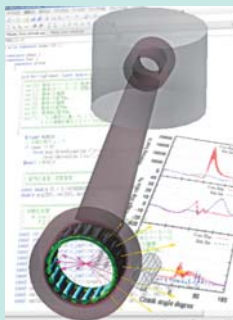


Yoshinobu SHIMAMURA  
Department of Mechanical  
Engineering,  
Faculty of Engineering,  
Shizuoka University



Hitoshi ISHII  
Emeritus Professor of  
Shizuoka University

## Two-Dimensional Dynamic Analysis of Cage Stress for Needle Roller Bearings that Support Connecting Rods in Reciprocating Engines



Tomoya SAKAGUCHI\*

In this paper, the author numerically analyzes cage stress in a connecting rod needle roller bearing by using a dynamic rolling bearing model considering both roller and cage motions as well as the cage elastic deformation. The analyses were conducted for four conditions in a small motorcycle engine: maximum torque, maximum power, maximum speed and overrun speed.

The results show that the cage stress rises at a moment immediately after ignition and during the intake stroke when the crank angle is approximately 90 degrees from the top dead center position. Additionally, it was determined that cage stress increases with the crank rotational speed.

### 1. Introduction

Single cylinder motorcycle engines adopt crankshaft assemblies, and the interface between the crankshaft and connecting rod (at the connecting rod large end) often incorporates a needle roller bearing because its starting torque is lower compared to a sliding bearing.

As demand for reduction in size and weight of connecting rods increases, the needle roller bearings used for supporting connecting rods are required to have greater load capacity. In order to increase load capacity of a bearing within a limited space, increase in length and number of rollers is the primary solution. However, this solution leads to thinner cage ribs spacing the rollers, resulting in a decrease in the cage mechanical strength. To address this issue, a cage must be designed to have the mechanical strength sufficient enough to avoid potential failure. Therefore, it is necessary to calculate stresses on the cage with higher accuracy.

The needle roller bearing motion at the crankshaft end of the connecting rod is fairly complicated. The inner ring raceway orbits around the center of crankshaft while the outer ring raceway oscillates relative to the inner ring raceway. The loads acting on the bearing are pressure load from the piston, inertia force from reciprocating motion and oscillating motion of the connecting rod, and centrifugal force from the crankshaft rotary motion.

Because of such a complex combination of motions, it is very difficult to measure in real-time the values of

forces and their resulting stresses within the needle roller bearing. Fujiwara, et. al. built a test machine that can simulate the load acting on the connecting rod large bearing and attempted to numerically determine the behavior of the cage. This approach, however, does not cover orbital motions<sup>1)</sup>.

To cope with the difficulties in experimental research into these motions, there have been attempts to build dynamic models involving the rollers and cage in order to determine numerically the time-dependent motions of these components<sup>1)-3)</sup>. Regrettably, other than the areas in contact with the rollers or raceway, the cage was regarded as a rigid body, and stress acting on the cage was not considered in any of these models.

The author has attempted to research the motion of rolling bearings through dynamic analysis<sup>4) 5)</sup> while being conscious about the cage's elastic deformation. Consequently, the author has learned that in planetary applications the stress occurring on the needle bearing cage increases as the bearing speed increases; an increase such that the calculated maximum principle stress in the cage exceeds the fatigue limit of the cage material resulting in a cage failure in a relatively short timeframe<sup>5)</sup>.

In this study, the author has applied a dynamic analysis code<sup>4)</sup>, originally developed for planetary applications, to analyze the effects of operating conditions on crankshaft end, needle bearing cage stress.

\*Advanced Technology R&D Center

## 2. Analysis Method

The components of this analysis include the piston, connecting rod, crankshaft, and the mating needle roller bearing as shown in Fig. 1. Major assumptions of this analysis are as follows:

1. Three (3) degrees of freedom with rollers, cage and connecting rod located on the yz plane.
2. Elastic deformation of the cage is considered using the mode synthesis method<sup>1), 6)</sup>.
3. The center axis of the crankshaft is fixed, and the crankshaft turns at a constant speed.
4. The piston is linked to the connecting rod via a smoothly rotating joint and smoothly reciprocates in the cylinder (friction is ignored while the piston is constrained to move only in the y direction as shown in Fig. 1).
5. The rollers, cage, and raceway are mutually in an elastic contact state, and the normal force working on them is defined by Hertz contact pressure.
6. Traction forces deriving from sliding on the raceway surface and acting on the rollers in the rolling direction are considered. Traction coefficient is modeled using a function that reflects the effect of proportion of oil film thickness to surface roughness<sup>7)</sup>.
7. Rolling contact forces acting between the rollers and raceway caused by the rolling viscosity drag occurring from oil film<sup>8)-10)</sup> and rolling direction component occurring from pressure of oil film<sup>8), 10)</sup> are considered. These forces are determined by the calculation techniques described by Zhou, et. al.<sup>10)</sup>

On the basis of these assumptions, the author has modeled the rollers, cage, connecting rod, piston, and crankshaft, as well as the interfering forces working between these components. As a result, the motions of these components, the deformation of the cage, and the resulting stresses are calculated.

## 3. Objects Being Analyzed

Table 1 summarizes the specifications of the engine and bearing and the lubrication conditions to be analyzed.

Table 2 summarizes the operating conditions of the engine being analyzed. These conditions are four typical operating conditions seen in actual motorcycle engines. Fig. 2 shows a plot of the time-dependent variation in piston load that occurs on the piston due

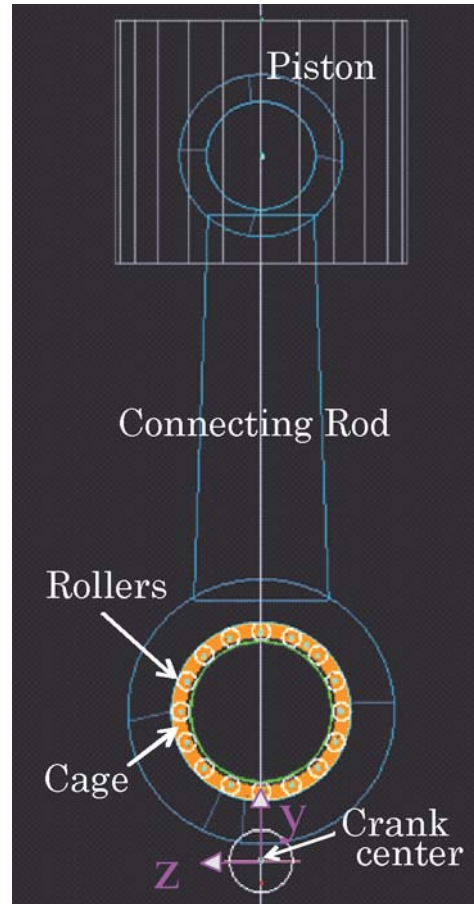


Fig. 1 Objects being analyzed, and coordinate system used

Table 1 Major specifications of the engine bearing, and lubrication conditions

Case for 4-cycle single-cylinder 125 cc engine	
Crank radius	27.6 mm
Connecting rod length	102.7 mm
Connecting rod mass	0.0552 kg
Connecting rod center of gravity position* (*: height relative to center of big end)	35.9 mm
Connecting rod moment of inertia	202 kg · mm <sup>2</sup>
Piston mass	0.0480 kg
Bearing specifications	
Bore diameter	26 mm
Outside diameter	33 mm
Roller diameter	3.495 mm
Roller length	10.8 mm
Number of rollers	16
Lubricating oil, kinematic viscosity	100.5 mm <sup>2</sup> /s @ 40°C 11.8 mm <sup>2</sup> /s @ 100°C
Representative temperature	135°C

Table 2 Operating conditions of the engine

Operating condition	Engine speed min <sup>-1</sup>	Max. piston load kN
Max. torque	5,000	16.3
Max. output	7,500	13.9
Max. speed	9,500	9.7
Overrun	10,500	7.6

i) Mode synthesis method is a technique to reproduce a complicated deformation by addition and/or subtraction of simple deformation modes.

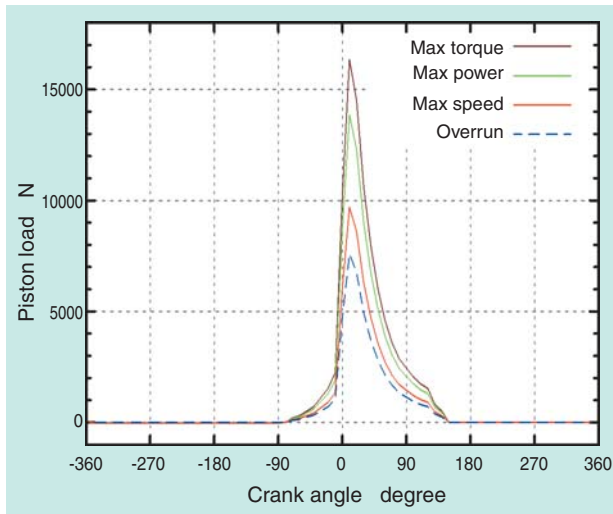


Fig. 2 Piston loads under various operating conditions

to combustion pressure. The “0 degree” position of the X axis represents a crank angle corresponding with the top dead center position.

#### 4. Results of Dynamic Calculation

Fig. 3 shows the time-dependent change in angular velocities of the major components, the piston load, the bearing load, the slip ratio on cage, and the maximum principle stress on the cage under maximum torque conditions. The variation in angular velocity of the outer ring shown in Fig. 3a) corresponds with the variation in oscillating motion of the outer ring. Also, this chart makes it apparent that the angular velocity of the cage varies in synchronization with variation in its oscillating motion. Fig. 3c) illustrates the slip ratio of the cage. The slip ratio of the cage is defined as a percent decrease in the effective cage rotational speed relative to the cage rotational speed when there is no slip on the raceway. When comparing slip ratio with the load on the bearing, the slip ratio is greater in a low load region as shown in Fig. 3b). Fig. 3d) plots maximum principle stresses on various points of the cage versus time (for overview of the record of maximum stresses over the entire area of the cage, the records for multiple points are indicated). “Com” in this chart stands for compression stroke, “Exp” explosion stroke, “Exh” exhaust stroke, and “Int” intake stroke. The principle stress soars up at the moment at which ignition occurs in the cylinder (0.024 s and 0.048 s), then gradually decreases.

Figs. 4 through 6 are time-dependent plots of cage loads and principle stresses under each of three additional operating conditions. Figures 4, 5, and 6 have higher speeds respectively. As indicated in the

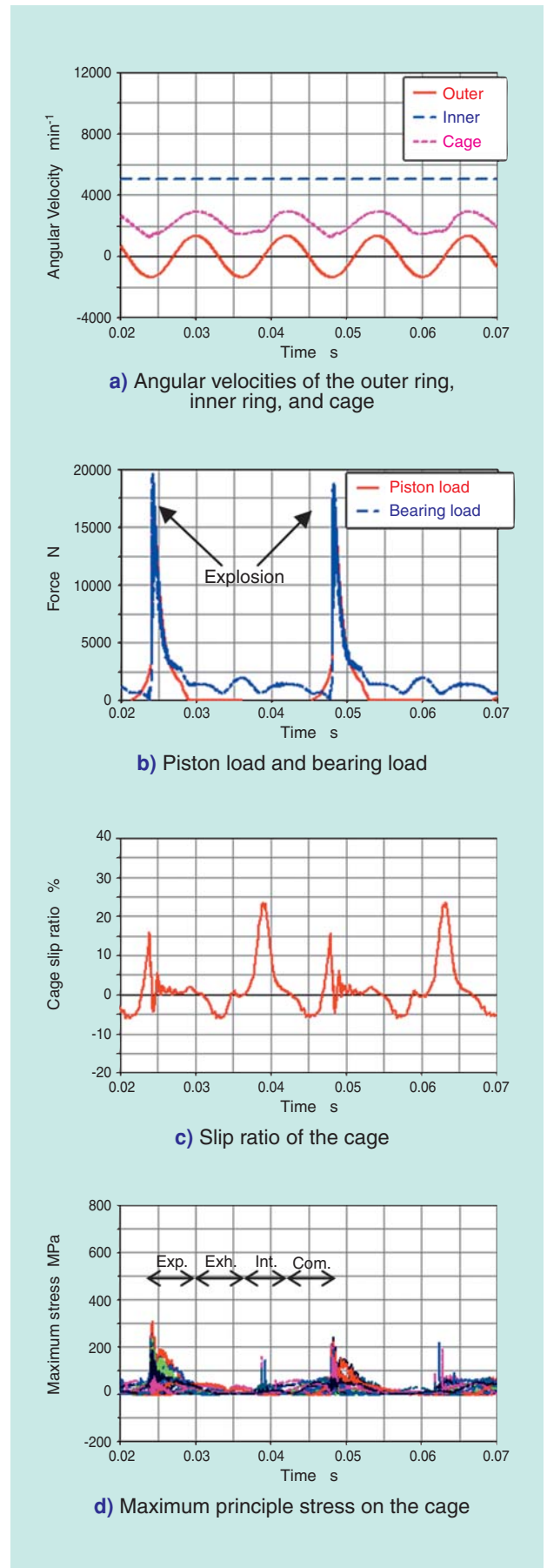


Fig. 3 Results of numerical analysis in the " Maximum-torque" conditions

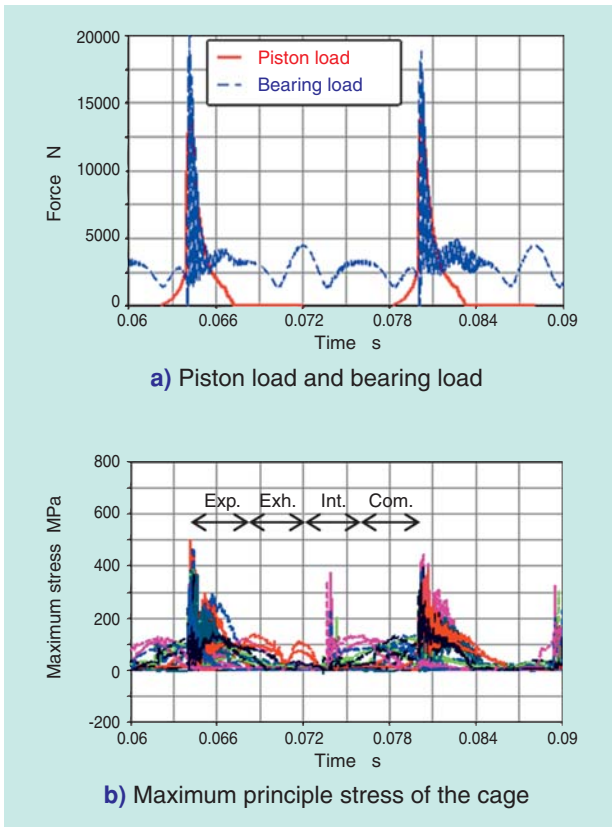


Fig. 4 Results of the numerical analysis in "Maximum-power" conditions

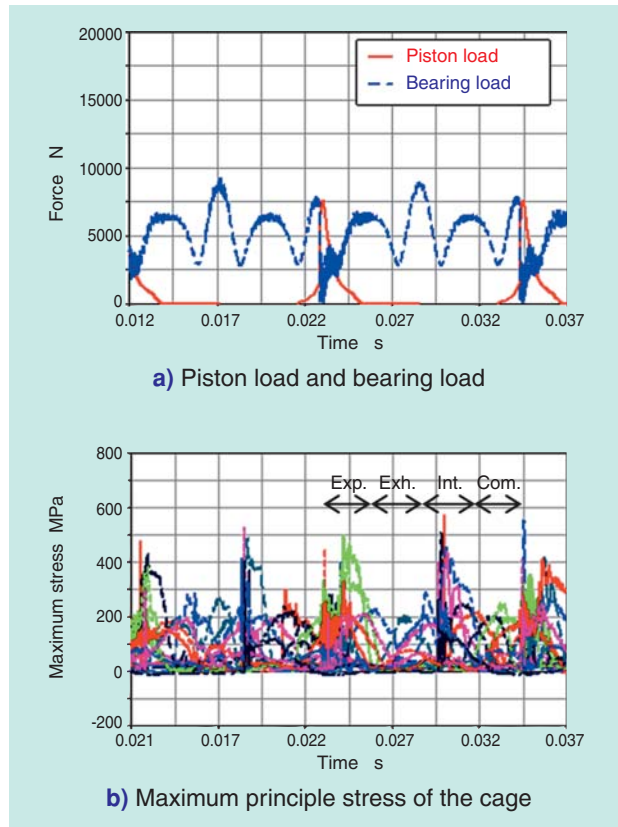


Fig. 6 Results of the numerical analysis in "Overrun" conditions

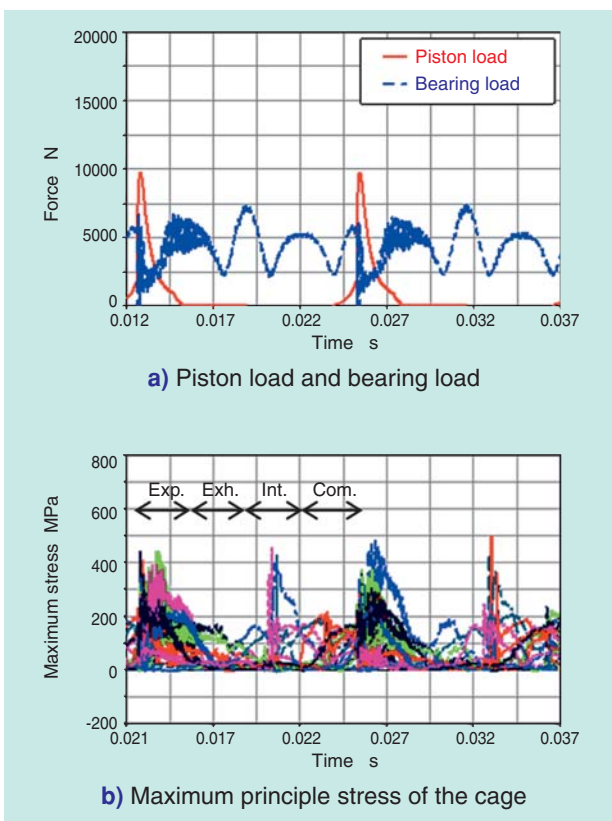


Fig. 5 Results of the numerical analysis in "Maximum-speed" conditions

force versus time graphs, when the rotational speed increases the bearing load during non-power strokes will be greater. This force increase is because of the inertia force of the piston and connecting rod. The direction of this inertia force at top or bottom dead center is away from the crank center: consequently, the direction of inertia is opposite to the explosion.

Therefore, the bearing load at ignition is relatively low while the engine is running at higher speed. With an increase in rotational speed, the stress on the cage during the intake stroke will be gradually increased. Likewise, with an increase in rotational speed, the stress on the cage at ignition will be greater. Nevertheless, the increase in stress at ignition is generally small compared with that during the intake stroke.

## 5. Reasons for Increased Cage Stress

As a result of the analysis above, the author has estimated that there are two major causes of cage stress increase:

- (1) The roller which has started orbital motion without slip pushes the cage.
- (2) The roller which has left the load zone, at around the 90-degree position in the intake stroke (crank angle relative to the top dead center) is acted upon by the centrifugal force and hits a cage rib.

The reasons for increased cage stress will be further discussed while referring further analysis results.

**Fig. 7** shows the bearing loads, cage slip ratios, and maximum principle cage stress versus the crank angle under maximum torque (lowest speed) and overrun (highest speed) conditions. A crank angle of 0 in these plots corresponds with top dead center, “Com./Exp.” is the period from compression stroke to power stroke, and “Exh./Int.” is the period from exhaust stroke to intake stroke.

Under maximum torque conditions as shown in **Fig. 7a**, the cage slip ratio increases immediately before ignition, and suddenly drops immediately afterwards. During this time, the maximum possible stress occurs owing to reason (1) mentioned above. The slip ratio of the cage will be highest at around the 90 degree point in the intake stroke, and a spike exists in the of cage stress plot. This peak stems from reason (2) mentioned above.

**Fig. 8** is a snapshot of the bearing motion at the moment where the maximum principle stress occurs during the maximum torque condition (crank angle 10.5 degrees). This figure illustrates the moment immediately after the top portion of bearing has entered the load zone due to combustion within the engine; thus the maximum principle load is occurring in the load zone. In this figure, the crankshaft and cage are rotating counterclockwise, the color contour of the cage indicates the magnitude of maximum principle stresses, and the piston (not shown) is situated above the diagram. The roller situated at the 2 o'clock position is applying a counterclockwise force to the corresponding cage rib. **Fig. 9a**) schematically illustrates this roller and its surrounding cage ribs and shows the pre-ignition situation. Due to inertia of the piston and connecting rod, the rollers in the upper half of the diagram are not subjected to load from the raceway; these rollers are pushed away (in the upward direction in the diagram) relative to the crank center owing to the

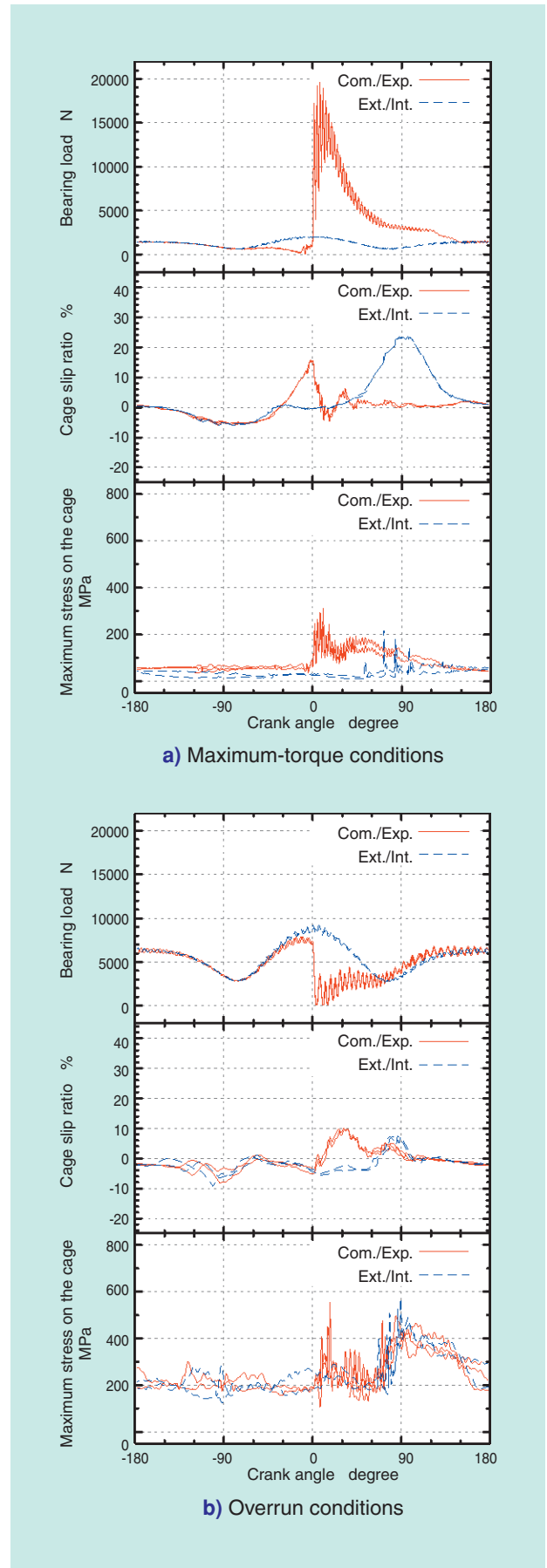


**Fig. 7** Bearing load, cage slip ratio and maximum principle stress on the cage relative to the crank angle

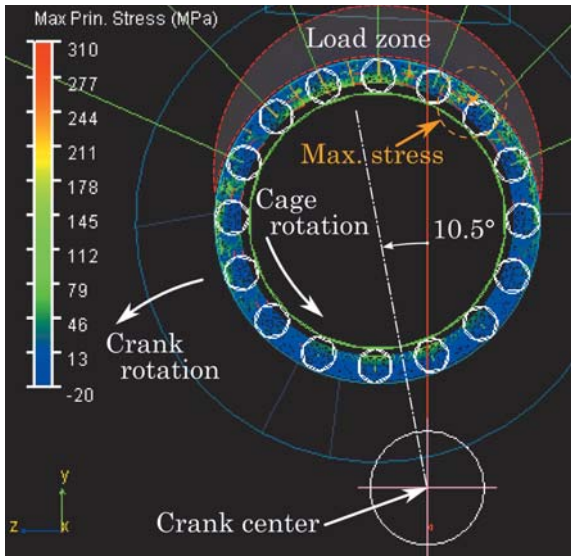
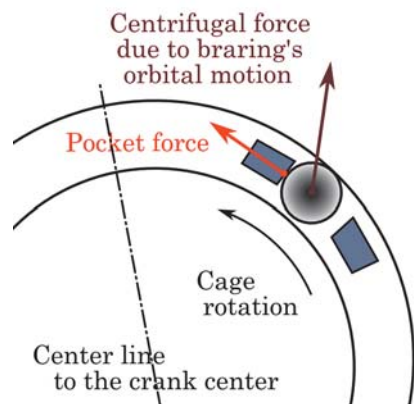
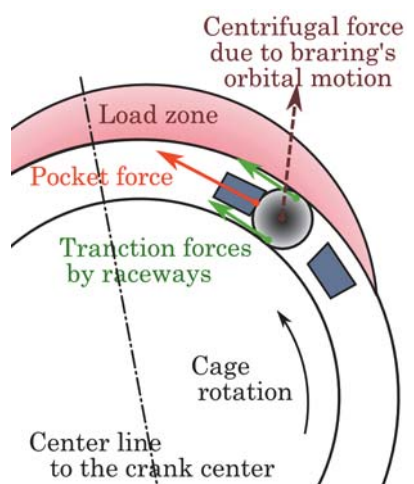


**Fig. 8** Configuration of the bearing where the maximum principle load acts on the cage under maximum torque conditions (explosion stroke, 10.5 degrees from top dead center)



**a)** Roller and cage in the unloaded zone immediately before explosion



**b)** Force acting on the cage rib at the moment of explosion

**Fig. 9** Stress increase mechanism for the cage at the moment of explosion

centrifugal force<sup>ii)</sup> on the rollers generated by the orbital motion of the bearing. Consequently, the roller at the 2 o'clock position comes into contact with the downstream cage rib during rotation causing the rib to deform. **Fig. 9b)** indicates the situation at the moment the explosion force has begun to act on the raceway. Indicating the effect of the piston load, the upper portion of **Fig. 9b)** shows the load zone. Being subjected to the sudden increase in loading from the raceway surface, the roller will begin to rotate rather than slide: consequently, this roller pushes the cage rib with a greater force, further deforming it. This describes the increase in cage stress owing to mechanism (1) above. The most likely reason why the roller at the 2 o'clock position generates the maximum stress is the simultaneous fulfillment of two conditions: first, the magnitude of the roller force (this force derives from centrifugal force occurring on the roller itself) acting on the cage rib is relatively large as shown in **Fig. 9a)**; and second, the magnitude of roller load from the explosion is relatively large, thus the frictional force from the raceway contact is large.

Within the results of the overrun-speed conditions shown in **Fig. 7b)**, the maximum principle load on the cage occurs at around the 90-degree point during the intake stroke. This results from cage stress increase mechanism (2) described previously. **Fig. 10** (intake stroke, 89.2 degrees after top dead center) shows the bearing in this situation. In **Fig. 10a)**, the roller at the 5 o'clock position, situated outside the load zone, collides with a cage rib. In this situation, the maximum stress occurs in the corner of the cage pocket, as shown in **Fig. 10b)**. This peak stress location coincides with the usual failure point of standard cages.

Now, referring to **Fig. 11**, cage stress increase mechanism (2) is further described. **Fig. 11** is a schematic rendering of the roller in the pocket where the maximum stress has occurred as described and shown in **Fig. 10**. In **Fig. 11** the piston is situated in the upper right, while the load zone is situated on the right. **Fig. 11a)** shows a snapshot just prior to the occurrence of the maximum principle stress. Consequently, the roller in the load zone at the 5 o'clock position applies a force accelerating the rotation of the cage towards the downstream cage rib. **Fig. 11b)** shows a snapshot immediately after the depiction in **Fig. 11a)**; wherein the maximum principle stress has occurred. Since the load zone shifts at a velocity greater than velocity of roller orbital motion, the roller is free from loading.

ii) The centrifugal force deriving from rotation of the roller around the bearing acts vertically onto the outer ring raceway; thus it does not affect rotation of the roller nor the magnitude of force acting on the cage.

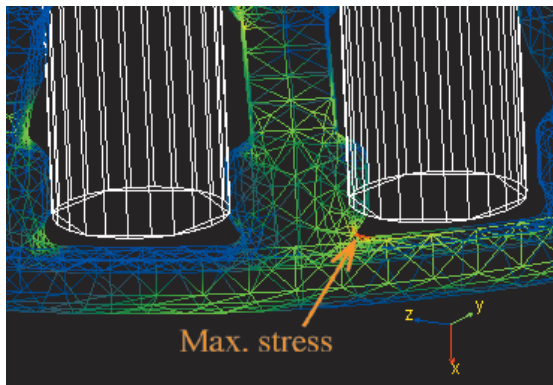
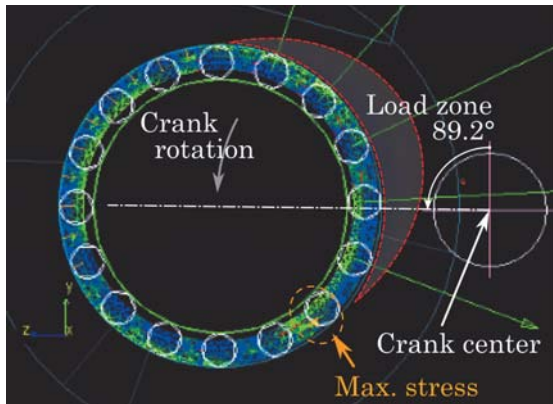


**Fig. 10** Situation where the maximum principle stress occurs on the cage under the overrun condition (air intake stroke, 89.2 degrees after top dead center)

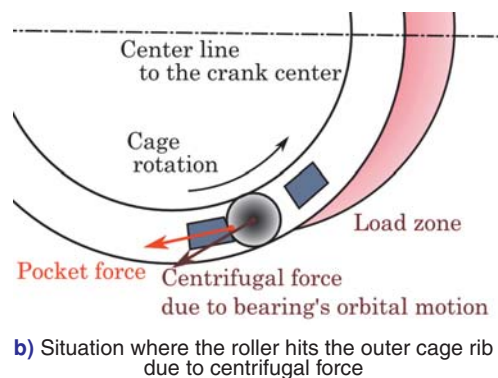
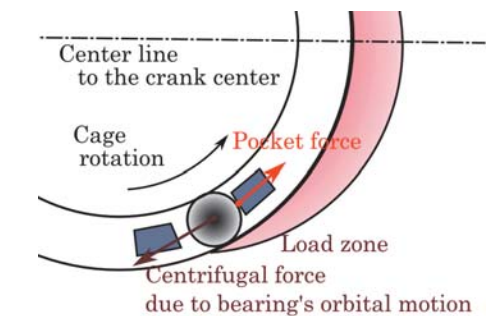


**Fig. 11** Stress rise mechanism on the cage at around the 90 degree point after top dead center

Consequently, this roller is forced toward the left by the centrifugal force due to orbital motion of the bearing; thereby this roller collides with the upstream (rear) cage rib. This collision force results in an increase of stress located at the cage pocket corner.

### 6. Effects of the Combustion Force and Crankshaft Rotational Speed on the Cage Maximum Principle Stresses

The maximum principle stresses occurred on the cage under the various operating conditions shown in **Table 2**. These stresses have been rearranged relative to the rotational speed of the crankshaft. **Fig. 12** graphically plots these results ("Each condition"). Under different piston loads the stress increases with the increase in rotational speed; however, there is no linear relation between the rotational speed and stress. This appears to be because the maximum torque condition (5,000 min<sup>-1</sup>) and the maximum output condition (7,500 min<sup>-1</sup>) are relatively low speed conditions, therefore maximum principle stress occurs due to mechanism (1) above. Similarly, under the maximum speed condition (9,500 min<sup>-1</sup>) and the overrun condition (10,500 min<sup>-1</sup>), each being a high-speed condition, maximum principle stress occurs due to mechanism (2) above. To verify this theory two scenarios were reviewed, where the piston load was fixed at zero (0 N, "None") and where the piston load was set using the maximum torque condition (maximum load 16.3 kN, "Max. Torque"). Using these loads, stresses under varying rotational speeds were calculated, and the results have been added to the plot in **Fig. 12**. It should be understood from this diagram that when no piston load is applied ("None"), the maximum principle stress on the cage increases in proportion to the 1.4th power of the crankshaft speed.

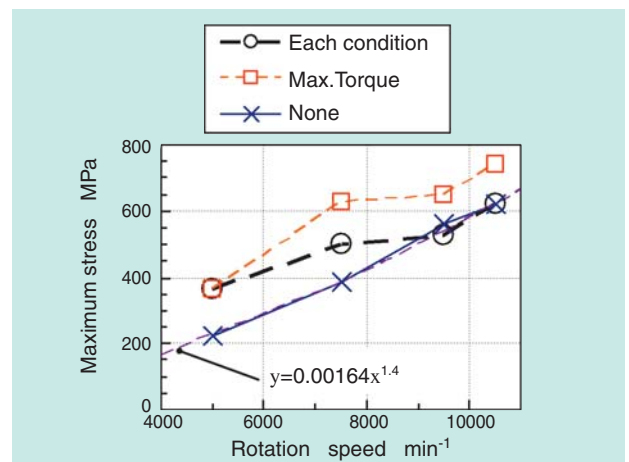


**Fig. 12** Maximum principle stresses on the cage relative to the crankshaft rotational speed

This is because the stress occurring in accordance with mechanism (2) is governed by the crankshaft speed. On the other hand, when the piston load is set under the maximum torque load ("Max. Torque"), the stress is greater over the entire speed range. The bearing load resulting from the inertia of the piston and connecting rod during the overrun (highest speed) condition stands at 9 kN (bearing load value at top dead center during exhaust or intake stroke in Fig. 6b), while the preset piston load (16.3 kN) is much greater. Due to this fact, the cage stress resulting from mechanism (1) increases beyond the maximum stress occurring due to mechanism (2).

## 7. Conclusion

A two-dimensional dynamic analysis has been completed for a needle bearing used at the crankshaft end of a connecting rod, which considered motion of the rollers, cage, and connecting rod as well as the elastic deformation of the cage, in order to study effect of operating conditions on the cage stress. The results of the analysis can be defined as follows:

- The following two mechanisms exist which increase the cage principle stress:
  - (1) Interference force between the rollers and cage deriving from a rapid change in slip ratio that results from the combustion force.
  - (2) Impact of a roller with the cage when the roller is transferred from the load zone to unloaded zone, and then accelerates due to the centrifugal force.
- Even when the crankshaft is turned without involving the combustive force, the maximum principle stress on the cage increases in proportion to the 1.4th power of crankshaft rotational speed. When combustive force causes piston load to occur, and if the piston load is greater than the sum of the inertia of the piston and connecting rod, then the stress on the cage will further increase.

NTN remains committed to the analysis and verification of the maximum stress on the cage under varied operating conditions through experiments; resulting in cages designed to improve reliability and optimize bearing performance.

## Reference

- 1) Fujiwara, H., Kobayashi, T., Fujii, K., Dynamic Analysis of Radial Needle Roller Bearings, Proceedings of the Tokai Branch Regular Meeting of the Japan Society of Mechanical Engineers, 51, 83, 2002.
- 2) Walters, C.T., The Dynamics of Ball Bearings, ASME J. Lub. Tech., 1, 1, 1971.
- 3) Gupta, P.K., Advanced Dynamics of Rolling Elements, Springer-Verlag New York Inc., 1984.
- 4) Sakaguchi, T. et al., Dynamic Analysis of Cage Stress in Needle Roller Bearings under Planetary Motions, Proc. ASME/STLE International Joint Tribology Conference 2007, 44189, 2007.
- 5) Sakaguchi, T., Dynamic Analysis for Needle Roller Bearings Under Planetary Motion, NTN Technical Review No. 75, p. 94, 2007.
- 6) Craig, R.R., Bampton, M.C., Coupling of Substructuring for Dynamic Analysis, AIAA 6, 7, 1313, 1968.
- 7) Sakaguchi, T., Harada, K., Dynamic Analysis Cage Behavior in a Tapered Roller Bearing, ASME J. Trib., 128, 604, 2006.
- 8) Houpert, L., Leenders, P., A Theoretical and Experimental Investigation into Rolling Bearing Friction, Proc. 1985 Eurotrib Conf., 1, Session III, Paper 2.8, 1985.
- 9) Aihara, S., A New Running Torque Formula for Tapered Roller Bearings Under Axial Load, Trans. ASME, J. Trib., 109, 7, 471, 1987.
- 10) Zhou, R.S., Hoeprich, M.R., Torque of Tapered Roller Bearings, Trans. ASME, J. Trib., 113, 7, 590, 1991.

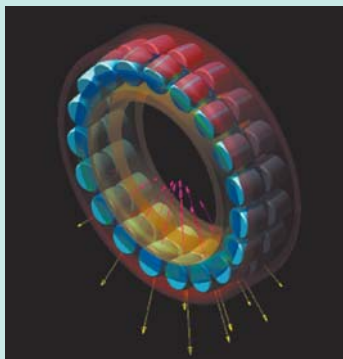
Photo of author



Tomoya SAKAGUCHI

Advanced Technology  
R&D Center

# Integrated Bearing Dynamic Analysis System (IBDAS)



Mariko SEKIYA\*

NTN has developed a new analysis system, Integrated Bearing Dynamic Analysis System (IBDAS), in 2011. IBDAS is a dedicated platform for dynamic rolling bearing analysis that is able to consider an elastic cage model and rolling elements with 6 degrees of freedom. Incorporating automation and a user-friendly computer interface, a large reduction in operation time can be achieved.

This paper compares static and dynamic analyses, provides a brief explanation of IBDAS, and gives examples of completed dynamic analyses.

## 1. Introduction

In 2011, NTN began promoting its unique dynamic analysis system for rolling bearings called IBDAS (Integrated Bearing Dynamic Analysis System) that is a dynamic analysis tool capable of not only accommodating six degrees of freedom for the rolling elements and cage (three translational and three rotational), but also outputting the stress distribution resulting from cage elastic deformation. Adoption of automatic analysis and a refined computer interface allows even new users to be able to execute a roller bearing dynamic analysis.

This article provides an overview of the advantages of dynamic analyses in comparison with static analyses, describes the features of IBDAS, and provides examples of completed dynamic analyses.

## 2. Features of Static and Dynamic Analyses

Mechanical analysis for bearings can be categorized into static analysis and dynamic analysis. Features and applications of each analysis type are summarized hereunder.

### 2.1 Static analysis

Static analysis is an analytical technique for determining various physical quantities in a stationary state by solving a system of equations, typically by balancing forces and moments. Generally these non-linear simultaneous algebraic equations are solved

through repeated calculation often utilizing the Newton-Raphson method. In bearing analysis, centrifugal force and gyro moment due to rolling element orbital motion are often considered; this is sometimes referred to as quasi-static analysis.

Static analysis is very useful in estimating load distribution, rigidity, and life of the bearing, providing an indispensable means for rolling bearing design. Conversely, static analyses are not capable of calculating frequently varying physical quantities in a non-stationary state. In particular, it is difficult to obtain necessary solutions for motion and stresses of a bearing retainer with static analyses alone. These factors cannot be easily measured experimentally; there are several reports about static analysis for these factors<sup>1) 2)</sup> with limited measurement conditions.

Additionally, the scope of static analyses is limited for bearings subjected to complicated external environments, such as bearings used under varying load and speed conditions. In cases such as these, connecting rod bearings within an engine one example bearing, studies need to be supported by dynamic analysis.

### 2.2 Dynamic analysis

Dynamic analysis is a technique where an equation of motion is developed for each element analyzed within the mechanical system. Thus, simultaneous ordinary differential equations are integrated over time. Numerical results are considered using numerical integration techniques, such as the Runge-Kutta method.

\*Automotive Business HQ. CAE Dept

Compared with static analyses, computational time for dynamic analyses is much greater. Nevertheless, dynamic analyses provide a useful tool for real-time simulation, allowing one to analyze frequently varying conditions, internal cage stresses, interaction forces between bearing components, and physical quantities such as rolling element skew and tilt.

One example of a rolling bearing dynamic analysis technique is ADORE (Advanced Dynamics of Rolling Elements) developed by Gupta <sup>3)</sup>; there are several reports of calculation with this technique <sup>4)</sup>. However, ADORE has drawbacks in that it can only handle a cage as a rigid body rather than an elastic body, and the scope of cage geometry ADORE handles is limited.

**Table 1** summarizes features of static and dynamic analyses.

**Table 1** Comparison of static and dynamic analyses

	Constructive formula/method of solution	Typical calculation technique	Typical applications	Calculation Time
<b>Static analysis</b>	Force-moment balance formula Solution of algebraic equation	Newton-Raphson method	Load distribution Rigidity Life	Relatively low
<b>Dynamic analysis</b>	Motion equation (translational, rotational) Numerical integration with differential equation	Runge-Kutta method	Non-static behavior In particular, behavior and stress of cage	High

### 3. Features of IBDAS

IBDAS is a dynamic analysis system for rolling bearings that enables automated calculations by using commercially available dynamic analysis software.

This system features a unique tribological contact model, an ability to handle the cage as an elastic body, and an automated data processing user interface. There features are briefly described hereunder.

#### 3.1 Tribology model

Contact modes within a bearing cannot be directly expressed with a standard function available within current commercially available, general-purpose, mechanics analysis software because of the presence of oil film. Therefore, a specifically designed sub routine was constructed.

Assuming that the contact mode between the rolling element and raceway surface is localized elastic contact, then, the contact pressure at the contact point is calculated in the following manner:

- In the case of roller bearings, a slice method is applied; thereby on the basis of each slice's load,

the contact pressure is calculated by Palmgren's simple formula <sup>5)</sup>.

- In the case of a ball bearing, contact pressure distribution is determined according to Hertz's contact theory.

For calculation of the tangential force between rolling element and raceway surface, the lubricant film parameter  $\Lambda$  is evaluated; thereby the relevant regime of boundary lubrication, mixed lubrication and hydrodynamic lubrication are determined. Lubricant film parameter  $\Lambda$  is defined as  $h/\sigma$ , which is the ratio of the minimum lubricant film thickness ( $h$ ) to mean square surface roughness ( $\sigma$ ) <sup>6)</sup>.

The tangential force coefficient  $\mu_{bd}$  used in the boundary lubrication regime can be determined by Kragelskii's <sup>7)</sup> formula (1) as follows:

$$\mu_{bd} = (-0.1 + 22.28s) \exp(-181.46s) + 0.1 \dots (1)$$

$s$ : slip rate

The tangential force coefficient  $\mu_{bd}$  used in the hydrodynamic lubrication regime can be determined by a simple theoretical formula proposed by Kimura, et. al. <sup>8)</sup>. The mixed lubrication regime is expressed by formula (2) and provides an interface that smoothly connects the boundary lubrication regime to hydrodynamic lubrication regime.

$$\mu_r = \begin{cases} \mu_{bd} & \text{if } \Lambda < 0.01 \\ \frac{\mu_{bd} - \mu_{hd}}{(0.01 - 1.5)^6} (\Lambda - 1.5)^6 + \mu_{hd} & \text{if } 0.01 \leq \Lambda < 1.5 \\ \mu_{hd} & \text{if } 1.5 \leq \Lambda \end{cases} (2)$$

As to the contact mode between the rolling element and raceway surface, rolling viscous resistance <sup>9)</sup> needs to be taken into account.

Tangential force factors for the forces acting between the rolling elements and cage, as well as between the raceway rings and the cage are determined by Formula (1).

For more detailed information about the tribology model used for IBDAS, refer to the paper by Harada and Sakaguichi <sup>10)</sup>.

#### 3.2 Elastic cage model

CMS method (Component Mode Synthesis) is used to build an elastic cage model. This is a technique for expressing the magnitude of deformation on an elastic body by linear superposition of given deformation modes <sup>11)</sup>.

Deformation modes are generated through analysis (known as super-element analysis) to obtain a minute-series model by processing a characteristic (mass, attenuation and rigidity) matrix deriving from a finite

element cage model on the basis of Guyan static reduction<sup>12)</sup>. Then, on the basis of the deformation mode information, stresses and deformation of the cage are calculated for the duration of the duty cycle within the dynamic analysis software. A finite element model which has not yet undergone static reduction has degrees of freedom modeled with more than ten thousands nodes. In contrast, NTN's elastic body model helps reduce the degrees of freedom down to scores of deformation models; thereby the work load for the calculation is significantly reduced.

In static reduction, degrees of freedom for specified nodes are left unchanged. Choice of these nodes (hereafter referred to as "boundary points") will greatly affect accuracy of the calculation: therefore, it is preferable to choose points where external forces are applied, where significant deformation is expected, or where significant mass is present<sup>12)</sup>.

For correlation, NTN compared the behavior of a tapered roller bearing retainer obtained by the mode synthesis method with experimentally obtained results<sup>13)</sup>.

In the experiment, a displacement sensor was installed onto the test bearing (tapered roller bearing, 32310U), and the test bearing was run at 1000 min<sup>-1</sup>; thereby the cage position was measured while varying axial load. Fig. 1(a) shows the measurements resulting from the experiment, and Fig. 1(b) graphically plots the results of calculation under the same conditions. Axial load  $F_a$  is made dimensionless by dividing by the basic dynamic load rating  $C_r$ , while the cage position from the center is rendered dimensionless by ratioing to the radial clearance between the cage pocket and roller.

Figs. 1(a) and 1(b) indicate that when the axial load is low ( $F_a/C_r=0.5\%$ ), the center of the cage shifts forward, in the direction motion and away from the direction of gravity. Additionally, when the axial load is

greater ( $F_a/C_r=8\%$ ), the center of the cage traces a near perfect circle. Thus, the experimental results of the cage behavior qualitatively matches the calculation results.

On the other hand, measurements of cage stress obtained from IBDAS are always lower compared with measurements obtained from the static analysis finite element method (hereinafter referred to as FEM). According to the dynamic analysis results under the conditions in Fig. 1, the cage stress can vary depending on the number of characteristic deformation modes: nevertheless, the calculated cage stress values resulting from the dynamic analysis are approximately 25% lower compared with stress values obtained from the FEM<sup>13)</sup>.

To address this problem within IBDAS, a correction coefficient for cage stress is calculated based on the results of the static analyses performed by the FEM and CMS methods.

Additionally, there has been concern about the underestimation of stress concentration at the cage pocket corner, wherein this underestimation can occur when the roller-to-cage contact location deviates from the midpoint<sup>14)</sup>.

To address this problem, IBDAS is capable of increasing the number of boundary points on the cage pocket rib. Fig. 2 shows the locations of boundary points set on a cage pocket in a tapered roller bearing (equivalent to 30310). In the test results shown in Fig. 3, the number of boundary points set on the cage pocket rib was varied, and then a radial load of 1 N was applied to the loading points (points 1 through 6) shown in Fig. 2. Fig. 3 graphically shows the ratio of pocket corner stress obtained by CMS to cage corner stress obtained by FEM. For more detailed information about the analysis, refer to bibliography source 14.

From Fig. 3, it should be understood that when the number of boundary setting points is 1, and if load

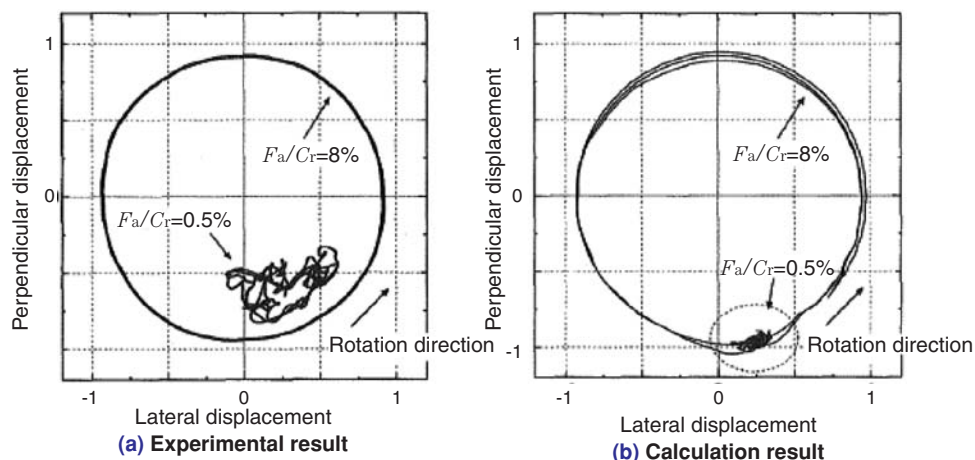
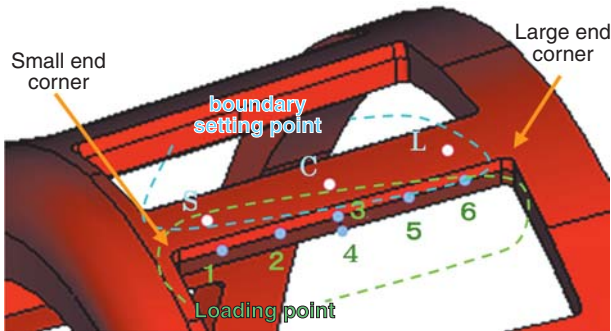
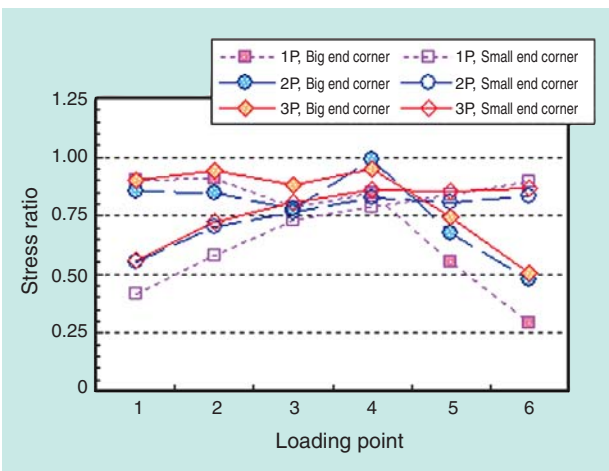


Fig. 1 Cage center behavior of a tapered roller bearing (32310U, 1000 min<sup>-1</sup>)

acts on load points 1 or 6, each of which is in close vicinity to the cage pocket corner, values resulting from the CMS method are significantly lower compared with values resulting from the FEM analysis. With an increase in number of boundary setting points, this trend is less apparent: if two or more boundary points are set, the minimum “CMS to FEM” stress ratio will be not smaller than 0.5.



**Fig. 2** Load points (1 through 6), boundary setting points (S, C, L), and stress measurement points (large end corner, and small end corner) on the cage



**Fig. 3** Ratio of cage stress determined by CMS to cage stress determined by FEM  
 1P: One boundary point (C), 2P: Two boundary points (S, L), Three boundary points (S, C, L)  
 Large end corner: Stress on the large end corner in cage pocket (Fig. 2, right)  
 Small end corner: Stress on the small end corner in cage pocket (Fig. 2, left)

#### 4. Computer Interface

One outstanding advantage of IBDAS is the adoption and ease of use of the computer interface. The computer interface helps simplify input/output operations and allows for the automation of the calculation processing section; thereby even new users of the software can easily analyze the behavior of rolling elements.

Through the computer interface IBDAS operation begins with the user entering a total of about 30 to 40 parameters including bearing type and size, lubricating oil type, temperature, operating conditions such as load and bearing speed, as well as numerical integration conditions. Note, however, that the user needs to develop a bearing mode shape file and upload the file during the data entry described above.

Once the user has completed data entry for all the condition parameters, IBDAS then automatically calculates the cage deformation mode information, constructs bearing model, and executes dynamic calculation.

When the calculation operation is complete, the user downloads the necessary data via the server and analyzes the results. Macros are provided for the acquisition of frequently referenced data including the behavior and stresses of the cage, contact force between associated bearing parts, and roller skew and misalignment; thus, the user can output necessary data without experiencing complicated post-process operation.

Fig. 4 illustrates an example of the work load reduction through automation and utilization of the new interface. Time-consuming data entry work and setup conditions are no longer necessary. At the same time, automated execution of calculations helps reduce the total work hours from 43 to a mere 2 hours. The work load has been dramatically reduced to 1/20 of what it was previously.

IBDAS can handle all rolling bearing types (deep groove ball bearing, angular ball bearing, cylindrical roller bearing, needle roller bearing, tapered roller bearing, and spherical roller bearing). IBDAS is also capable of model selections based on operating conditions—the user can select from a two-dimensional model (planar constraints: two degrees of freedom for translational motion, one degree of freedom for rotational motion) and a three-dimensional model (three degrees of freedom for translational motion, three degrees of freedom for rotational motion). Operation of planetary systems, eccentric rotation, and motion of connecting rods, etc. can be analyzed.

The user may also prepare a user-defined application file, such that IBDAS can flexibly handle operating conditions not listed above.

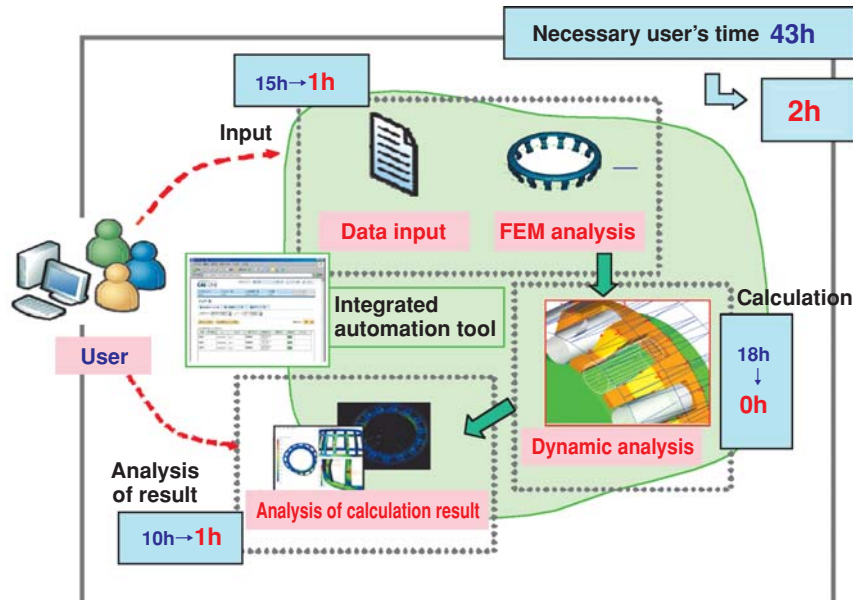


Fig. 4 Flow of dynamic analysis and example of time reduction due to IBDAS (light blue: previous system, pink: IBDAS)

### 5. Disclosed Examples of NTN's Dynamic Analysis

In order to present typical examples of the application of dynamic bearing analyses, the section hereunder describes NTN's history of dynamic analyses up to the release of IBDAS. Note that the year indicated is the year the information was first published.

First, in 2000, using NTN's proprietary developed codes, the cage behavior and forces acting on the cage within a connecting rod needle roller bearing were calculated<sup>15) 16)</sup> and compared with the experimentally determined cage behavior. This analysis was focused on the large end connecting rod needle roller bearing, which is a typical example of dynamic operating conditions. This model was a two-dimensional, simplified dynamic model whose degrees of freedom was decreased with planar constraints.

Eventually, a commercially available dynamic analysis software package was obtained. In 2002, NTN disclosed results of its two-dimensional analysis of cylindrical roller bearing cage behavior<sup>17) 18)</sup>. NTN also released results of its three-dimensional, rigidly modeled cage analysis (an evolution from the aforementioned two-dimensional analysis) for a tapered roller bearing<sup>10) 19) 20)</sup>; wherein NTN attempted to review contact forces between the rollers and the retainer used in NTN's newly developed bearing.

In 2006, more advanced three-dimensional analyses became possible, which allowed the cage to be handled as an elastic body using the mode synthesis method<sup>21)</sup>. Eventually, the mode synthesis

method was incorporated into the two-dimensional analysis operation for analyzing needle roller bearings undergoing planetary motion<sup>22)</sup>. Eventually, NTN attempted to verify the accuracy of the mode synthesis method through the three-dimensional analysis of a cage in a tapered roller bearing<sup>13) 14)</sup>.

In 2011, the dynamic analysis techniques for various rolling bearing types were combined and organized into a unique user-friendly system—IBDAS.

For further example, the readers of this article are encouraged to refer to "Two-Dimensional Dynamic Analysis of Cage Stress for Needle Roller Bearings that Support Connecting Rods in Reciprocating Engines" in this issue of the NTN Technical Review.

Table 2 Progress in technique for dynamic analysis for rolling bearings at NTN

Year of outside publication	Contents of publication
2000	Analysis of a needle roller bearing cage used in a connecting rod; according to NTN's propriety development code (literatures 15 and 16)
	Introduction of commercially available dynamic analysis software
2002	Two dimensional analysis of a cage (rigid model) in a cylindrical roller bearing using commercially available dynamic analysis software (literatures 17 and 18)
2004	Three dimensional analysis of a cage (rigid model) in a tapered roller bearing (literatures 19 and 20)
2006	Stress analysis of a cage (elastic model) in cylindrical roller bearing, taking elasticity into account (literature 21)
2007	Two dimensional analysis of a needle roller bearing in planetary motion (elastic model) (literature 22)
2011	Release of integrated dynamic analysis system IBDAS

## 6. Conclusion

This article has compared the techniques of static and dynamic analyses, explained the advantages of the dynamic analysis system IBDAS, and summarized NTN's typical experiences using dynamic analysis.

Through the adoption of dynamic analysis models, stresses and behavior of the bearing cage under varied operating conditions are clarified (this achievement was impossible using static analysis techniques). At the same time, automation of the analysis operation has helped to greatly decrease the analysis time required.

NTN will promote utilization of both static and dynamic roller bearing analysis techniques in order to further enhance its ability to develop better bearing designs and support its products.

## Reference

- 1) For example: Kakuta, K., Kohno, T., Ohta, H., Ota, H., Generating Mechanism of Forces Acting on Retainer of Ball Bearings Supporting Unbalanced Rotating Shaft, Transactions of the Japan Society of Mechanical Engineers, 62-600, C 3210-3215, 1996.
- 2) Fujiwara, H., Fujii, K., Nakazeki, T., Retainer Forces in Cylindrical Roller Bearings, NTN Technical Review No. 68, p. 63-66, 2000.
- 3) Gupta, P.K., Advanced Dynamics of Rolling Elements, Springer-Verlag, 1984.
- 4) Gupta, P.K., Dynamics of rolling element bearings, Parts I, II, III and IV, Journal of Lubrication Technology, ASME Trans., 101, 293-326, 1979.
- 5) Gupta, P.K., Advanced Dynamics of Rolling Elements, Springer-Verlag, 39, 1984.
- 6) Yamamoto, Y. and Kaneta, M., Tribology, Rikogakusha, 162, 1998.
- 7) Kragelskii, I.V., Friction and Wear, Butterworths, 1965.
- 8) Muraki, M., Kimura, Y., Traction Characteristics of Lubricating Oils (Part 2), Journal of Japan Society of Lubrication Engineers, 28, 10, 753-760, 1983.
- 9) Zhou, R.S. and Hoeprich, M.R., Torque of Tapered Roller Bearings, ASME J. Tribology, 113, 7, 590-597, 1991.
- 10) Harada K., Sakaguchi, T., Dynamic Analysis of a High-Load Capacity Tapered Roller Bearing, NTN Technical Review No. 73, 20-29, 2005.
- 11) Craig, R.R., and Bampton, M.C.C., Coupling substructures for dynamic analysis, AIAA J., 6, 7, 1313-1319, 1986.
- 12) Nagamatsu, A., Okuma, M., Component mode synthesis, Baifukan, 1991.
- 13) Sakaguchi, T. and Harada, K., Dynamic Analysis of Cage Stress in Tapered Roller Bearings Using Component-Mode-Synthesis Method, ASME J. Tribology, 131, 011102 1-9, 2009.
- 14) Sakaguchi, T., Measurement Precision of Cage Stress in Tapered Roller Bearings Using Component-Mode-Synthesis Method, Proceedings of Japan Society of Tribologists Tribology Conference, 279-280, 2010.
- 15) Fujiwara, H. and Kobayashi, T., Dynamic Analysis of Needle Roller Bearings in Connecting Rod Big-End Applications, Proc. Int. Trib. Conf., Nagasaki 2000, 1841-1846, 2001.
- 16) Fujiwara, H., Kobayashi, T., Dynamic Analysis of Needle Roller Bearings in Connecting Rod Big-End Applications, NTN Technical Review No. 69, 89-96, 2001.
- 17) Sakaguchi, T., Ueno, K., Kobayashi, T., Analysis of cage behavior on cylindrical roller bearings, Proceedings of Japan Society of Tribologists Tribology Conference, 415, 2002.
- 18) Sakaguchi, T., Ueno, K., Dynamic Analysis of Cage Behavior in a Cylindrical Roller Bearing, NTN Technical Review No. 71, 8-17, 2003.
- 19) Harada, K. and Sakaguchi, T., 3D dynamic analysis of cage behavior on tapered roller bearings (1st report, behavior measurements), Proceedings of Japan Society of Tribologists Tribology Conference, 501, 2004.
- 20) Sakaguchi, T. and Harada, K., 3D dynamic analysis of cage behavior on tapered roller bearings (2nd report, calculation results), Proceedings of Japan Society of Tribologists Tribology Conference, 503, 2004.
- 21) Sakaguchi, T. and Harada, K., Dynamic Analysis of Cage Stress in Tapered Roller Bearings, Proc. ASIATRIB., Kanazawa 2006, 649-650, 2006.
- 22) Sakaguchi, T., Dynamic Analysis for Needle Roller Bearings Under Planetary Motion, NTN Technical Review No. 75, 94-99, 2007.

Photo of author



Mariko SEKIYA

Automotive Business HQ.  
CAE Dept

## Hybrid PEEK Sliding Bearing

Takuya ISHII\*  
Ken YASUDA\*\*



PTFE-based bushings are used for the main spindle bearings of air conditioner compressors. Recently, demand has increased for compressors with enhanced efficiency, reduced size, and lighter weight. To meet these requirements, NTN has developed Hybrid PEEK Sliding Bearings, which have injection molding PEEK resin layers of 0.5 mm thickness on the bores of sintered metal bushings, with the objective of improving friction/wear properties and anti-seizure performance. This article introduces the characteristics, structure and performances of Hybrid PEEK Sliding Bearings.

### 1. Introduction

Improved energy efficiency is needed for both household and commercial air conditioners. Most of the power consumption of an air conditioner is due to operation of the air compressor. Therefore, the air compressor in an air conditioner system needs to be very energy efficient<sup>1)</sup>. The structure of a typical air compressor for an air conditioner is shown in Fig. 1 along with the locations of bearings used. The main spindle bearings (PTFE resin bushings) have to satisfy requirements for improved friction-abrasion quality and seizure resistance, because refrigerant liquefied by over-compression can cause refrigeration oil to flow out via the friction surface. This article presents information about NTN's unique hybrid PEEK bearing that hybridizes newly developed sintered metal alloy and resin material in order to meet these requirements.

### 2. Performance Improvement for Resin Sliding Bearing

Compared with rolling bearings, resin sliding bearings are inferior in terms of heat resistance. Even a super engineering plastic material featuring relatively high heat resistance can melt and wear out due to poor heat releasing performance.

A resin sliding bearing boasting high heat releasing

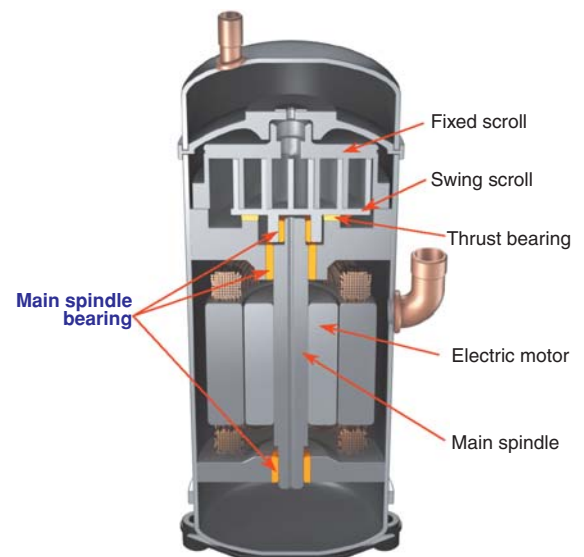


Fig. 1 Typical structure of air-conditioner compressor

performance solves this issue with hybridization of a thin-walled resin material and a metal layer. This sliding bearing is a PTFE resin bushing<sup>2)</sup> (Fig. 2) that is used as the main spindle bearing in an air conditioner compressor. However, because of a limitation in the manufacturing process, the resin material used is limited only to PTFE. If refrigeration oil flows out via the friction surface as in the case of the compressor main spindle, the oil attacks the thin resin layer, exposing the sintered metal layer and

\*Composite Material Products Division Composite Material Engineering Dept

\*\*NTN Engineering Plastics Corp. Engineering Dept

potentially causing bearing seizure. Furthermore, there have been mounting needs for lower bearing torque and improved abrasion resistance. To address this trend, NTN has developed the new hybrid PEEK bearing.

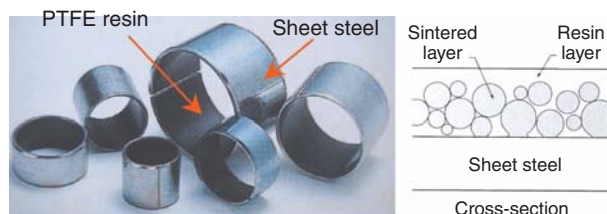


**Fig. 2** Three-layered PTFE resin bushing (sheet steel + porous sintered bronze material + PTFE)

### 3. Hybrid PEEK Bearing

#### 3.1 Features

Note that a conventional PTFE resin bushing is fabricated by impregnating a sintered intermediate layer on sheet steel with PTFE resin and baking the intermediate layer. In contrast, with NTN's new hybrid PEEK bearing, a layer of 0.5 mm thick PEEK resin is formed onto the bore surface of a sintered alloy bushing through an injection molding process. PEEK resin excels in heat resistance, abrasion resistance, oil/chemical resistance and fatigue resistance. Hybridization with a metal layer helps achieve dramatically improved heat releasing performance compared with bearings consisting of PEEK resin material alone.

- (1) **The new product excels in seizure resistance (comparison with conventional product: five times or more)**
- (2) **Lower friction/reduced abrasion quality (comparison with conventional product: 2/3 in terms of coefficient of friction, 1/3 in terms of abrasion)**

\* Conventional product: PTFE resin bushing

#### 3.2 Structure and constituent materials

**Fig. 3** shows a simplified illustration of NTN's newly developed hybrid PEEK bearing. The PEEK resin material (NTN material name: BEAREE PK5307) forms the bearing bore surface that is slightly in contact with the matching shaft, and includes a blend of special filling material that boasts good friction-abrasion quality while still being capable of forming a thin film through an injection molding process. The bushing is made of a ferrous sintered alloy.

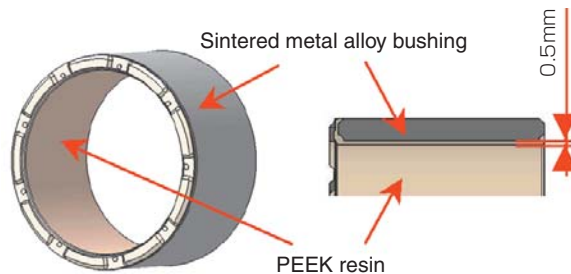


**Fig. 3** Structure of hybrid PEEK sliding bearing

### 3.3 General physical properties

**Table 1** summarizes general physical properties of PEEK resin (BEAREE PK5307).

**Table 1** General physical properties of BEAREE PK5307

Characteristics	Test method	Unit of measurement	Characteristic value
Specific gravity	ASTM D792	—	1.42
Tensile strength	ASTM D638	MPa	83
Bending strength	ASTM D790	MPa	142
Young's modulus in flexure	ASTM D790	MPa	5,200
Coefficient of linear expansion (R.T.~150°C)	TMA method	1/°C	MD: 3.4×10 <sup>-5</sup> CD: 5.3×10 <sup>-5</sup>
Izod impact strength	ASTM D256 (notched)	J/m	30
Rockwell hardness	ASTM D785	R scale	117

※All the values above are representative.

### 3.4 Comparison of various features of bearings

**Table 2** compares NTN's new hybrid PEEK bearing product to a conventional PTFE resin bushing. Comparison test data is given in Sec. 3.5, showing NTN's newly developed hybrid PEEK bearing excels in seizure resistance and friction-abrasion performance.

**Table 2** Comparison of various bearing features

Characteristics		Hybrid PEEK bearing	PTFE resin-based bushing
Composition	Surface layer (sliding surface)	PEEK resin (0.5mm)	PTFE resin (0.05mm)
	Intermediate layer	None	Sintered bronze (0.3mm)
	Backing metal	Sintered metal alloy	Sheet steel
Form		Bushing (without split)	Bushing (with split)
Resin material forming process		Injection molding	Impregnation forming
Seizure resistance		◎	△
Abrasion resistance		◎	○
Friction resistance		◎	○

◎ : Excellent ○ : Good △ : Acceptable

### 3.5 Bearing performance

#### 3.5.1 Seizure resistance

Seizure resistance testing was performed with the hybrid PEEK bearing, a PTFE resin bushing and a PEEK resin bearing. Fig. 4 shows a schematic of the radial tester used, and Table 3 summarizes the applied test conditions. The test procedure is summarized as follows:

##### <Test procedure>

- (1) Oil flows throughout the test rig and the shaft rotates.
- (2) Increase the bearing contact pressure by 0.8 MPa every 3 minutes, so that the contact pressure reaches 17 MPa, 1 hour after start of the test.
- (3) When contact pressure of 17 MPa is reached, oil circulation is stopped; oil is drained away from the bottom of the lubrication system, and then the bearing runs until seizure (30 min. at maximum).

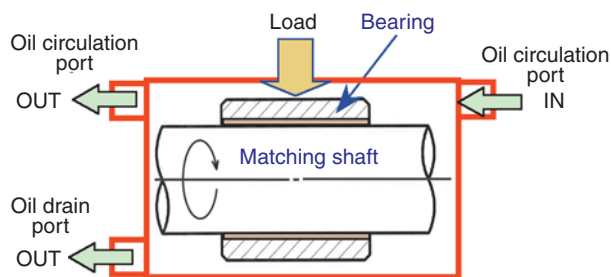


Fig. 4 Radial-type test machine

Table 3 Test conditions

Characteristics	Contents
Bearing size	Bore dia.: 30 mm, width: 20 mm
Operating internal clearance	0.09mm
Contact pressure	max. 17 MPa (load 10 kN)
Sliding velocity (two conditions)	8.5m/s (5,400min <sup>-1</sup> ) 14.1m/s (9,000min <sup>-1</sup> )
Lubricating oil	Ether-based refrigerating oil (temperature at circulation: 90°C, flow rate: 100 mL/min)
Matching shaft	FCD600 (0.4 μmRa)

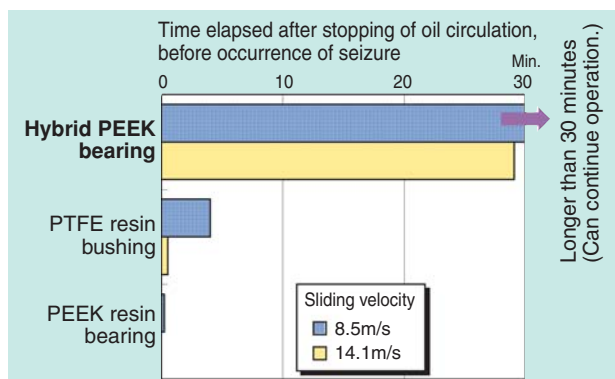


Fig. 5 Seizure resistance

- (4) A bearing temperature rise in excess of 10°C marks the occurrence of seizure.

Fig. 5 provides data about the time elapsed before seizure with the tested bearings. NTN's hybrid PEEK bearing is superior to the PTFE resin bushing in terms of seizure resistance quality. As illustrated in Fig. 5, the PEEK resin bearing, not hybridized with a metal layer, seizes at an earlier stage of the seizure resistance test.

#### 3.5.2 Friction-abrasion characteristics

A radial friction-abrasion test was performed with the hybrid PEEK bearing and a PTFE resin bushing. These parts were subjected to a radial friction-abrasion test in lubricating oil under the test conditions summarized in Table 4.

Fig. 6 shows the relationship between test duration and wear depth, and Table 5 gives data for the coefficient of dynamic friction. After 30 hours from the

Table 4 Test conditions

Characteristics	Contents
Test machine	Shaft rotation radial test machine (Fig. 4)
Bearing size	Bore dia.: 30 mm, width: 20 mm
Operating internal clearance	0.09mm
Contact pressure	17 MPa (load 10 kN)
Sliding velocity	4.7m/s (3,000min <sup>-1</sup> )
Lubricating oil (circulation)	Ether-based refrigerating oil (temperature: 90°C, flow rate: 100 mL/min)
Matching shaft	FCD600 (0.4 μmRa)
Duration	120h

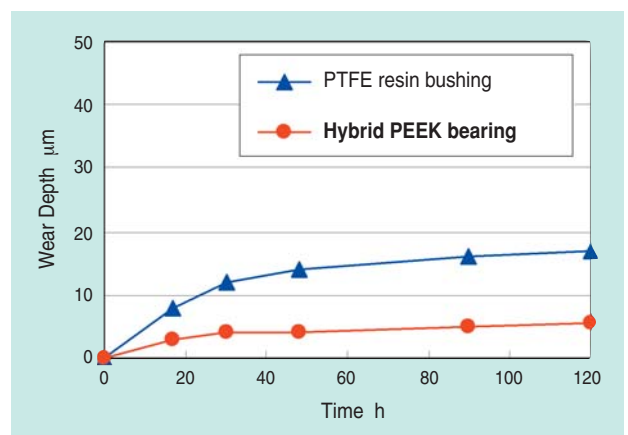


Fig. 6 Wear depth versus testing time

Table 5 Coefficient of dynamic friction

Bearing	Coefficient of dynamic friction (120 hours after start of test)
Hybrid PEEK bearing	0.006
PTFE resin bushing	0.009

start of the test, wear depth remains virtually unchanged. The hybrid PEEK bearing excels in friction-abrasion quality. Compared with the PTFE resin bushing, the hybrid PEEK bearing boasts 2/3 the coefficient of friction and 1/3 the wear depth.

### 3.5.3 Effect of contact pressure on coefficient of friction

The effect of contact pressure on the coefficient of friction was tested for the hybrid PEEK bearing and a PTFE resin bushing under the test conditions summarized in **Table 6**. The contact pressure on the test samples in lubricating oil was increased by 1 MPa every minute, beginning with 1 MPa up to a maximum pressure of 10 MPa. **Fig. 7** graphically plots the results of the effect of contact pressure on the coefficient of dynamic friction.

Compared with a conventional PTFE resin bushing, NTN's newly developed hybrid PEEK bearing boasts greater load capacity. Its coefficient of friction is about 2/3 that of the PTFE resin bushing. The coefficient of friction with NTN's hybrid PEEK bearing tends to be lower, along with lower contact pressure.

**Table 6** Test conditions

Characteristics	Contents
Test machine	Shaft rotation radial test machine ( <b>Fig. 4</b> )
Bearing size	Bore dia.: 30 mm, width: 20 mm
Operating internal clearance	0.09mm
Contact pressure	max. 1–10 MPa (load 6 kN)
Sliding velocity	4.7m/s (3,000min <sup>-1</sup> )
Lubricating oil (circulation)	Ether-based refrigerating oil (temperature: 90°C, flow rate: 100 mL/min)
Matching shaft	FCD600 (0.4μmRa)

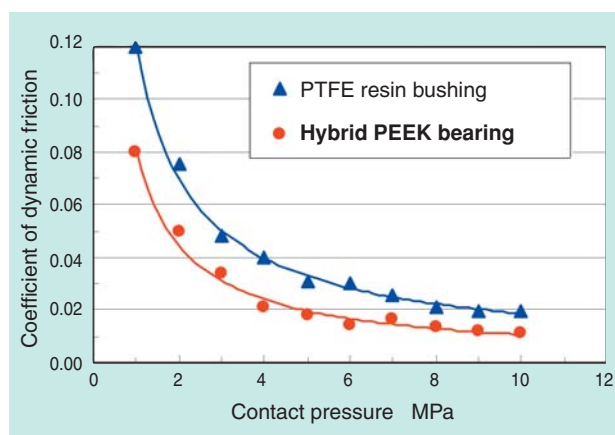


**Fig. 7** Effect of contact pressure on coefficient of friction

## 3.6 Environment resistance

### 3.6.1 Heat cycles

To determine the variation in adhesion of PEEK resin to the sintered metal alloy bushing resulting from repetition of a thermal expansion-contraction cycle, a shear fracture test was executed with samples before and after undergoing heat cycles (**Table 7**). As illustrated in **Fig. 8**, shear force was applied to the PEEK resin layer on the bearing bore surface. Then, the shear fracture load was applied to the area of the bore surface within the sintered metal alloy bushing in order to determine the shear strength of the PEEK bearing. **Table 8** summarizes the shear stress values obtained from NTN's newly developed hybrid PEEK bearing both before and after application of heat cycles.

The results of the test determined that the PEEK resin member did not change in external appearance, such as loosening from the sintered metal alloy bushing. At the same time, virtually no deterioration was found in shear strength. This is because of improved adhesive power owing to the anchoring effect of recesses on the surface of the sintered metal alloy bushing. The PEEK sliding bearing that underwent the shear fracture test had a mixture of fractured PEEK resin in recesses of the sintered bushing and inter-surface fracture between the PEEK resin and sintered metal alloy bushing.

Furthermore, the change in frictional shear strength

**Table 7** Heat cycle test conditions

Characteristics	Conditions
Pattern	-40°C (30 min.) ⇔ 165°C (30 min.)
Number of repetitions	50 times

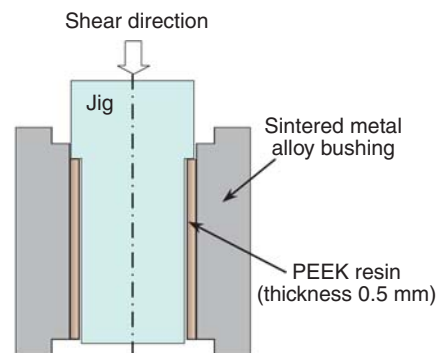


**Fig. 8** Schematic view of shear test rig

**Table 8** Result of shear test

Characteristics	Before heat cycle (original state)	After heat cycle
Shear strength	3.62MPa	3.53MPa
Rate of change	(Reference)	-2.6%

before and after heat cycles is approximately 0.1 MPa, which was calculated along with the results shown in Fig. 7 (the product of contact pressure and coefficient of friction). Thus, there are no problems expected using the PEEK resin bearing in air compressors.

### 3.6.2 Oil resistance

To determine the change resulting from long use in oil regarding the adhesion between the PEEK resin and sintered metal alloy, as well as the dimensional variation of the PEEK resin layer, NTN implemented an oil immersion test under conditions summarized in Table 9. Figs. 9 and 10 summarize the relationship between oil immersion time and shear strength, as well as change in bearing bore diameter. No change in appearance was found on the bearing samples that underwent oil immersion. There is virtually no effect of

Table 9 Oil immersion test conditions

Characteristics	Conditions
Immersion oil	Ether-based refrigerating oil
Temperature	150°C
Duration	100h, 300h, 500h

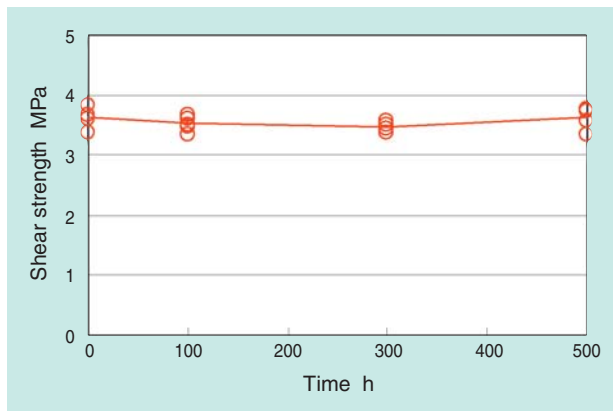


Fig. 9 Relation between oil immersion time and shear strength

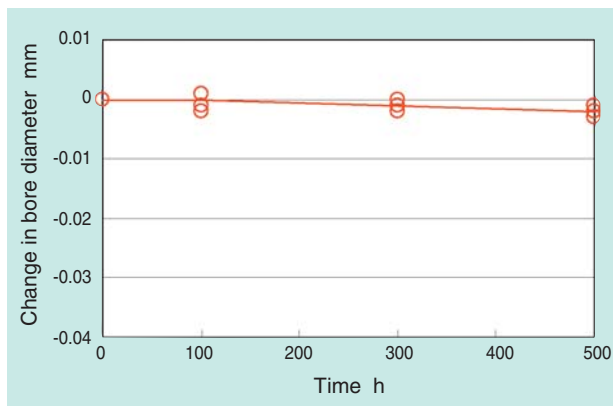


Fig. 10 Relation between oil immersion time and change in bearing bore diameter

oil immersion on shear strength and the bore dimension of the PEEK resin bearing.

## 4. Conclusion

Compared with a conventional PTFE resin bushing, NTN's hybrid PEEK bearing boasts much improved seizure resistance quality and friction-abrasion characteristics.

NTN will attempt to further expand the scope of possible applications of the hybrid PEEK bearing not only to household and commercial air conditioner compressors, but also to automotive air conditioner compressors. At the same time, aiming at further improvement in functionality and reduction in size and weight, NTN will mobilize all of its sliding bearing technologies (resin bearings, sintered oil-impregnated bearings, fluid dynamic pressure bearings) to develop and commercialize highly functional bearing products, positively contributing to energy savings, efficiency improvement, and reduction in size and weight of industrial machinery.

## Reference

- 1) Sato, H. et al., High Efficiency and Large Capacity 3D Scroll Compressor GU Series, Mitsubishi Heavy Industries Technical Review, 43, 2, 10, 2006.
- 2) MLE bearing, Cat. No. 5116-II/J, NTN, 2006.

## Photo of authors



Takuya ISHII  
Composite Material  
Products Division  
Composite Material  
Engineering Dept



Ken YASUDA  
NTN Engineering Plastics Corp.  
Engineering Dept

## Air Spindle for Ultra High-precision Machine Tools



Teruyoshi HORIUCHI\*  
Kazuyuki AONO\*

Air spindles are used in applications such as inspection equipment for semiconductor wafers and hard disks. At NTN, we are using our skills and experience to produce air spindles for ultra-high-precision machine tools.

### 1. Introduction

Thanks to excellent rotary characteristics resulting from non-contact construction, air spindles have been contributing to performance improvement in various industrial fields, including disk-type data storage media production and semiconductor device inspection. Furthermore, air spindles have been increasingly regarded as a promising tool for accuracy improvement in precision machining processes for nonspherical lenses and special metal dies.

This trend is promoted by users' mounting demands for digital cameras with higher functionality, cellular phones with built-in ultra-compact cameras, and smartphones, each of which require compact, high-precision nonspherical image-capturing lenses.

This paper describes typical performance & assessment results and an explanation of the control scheme for NTN air spindles for machine tools, targeting the production process for nonspherical lenses.

### 2. Nonspherical Lens

Generally, when configuring an optical system by using spherical lenses of the single radius form, it is necessary to combine multiple lenses to correct aberrations associated with individual lenses; consequently, the construction of the optical system is complicated. In contrast, a nonspherical lens such as a one in Fig. 1 is formed with a plurality of spherical faces; therefore, even one spherical lens can minimize

aberration, and provides a smaller and simpler solution. However, unlike production of simple spherical lenses which can be readily finished with lapping, small lot production of nonspherical lenses involves first trace-cutting of multiple-curved faces with a cutting tool, and then finishing with lapping. The usual mass-production technique for nonspherical lenses is forming with metal dies. For high-efficiency forming, the metal dies must have accurately finished internal profiles consisting of complicated curved faces. This requirement can be met with a machining spindle which features minimized rotational runout and dimensional variation.

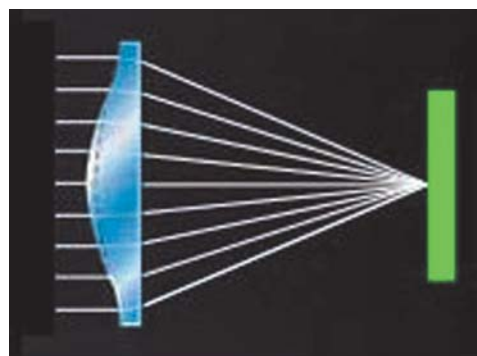


Fig. 1 Nonspherical lens

\* Aberration is a phenomenon where light having passed a lens does not converge on a narrow point on the optical axis, and the resultant image appears to be blurred or distorted.

### 3. Features of Air Spindles for Machine Tools

Previously, air spindles were very often used in an upright attitude. In contrast, NTN's newly developed air spindle is intended for horizontal installation such as shown in Fig. 2. The major targeted applications of this air spindle product are precision turning centers and grinding machines.

For evaluation purposes, we have fabricated a prototype air spindle for a machine tool (hereinafter referred to as “newly developed product”), and Table 1 summarizes the major specifications for this newly developed product. The drive motor used is capable of continuous operation at 20,000 min<sup>-1</sup>: the newly developed air spindle boasts high degree of accuracy, and features radial and axial NRRO (Non Repetitive Runout) values of 0.010 μm or smaller. This air spindle is more reliable, thanks to its non-contact type seal that more reliably prevents possible ingress of chips and coolant into the bearing. Furthermore, this NTN product is less affected by variations in temperature. This is achieved thanks to several innovations: (a) the well-thought-out cooling structure, which helps mitigate heat buildup during continuous

air spindle operation; (b) component design intended to minimize heat buildup during operation; and (c) careful selection of materials for limited thermal expansion properties.

### 4. Evaluation of Rotational Accuracy

NTN's typical air spindle evaluation method is described below, along with actual accuracy measurements of NTN's newly developed air spindle product.

#### 4.1 Non Repetitive Runout (NRRO) accuracy (1) Method for measurement and evaluation

The rotary shaft is allowed to run at a constant speed. The runout of an arbitrary point on the rotary shaft is measured when the rotary shaft has just completed one full rotation, and the difference between this measurement and the measurement at the start of the rotation is determined. Then, this difference is acquired for 2,000 successive rotations; the maximum value of this difference is taken as the non-repetitive runout (NRRO) for evaluation purposes of the spindle accuracy.

The analyzer used is an electrostatic, capacitance

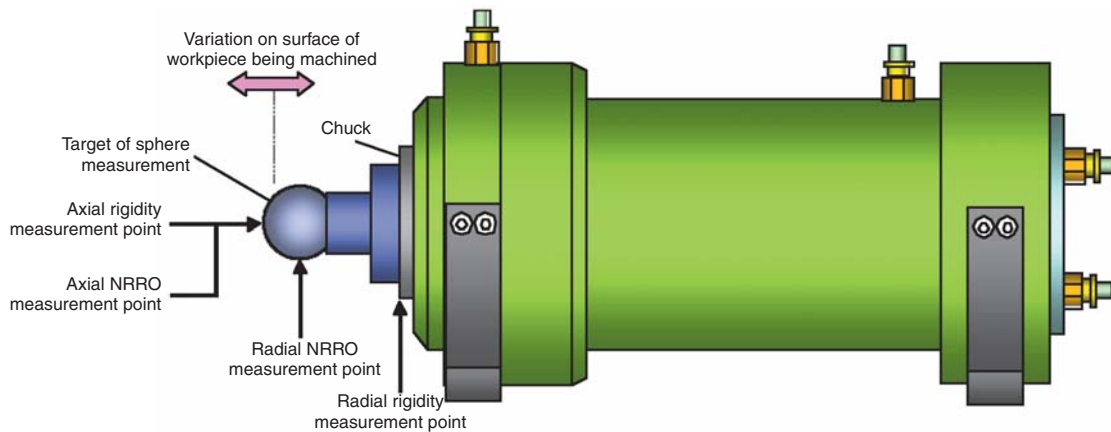


Fig. 2 Accuracy measurement points

Table 1 Specifications

Characteristics (at bearing feed air pressure 0.49 MPa)		Guaranteed value
Max. rotational speed		20,000min <sup>-1</sup>
Radial rigidity		45N/μm
Axial rigidity		227N/μm
NRRO	Radial	0.010 μm max.
	Axial	0.010 μm max.
Rotational speed fluctuation (jitter)		within ±0.01%
Variation on surface of workpiece being machined (at constant rotational speed)		1 μm max.

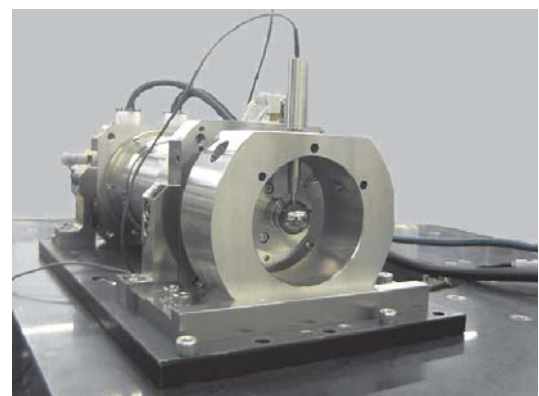


Fig. 3 Test rig for NRRO measurement

type non-contact displacement gage (MicroSense from ADE) with a measuring resolution of  $0.001 \mu\text{m}$ , and the accuracy was measured on a spherical measurement target shown in Fig. 3.

**(2) Result of measurement**

At the rotational speed of  $20,000 \text{ min}^{-1}$ , radial and axial NRRO were measured. Figs. 4 and 5 show the actual measured values. The new product, incorporating the improvements described earlier—heat buildup prevention arrangement, sealing performance of improved mechanisms including improved chuck—has stably achieved runout of  $0.007 \mu\text{m}$  or less. Therefore, it has been determined that the new product satisfies the guaranteed values.

**(3) Drive system**

To be able to run an AC motor, sinusoidal current needs to be fed into its motor coil. The drive system for an AC motor can be categorized into “linear drive system” and “PWM (pulse width modulation) drive system” types, depending on the method for generating the sinusoidal current.

With the linear drive system represented in Fig. 6, a sinusoidal command voltage is power-amplified to drive the motor. Though boasting higher control accuracy, this system involves greater loss at the amplifier; consequently, it is difficult to achieve larger capacity—a drawback that needs to be solved.

With the PWM drive system represented in Fig. 7, the pulse width of command voltage is adjusted in

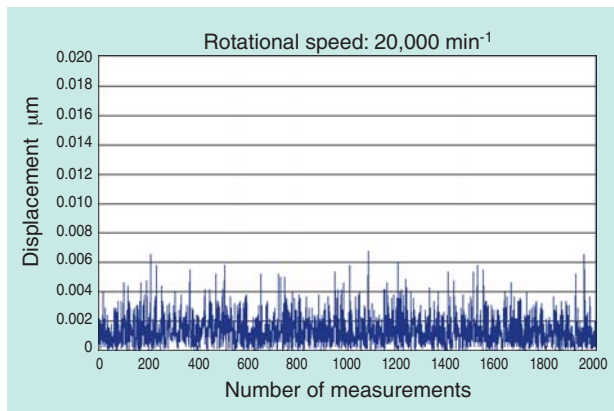


Fig. 4 Radial NRRO on linear drive system

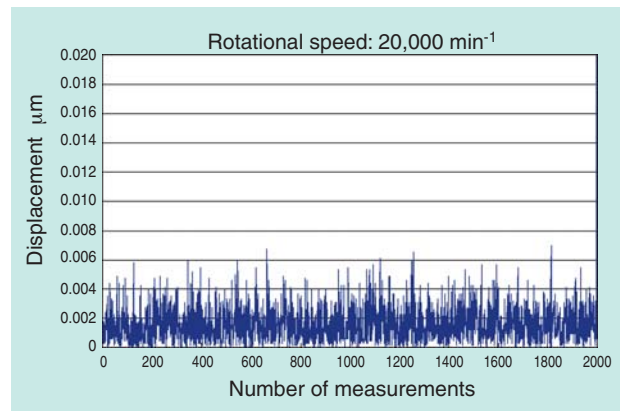


Fig. 5 Axial NRRO on linear drive system

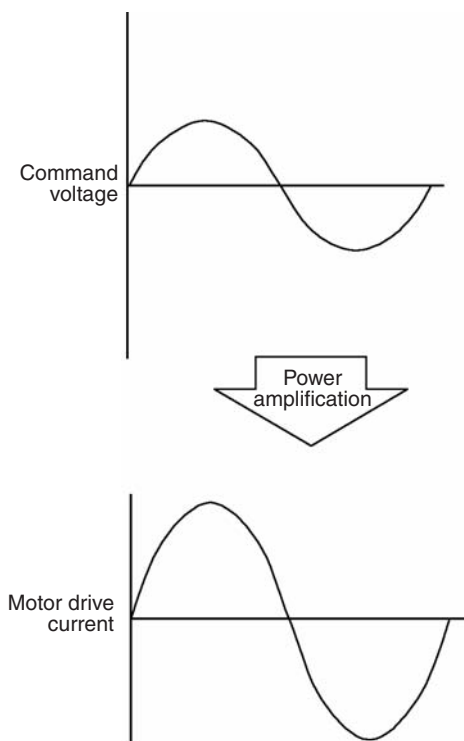


Fig. 6 Linear drive system

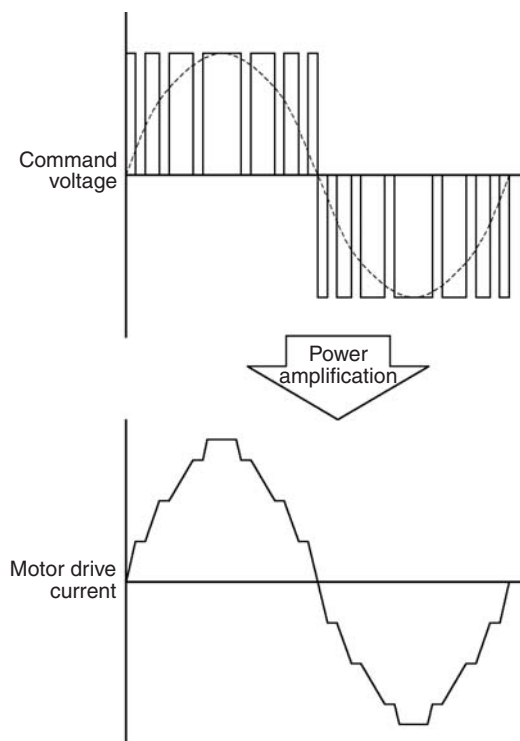


Fig. 7 PWM drive system

proportion to the amplitude of the sinusoidal wave by switching ON/OFF power, and then the voltage pulses are power-amplified to generate the current that approximates the sinusoidal wave in order to drive the motor. This system is highly versatile and highly efficient, and can readily offer higher output. However, noise occurring from switching can adversely affect accuracy of the air spindle; consequently, this drive system is inferior to the linear-type drive system in terms of accuracy.

NTN's newly developed air spindle is combined with a dedicated high-capacity linear drive-type driver to achieve higher accuracy.

#### (4) Evaluation results of NRRO by drive system

NTN prepared two systems for comparison of NRRO performance. Both used the same combination of air spindle proper and electric motor, while two different drive systems – linear and PWM – were applied, and the NRRO compared between the two. Fig. 8 shows plotting of measured radial NRRO values obtained from the PWM drive system. With the PWM drive system, the peak reached 0.018  $\mu\text{m}$ , owing to effect of switching noise; this means the amplitude of displacement with the PWM drive system is more than twice as great compared with the linear drive system in Fig. 4.

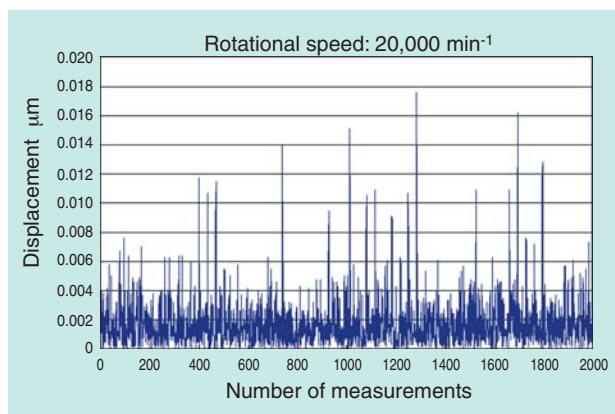


Fig. 8 Radial NRRO on PWM drive system

### 4.2 Rotational speed fluctuation (jitter)

#### (1) Method for measurement and evaluation

Jitter is a numerical measure for defining the severity of rotational speed fluctuation. A control rotary encoder is included in the air spindle. The origin pulse from the rotary encoder (one pulse per rotation) is fed into the analyzer used. Proportion of fluctuation in rotational cycle ( $\Delta t$ ) to theoretical value ( $T$ ) is referred to as jitter and is used as a measure for determining quality of rotational accuracy with the air spindle.

$$\text{Jitter (\%)} = \pm \{ (\Delta t / T) \times 100 \} / 2$$

#### (2) Evaluation results of jitter by drive system

Magnitude of jitter was measured for both the linear drive system and the PWM drive system. The resultant actual measurements are summarized in Tables 2 and 3. Jitter is smaller with the linear drive system, and accuracy of PWM is inferior owing to the adverse effect of noise.

## 5. Functions and Construction Required on Air Spindle for Machine Tool

#### (1) Heat buildup prevention features

Mitigation of heat buildup on air spindle is a difficult challenge if the air spindle is used on a machine tool intended for highly accurate machining operation. This is because the components in bearings within the air spindle can expand or shrink due to fluctuation in temperature, and the resultant displacement will be transferred to the workpiece being machined. The typical contributing factors for temperature fluctuation can include fluctuation in room temperature, and heat generation from the drive and bearing. To mitigate these heat buildup factors, the NTN's newly developed air spindle has adopted the following features:

##### [1] Water cooling structure

A water jacket is adopted to enclose the entire bearing system and motor for efficient cooling of the air spindle.

##### [2] Use of low thermal expansion materials

Low thermal expansion materials such as invar are used for certain bearing components to mitigate thermal displacement.

Table 2 Measurement result of jitter on linear drive system

Rotational speed $\text{min}^{-1}$	Displacement $\Delta t$ nsec					Jitter $\pm\%$
	500	1800	5400	10000	15000	
500	213.0	180.1	190.9	205.5	195.0	0.00009
1800	82.1	72.7	68.5	84.3	67.6	0.00013
5400	33.5	28.2	27.9	31.8	26.5	0.00015
10000	20.8	21.2	17.4	21.2	18.8	0.00018
15000	14.1	12.2	11.5	13.6	14.3	0.00018
20000	9.3	10.3	10.9	10.8	10.2	0.00018

Table 3 Measurement result of jitter on PWM drive system

Rotational speed $\text{min}^{-1}$	Displacement $\Delta t$ nsec					Jitter $\pm\%$
	500	1800	5400	10000	15000	
500	101429.1	97723.3	77618.2	93284.7	89962.5	0.04226
1800	5664.6	5950.3	6932.7	5636.8	5379.7	0.01040
5400	685.8	752.9	531.4	582.7	781.4	0.00352
10000	237.5	191.5	220.1	357.4	268.6	0.00300
15000	128.3	117.8	163.6	135.4	149.5	0.00205
20000	162.3	72.8	121.3	184.2	97.2	0.00307

**[3] Improved shape**

Certain foot components that support the air spindle include a movable portion in order to accommodate axial thermal displacement.

The air spindle was continuously run at a speed of 20,000 min<sup>-1</sup>. Fig. 9 plots the resultant variation on the surface of the workpiece being machined. As illustrated by this diagram, NTN's newly developed air spindle achieves a stable state within several minutes after the start of operation, and regulates the variation on the surface of the workpiece to 1 μm or smaller.

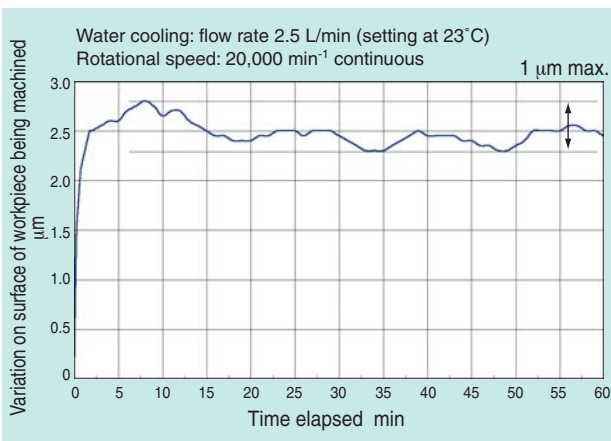


**Fig. 9** Variation on surface of workpiece being machined

**(2) Sealing performance**

Foreign matter trapped in the bearing of an air spindle will jeopardize rotational performance and may lead to catastrophic bearing damage such as seizure. Air spindles for machine tools may be used in severe operating conditions where they are subjected to splashes of cutting chips and coolant. Air spindles are equipped with a non-contact seal mechanism to protect the bearing from these attacks. This seal mechanism includes a narrow labyrinth gap between the rotary shaft and fixed portion (housing); compressed air for air-sealing is allowed to flow through this gap to prevent cutting chips and coolant from entering the bearing. To verify sealing performance of this sealing system, the air spindle was continuously run for 24 hours under coolant splash.

**(3) Chuck mechanism**

For easy mounting/dismounting of the workpiece, the air spindle is equipped with a vacuum chuck mechanism. A workpiece is firmly attracted to the chuck by the pressure difference relative to atmospheric pressure, because air between the workpiece and table is evacuated from the opposite-to-table side through vent holes situated along the shaft core of the rotational shaft. The opposite-to-table side is provided with a non-contact seal, drain trap and drain port; this layout prevents the coolant from entering the bearing (otherwise the coolant can be drawn into the bearing through the air vent holes when the work piece is chucked).

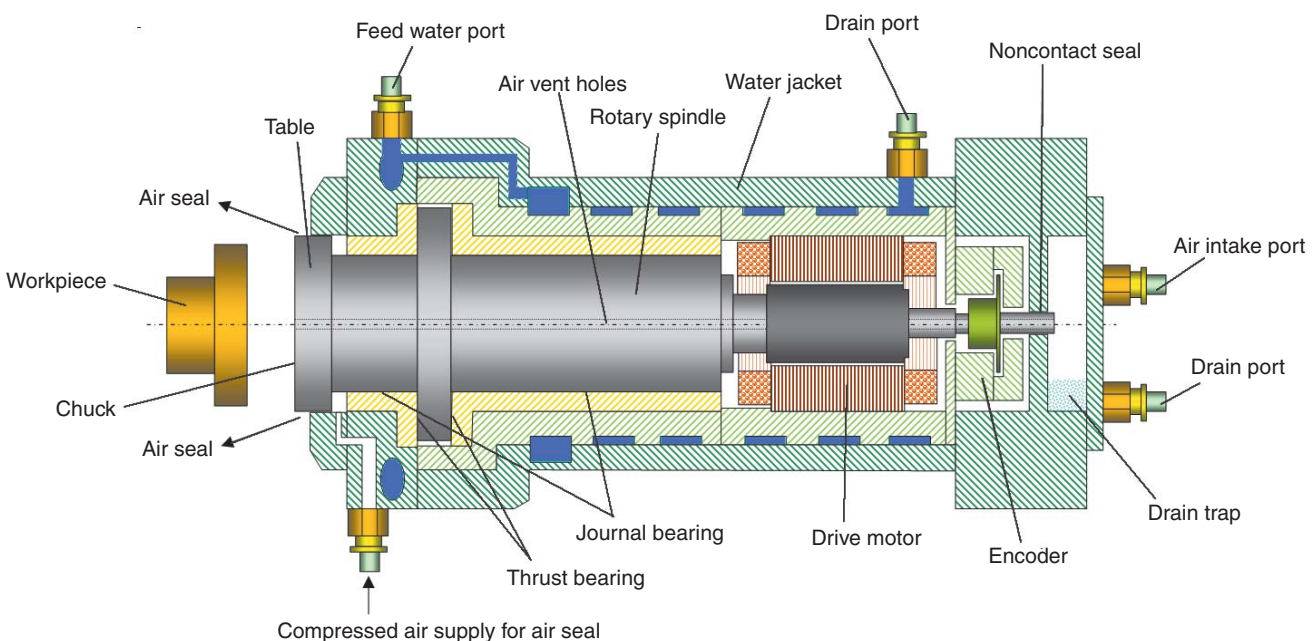


**Fig. 10** Internal structure of NTN's air spindle for machine tool

## 6. Conclusion

NTN has performed performance evaluation tests for its newly developed air spindle for ultra high-precision machine tools that meet contemporary users' needs, and verified the commercial usefulness of this product.

So far, NTN has designed and marketed optimal mechanical structure and control systems that meet the cost and performance that users demand. However, our engineering challenges moving forward will be further complicated and more demanding. To be able to promote users' acceptance and propagation of NTN products throughout its users, continued engineering improvements for enhanced performance, as well as timely performance verification, will be increasingly important.

On the basis of its accumulated technologies and knowledge, NTN will further develop and improve its air spindle product, and continue to seek new applications for the products.

## Reference

- 1) Horiuchi, T., Aono, K., Hiyoshi, H., Development of Aerostatic Bearing Spindle for Precision Machine Tool, NTN Technical Review No. 74, P. 32-35, 2006.

## Photo of authors

---



Teruyoshi HORIUCHI

Precision Equipment Division  
Product Engineering Dept



Kazuyuki AONO

Precision Equipment Division  
Product Engineering Dept



**2010 'Cho' Monodzukuri Innovative Parts and Components Awards—Automotive Component Award**

**Torque Diode for Seat Lifter**

Masahiro KAWAI

**1. Introduction**

This torque diode for seat lifters received the Automotive Component Award at the 2010 'Cho' Monodzukuri Innovative Parts and Components Awards, which are sponsored by the Conference for the Promotion of Monodzukuri and the Nikkan Kogyo Shimbun (Business & Technology Daily News) with support from the Ministry of Economy, Trade and Industry and The Japan Chamber of Commerce and Industry.

The torque diode for seat lifters is used in the mechanical device for manually adjusting the height of a vehicle seat. The torque diode has the merits of quiet operation, while allowing for invariable adjustment with only a small amount of force needed to operate. It also contributes to making vehicle seats more compact and more comfortable.

**2. Structure of Torque Diode for Seat Lifters**

The torque diode for seat lifters is a product that was developed jointly with Shiroki Corporation as a new mechanical device that controls transmission of torque between the input and output shafts.

Beginning with a wedge-shaped clutch structure (see Fig. 1) and by combining the high-precision press operations and lubrication techniques that NTN has developed in its bearing technologies, NTN has succeeded in creating a product that meets the needs of the market.

In order to meet the price requirements of the market, the amount of cutting required was greatly reduced by adopting a new high-precision press

process(see Fig. 2). In 2002, for the first time we began sales in Japan as a clutch for high-performance lever-operated manual seat lifters.

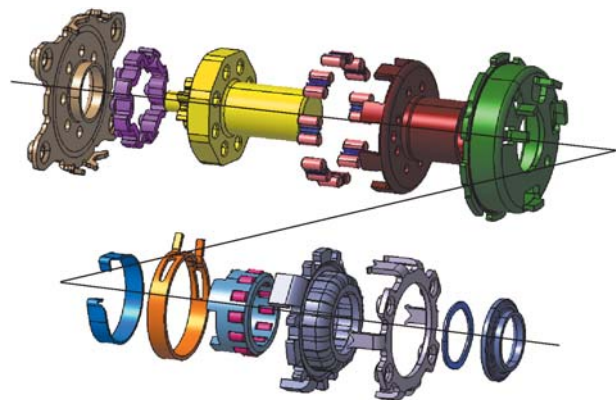


Fig. 2 Component parts

**3. Conclusion**

At this time, vehicle seats with manual lifters are growing at a rate of about 80% according to our estimates. So we are contributing a great deal to the popularity of the level-operated seat lifter models.

For now, we will advance the development of products to achieve better performance with the goal of expanding in markets overseas.

Photo of author

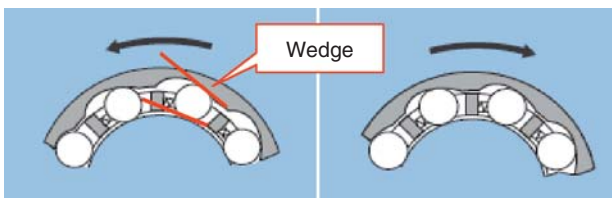


Fig. 1 Wedge-shaped clutch (one-way clutch)  
(left: clutch engaged, right: clutch idle)



Masahiro KAWAI  
Automotive Business HQ  
Axle Unit Engineering Dept.



## First Certificate of Tribology Heritage

# Journal Rolling Bearing for the 0 “Zero” Series Shinkansen Trains

Kouya OHIRA\*

Masanori UENO\*\*

### Overview

At the 55th General Meeting of the Japanese Society of Tribologists, NTN’s journal rolling bearing for the 0 Series Shinkansen trains was recognized as a tribology heritage. <sup>1)</sup> A system of honoring tribology heritages was established this year with the goal of identifying actual products related to tribology that contributed significantly to the advancement of science and technology and to preserve technologies.

These journal bearings were developed for the 0 Series Shinkansen as Japan’s first high-speed train put into operation when the Tokaido Shinkansen Line commissioned in 1964. These journal bearings are comprised of double-row cylindrical roller bearing and single-row deep-groove ball bearing. Journal bearings bear the radial load, which is the weight of the train, and the axial load, which occurs when traveling around curves. The cylindrical roller bearings carry radial load, while the deep-groove ball bearing bears the axial load.

Moreover, in order to prevent the ball elements from slipping on the raceways surface when no axial load is present, the deep groove ball bearing is preloaded using a disc spring. Before Shinkansen, journal bearings on conventional trains were grease-lubricated. In contrast, Shinkansen trains were the first to adopt journal bearings lubricated by oil bath lubrication system because these bearings have to operate at high speeds for a prolonged time.

As a result of journal bearing design development and testing, a variety of specification and inspection standards were established with the guidance of the Japanese National Railways (now JR). A variety of the

standards from that time have been contributing greatly to the advancement of bearings for railway.

Shinkansen journal bearings are one key industrial product that has continued to support the high speed, safety and comfort of Shinkansen trains to this day. These rolling bearings were recognized as an important tribology heritage that made a great contribution to the advancement of tribology history as a milestone for journal bearings in high speed trains, leading to this designation.

Since the importance of the railway industry continues to grow, there are demands for bearings that are able to provide even higher speed, greater reliability and longer life because trains offer high-speeds, high-capacity means of transportation with low environmental impacts. We will continue to research and develop journal bearings for railway that take safety and economy into consideration while being good for the environment.

This journal bearing model is being displayed in the first-floor lobby of our Industrial Technical Center in Kuwana-shi, Mie.

### References

- 1) Tribology Heritage #3: Journal Bearings for 0 Series Shinkansen Trains, Journal of Japanese Society of Tribologist, Vol. 56, No. 7, p. 402, 2011.



Fig. 1 Certificate of Tribology Heritage



Fig. 2 Commendation from Japanese Society of Tribologist (From the left: Masayuki Mori, President, Japanese Society of Tribologist, and Yosikazu Fukumura, Executive Director, NTN CORP.)

\* Industrial Technical Center

\*\*Industrial Business Headquarters, Construction Machinery and Railway Engineering Department

## Sealed Self-Aligning Roller Bearing (ULTAGE WA Type)

With an additional seal that prevents the ingress of foreign matter,  
load capacity of the world's highest level

**Longer bearing life, higher reliability and easier handling!**



### Features

**[1] Worlds highest load capacity**

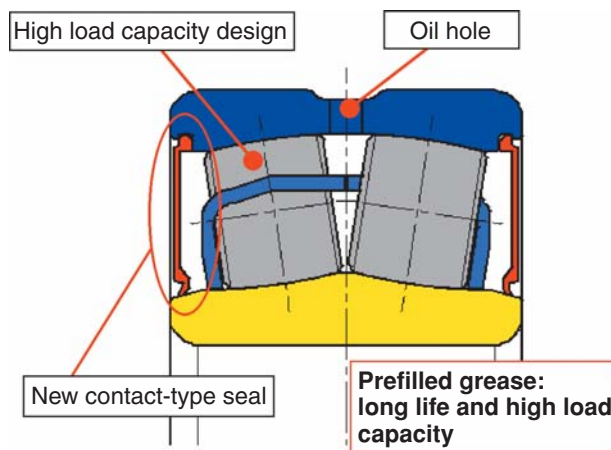
- Adoption of the ULTAGE EA type internal design

**[2] Compact design that minimizes space taken up by seals in an assembly**

- Use of a special contact-type rubber seal design prevents the ingress of contaminants.
- Contact pressure of the seal on the bearing remains unchanged in spite of alignment operation on the bearing; the seal maintains its dust-prevention performance during misalignment conditions.

**[3] Long-life grease used as standard**

### Structure



### Applications

- **Raw material transportation conveyors**  
(in steel mills, thermal power generation stations, mines, etc.)
- **Parts possibly attacked by salty air**  
(transportation equipment in harbors; and construction machinery, etc.)

# ULTAGE Sealed Four-Row Tapered Roller Bearing for Rolling Mill Roll-Necks

Through optimized bearing design, we have greatly improved load resistance, load capacity and sealing performance, **helping extend bearing replacement cycles** and **improving reliability** of the bearing during rolling mill operation!



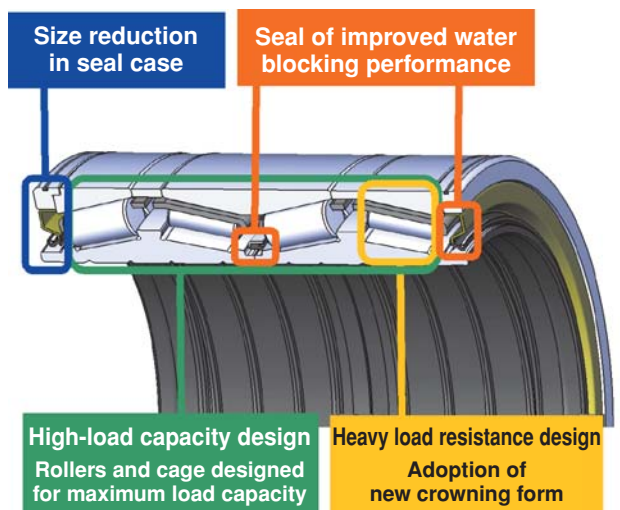
## Features (compared to previous models)

- [1] Worlds highest-load capacity design**
  - Bearing rating life improved by as much as 1.8 times.
- [2] New crowning form improves load distribution**
  - Heavy load resistance more than doubled (world's best)
- [3] Improved Seal Performance**
  - Water resistance more than doubled

## Applications

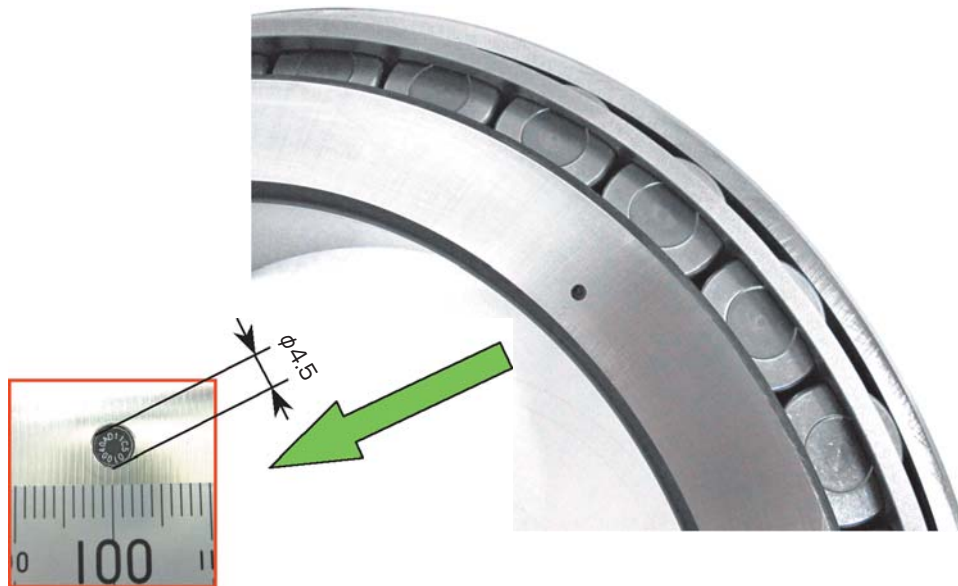
- Steel mill roll-neck bearings

## Structure



## IC Tag Integrated Bearing

The industry's first! Electronic data can be recorded inside the bearing itself.  
**Enhanced reliability about regular inspection information, and simplification of otherwise time-consuming information management procedure!**



### Features

- [1] Confirmation of quality data reading can be conducted from the bearing itself.
- [2] Users can write and read usage history to the bearing itself.
- [3] Management items can be set freely.

### Applications

- Construction machinery, mining equipment, aircraft, wind power generation facilities, rolling stock, etc.  
 (suitable for applications that require regular maintenance)

### Structure (examples of applications and typical contents of data being displayed)

[Image of use]



[Examples of data sets used for bearing life management]

**(Bearing quality information)**

1	Product name
2	Bore dia., outside dia., precision of bearing width, gap information, etc.
3	Serial No.
4	Manufacture date, inspection date, shipping date

**(User management information)**

1	ID No. of machine that is equipped with the bearing in question
2	Date where the bearing is installed to the machine
3	Date where inspection takes place
4	Accumulated operating hours

# Large Bearing with Integrated Rotary Sensor

First in the industry!

NTN has created large bearings with incorporated rotary sensors!

Using this, **a fewer number of parts and components are needed** for installing a rotary sensor and the **time needed for installing and adjusting the sensor is virtually eliminated**



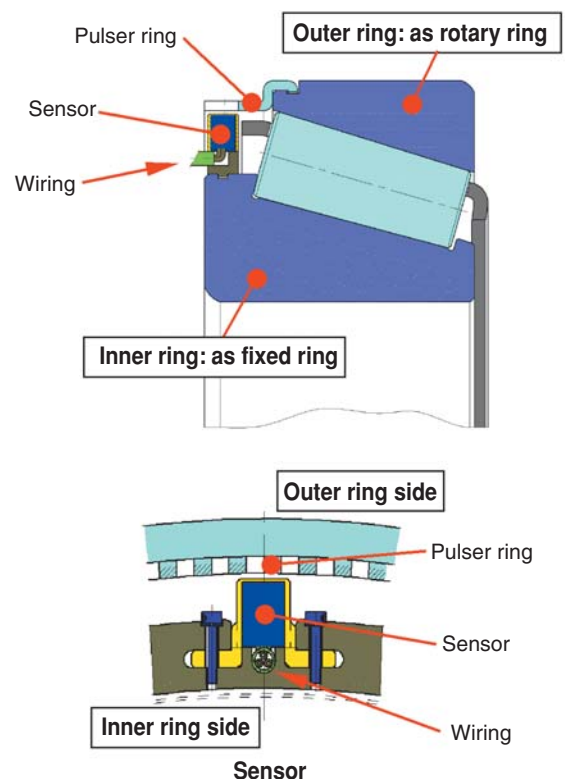
## Features

- [1] Rotary sensor is built into the bearing.
- [2] A unique design has been adopted to prevent possible disconnection of electric wire between the shaft and inner ring even if creeping (slipping) occurs between the shaft and inner ring.
- [3] Can be used immersed in oil.
  - Even in oil at 120°C, the sensor reliably detects the bearing speed (can depend on oil type and additives).
- [4] Can reliably operate under vibrating conditions.
  - Even in severe vibrating conditions with vibration acceleration of 10 G, the sensor reliably detects the bearing speed.

## Applications

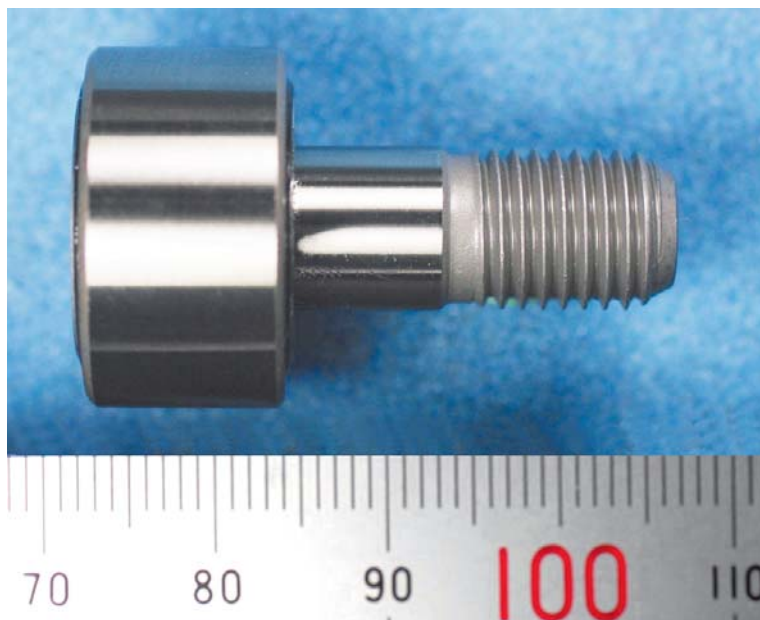
- Construction machinery, steelworks facilities, wind power generation facilities, ventilators, etc.

## Structure (example: tapered roller bearing)



## New Standard Cam Follower

Compared to conventional cam followers, this product boasts **longer life and lower torque** even in severe applications



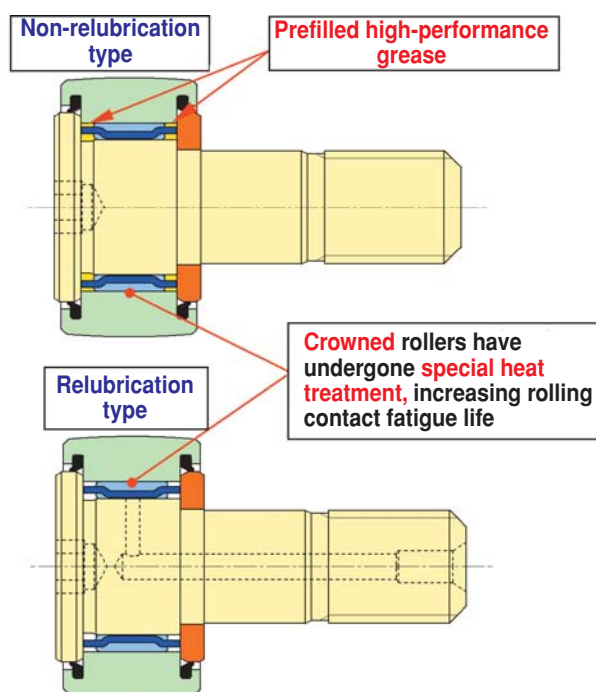
### Features (compared to previous models)

- [1] **Longer rolling fatigue life achieved.**
  - More than double the fatigue life when compared to previous designs (with prefill of high-performance grease)
- [2] **Non-relubrication type is prefilled with high-performance grease, boasting greater wear resistance and much lower starting torque at low temperatures.**
  - 35% reduction in starting torque (at -20°C)
- [3] **Installation and lubrication methods remain the same as those of current standard products (fully compatible)**

### Applications and series model numbers

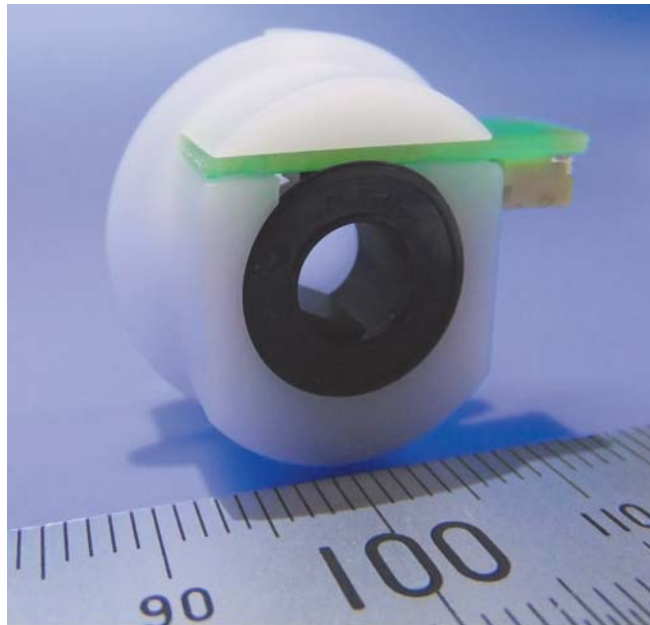
- Transportation equipment, machine tools, printing presses, press machines, etc.
- **NTN KR (V) 16–26 series models**  
With cages of outer ring outside diameters  $\phi$  16–26 mm (stud diameter  $\phi$  6–10 mm), or full complement type roller cam followers

### Structure



## Rotary Sensor-Integrated Sliding Bearing

Combining resin sliding bearings and sensors **helps simplify the installation of the bearings into the machine**. The design promotes reliability in monitoring of running state of the machine, **helping reduce time needed for maintenance work** on the machine



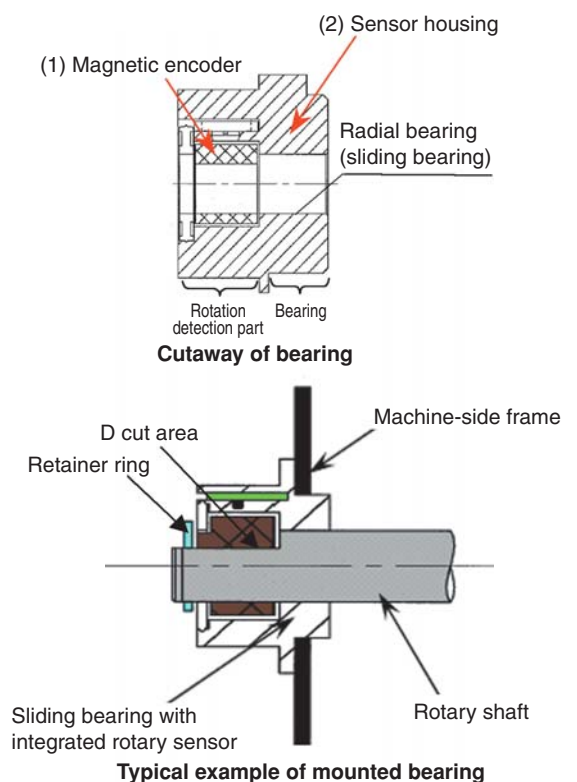
### Features

- [1] **Unitized sliding bearing and rotary (magnetic) sensor**
  - Easy handling and compact size
- [2] **Greater freedom in designing wiring route**
  - Selectable orientation of the connector during mounting.
- [3] **Wide input voltage range (3–26 V)**
  - Compatible with diverse machinery and specifications
- [4] **Greater freedom for forms of bearings and product outer diameters**
  - Customized design possible

### Applications

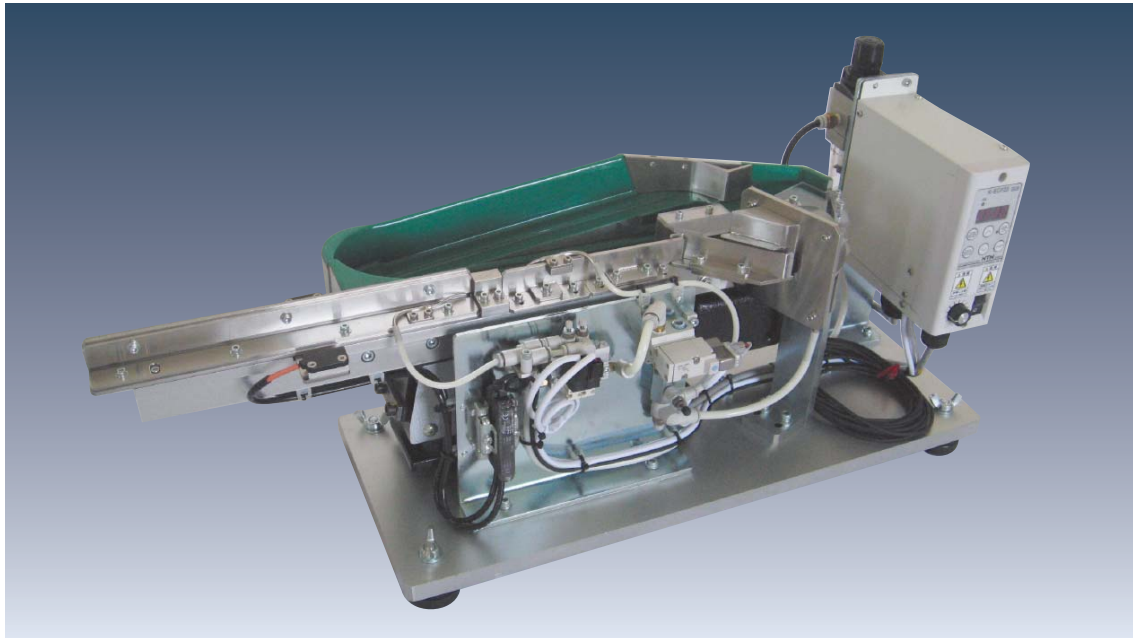
- Rotary drives in office automation equipment, measuring equipment, etc.

### Structure



## Monodrive Two-way Feeder with Spring Separation Mechanism

Enhances functionality of automatic spring parts feeding system.  
**Reduces necessary floor space** while **realizing reliable parts feeding!**



### Features

As automatic feeding system for tangled springs

#### [1] Compact

- Required floor space is about half (compared to bowl type models).
- Newly-developed spring separation mechanism has been integrated into a compact monodrive two-way feeder.

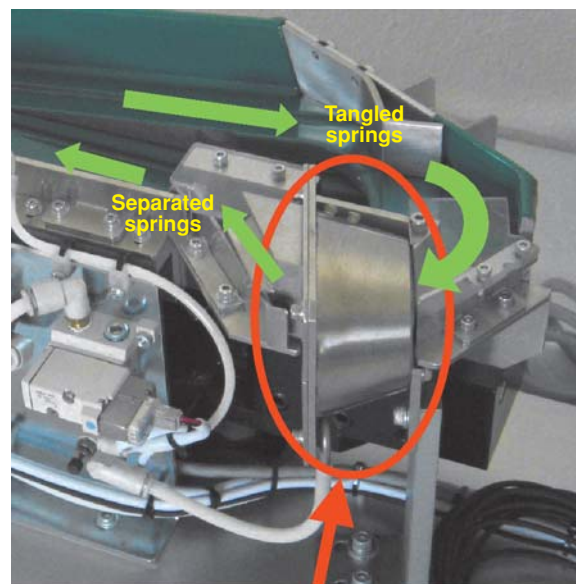
#### [2] Stable supply

- Tangled springs are rapidly and reliably separated and transported by the separation mechanism.

### Applications

- Automatic feeding equipment for small diameter coil springs (diameters of up to 2–5 mm)

### Structure



Spring separator

# Compact, Variable Frequency Controller for Parts Feeders

Numerous functions are combined to contribute to a **reduction in necessary floor space** and **improvement in production efficiency**



## Features

- [1] **Reduced floor space (compared to previous models)**
  - Volume: 1/3 (K-ECG25)–2/3 (K-ECH45)
- [2] **Numerous functions**
  - Resonance point tracking function (included in high-performance types)
    - Up to 30% reduction in electricity consumption
  - Constant amplitude function (included in high-performance types)
    - Transportation speed remains unchanged regardless of variation in the volume of loaded work pieces.
  - Works depleted detection, and inching operation functions (included in all types)

## Comparison of parts feeder product types



## Lineup

Note: For details about applicable parts feeder unit being controlled, please refer to NTN's relevant parts feeder catalog.

Model	Size mm	Weight kg	Applicable units	Constant amplitude & resonance point tracking functions
K-ECF25	W60×H140×D142	About 1.1	K10–K20, N25, L20S, 05–S30, etc.	No (standard type)
K-ECG25		About 1.2		Yes (high-performance type)
K-ECH45	W82×H140×D142	About 1.7	K20·1, N25–N40, G50	No (standard type)
K-ECJ45		About 1.7		Yes (high-performance type)